Measurements of hydroxyl radical reactivity and formaldehyde in the atmosphere

Danny Russell Cryer

Submitted in accordance with the requirements for the degree of

Doctor of Philosophy

The University of Leeds

School of Chemistry

September, 2016

The candidate confirms that the work submitted is his own, except where work which has formed part of jointly-authored publications has been included. The contribution of the candidate and the other authors to this work has been explicitly indicated below. The candidate confirms that appropriate credit has been given within the thesis where reference has been made to the work of others.

The observations of OH reactivity presented in Chapter 5 of the thesis have appeared in publication as follows:

Stone, D., Whalley, L. K., Ingham, T., Edwards, P. M., Cryer, D. R., Brumby, C. A., Seakins, P. W. and Heard, D. E.: *Measurement of OH reactivity by laser flash photolysis coupled with laser-induced fluorescence spectroscopy,* Atmospheric Measurement Techniques, 9, 2827-2844, 2016.

I was responsible for the ambient measurements of OH reactivity that were made during the York 2014 ‘missing’ OH reactivity campaign, along with L. K. Whalley and D. E. Heard, and for the processing and analysis of the observational data.

Acknowledgements

So the time has finally come to write the acknowledgements after finishing the rest of this book. I have to say it felt like this day would never come! There are a number of people I need to thank who have helped me in a manner of ways through the course of my PhD, without help from these people this work would not have been possible.

Firstly I would like to thank my supervisors Dwayne and Lisa for their support and guidance over the past four years. I would also like to thank them for providing me with the opportunity to do this PhD in the first place. I also need to thank past and present members of the Heard group who I have worked alongside. I would like to thank Trev in particular for all the help and advice he has given me both in the lab and in the field. Due to the collaborative nature of the fieldwork I have been involved in there are many people from other institutions who are due acknowledgement and thanks. However, there are far too many for them to individually name them all here so I would like to thank everybody who I have worked with in the field.

During my four years in Leeds I've met many people both inside and outside of the department. In particular I would like to thank Charlotte for her unwavering support and confidence in me. I'm sure I would have lost considerably more hair writing this thesis without her! Thanks are also due to Anna for her friendship and the often late night tea/coffee breaks that I'm sure stopped both of us losing the plot! Furthermore I would also like to thank my friends Graham, Adam, Laura and many others (there are too many to name) for providing me with a social life.

No acknowledgements would be complete without mentioning my family. I would like to thank my parents for supporting me not only through my PhD, but through life in general. The time and effort they invested in my education through my school years made this PhD possible.

Abstract

Results from the laboratory characterisation of a new design of hydroxyl radical (OH) flow reactor are presented. Further to this details of its coupling with a gas chromatograph time of flight mass spectrometer (GC-TOF-MS) system, to form a new instrument for the identification of 'missing' OH reactivity is discussed. Preliminary measurements in ambient air demonstrated the potential value of this system which could be used to chemically identify 'missing' OH sinks in various environments, and also to determine bimolecular rate coefficients for their reaction with OH. Observations of OH reactivity and formaldehyde (HCHO) are presented from an urban background site in York in the summer of 2014. OH reactivity was measured using laser flash photolysis coupled with laser induced fluorescence spectroscopy (LFP-LIF). The average 'missing' OH reactivity was ~27 % when measurements were compared with values predicted by a calculation that utilised measured concentrations of a very detailed suite of volatile organic compounds (VOCs). It is concluded that a combination of unidentified VOCs and products of VOC photo-oxidation account for this discrepancy. HCHO was measured using a new fast response (1 s time resolution) laser induced fluorescence (LIF) spectroscopy instrument and some evidence of daytime diurnal behaviour suggested that the dominant HCHO source was photo-chemical (~1.3 ppb diurnal peak). Observations of OH reactivity and HCHO are also presented from a coastal site in Weybourne, Norfolk, using the same instrumentation during the summer of 2015. The average 'missing' OH reactivity was ~44 %. It is concluded that much of the 'missing' reactivity was likely due to unmeasured VOCs and their photo-oxidation products. Strong diurnal behaviour of HCHO was observed and is consistent with an atmosphere where the dominant source is photo-chemical (~1.1 ppb diurnal peak). Unusual behaviour was observed for HCHO during a thunderstorm where sharp fluctuations in concentration were observed. It has so far not been possible to conclude the exact cause of this, however, it is suggested that the source was marine. Finally, preliminary results from three experiments of an intercomparison of OH reactivity instrumentation are presented. The results demonstrate the reliability of the Leeds LFP-LIF instrument for the measurement of ambient OH reactivity.

Table of Contents

List of Abbreviations

BEARPEX	Biosphere effects on aerosols and photochemistry experiment
BNC	Berkeley Nuceleonics Corporation
BST	British summer time
BVOC	Biogenic volatile organic compound
CABINEX	Community atmosphere-biosphere interactions experiment
CalNex	California Nexus
CIMS	Chemical ionisation mass spectrometer
ClearFlo	Clean air for London
CPM	Channeltron photomultiplier
CRM	Comparative reactivity method
CWT	Concentration weighted trajectory
DOAS	Differential optical absorption spectroscopy
DOMINO	Diel oxidant mechanisms in relation to nitrogen oxides
FAGE	Fluorescence assay by gas expansion
FMI	Finnish meteorological institute
GABRIEL	Guyanas atmosphere biosphere exchange and radicals intensive experiment with the Learjet
GC	Gas chromatograph
GC-FID	Gas chromatograph coupled with flame ionisation detector
GC-PID	Gas chromatograph coupled with photoionisation detector
GC-TOF-MS	Gas chromatograph coupled with time of flight mass spectrometer
GCxGC-FID	Comprehensive gas chromatograph coupled with flame ionisation detector
GCxGC-TOF-MS	Comprehensive gas chromatograph coupled with time of flight mass spectrometer
HPLC	High performance liquid chromatography
HUMPPA-COPEC	Hyytiälä united measurement of photochemistry and particles – comprehensive organic particle and environmental chemistry
HYSPLIT	Hybrid single particle lagrangian integrated trajectory model
IC	Ion chromatography

ICOZA	Integrated chemistry of ozone in the atmosphere
ID	Inner diameter
IR	Infra-red
IUPAC	International union of pure and applied chemistry
LFP-LIF	Laser flash photolysis coupled with laser induced fluorescence spectroscopy
LIF	Laser induced fluorescence
LOPAP	Long path absorption photometry
LP-DOAX	Long path differential optical absorption spectrometery
LSCE	Laboratory of the sciences of climate and the environment
MAX-DOAS	Multiaxis differential optical absorption spectrometry
MCM	Master chemical mechanism
MCMA	Mexico City metropolitan area
MEGAPOLI	Megacities: emissions, urban, regional and global atmospheric pollution and climate effects, and integrated tools for assessment and mitigation
MPIC	Max Planck Institute for Chemistry
NOAA	National Oceanic and Atmospheric Administration
NPL	National Physical Laboratories
NPT	National pipe thread
OASIS	Ocean-atmosphere-sea ice-snowpack
OD	Outer diameter
OP3	Oxidant and particle photochemical processes
ORSUM	OH reactivity specialists uniting meeting
PMT	Photomultiplier tube
PMTACS-NY	PM2.5 technology assessment and characteristics study – New York
PMTACS-NY-WFM	PM2.5 technology assessment and characteristics study – New York – Whiteface Mountain
POPR	Perturbed ozone production rate
PRD	Pearl river delta
PRF	Pulse repetition frequency
PRIDE-PRD	Program of regional integrated experiments on air quality over the pearl river delta

PROPHET	Program for research on oxidants: photochemistry, emissions and transport
PT	Pressure transducer
PTR-MS	Proton transfer mass spectrometer
QCLS	Quantum cascade laser spectrometer
RACM	Regional atmospheric chemistry model
SAPHIR	Simulation of atmospheric photochemistry in a large reaction chamber
SAPHIR-PLUS	SAPHIR plant chamber unit for simulation
SCAPE	Schenandoah cloud and photochemistry experiment
SHG	Second harmonic generator
SLM	Standard litres per minute
SOS	Southern oxidants study
SRS	Stanford research systems
TDLAS	Tuneable diode laser absorption spectroscopy
TexAQS	Texas air quality study
THG	Third harmonic generator
TOF-MS	Time of flight mass spectrometer
TOHLM	Total OH loss rate method
TORCH	Tropospheric organic chemistry experiment
TRAMP	TexAQS radical measurements project
TTL	Transistor transistor logic pulse
UEA	University of East Anglia
UPS	Uninteruptable power supply
UTC	Coordinated universal time
UV	Ultra-violet
VOC	Volatile organic compound
WACL	Wolfson Atmospheric Chemistry Laboratories
WAO	Weybourne Atmospheric Observatory

List of Figures

List of Tables

Chapter 1 - Introduction

1.1 Atmospheric chemistry

The field of atmospheric chemistry is composed largely of three interdependent disciplines; these are field measurements, laboratory measurements and computer modelling. Observations from field measurements are used to investigate atmospheric processes and composition. They can be used to build and test the quality of global climate and air quality models by comparison with their predictions. Model simulations contain the current state of our knowledge of the atmosphere and can also be used to predict future change. Laboratory measurements are used to determine physical constants such as rate coefficients for use in computer models, and to complement analysis of data recorded in the field. They can also be used to investigate complicated chemical and physical processes which occur in the atmosphere, ranging from single reaction kinetic studies to complex multiple reaction studies in atmospheric simulation chambers. Further to this, laboratory measurements are often used as a means to test and characterise instrumentation prior to field deployment.

Managing air quality and climate change are two of the biggest environmental challenges we face as a society. Poor air quality resulting from pollution contributes to over two million premature deaths worldwide each year (World Health Organisation, 2005). Over the previous few decades there has been an international effort to reduce the level of pollutants emitted into the atmosphere. However, decreasing emissions do not scale linearly with the level of pollutants that are detected in the air, and pollutants can also travel long distances and adversely affect air quality across boarders and continents (European Environment Agency, 2008, Maas and Greenfelt, 2016). The work presented in this thesis is particularly relevant to the production of Tropospheric ozone. It is a major pollutant and greenhouse gas which is formed through the removal of volatile organic compounds (VOCs), in the

presence of nitrogen oxides (NO_x), from the atmosphere by reaction with the hydroxyl radical, (OH) (Sillman, 1999). It can also be formed during long range transport of air masses from the pollutant emission sources. In order to accurately predict changes in Tropospheric O_3 and plan effective mitigation strategies, it is crucial that we have a clear understanding of the range of VOCs that are removed from the atmosphere by OH. The measurement of OH reactivity (the pseudo first order rate coefficient for OH loss) provides a valuable tool to test our understanding of this. Additionally, measurement of gas phase formaldehyde is a useful investigative tool as it acts as an overall tracer of VOC removal by OH. The ability of a computer model simulation to accurately predict formaldehyde levels as measured in the field has the potential to highlight uncertainties in our understanding of VOC + OH chemistry. This thesis investigates the completeness of our knowledge of the VOCs that are removed from the atmosphere by OH, in two contrasting chemical environments. Chapter 2 describes the methodologies and experimental techniques used to measure OH reactivity and formaldehyde for this work. Chapters 5 and 6 present field observations of OH reactivity and formaldehyde that were made at an urban background site in York and a coastal site in Norfolk, respectively. Further to this Chapter 4 details the laboratory characterisation of a new field instrument that can be used to investigate the chemical identity of currently unidentified VOCs which react with OH, and also measure rate coefficients for their reaction with OH. In Chapter 3 results from an intercomparison study are presented where 9 instruments for the measurement of OH reactivity simultaneously sampled gas from an atmospheric simulation chamber.

1.2 RO_x in the troposphere

1.2.1 Overview of chemistry

The troposphere occupies the first ~15 km of the atmosphere and the lowest ~1 km is known as the boundary layer (Holloway and Wayne, 2010). Approximately 90% of atmospheric mass resides in the troposphere (Wayne, 2000). RO_x, the collective term for hydroxyl radicals (OH), hydroperoxyl radicals (HO_2) and alkoxy radicals (RO_2), plays a central role in controlling tropospheric pollutant and greenhouse gas levels. Therefore complete and detailed knowledge of RO_x chemistry is crucial when assessing the impact of ever changing emissions on air quality, climate and health. A

significant portion of this work is focussed on the chemistry of OH in the troposphere, and its removal via reaction with volatile organic compounds (VOCs).

1.2.2 RO_x formation

R 1.1 and R 1.2 show the photolysis of ozone and subsequent reaction of the product $O(^1D)$ with water vapour, this is the main pathway for the formation of tropospheric OH.

$$O_3 + h\nu_{(\lambda<340\ nm)} \rightarrow O_2 + O(^1D) \qquad \textbf{R 1.1}$$

$$O(^1D) + H_2O \rightarrow 2OH \qquad \textbf{R 1.2}$$

However, $O(^1D)$ can also undergo collisional quenching with a bath gas M (most commonly O_2 or N_2) to form $O(^3P)$ which can react with O_2 in the presence of M to reform ozone, R 1.3 and R 1.4. Only a small fraction (< 3 %) of $O(^1D)$ formed through photolysis of O_3 leads to the production of OH, with the rest reacting back again to O_3 (ESPERE, 2017).

$$O(^1D) + M \rightarrow O(^3P) + M \qquad \textbf{R 1.3}$$

$$O(^3P) + O_2 + M \rightarrow O_3 + M \qquad \textbf{R 1.4}$$

The processes shown in R 1.1, R 1.2, R 1.3 and R 1.4 are displayed in Figure 1.1 in addition to other atmospherically relevant processes involving RO_x.

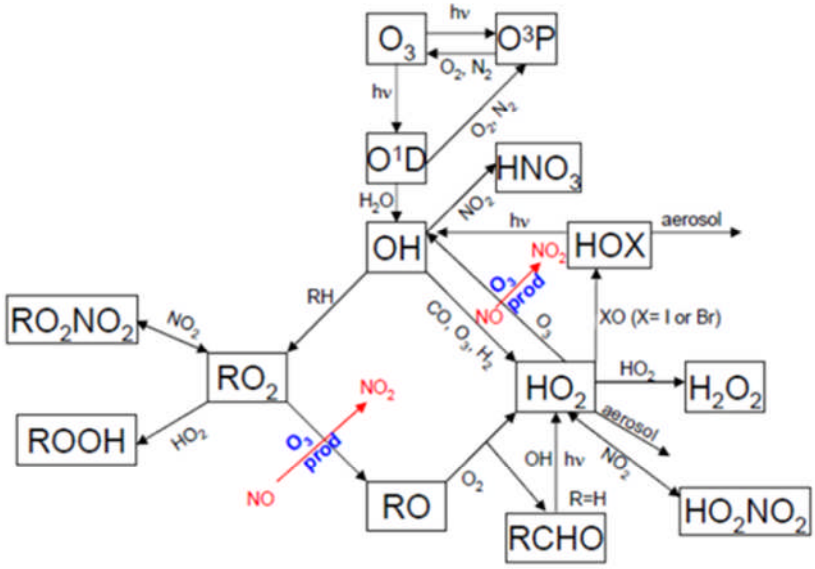

Figure 1.1: Schematic to show a simplified RO_x reaction cycle, halogen atoms are represented by X and alkyl groups are represented by R. Taken from Smith (2007).

OH can oxidise VOCs such as alkanes to produce alkylperoxy radicals (RO_2) that can react with NO to form alkoxy radicals (RO). Dioxygen can react with RO to form a carbonyl compound and hydroperoxyl radicals (HO_2). HO_2 can react with NO to reform OH. R 1.5- R 1.9 summarise these reactions where R represents an alkyl group and R' represents an alkyl group with one less carbon than R (Finlayson-Pitts and Pitts, 2000). The process is known as RO_x cycling.

$$RH + OH \rightarrow R + H_2O \quad \textbf{R 1.5}$$

$$R + O_2 + M \rightarrow RO_2 + M \quad \textbf{R 1.6}$$

$$RO_2 + NO \rightarrow RO + NO_2 \quad \textbf{R 1.7}$$

$$RO + O_2 \rightarrow R'CHO + HO_2 \quad \textbf{R 1.8}$$

$$HO_2 + NO \rightarrow OH + NO_2 \quad \textbf{R 1.9}$$

In R 1.7 and R 1.9 NO_2 is formed, which is photolysed to produce $O(^3P)$ (R1.10) which can then react to produce ozone (R1.4), this is the only pathway for the formation of ozone in the troposphere. Tropospheric ozone is a greenhouse gas and can also cause adverse health effects. Thus in high NO_x (the collective term for NO and NO_2) environments such as urban areas where vehicular emissions are high, it is important that factors affecting the RO_x budget are well characterised and understood. Tropospheric ozone production is discussed in more detail in Section 1.3.

$$NO_2 + h\nu_{(\lambda<420\ nm)} \rightarrow O(^3P) + NO \quad \textbf{R 1.10}$$

Aside from R 1.1 and R 1.2, there are several other pathways for RO_x formation which are typically most significant in polluted environments (Finlayson-Pitts and Pitts, 2000). R 1.11 - R 1.13 show the photolysis of formaldehyde (HCHO) and subsequent reaction of both products to produce HO_2. It should be noted here that photolysis of other carbonyl species other than HCHO, such as longer chain aldehydes and ketones, can also lead to the production of RO_x. The atmospheric chemistry of HCHO is of particular relevance to this thesis and ambient measurements are presented and discussed in Chapters 5 and 6.

$$HCHO + h\nu_{(\lambda<338\ nm)} \rightarrow H + HCO \quad \textbf{R 1.11}$$

$$HCO + O_2 \rightarrow CO + HO_2 \quad \textbf{R 1.12}$$

$$H + O_2 + M \rightarrow HO_2 + M \quad \textbf{R 1.13}$$

The photolysis of nitrous acid (HONO) also produces OH (R 1.14) (Johnston and Graham, 1974), as does the photolysis of hydrogen peroxide (H_2O_2) and alkyl peroxide (ROOH) (R 1.15 and R 1.16) (Jacob, 1999). Halogen oxoacids (HOX, where X commonly represents Cl, Br or I) can also be photolysed to produce OH (R 1.17).

$$HONO + h\nu_{(\lambda<400\ nm)} \rightarrow OH + NO \quad \textbf{R 1.14}$$

$$H_2O_2 + h\nu_{(\lambda<340\ nm)} \rightarrow 2OH \quad \textbf{R 1.15}$$

$$ROOH + h\nu_{(\lambda<300\ nm)} \rightarrow OH + RO \quad \textbf{R 1.16}$$

$$HOX + h\nu_{(\lambda<480\ nm)} \rightarrow OH + X \quad \textbf{R 1.17}$$

Another route for the production of OH is the reaction between ozone and alkenes. Ozone can add to the double bond of an alkene to form a carbonyl compound and energy rich intermediate (Atkinson, 2007, Atkinson and Carter, 1984). This is known as a Criegee intermediate and can either be quenched by collisions with M, or it can decompose in a variety of ways and sometimes form OH (Heard et al., 2004). R 1.18 and R 1.19 demonstrate this type of OH formation by example of ethene reacting with ozone.

$$CH_2 = CH_2 + O_3 \rightarrow H_2CO + [H_2COO]^* \quad \textbf{R 1.18}$$

$$[H_2COO]^* \rightarrow OH + HCO \quad \textbf{R 1.19}$$

The OH yield from this type of reaction has been shown to be dependent on several factors. For the reaction of ozone with ethene the OH yield has been reported as ~16 %, whereas for more substituted alkenes, and those with different isomeric properties, higher yields (e.g. 90 % for 2,3-dimethyl-2-butene) have been reported. OH yields have also been found to vary as a function of pressure. A recent review of Crigee intermediates formed during tropospheric ozonolysis can be found in Taatjes et al. (2014).

1.2.3 RO_x termination

Pathways for RO_x termination are different in high and low NO_x environments. In high NO_x environments RO_x propagation by R 1.7 and R 1.9 is rapid resulting in the partitioning of RO_x being skewed towards OH. Nitric acid (HNO_3) formation from

the reaction between OH and NO_2 is a dominant RO_x termination mechanism in these environments, R 1.20 (Finlayson-Pitts and Pitts, 2000). In low NO_x environments there is less RO_x propagation due to a lack of NO, in this case radical-radical reactions present the main termination mechanism, most commonly R 1.21 and R 1.22. The products of R 1.20, R 1.21 and R 1.22 can all lead to permanent radical loss through dry or wet deposition on surfaces or particles (Wayne, 2000).

$OH + NO_2 + M \rightarrow HNO_3 + M$ **R 1.20**

$HO_2 + HO_2 \rightarrow H_2O_2$ **R 1.21**

$HO_2 + RO_2 \rightarrow ROOH$ **R 1.22**

1.3 Tropospheric ozone production

The atmospheric chemistry of ozone in the troposphere plays a key role in numerous processes relating to air quality and climate change as it is both a pollutant and a greenhouse gas. O_3 is a major constituent of photochemical smog and is a known respiratory irritant, exposure to excessive levels has been shown to be linked with increased mortality rates in a number of European cities; daily deaths have been shown to increase by 0.3 % per every ~5 ppb increase in O_3 exposure (World Health Organisation, 2005). In addition to this, tropospheric O_3 is damaging to crops; it can harm yields and reduce quality (Krupa et al., 1998). Tropospheric O_3 is often produced as a product from the photo-oxidative processing of VOCs in the presence of NO_x through the reaction of $O(^3P)$ with O_2, where $O(^3P)$ was formed from the photolysis of NO_2 that resulted from the reaction between NO and RO_2, or HO_2.

Environments are often characterised as NO_x or VOC limited when considering O_3 production. When the loading of NO_x in the atmosphere is low, catalytic RO_x cycling (as described in Section 1.2) is slow, meaning that there is a high frequency of radical termination reactions and net O_3 destruction. As the level of NO_x increases, there is a linear increase in O_3 production until a threshold (known as the O_3 compensation point) is reached. At this point there is a change from net O_3 destruction, to net O_3 production. At NO_x levels beyond this point the linear increase in O_3 production continues. However, there comes a point where the termination reaction of OH with NO_2 (R1.20) begins to slow down the cycling of RO_x (because OH is lost) and subsequently the rate of O_3 production reaches a maximum. As NO_x increases beyond this maximum, the rate of O_3 production begins to decrease. The

maximum in O_3 production signifies a transition from a NO_x limited to a VOC limited atmosphere (Sillman, 1999) and is illustrated in Figure 1.2(a). The rate of O_3 production is sensitive changes in the level of VOCs present, similar to the relationship with NO_x this is non-linear (Sillman and He, 2002). Ozone isopleths are commonly used to visualise the relationship between the rate of O_3 production, and the level of NO_x and VOCs; an example is shown in Figure 1.2(b).

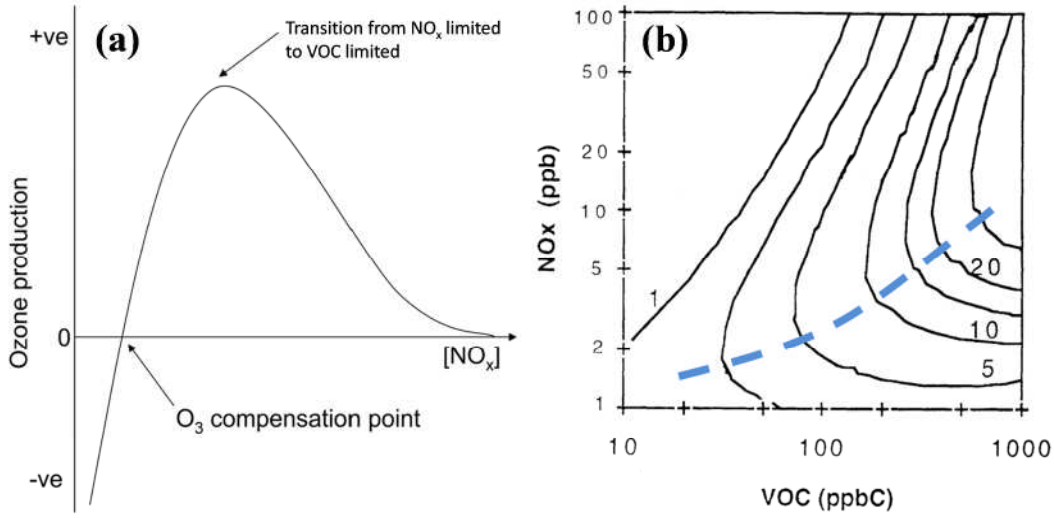

Figure 1.2: (a) Changes in ozone production over a range of [NO_x]. Adapted from Edwards (2011). (b) Example O_3 isopleth showing rates of production in ppb h^{-1} as a function of VOC (ppbC = ppb × carbon number) and NO_x (ppb). The transition from VOC limited to NO_x limited is represented by the dashed blue line. Adapted from Sillman (1999).

In order to devise effective O_3 mitigation strategies it is paramount that the O_3 production regime is fully understood in the environment in question. The O_3 production regime is not solely dictated by the emissions present at the source; it can change as emissions are transported. For example O_3 production could be VOC limited in an urban environment where there is a high loading of fresh vehicular emissions but as the air mass is transported further away and NO_x is depleted due to the formation of HNO_3 and organic nitrates the regime can transition to being NO_x limited.

There are multiple indirect approaches for determining O_3 production regime described in the literature where measured indicators are used to reflect cumulative processing of NO_x and VOC emissions. The ratio of the production rates of H_2O_2 to HNO_3 ($p(H_2O_2 + ROOH):p(HNO_3)$) is one such indicator. When the ratio is greater than 0.9, the O_3 production regime is typically NO_x limited, as the production of

peroxides constitute major radical loss. When the ratio is less than 0.1 the O_3 production regime is typically VOC limited, as the loss of radicals through formation of peroxides is insignificant and NO_2 is a dominant sink of OH (Sillman, 1999). Another indicator reported is the total concentration of reactive nitrogen (NO_y), a modelling study reported by Milford et al. (1994) showed that when NO_y is below a threshold in the range 10 – 25 ppb the O_3 production regime is predicted to be NO_x limited, whereas when NO_y is above a threshold in the range 20 – 30 ppb the O_3 production regime is predicted to be VOC limited. Tropospheric ozone and the concept of NO_x and VOC limiting environments bear particular importance to Chapter 6 of this thesis where measurements are presented from a campaign at a UK coastal site, a major aim of which was to measure the rate of O_3 production directly.

1.4 FAGE detection of OH

A large portion of the work presented in this thesis is focussed on the measurement of OH reactivity (defined in Section 1.5.1) using the laser flash photolysis coupled with laser induced fluorescence spectroscopy technique (LFP-LIF, described in Section 1.5.1). A key requirement of this technique is the sensitive and selective detection of OH using the fluorescence assay by gas expansion (FAGE) technique, the principles of which are described in this section.

Hard et al. (1979) pioneered the FAGE technique for the detection of OH; through the course of development several modifications have been necessary to overcome various chemical and spectral interferences (Heard and Pilling, 2003). In the FAGE technique, air is sampled through a pinhole into a low pressure (~2 Torr) cell where it expands and OH is detected by laser induced fluorescence (LIF) spectroscopy. The use of low pressure minimises interference from photolysis of ozone and consequent formation of OH (R 1.1 and R 1.2) through a reduction in the number density of H_2O vapour; interference from Rayleigh and Mie scattering is also reduced.

In early FAGE instruments 282 nm laser light was used for OH excitation, the wavelength of the induced fluorescence was longer than the scattered laser light meaning it could be easily discriminated. Smith and Crosley (1990), however, reported results from a modeling study which revealed the presence of a significant ozone interference with this excitation regime with the use of high energy low pulse repetition frequency (PRF) lasers. Following this the FAGE community adapted to

excite using 308 nm low energy high PRF lasers. The absorption cross section of ozone at 308 nm is ~9.8×10^{-19} cm^2 compared with ~2.8×10^{-18} cm^2 at 282 nm (Sander et al., 2003), thus after the change in excitation regime the ozone interference was no longer significant. An added benefit to the 308 nm excitation regime was an increase in sensitivity due to the absorption cross section of OH being ~6 times higher than at 282 nm (Heard and Pilling, 2003).

The gating of the fluorescence detector and function of the vacuum pump systems are crucial when exciting OH at 308 nm with a low energy higher PRF laser in FAGE. When OH is excited at 308 nm the resulting laser induced fluorescence is also at ~308 nm, a process known as on-resonance fluorescence. In such a system it is vital that the gating of the fluorescence detector is timed carefully in order to discriminate fluorescence against laser scatter. The efficiency of the pump system becomes very important with the use of high PRF lasers. It needs to remove air fast enough so that the excitation region within the FAGE cell is completely cleared between laser pulses in order to avoid cumulative ozone interference. For example if the laser PRF is 5 kHz the pump system should have the capability to clear the excitation region within 200 μs.

1.5 Measurement of OH reactivity

1.5.1 Definition and motivation for measurement

It is important that computer model simulations accurately predict OH levels because OH is the primary tropospheric oxidising agent. It is responsible for the removal of many trace species including greenhouse gases and compounds that pose health hazards such as CO and benzene (Heard and Pilling, 2003). Concentrations of ambient OH measured in the field are frequently compared with concentrations outputted from zero-dimensional box models that do not take transport of the air mass into account. This is a very good way to test our understanding of the atmospheric chemistry of OH at the time and place of field measurement. The zero-dimensional box model - measurement comparison approach is acceptable for OH as it is a very short lived intermediate, meaning that its concentration is exclusively determined by chemistry, not transport. In the recent review by Stone et al. (2012) there is extensive discussion of OH and HO_2 field measurement and model comparisons.

Direct measurement of OH reactivity can help us as an investigative tool in the search for the source of discrepancies between model simulations and measured OH levels. The measurement of OH reactivity is central to this thesis and observations from field measurements are presented in Chapters 5 and 6. Some results from an intercomparison study where different techniques were used to measure OH reactivity are also presented in Chapter 3. The present and following five sections detail the motivation, theory behind, methods used, and the instruments reported in the literature for total OH reactivity measurements.

As the lifetime of OH is very short, ranging from approximately 1s in the cleanest to approximately 1 ms in polluted environments (O'Brien and Hard, 1993), its concentration in ambient air can be assumed to be in the steady state (Ren et al., 2008). When in the steady state, it can be assumed that the sum of the rates of production, and the sum of the rates of loss of OH are equal, E 1.8. $[OH]$ is the steady state concentration of OH, $\sum_i P_{OH}^i$ is the total OH production rate and $\sum_j L_{OH}^j [OH]$is the total OH loss rate.

$$\frac{d[OH]}{dt} = \sum_i P_{OH}^i - \sum_j L_{OH}^j [OH] = 0 \qquad \textbf{E 1.1}$$

When OH is reacting under pseudo – first order conditions (concentrations of sinks higher than OH concentration to the extent that they can be assumed constant), total OH reactivity can be defined as the pseudo – first order rate coefficient for OH loss (k'_{OH}). By inspection of E 1.1, k'_{OH} is equal to $\sum_j L_{OH}^j$, which (if all chemical OH removal processes are assumed to be bimolecular) is equal to $\sum_j k_{OH+Zj}^j [Z_j]$, E 1.8. k_{OH+Zj}^j is the bimolecular rate coefficient for the reaction of OH and a compound responsible for its removal from the atmosphere (an OH sink). $[Z_j]$ is the concentration of such a sink.

$$k'_{OH} = \sum_j L_{OH}^j = \sum_j k_{OH+Zj}^j [Z_j] \qquad \textbf{E 1.2}$$

As discussed above it is important that the OH concentration is accurately predicted by models. If model OH predictions are greater than field measurement values, it is likely that there are compounds removing OH from the atmosphere that are not used to constrain model simulations. These are commonly known as ‘missing’ sinks which are not routinely measured during field campaigns. It is also worth noting,

however, that the OH concentration could be under predicted by a model simulation when there are still 'missing' sinks. This is often the case when there are 'missing' OH sources that outweigh the 'missing' sinks.

Approximately 10^4 - 10^5 organic species in the atmosphere have been identified, however the real number present could be much greater (Goldstein and Galbally, 2007). Lewis et al. (2000) reported the identification of over 500 organic species and suggested that many studies prior to theirs may have underestimated VOC levels, this highlights the difficulty in measuring a complete suite of VOCs. Clearly the measurement of every atmospheric species that could react with OH is not possible (Wood and Cohen, 2006). Direct measurement of k'_{OH} allows assessment of the extent to which 'missing' sinks are removing OH from the atmosphere.

Field measurements of total OH reactivity can be compared with calculated estimates ($k'_{OH(calc)}$). These estimates are calculated as the sum of the product of co-located concentration measurements of known OH sinks ($[A_j]$), and their respective bimolecular rate coefficients for reaction with OH (k^j_{OH+Aj}), E 1.8.

$$k'_{OH(calc)} = \sum_j k^j_{OH+Aj}[A_j] \qquad \textbf{E 1.3}$$

Zero-dimensional chemical box models can also be used to estimate total OH reactivity ($k'_{OH(mod)}$). These estimates are typically larger than those calculated with E 1.8 because they take unmeasured OH reactive products of photo-oxidation into account.

The difference between k'_{OH} and the reactivity calculated or modeled using co-located VOC concentration measurements is termed the 'missing' reactivity. Direct measurement of total OH reactivity allows us to test the hypothesis that unmeasured sinks are reacting with OH and are also the cause of model over prediction (Kovacs et al., 2003). Chapter 4 of this thesis details the development of new instrumentation to detect and identify species that contribute to 'missing' OH reactivity. In Chapters 5 and 6 field measurements of OH reactivity are presented and in Chapter 3 results from an inter-comparison of OH reactivity instrumentation are presented. There are three techniques with which it is possible to measure OH reactivity, these are described in the following five sections. A review of OH reactivity measurements in

the literature is presented in Section 1.5, the reader is also referred to a recent review by Yang et al. (2016) for details of published field measurements.

1.5.2 Total OH loss rate method (TOHLM)

Kovacs and Brune (2001) outlined the first experimental method for direct measurement of total OH reactivity. The method used here is referred to as the total OH loss rate method (TOHLM). In this method, ambient air is introduced to a reaction flow tube where there is an artificially high level of OH, achieved by use of a mercury lamp in a humidified nitrogen flow. The flow rate in the reaction tube is kept constant and thus it is possible for OH reaction time to be systematically altered through variation of the distance between the mercury lamp and the (LIF) detection cell inlet. Assuming pseudo first order conditions for the decay of OH (concentrations of compounds reacting with OH can be assumed constant as they are much higher), E 1.8 can be used to calculate $k'_{OH(raw)}$ (the OH decay observed before any correction scheme is applied). S_{OH} is the OH LIF signal at a set distance between lamp and detection inlet, S_{OH_0} is the OH LIF signal at the minimum distance, and t is the reaction time.

$$\ln\left(\frac{S_{OH}}{S_{OH_0}}\right) = -k'_{OH(raw)}t \qquad \textbf{E 1.4}$$

$k'_{OH(raw)}$ has to be adjusted to account for both wall loss of OH in the flow tube and the reaction between HO_2 and NO causing OH formation. E 1.5 is used for this adjustment.

$$k'_{OH} = k'_{OH(raw)} - k'_{OH(wall)} + k_{NO+HO_2}[NO]\frac{S_{HO_2}}{S_{OH}} \qquad \textbf{E 1.5}$$

Where $k'_{OH(wall)}$ is the rate constant for the loss of OH to the flow tube walls, k_{NO+HO_2} (8.8×10^{-12} cm^3 molecule^{-1} s^{-1} at 298 K) is the bimolecular rate constant for the reaction between NO and HO_2 (Atkinson et al., 2004), $[NO]$ is the concentration of NO and S_{HO_2} is the OH LIF signal that represents HO_2 (Ingham et al., 2009). The diagram in Figure 1.3 illustrates the key features of an instrument that used the flow tube with sliding injector technique for measurement of total OH reactivity.

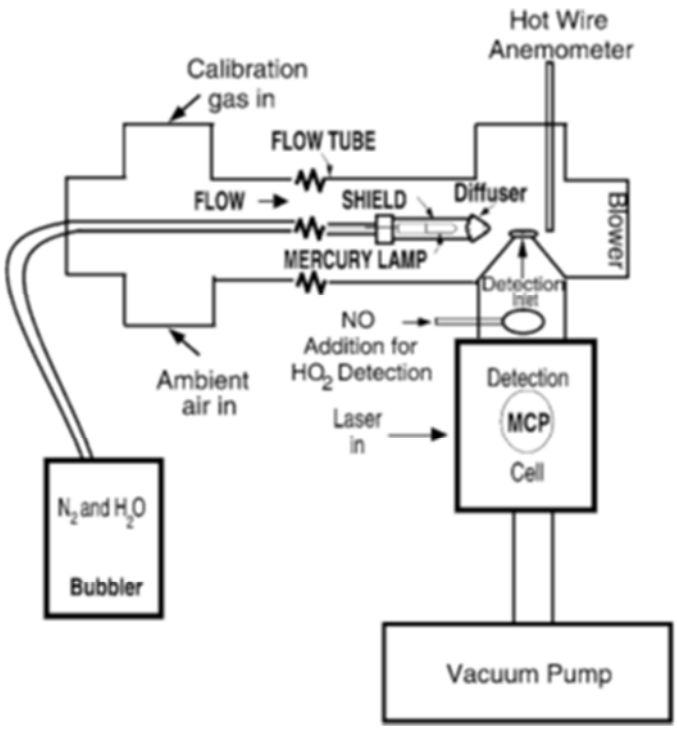

Figure 1.3: Diagram of the Total OH Loss Measurement (TOHLM) instrument used for the measurements of total OH reactivity. Taken from Kovacs and Brune (2001).

A flow tube with sliding injector technique but with a different detector also exists and was first reported by (McGrath, 2010); the method of detection used is chemical ionisation mass spectrometry (CIMS). This instrument was deployed during the OASIS campaign in Alaska to record the first total OH reactivity measurements in an arctic environment (McGrath et al., 2009), it was also deployed during the NIFTy campaign at a forested site (McGrath, 2010). A similar instrument is also reported to have been constructed by the German Weather Service (Heard, 2012). Full details of measurements using the flow tube with sliding injector - CIMS technique are not currently present in the literature.

1.5.3 Laser flash photolysis coupled with laser induced fluorescence spectroscopy (LFP-LIF)

The feasibility of a second laser induced fluorescence method for the measurement of total OH reactivity was demonstrated by Calpini et al. (1999) and Jeanneret et al. (2001). This method is termed as the laser flash photolysis coupled with laser induced fluorescence spectroscopy (LFP-LIF) technique and was first successfully implemented by Sadanaga et al. (2004b) for field measurements in urban Tokyo. A schematic of the instrument used is shown in Figure 1.4.

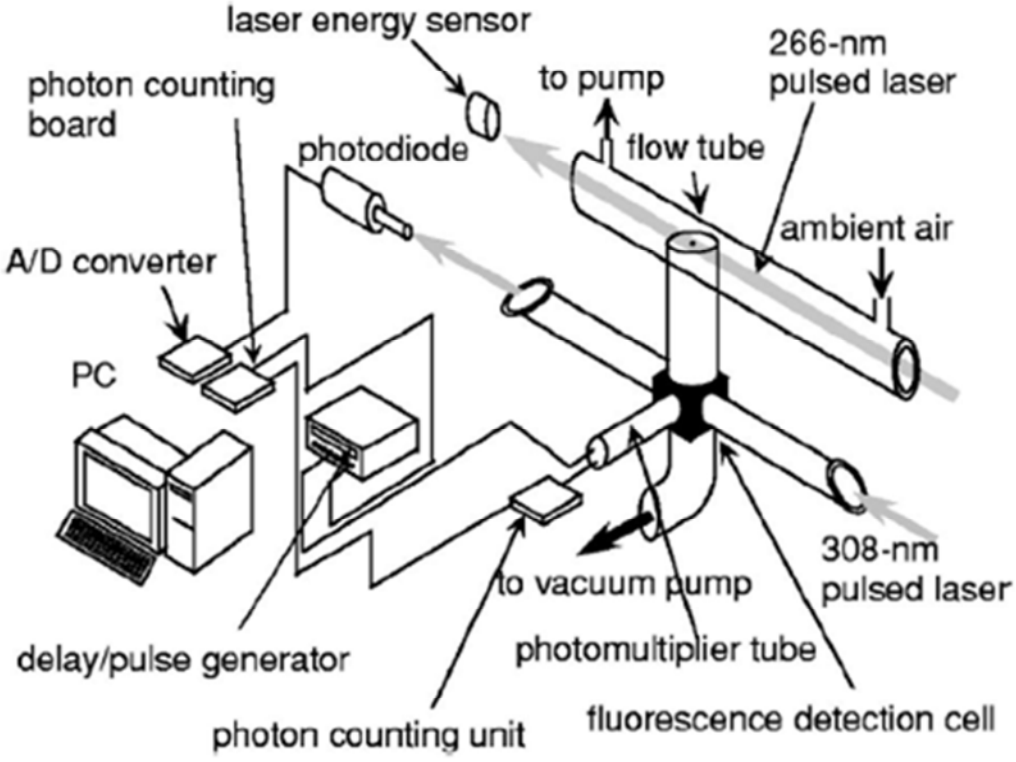

Figure 1.4: Schematic of the Tokyo Metropolitan University laser induced fluorescence pump and probe instrument. Taken from Sadanaga et al. (2004b).

OH is produced in a reaction flow tube by photolysis of O_3 using a 266 nm pump laser and subsequent reaction of $O(^1D)$ with water vapour present in ambient air (R 1.1 and R 1.2). The OH decay is then recorded in real time by FAGE (described in Section 1.4). Similar to the flow tube with sliding injector technique, this method relies on the assumption that the decay of OH is occurring under pseudo first order conditions. E 1.6 (essentially E 1.4 rearranged) can be used to represent the pseudo first order OH decay.

$$S_{OH} = S_{OH_0}\exp(-k'_{OH(raw)}t) \qquad \textbf{E 1.6}$$

When a single exponential curve is fitted to the observed OH decay signal, the expression of the fitted curve can be used to obtain a value for $k'_{OH(raw)}$. Similar to the flow tube with sliding injector technique, corrections have to be made to account for physical processes that affect the OH decay signal, such as escape of OH from the detection zone in the flow tube by diffusion and turbulence (Sadanaga et al., 2004b). To achieve this, the decay of OH in zero air ($k'_{OH(zero)}$) has to be recorded, E 1.8 is then used to calculate k'_{OH}.

$$k'_{OH} = k'_{OH(raw)} - k'_{OH(zero)} \quad \textbf{E 1.7}$$

Interference is also possible from the HO_2 + NO reaction at high NO (but only above ~20 ppbv); this scales with NO concentration and is much smaller than in the flow tube with sliding injector technique (where corrections need to be made above ~5 ppbv). Often in the literature ambient air samples have either been diluted prior to analysis to avoid this interference, or when NO was very high measurements have been omitted from further analysis due to the large uncertainty incurred (Yoshino et al., 2012). Lou et al. (2010) have reported that k'_{OH} can be estimated using a bi-exponential fit (to account for radical recycling) to within less than 10 % error at NO levels of up to 30 ppbv.

The LFP-LIF method was used for the measurements of OH reactivity presented in this work (Chapters 3, 5 and 6). Specific details of the instrument used can be found in Chapter 2 and also in a recent publication by Stone et al. (2016).

1.5.4 Comparative reactivity method (CRM)

Sinha et al. (2008) first reported the comparative reactivity method (CRM) for the measurement of total OH reactivity. Pyrrole (a compound that is not commonly found in ambient air) competes with trace species in ambient air to react with OH. E 1.8 is used to calculate $k'_{OH(raw)}$ where C_1 is the concentration of pyrrole detected when no OH is generated, C_2 is the concentration of pyrrole detected when OH is generated in the absence of ambient air, C_3 is the concentration of pyrrole detected when OH is generated in the presence of ambient air and k_{Py+OH} is the rate constant for the reaction between pyrrole and OH (1.03×10^{-10} cm^3 $molecule^{-1}$ s^{-1}), which is widely reported in literature (Wallington, 1986).

$$k'_{OH(raw)} = \frac{C_3 - C_2}{C_1 - C_3} k_{Py+OH} C_1 \quad \textbf{E 1.8}$$

Figure 1.5 shows a diagram of the glass reactor used in the majority of CRM studies of total OH reactivity. Pyrrole and ambient or zero air are introduced through arm A. Humidified Nitrogen is flowed through arm B where UV radiation from a Hg pen-ray lamp is used to produce OH. The exhaust is pumped out of arm C and arm D is used to transfer the analyte to the Proton Transfer Mass Spectrometer (PTR-MS) for the detection of pyrrole.

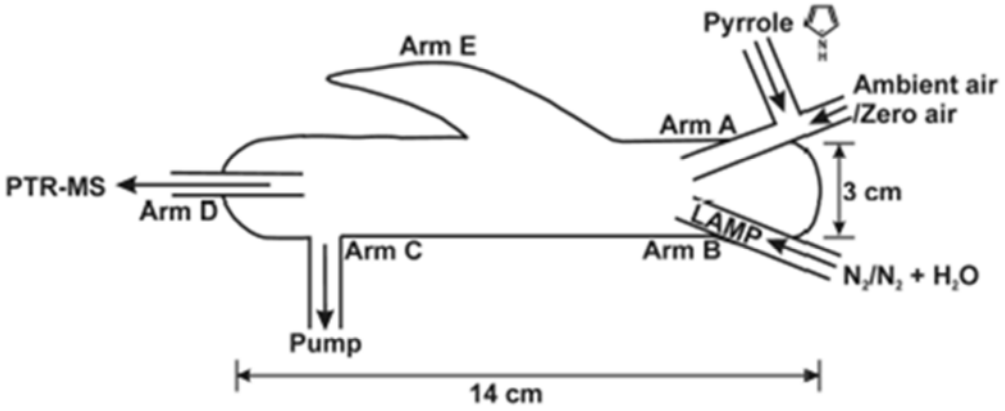

Figure 1.5: Schematic diagram of the glass reactor used in a comparative reactivity method (CRM) instrument for measurement of total OH reactivity. Taken from Sinha et al. (2008).

Total OH reactivity measurements made using the CRM also have to be adjusted to account for HO_2 + NO recycling. The adjustment is made by systematic addition of NO to the reactor and analysis of the absolute changes in OH reactivity. These changes are then plotted against NO concentration, and linear functions from linear best fits are used to correct $k'_{OH(raw)}$ values to k'_{OH} values. In contrast to the flow tube with sliding injector and laser flash photolysis methods, all CRM measurements are corrected, even at very low NO concentrations.

Nölscher et al. (2012a) have recently reported that a CRM instrument with a Gas Chromatograph - Photoionisation Detector (GC - PID) in place of a PTR-MS has potential as an economical instrument for total OH reactivity measurements. However, an instrument of this type has not yet been extensively used for field measurements.

1.5.5 Instrumentation in the literature

Flow tube with sliding injector, laser flash photolysis and comparative reactivity method instruments have all been used extensively for the measurement of total OH reactivity by various research groups worldwide. Table 1.1 provides a summary of the instruments currently in the literature that have been used for the measurement of total OH reactivity.

Technique	Group	$k'_{OH(physical)}$ (s^{-1})	Uncertainty (1σ)	Reference
TOHLM (LIF)*	Pennsylvania State University, USA	5.1 ± 0.6	± 14 %	Kovacs et al. (2003)
TOHLM (LIF) ‡	University of Leeds, UK	1.6 ± 0.4	± 10 %	Ingham et al. (2009)
TOHLM (LIF) †	Pennsylvania State University, USA	Not available	Not available	Mao et al. (2010)
TOHLM (LIF)	Indiana University, USA	3.6 ± 0.2	± (1.2 s^{-1} + 4 %)	Hansen et al. (2014)
TOHLM (CIMS)**	University of Colarado, USA	Not available	Not available	McGrath (2010)
TOHLM (CIMS)**	German Weather Service, Germany	Not available	Not available	Heard (2012)
LFP-LIF	Tokyo Metropolitan University, Japan	3.0 ± 0.15	± 10 %	Sadanaga et al. (2004b)
LFP-LIF	Jülich Forschungszentrum, Germany	1.4 ± 0.3	± 10 %	Lou et al. (2010)
LFP-LIF**	University of Lille, France	Not available	Not available	Amedro et al. (2012)
LFP-LIF	University of Leeds,UK	1.1± 1.0 s^{-1}	± 6 %	Stone et al. (2016)
CRM (PTRMS)	Max Planck Institute for Chemistry, Mainz, Germany	Not applicable	25 %	Sinha et al. (2008)
CRM (PTRMS)	University of Colarado, USA	Not applicable	30 %	Kim et al. (2011)
CRM (GC-PID)	Max Planck Institute for Chemistry, Mainz, Germany	Not applicable	25 %	Nölscher et al. (2012a)
CRM (PTRMS)	Mines Douai National Graduate School of Engineering, France	Not applicable	17-25%	Michoud et al. (2015)
CRM (PTRMS)	Laboratory of the Sciences of Climate and the Environment (LSCE), France	Not applicable	35 %	Zannoni et al. (2016)

Table 1.1: Instruments for the direct measurement of total OH reactivity that have been reported in the literature. * Total OH Loss rate Method (TOHLM) instrument, no longer in operation. ‡ Instrument no longer in operation. † A new TOHLM instrument was built at Pennsylvania State University. ** No published data available from field measurements. Values were correct at the time of publication. $k'_{OH(physical)}$ can be considered as the instrument artefact and is not applicable to CRM type instruments.

In addition to the instruments listed in Table 1.1, a new instrument for the measurement of total OH reactivity has been developed at the University of Leeds as a replacement for the old flow tube with sliding injector instrument described by Ingham et al. (2009). Full details of this new instrument are presented in this work.

1.5.6 Comparison of techniques

Laser flash photolysis pump and probe instruments present the only method for recording total OH reactivity in real time, thus they are ideally suited for measurements in places where trace species composition is highly variable, e.g. urban environments. This is due to their averaging times being considerably shorter

than for the TOHLM or CRM technique. They also produce zero HO_2 initially, whereas the flow tube with sliding injector and comparative reactivity method instruments do produce HO_2 initially, due to the use of an Hg(Ar) penray lamp (Lou et al., 2010) at 185 nm to photolyse water vapour to give OH and H. A result of this is that correction for interference from HO_2 + NO is only necessary at high NO (above approximately 20 ppbv). This is another reason why pump and probe instruments are suited to urban environments. In contrast, flow tube with sliding injector measurements require correction when NO is above approximately ~1 ppbv (Shirley et al., 2006) and comparative reactivity method measurements require corrections to be made when any NO is detected (Michoud et al., 2015). A disadvantage to the laser flash photolysis pump and probe technique is that the instrument requires two lasers which incurs additional cost and can be technically more demanding. As discussed in Section 1.4.4 a new comparative reactivity method instrument with a GC-PID detector is reported to have potential as a relatively low cost instrument for total OH reactivity measurement. Photolysis of pyrrole and VOCs within the OH reactors of comparative reactivity method instruments has also been reported to affect measurements of k'_{OH}, full details of the significance of this effect have recently been reported by Michoud et al. (2015).

1.6 Review of ground-based OH reactivity measurements

1.6.1 Forest atmospheres with low anthropogenic influence

Di Carlo et al. (2004) reported the first total OH reactivity measurements from a forested site at Great Lakes, MI, USA during the the program for research on oxidants: photochemistry, emissions and transport (PROPHET) campaign. Missing OH reactivity was observed to be exponentially dependant on temperature above 284 K, below 284 K the missing OH reactivity was less than 0.5 s^{-1}. It was found to be as high as ~4 s^{-1} at around 297 K. The authors concluded that this missing reactivity could have been caused by emissions of biogenic volatile organic compounds (BVOCs) such as terpenes which also display a temperature dependant emission. Figure 1.6 demonstrates the exponential dependence of missing reactivity on temperature.

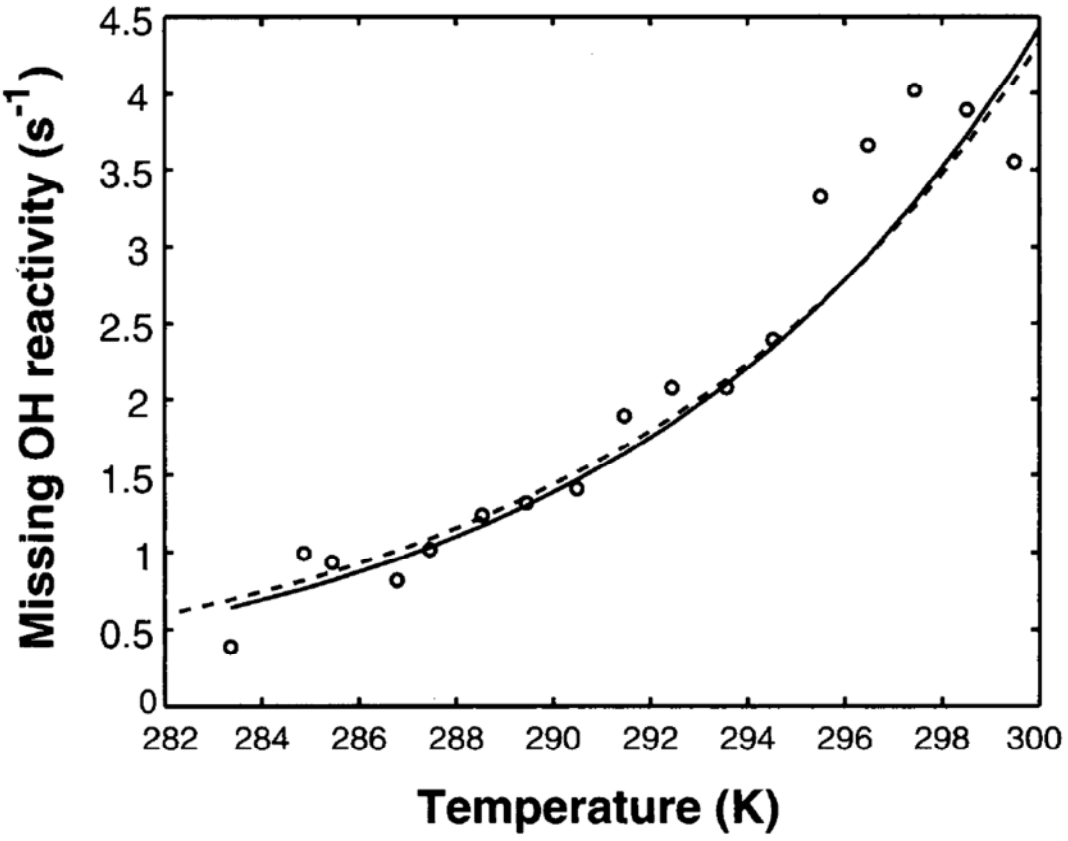

Figure 1.6: Missing OH reactivity observed by Di Carlo et al. (2004) at a forested site in Great Lakes, MI, USA. The solid line has been fitted to the data points shown; the dashed line is a derived temperature dependence of terpene emissions. Taken from Di Carlo et al. (2004).

Measurements of total OH reactivity have been reported from a forested site at Whiteface Mountain, NY, USA during the PMTACS-NY Whiteface Mountain campaign (Ren et al., 2006b). The measured and calculated reactivities were in good agreement and no relationship was found between the magnitude of the missing reactivity and temperature, in contrast to the temperature dependent missing reactivity reported from PROPHET. Figure 1.7 shows the campaign average relationship between k'_{OH} and $k'_{OH(calc)}$.

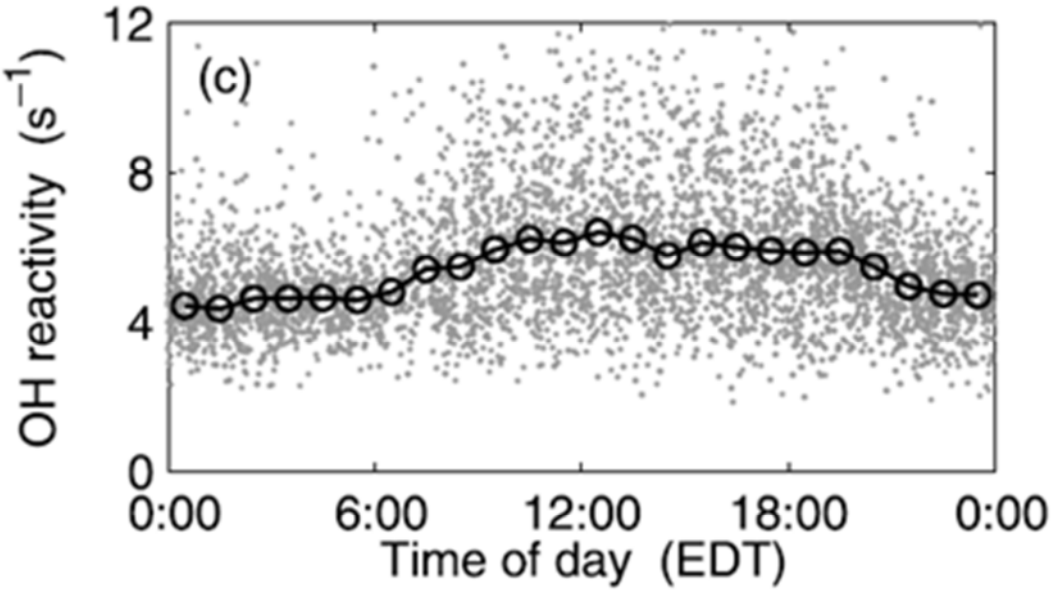

Figure 1.7: Plot showing all k'_{OH} values measured campaign (small dots) and the campaign average $k'_{OH\,(calc)}$ (large circles connected with a line) during the PMTACS-NY WFM campaign. Taken from Ren et al. (2006b).

Sinha et al. (2008) reported total OH reactivity measurements from a tropical rainforest site, however only 2 hours of data were obtained. The measurements were taken at the Brownsberg national park in Suriname and the average reactivity was approximately 53 s^{-1}. $k'_{OH(calc)}$ was determined using concentrations of OH reactive species that were measured prior to the two hours of reactivity measurements, the average missing reactivity was ~65 %.

Whalley et al. (2011) and Edwards et al. (2013) reported high total OH reactivity measurements from a rainforest during the OP3-I campaign in the Sabah Region of Malaysian Borneo. Diurnal behaviour was observed in the form of a peak around midday. The entire campaign diurnal average k'_{OH} was ~29 s^{-1}. Edwards et al. (2013) reported missing reactivity determined by comparison with a chemical box model, of approximately 53 %. When this box model was forced to include a greater contribution from photo-oxidation products by constraint to observed OH levels (which were also underestimated by the model by approximately 70 %), the missing reactivity decreased to ~38 %. This indicated that missing sources of OH as well as sinks contributed to the discrepancy of measured k'_{OH} and $k'_{OH\,(calc)}$.

Sinha et al. (2010) reported total OH reactivity measurements taken in 2008 from within the canopy of a Finnish boreal forest. The averaged OH reactivity observed

during the campaign was ~9 s^{-1}. Diurnal behaviour was not observed and the lowest reactivities were below the limit of detection (3.5 s^{-1}) whereas the largest were typically around 20 s^{-1}. Except during one episode of high pollution where values of up to 60 s^{-1} were reported, the authors concluded that this was due to biogenic emissions from a local saw mill, which had previously been reported as a strong source of VOCs (particularly monoterpenes) at the site (Eerdekens et al., 2009). On average, approximately 50% missing reactivity was observed during this campaign and it was concluded that its cause was many unmeasured primary BVOCs at low levels, not products of photo-oxidation. This is because the measurements were taken from within the canopy so it is unlikely that there were high concentrations of unmeasured oxidation products. Also contributions to calculated OH reactivity from measured primary emissions were higher than their measured oxidation products.

Hansen et al. (2013) reported total OH reactivity measurements from the community atmosphere-biosphere interaction experiment (CABINEX) campaign that took place during the summer at the same site in Great Lakes MI, USA as the PROPHET 2000 campaign (Di Carlo et al., 2004). The flow tube with sliding injector technique was used to take measurements at 21 m and 31 m above, and 6 m below the deciduous forest canopy. The missing reactivities were found to be ~42 % and ~43 % above the canopy (21 m and 31 m, respectively). Measurements of total OH reactivity within the canopy were found to be in good agreement with the calculated reactivities. Missing reactivity above the canopy was observed to have a similar exponential dependence on temperature to that observed by (Di Carlo et al., 2004). However, the authors concluded that during CABINEX 2009 missing reactivity was most likely due to unmeasured BVOC oxidation products, rather than BVOCs.

The comparative reactivity method was used by Nölscher et al. (2012b) to measure both in canopy and above canopy total OH reactivities from a boreal forest site in Finland during the HUMPPA-COPEC 2010 campaign. Values varied throughout the course of the campaign and reactivity was typically higher inside the canopy for the majority. However, reactivity was found to be higher above the canopy when plumes from Russian wildfires were transported to the site. Missing reactivity was only assessed for above canopy measurements and was found to be ~68 % on average for the whole campaign. Table 1.2 provides a summary of all total OH reactivity field measurements at forested sites with low anthropogenic influence in the literature.

Campaign	Dates	Technique	Location	Average $k'_{OH(missing)}$ (s^{-1})	Reference
PROPHET	Jul – Aug, 2000	TOHLM (LIF)	Great Lakes, MI, USA	~50 % * (~10 m above canopy)	Di Carlo et al. (2004)
PMTACS-NY-WFM	Jul – Aug, 2002	TOHLM (LIF)	Whiteface Mountain, NY, USA	Small *† (within canopy, on ground)	Ren et al. (2006b)
GABRIEL	Oct, 2005	CRM (PTRMS)	Brownsberg, Brokopondo, Suriname	~65 % *(within canopy, ~35 m above ground)	Sinha et al. (2008)
OP3-I	Apr – May, 2008	TOHLM (LIF)	Sabah, Borneo, Malaysia	~53 % ** (within canopy, ~5m above ground)	Edwards et al. (2013)
BFORM	Aug, 2008	CRM (PTRMS)	Hytiälä, Juupajoki, Finland	~50 % * (within canopy, ~12 m above ground)	Sinha et al. (2010)
CABINEX	Jul – Aug 2009	TOHLM (LIF)	Great Lakes, MI, USA	~42 %* (~21 m above canopy)	Hansen et al. (2014)
				~43 %* (~31 m above canopy)	
				Small*† (~6 m below canopy)	
HUMPPA-COPEC	Jul – Aug 2010	CRM (PTRMS)	Hytiälä, Juupajoki, Finland	~68 % * (~24 m above canopy)	Nölscher et al. (2012b)

Table 1.2: Summary of total OH reactivity field measurements taken at forested sites with low anthropogenic influence. *Average missing reactivity determined by comparison with $\boldsymbol{k'_{OH(calc)}}$, determined using just measured sinks. **Average missing reactivity determined by comparison with $\boldsymbol{k'_{OH(mod)}}$ determined considering model generated intermediates. †Average missing reactivity could not be determined due to a lack of numerical values in the literature.

A total of seven field measurements of total OH reactivity have been reported for forested sites. In the majority of which, significant levels of missing reactivity have been observed. Four measurements have been made using the flow tube with sliding injector technique and another three with the comparative reactivity method.

Perhaps one of the most striking studies is that of Di Carlo et al. (2004), where the missing reactivity in a mixed transition forest site during the PROPHET 2000 campaign was found to be exponentially dependent upon temperature when measured using the flow tube with sliding injector technique. Missing reactivity ranged from 0.5-3.7 s^{-1} as temperature increased from 284 K to 299 K and was concluded to be due to unmeasured BVOC emissions which were also expected to be temperature dependent. Most recently (Hansen et al., 2013) have reported total OH reactivity measurements from the same site using the same method and observed a similar temperature dependence during the CABINEX 2009 campaign. However, in this case it was found to be inconsistent with predictions for the

temperature dependence of BVOC emissions; this led to the conclusion that unmeasured photo oxidation products contributed the most to missing reactivity.

No such temperature dependency has been described at sites other than the one used for PROPHET 2000 and CABINEX 2009, however during HUMPPA-COPEC 2010 the greatest missing reactivity was recorded after a period of elevated temperature. Also in other campaigns such as OP3-I in Borneo the temperature did not fluctuate significantly throughout the course of measurement meaning that any temperature dependency could not have been properly assessed (Edwards et al., 2013).

In contrast to OH reactivities reported from other forested sites, no significant missing reactivity was observed during the PMTACS-NY-WFM campaign in 2002 (Ren et al., 2006b). The small amount of missing reactivity reported was not found to be temperature dependant, the daytime campaign average temperature was 291 K (a temperature at which significant missing reactivity would not have been observed at the PROPHET 2000 site). This and the observation that isoprene only accounted for small portion of calculated OH reactivity (as opposed to PROPHET 2000 where it accounted for a much larger portion), led to the conclusion that the small and high missing reactivities at Whiteface Mountain and the PROPHET site, respectively were due to differences in BVOC emissions.

Two measurements of total OH reactivity have been reported for tropical rainforests. Sinha et al. (2008) reported measurements from project GABRIEL (2005). Only a small quantity (~2 hours) of data were collected due to a lack of availability of the PTR-MS instrument that was also being used for hydrocarbon measurements. However, the average missing reactivity that could be determined was ~65 % (Edwards, 2011). A much more extensive survey of OH reactivity in a tropical rainforest has since been reported by Whalley et al. (2011) and (Edwards et al., 2013) for the OP3-I campaign in Malaysian Borneo. The average missing reactivity for the entire campaign was also high and box modeling indicated that missing OH sources influenced the discrepancy between measured k'_{OH} and $k'_{OH(calc).}$

Two sets of measurements (both from summer) have been reported from the same site in a boreal forest (Hyytiälä, Juupajoki, Finland). Sinha et al. (2010) found there to be approximately 50 % average missing reactivity from in-canopy measurements. More recently a much more extensive set of total OH reactivity measurements (above-canopy and in-canopy) have been reported by Nölscher et al. (2012b).

Missing reactivity was only assessed for above-canopy measurements due to availability of hydrocarbon data and averaged ~68 % for the entire campaign. Similar to PROPHET 2000, HUMPPA-COPEC 2010 and CABINEX 2009, large missing reactivity was associated with high temperatures; missing reactivity was ~89 % during a hot period at the start of the campaign. This led to the conclusion that unmeasured BVOCs significantly contributed to missing reactivity as Yassaa et al. (2012) reported that high temperatures were accompanied by BVOC emission diversification at this site.

In summary, there are large gaps in our knowledge of the OH chemistry in forested environments where total OH reactivity has been directly measured. Further field measurements from a variety of forest biomes in conjunction with leaf enclosure studies are required to assess the global misunderstanding.

1.6.2 Urban atmospheres

The first field measurement of total OH reactivity was at an urban site and was reported in 2001, a full analysis of the results was published in 2003 (Kovacs and Brune, 2001, Kovacs et al., 2003). The measurements were taken at an urban background site in Nashville, TN, USA during the summer of 1999. The measured reactivity was considerably larger than that initially calculated from co-located VOC concentration measurements (~30 %). The authors concluded that the cause for this missing reactivity was VOCs that were either not included in the suite of ambient concentration measurements, or that some of the OH reactive compounds present were below the limit of detection. Anthropogenic VOC emissions from a nearby tunnel were scaled down proportionally using the CO concentration. The scaled down concentrations of species that were below the limit of detection at the measurement site were then included in the calculation of total OH reactivity. This led to a reduction in the average missing reactivity so that it was ~10 %.

Di Carlo et al. (2004) have reported total OH reactivity measurements from an urban background site at LaPorte, TX, USA. The measurements were taken at an airport where the air mass was influenced by anthropogenic emissions from Houston, petrochemical plants and a nearby shipping canal. The magnitude of the average missing reactivity was small (~4 %) and no temperature dependence was observed.

Summer measurements from an urban background site in New York City, NY, USA have also been reported (Ren et al., 2003b, Ren et al., 2003c). The total OH

reactivity was about twice that observed in Nashville and the 'missing' OH reactivity was ~10 %.

OH reactivity measurements were taken in 2003 at a site located in the Mexico City Metropolitan Area (MCMA) (Shirley et al., 2006). Strong diurnal behaviour was observed, reactivity was found to be extremely high (approximately 120 s^{-1}) during the morning rush hour, about five times higher than the peak observed in PMTACS-NY 2001. 72 % of the measured OH reactivity was attributable to VOCs and the diurnal profile of NO_x was similar to that for OH reactivity, and suggests that vehicular emissions were a driver in the daily changes observed in OH reactivity. The average missing reactivity for the whole campaign was approximately 30 %.

Sadanaga et al. (2004b) reported the first field measurements of total OH reactivity using the laser induced fluorescence pump and probe technique from a site in urban Tokyo during the summer. Following this a more in detailed report of these measurements has been given by Sadanaga et al. (2005). Yoshino et al. (2006) have since reported winter, spring and autumn measurements from the same site. Measured OH reactivity ranged from 10 to 100 s^{-1}during observations for all four seasons. During summer measurements OH reactivity was found to correlate well with NO_x levels. During winter, spring and autumn NO_x was generally high and OH reactivity was found to correlate well with NO levels. Significant missing reactivity (~30%) between calculated values and observed values was observed in summer, spring and autumn. On the other hand the missing reactivity was much lower (~5%) in winter, indicating that missing OH sinks in urban Tokyo are related to photochemical activities.

In 2004, OH reactivity measurements were taken during winter at the same site as PMTACS-NY 2001 (a summer campaign) (Ren et al., 2006a). Diurnal behaviour was present in the form of two peaks in reactivity. These peaks were seen in the morning and afternoon and were likely due to increased vehicular emissions at these times. There was overall good agreement between calculated and measured reactivities, however there was clearly 'missing' OH reactivity during the rush hour as demonstrated by the plots in Figure 1.8.

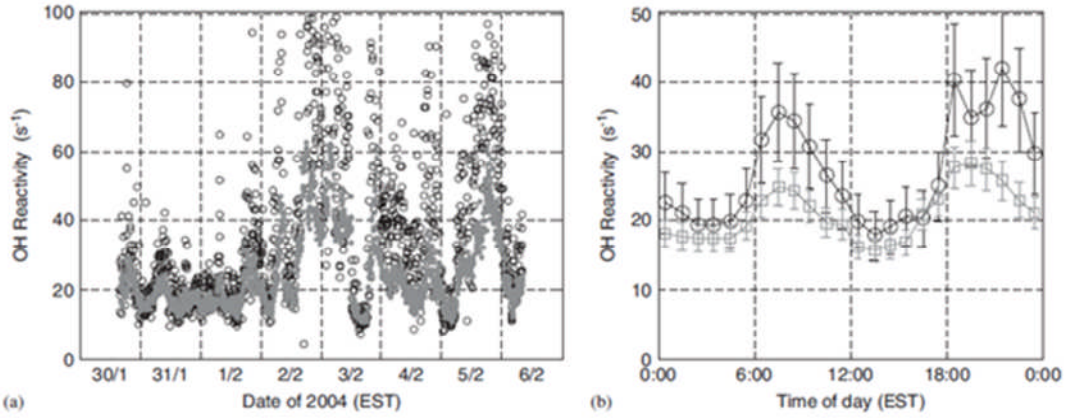

Figure 1.8: (a) Plot showing the relationship between measured (circles) and calculated (grey dots) total OH reactivities from a field campaign during the winter in New York City, 2004. (b) Plot showing the campaign average diurnal profiles of measured (circles) and calculated (squares) total OH reactivities. Taken from Ren et al. (2006a).

Sinha et al. (2008) reported total OH reactivity measurements from an urban site in Mainz, Germany during the summer, the average value was ~10.4 s^{-1}. A diurnal peak in reactivity was also observed during the afternoon. Missing reactivity could not be assessed as no co-located VOC concentration measurements were taken so no comparison between calculated and observed reactivity could be made.

Mao et al. (2010) reported total OH reactivity measurements from an urban background site near Houston, TX, USA during the TRAMP 2006 campaign. A diurnal peak was observed due to the morning rush hour and on average the agreement between measured and calculated reactivities was very good, as demonstrated by Figure 1.9.

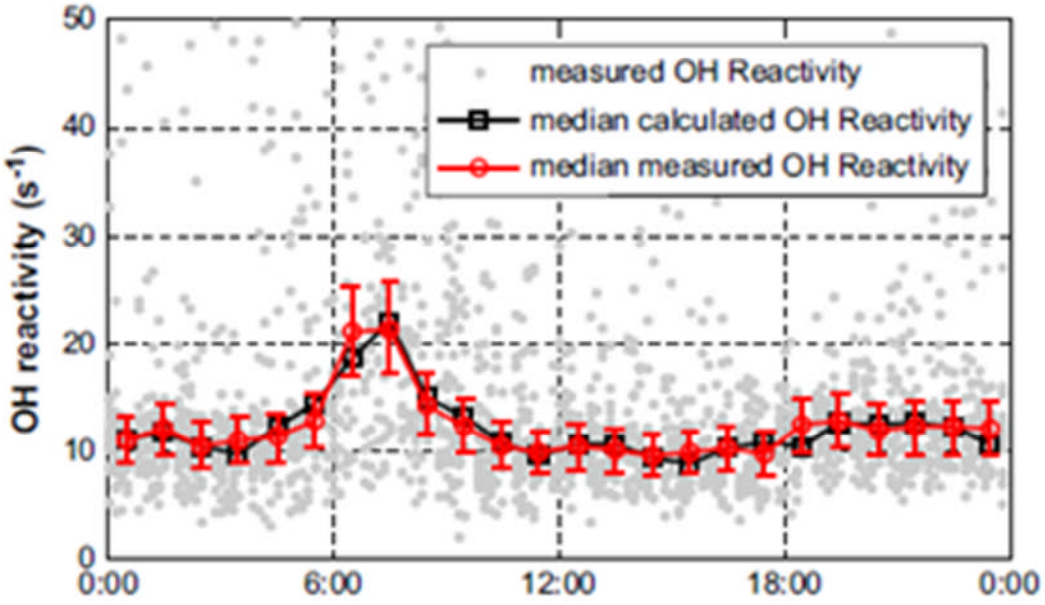

Figure 1.9: Plot showing the relationship between the diurnal average measured (red circles) and calculated (black squares) observed during the TRAMP 2006 campaign. Taken from Mao et al. (2010).

Chatani et al. (2009) first reported total OH reactivities from the centre of the metropolitan area of Tokyo in the summer of 2007. More recently Yoshino et al. (2012) have reported measurements from the same site for the winter of 2007 and the autumn of 2009. The missing reactivity observed in all three data sets was similar to that reported from Hachioji (Sadanaga et al., 2004a, Sadanaga et al., 2005, Yoshino et al., 2006). The total OH reactivity in the summer 2007 measurements ranged from 15 to 70 s^{-1}. Model predictions reported by Chatani et al. (2009) indicated that products of photo-oxidation and primary species were responsible for missing reactivity (~26.5% average). The total OH reactivity in the winter 2007 measurements ranged from 10 to 80 s^{-1}. The winter 2007 data were excluded from missing reactivity analysis due to high morning rush NO levels (no diurnal average for morning rush available, however average daytime NO was 37.4 ppbv) causing OH recycling (from HO_2 + NO) and consequently large uncertainties. Total OH reactivity in the autumn 2009 measurements also ranged from 10 to 80 s^{-1} and significant missing reactivity was observed (~34.7% on average).

The first total OH reactivity measurements for a European megacity were taken in Paris during the 2010 MEGAPOLI campaign reported by Dolgorouky et al. (2012). Reactivity had a strong dependence on the origin of the air mass present. When

polluted continental air masses were present at the site, average measured reactivities were approximately 120-130 s^{-1} and the missing reactivity was the highest ever registered in an urban area (approximately 74 %). However, when cleaner marine influenced air masses reached the site the OH reactivity was approximately 20 s^{-1} and the average missing reactivity was low (approximately 12 %). The authors concluded that oxidised compounds from photo chemically processed anthropogenic emissions were the cause of such high missing reactivity.

A recent study by Brune et al. (2016) presented observations of OH reactivity that were made during the California Nexus (CalNex) campaign at an urban background site south of Bakersfield , CA, US. The measurements were made in a car park in close proximity (<1 km) to a major road and a few hundred metres from agricultural land. A diurnal trend in OH reactivity (ranging from ~10 – 25 s^{-1}) was observed that showed evidence of influence from morning rush hour traffic emissions. The 'missing' OH reactivity determined through comparison of the measurements with model predictions was ~41 % on average. The site used for OH reactivity measurements during CalNex shared similarities with the site used for OH reactivity measurements in York that are presented in Chapter 5 of this thesis. Both were on the edge of a large city, near agricultural land and main roads.

One of the studies most relevant to the work presented in this thesis is that reported by Whalley et al. (2016) where measurements of OH reactivity made in urban London are presented from the clean air for London (ClearFlo) campaign. The measurements were made using the same LFP-LIF instrument that is described in Chapter 2 of this thesis and was used to make the measurements of OH reactivity that are presented in Chapters 5 and 6. The results showed a strong diurnal peak (~27 s^{-1}) in the mornings due to rush hour traffic emissions. When concentrations of all of the measured OH sinks were used in a model simulation, the predicted OH reactivity was typically ~15 % lower than the measured OH reactivity. Further discussion of the observations from ClearFlo are discussed in the context of the results from this work in Chapters 5 and 6. A summary of OH reactivity measurements in the literature is presented in Table 1.3.

Campaign	Dates	Technique	Location	Average $k'_{OH(missing)}$ (s^{-1})	Reference
SOS	Jun – Jul, 1999	TOHLM (LIF)	Nashville, TN, USA	~10 % *	Kovacs et al. (2003)
TexAQS	Aug – Sep, 2000	TOHLM (LIF)	La Porte, TX, USA	~4 % *	Di Carlo et al. (2004)
PMTACS-NY	Jun – Aug, 2001	TOHLM (LIF)	New York City, NY, USA	~10 % *	Ren et al. (2003b)
MCMA	Apr, 2003	TOHLM (LIF)	Iztapalapa, Mexico City, Mexico	~30 % *	Shirley et al. (2006)
-	Jul and Aug, 2003 Jan, Feb ,May and Nov, 2004	LFP-LIF	Hachioji, Tokyo, Japan	~30 % (summer, spring and autumn) ~5 % (winter)	Yoshino et al. (2006)
-	Jan – Feb, 2004	TOHLM (LIF)	New York City, NY, USA	Small * †	Ren et al. (2006a)
-	Aug, 2005	CRM (PTRMS)	Mainz, Rhineland-Palatinate, Germany	***	Sinha et al. (2008)
TRAMP	Aug – Sep, 2006	TOHLM (LIF)	Houston, TX, USA	Small *	Mao et al. (2010)
-	Aug and Dec, 2007 Oct, 2009	LFP-LIF	Koto-Ku, Tokyo, Japan	~27 % (summer) ~35% (autumn)	Yoshino et al. (2012)
MEGAPOLI	Jan – Feb 2010	CRM (PTRMS)	13th District, Paris, France	~54 % *	Dolgorouky et al. (2012)
CalNex	May-Jun 2010	TOHLM (LIF)	Bakersfield, CA, US	~41 %**	Brune et al. (2016)
ClearFlo	Jul- Aug 2012	LFP-LIF	North Kensington, London, UK	~15 %**	(Whalley et al., 2016)

Table 1.3: Summary of total OH reactivity field measurements taken at urban sites with low anthropogenic influence. Data from field measurements at Hachioji are also available in other publications (Sadanaga et al., 2005, Sadanaga et al., 2004b, Sadanaga et al., 2004a). Data from field measurements at Koto-Ku are also available in Chatani et al. (2009). *Average missing reactivity determined by comparison with $\boldsymbol{k'_{OH(calc)}}$. **Average missing reactivity determined by comparison with $\boldsymbol{k'_{OH(mod)}}$. ***Missing reactivity was not assessed due to there being no co-located VOC concentration measurements. †Average missing reactivity could not be determined due to a lack of numerical values in the literature.

OH reactivity measurements from urban and urban background sites are more widely reported in literature than measurements for forested environments. Measurements taken using all three techniques have been reported and in general missing reactivity is lower than it is at forested sites.

Measurements from New York and Tokyo urban background sites, and a central Tokyo site have been reported for both summer and winter (Ren et al., 2003b, Yoshino et al., 2006, Yoshino et al., 2012). At the background sites the average missing reactivity was found to be lower in winter than summer (~30 % compared with ~5 % for the Tokyo background site); thus indicating that photo-oxidation products of primary emissions account for a large portion of missing urban reactivity. This is because concentrations of primary emissions are typically higher in winter than summer due to lower actinic flux and a compressed boundary layer. The missing reactivity at the central Tokyo site in winter could not be fully assessed; this was due to very high NO_x (NO: 37.4 ppbv, NO_2: 35.8 ppbv) levels leading to large experimental uncertainty from HO_2 + NO recycling.

Missing urban reactivity is often lower when large portions of $k'_{OH(calc)}$ or $k'_{OH(mod)}$ are accounted for by known OH reactive pollutants such as NO_x and CO. The missing reactivities reported from PMTACS-NY-2001 and MCMA (~10 % and ~30 %, respectively) demonstrate this. On average in PMTACS-NY-2001 NO_x and CO accounted for 42 % and 12 % of the campaign average $k'_{OH(calc)}$, respectively, whereas in MCMA NO_x and CO accounted for 12 % and 7 % of the campaign average $k'_{OH(calc)}$, respectively.

In summary, the percentage of 'missing' OH reactivity at urban background and central urban sites is typically smaller than for forested sites, however there are still gaps in our knowledge. Where missing reactivity has been observed, a common conclusion is that it was a result of unmeasured concentrations of primary emissions and their photo-oxidation products not being included in the calculation of $k'_{OH(calc)}$ or $k'_{OH(mod)}$. Measurements of OH reactivity from an urban background site in York are presented in Chapter 5 of this thesis.

1.6.3 Rural and other atmospheres

In 2005 OH reactivity measurements from a rural site in an Appalachian valley in Rock Springs, PA, USA were reported (Ren et al., 2005). The site was surrounded by agricultural fields, near to a road and close enough to some large cities to be influenced by anthropogenic emissions (Ren et al., 2003a). No co-located VOC concentration data were available so missing reactivity could not be assessed. When

a computer model was constrained using measured total OH reactivity, OH and HO_2 mixing ratio predictions were in good agreement with field measurements.

Total OH reactivity measurements from 2004 at a coastal site in Weybourne, Norfolk, UK were reported by Lee et al. (2009). The average measured OH reactivity was ~4.9 s^{-1} with minimum and maximum values of ~1.3 and ~9.7 s^{-1}, respectively. No diurnal behaviour was observed owing to the variety of air masses that reached the site; UK/South Westerly Air and Northerly Air. These acted upon the site at irregular intervals and OH reactivity was found to be variable during episodes of UK/South Westerly air but less so with Northerly air. Also, it was typically higher during episodes of UK/South Westerly air than Northerly air. Missing reactivity was first calculated using co-located VOC concentration measurements and was found on average to be 1.9 s^{-1} (~40%). Secondly, the Master Chemical Mechanism (MCM) (Jenkin et al., 1997, Saunders et al., 2003) was used to model missing reactivity and on average this was found to be 1.4 s^{-1} (~30%). Whilst there was better agreement between measured and modeled reactivity, missing reactivity is still significant, even in episodes of clean air. The authors concluded that the missing reactivity was likely to be due to many high molecular mass VOCs at low concentrations which were not included in the suite of VOC measurements. In Chapter 6 of this thesis measurements of OH reactivity from the same site in Weybourne are presented and comparisons are made with the OH reactivity calculated using the concentrations of measured OH sinks.

In 2006 total OH reactivity measurements were reported from a regional background site in the Pearl River Delta (PRD), China (Lou et al., 2010). The measured total OH reactivities ranged from 10 to 120 s^{-1}. Diurnal behaviour was observed and correlated well with anthropogenic pollutant levels such as CO, NO_2 and propene. Total OH reactivity was calculated from co-located VOC concentration measurements and on average missing reactivity was ~50 %. In an attempt to account for some of the missing reactivity, the Regional Atmospheric Chemistry Model (RACM) was used to predict total OH reactivity by taking into account the reactions with OH of photo-oxidation products of the measured VOCs. Three models were used to predict OH reactivity. The first and most basic model used only data from the co-located VOC measurements and rate constants. The second took into account additional recycling of OH. The third was constrained using OH concentrations measured during the field campaign. Similar to the calculated OH

reactivities, the correlation between model prediction and observed OH reactivity was good. Missing reactivity was reduced to approximately 10 % using the basic RACM model predictions for daytime measurements, however it was still found to be significant (approximately 30 %) for night time measurements.

Sinha et al. (2012) reported winter total OH reactivity measurements taken in 2008 from southern Spain at a site near the Atlantic Ocean, the campaign average reactivity was 18 s^{-1}. Total OH reactivity was found to be very dependent on the origin of the air mass present. Assessment of the missing reactivity at this site was not possible due to an absence of certain key VOC measurements. Table 1.4 provides a summary of all total OH reactivity field measurements that have been taken at sites, that are not forested or urban, but do have significant anthropogenic influence.

Campaign	Dates	Technique	Location	Average $k'_{OH(missing)}$ (s^{-1})	Reference
-	May – Jun, 2002	TOHLM (LIF)	Rock Springs, PA,USA	***	Ren et al. (2005)
TORCH-2	May, 2004	TOHLM (LIF)	Weybourne, Norfolk, UK	~40 % * ~30 % **	Lee et al. (2009)
PRIDE-PRD	Jul, 2006	LFP-LIF	Guangzhou, Guandong, China	~50 % * Small **†	Lou et al. (2010)
DOMINO	Nov – Dec, 2008	CRM (PTRMS)	El Arenosillo, Magazón, Spain	***	Sinha et al. (2012)

Table 1.4: Summary of total OH reactivity field measurements taken at rural or urban sites. *Average missing reactivity determined by comparison with $\boldsymbol{k'_{OH(calc)}}$. **Average missing reactivity determined by comparison with $\boldsymbol{k'_{OH(mod)}}$. ***Missing reactivity was not assessed due to there being no co-located VOC concentration measurements. †Average missing reactivity could not be determined due to a lack of raw data in the literature.

Total OH reactivity measurements have also been reported from several rural and coastal sites where the air mass is periodically influenced by anthropogenic emissions. Only for two of these campaigns could the missing reactivity be assessed. Missing reactivities were reported from comparisons with calculated and modeled reactivities, for both campaigns the missing reactivity was smaller when modeled values were used.

Missing reactivity was assessed during both the TORCH-2 campaign and the PRIDE-PRD campaign. When determined by comparison of measured reactivities with those calculated from co-located VOC concentration measurements the average missing reactivities for TORCH-2 and PRIDE-PRD were approximately 40 % and

50 % respectively. When the MCM model was used to predict OH reactivity at the TORCH-2 site the missing reactivity was reduced to approximately 30 % indicating that unmeasured VOCs contributed significantly to OH reactivity as well as unmeasured photo oxidation products. When the RACM model was used to predict OH reactivity at the PRIDE-PRD site, the predicted reactivity was reduced so that it was in good agreement with measured values, thus indicating that photo-oxidation products of primary emissions were significant contributors to OH reactivity.

1.7 Limitations of OH reactivity measurements

In the majority of OH reactivity field measurements that have been made in a range of atmospheres, 'missing' OH reactivity has been reported. A common conclusion is that this is due to species reacting with OH that were not measured by co-located OH sink concentration measurements, and so were not considered when making a prediction of OH reactivity using a calculation or computer model. The origin and identity of these compounds is open to speculation and no rigorous method for their quantification and identification is described in the literature. Kato et al. (2011) reported a method to estimate the contribution from detectable, however unidentifiable, VOCs to 'missing' OH reactivity. A relative rate analysis of gas chromatograph flame ionisation detector (GC-FID) peaks was used to determine biomolecular rate coefficients for the reactions between such species and OH. This study is described in detail in Chapter 4 of this thesis where the development of new instrumentation for the identification of species contributing to 'missing' OH reactivity is also described.

1.8 Formaldehyde in the troposphere

Section 1.2 details the chemistry of the photo-oxidation of VOCs in the troposphere, via the HO_x cycle, which is driven through a catalytic conversion between OH and HO_2, and NO and NO_2. Whilst HCHO plays a key role in the HO_x cycle as a photolytic source of HO_2 (R 1.11), it is also a dominant byproduct of VOC photo-oxidation (Lee et al., 1998). Consequently HCHO is often viewed as a trace species for overall VOC oxidation (DiGangi et al., 2011). It can be measured from space using satellites, and observations provide a proxy for mapping emissions of VOCs that would be more challenging to measure themselves (Palmer et al., 2001, Chance

et al., 2000). For example Isoprene emissions can be mapped in this way (Palmer et al., 2003).

HCHO is a useful target species in atmospheric modelling studies to assess the accuracy of oxidation schemes. Whalley et al. (2016) reported better accuracy of HCHO predictions by a zero-dimensional chemical box model to be concurrent with better agreement between measured and modelled OH reactivity in the urban atmosphere of London. In addition to production from photo-oxidation of VOCs, HCHO is also a primary pollutant emitted directly from a number of sources such as incomplete combustion of fossil fuels and has also been shown to be a direct biogenic and soil emission (Anderson et al., 1996, Kaiser et al., 2015).

Whilst the importance of HCHO as a trace species in the atmosphere, and the usefulness of its measurement is highlighted above, the chemistry of HCHO in indoor atmospheres is also important. HCHO is the most common and best known indoor pollutant (Salthammer et al., 2010). There are a number of direct indoor HCHO sources ranging from combustion of tobacco, to emissions from building materials or consumer products (IARC, 2006, Kelly et al., 1999). There are also a complex range of secondary indoor HCHO sources such as the ozonolysis of terpenes (Nazaroff and Weschler, 2004, Uhde and Salthammer, 2007). However, the contribution from secondary HCHO to indoor atmospheres is not fully understood and is an active field of research.

Understanding the outdoor and indoor atmospheric chemistry of HCHO is crucial in managing air quality as high levels are known to cause adverse health effects in humans, HCHO is a known carcinogen and respiratory irritant (Kaden et al., 2010). The iterative process of measuring HCHO in an atmosphere and comparing the observations to predictions from computer models serves as a strong investigative tool to improve our understanding. To maximise the potential for such study and provide adequate scope to fully investigate HCHO sources, it is desirable to be able to measure rapid changes in HCHO in ambient air. A new LIF instrument for this is described in Chapter 2 which is capable of making HCHO measurements every second. Laboratory measurements made with this instrument are presented in Chapter 4 where HCHO was observed in experiments conducted to characterise new instrumentation for the identification ‘missing’ OH reactivity. Measurements of HCHO in ambient air are presented in Chapters 5 and 6. Many methods for the

measurements of HCHO in the atmosphere are reported in the literature. Those used most frequently in the field of atmospheric chemistry are described in Section 1.8 and a review of a selection of ambient measurements reported in the literature is presented in Section 1.9.

1.9 Measurement of formaldehyde

1.9.1 Direct spectroscopic measurement

Many measurements of HCHO as a trace species in the atmosphere are made using spectroscopic techniques where HCHO is detected directly in ambient air, there is no derivitisation prior to detection. Möhlmann (1985) reported the first direct spectroscopic measurement of gas phase HCHO, where detection was achieved using LIF and ~10 ppb of gas phase HCHO could be determined in 100s. More recently measurements of HCHO using LIF have been reported where significantly lower levels can be detected. Hottle et al. (2008) reported that measurements as low as ~0.051 ppb could be made in 1s using LIF where HCHO was excited in the $5_{0,5} \leftarrow 5_{1,4}$ rotational transition of the 4 $A^1A_2 \leftarrow X^1A_1$ vibronic band at 353.370 nm. A new instrument for the measurement of HCHO using this technique is described in this work and full experimental details are presented in Chapter 2, the key features of the technique are summarised here.

For the measurement of HCHO by LIF ambient air is sampled into a low pressure cell (130 Torr) where it is irradiated with pulsed UV radiation at 353.370 nm from a laser light source. Molecules of HCHO in the gas sampled become electronically excited into a higher vibrational energy level. From here they undergo collisional quenching with other molecules present in the gas to a lower vibrational energy level of the electronically excited state, where relaxation back to the ground electronic state occurs resulting in broadband (laser induced) fluorescence at 390 – 550 nm. Figure 1.10 summarises this process.

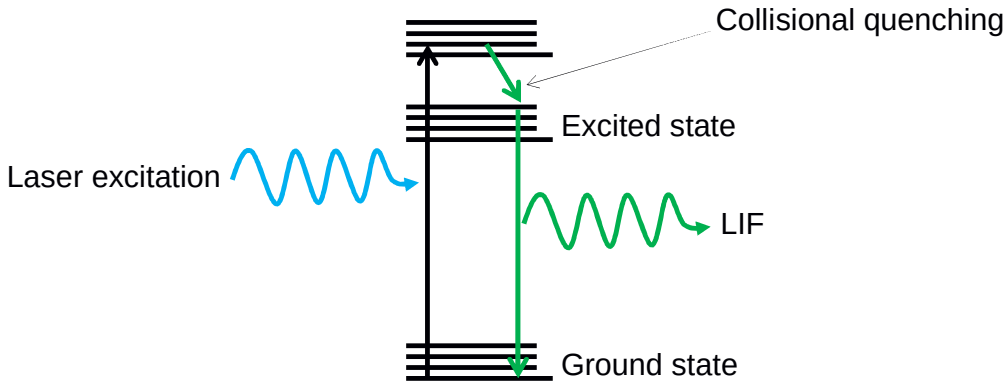

Figure 1.10: Schematic energy level diagram to illustrate the key processes occurring during LIF measurement of gas phase HCHO.

Photons resulting from LIF are detected using a PMT and photon counter. A background signal, recorded at an 'offline' wavelength where photons from HCHO LIF are not observed, is subtracted. The background subtracted HCHO LIF signal determined is proportional to the level of HCHO present in the gas sampled. It is used in conjunction with a calibration factor, determined through the addition of known quantities of HCHO to the instrument, to determine the level of HCHO that was present.

Another direct spectroscopic method for the measurement of HCHO in ambient air is differential optical absorption spectroscopy (DOAS). Unlike HCHO LIF this method is absolute and no calibration of the instrumentation is required. There are two variations of DOAS that are often used for the measurement of HCHO as a trace species in ambient air long path (LP) and multi axis (MAX) DOAS. An in depth discussion of the LP-DOAS and MAX-DOAS techniques is beyond the scope of this work, however, the key features of each technique are summarised here.

In LP-DOAS there are two key pieces of instrumentation; a light source and a spectrometer which are arranged such that light can be sent and received through the atmosphere studied. A continuous light source is typically used for this and a range of wavelengths (dependant on the species of study) is scanned using the spectrometer. Spectra recorded during the LP-DOAS measurement of HCHO are typically for near-UV radiation. Interferences arise from the presence of species other than those targeted, which are known to absorb (e.g. NO_2 and O_3) in the same wavelength region. Contributions for these are subtracted using appropriate reference spectra which are measured at regular intervals during the course of

operation of the instrument. A reference spectrum for the target species is then fitted to the resulting spectra and a concentration is determined using the Beer-Lambert law.

When measurements are made by MAX-DOAS scattered sunlight is used as the light source instead of, for example, a lamp which could be used in LP-DOAS. An advantage to the MAX-DOAS technique is that spectra can be recorded at discreet viewing angles, meaning that vertical concentration gradients of target species can be measured. A telescope is often used to achieve variation of the viewing angle and focusses light into an optical fibre so that it can be transmitted to a spectrometer. The spectra are typically recorded for mid-UV radiation and are processed in a similar manner to the description above for LP-DOAS to account for other species known to absorb in the studied region. The concentrations are determined using the Beer-Lambert law.

The limits of detection for a measurement of HCHO by LP-DOAS or MAX-DOAS are typically significantly higher than measurements made by LIF. MacDonald et al. (2012) reported that measurements made using LP-DOAS at a rainforest in Malaysian Borneo were subject to a limit of detection of 300-400 ppt for a measurement made over 60 minutes. A further disadvantage to the DOAS techniques is that meteorological factors such as cloud and fog can result in measurements that are subject to greater uncertainty. Cloud cover can be particularly obstructive for MAX-DOAS measurements as it results in a decrease in the intensity of natural sunlight that is used to record spectra.

A third direct spectroscopic technique that is used for the measurement of atmospheric HCHO is tuneable diode laser absorption spectrometry (TDLAS) (Fried et al., 1997). In this technique ambient air is drawn into a multipass absorption cell, where IR radiation from a diode laser is used to scan a HCHO absorption feature at 2831.6417 cm^{-1} (Fried and Richter, 2006). A reference spectrum for HCHO is then subtracted from the resulting absorption spectrum to determine a concentration of HCHO. Fried et al. (2003) reported a 2σ limit of detection in the range 50-80 ppt for measurements made over one minute using this technique. In addition to tunable diode lasers, similar systems that utilise quantum cascade lasers have also been reported e.g. Choi et al. (2010).

1.9.2 Indirect spectroscopic measurement

In addition to the direct spectroscopic methods for HCHO measurement described in Section 1.8.1 it is possible to measure HCHO indirectly using spectroscopic methods. The most common such method reported in the literature is Hantzsch Fluorimetry and was first reported by Kelly and Fortune (1994). The majority of measurements reported in the literature that were obtained using this technique were made using a commercial instrument (AL4001 or similar, Aerolaser GmbH, Germany) The basis of the measurement of HCHO using this technique relies upon a liquid phase reaction of HCHO to produce a product which can be detected by fluorescence. For this to be possible gas phase HCHO must first be transferred to the liquid phase. Ambient air is flowed into a stripping coil which also receives a flow of an aqueous solution of sulphuric acid, within this coil gas phase HCHO enters the liquid phase with an efficiency of 98 % (Kaiser et al., 2014). The solution is isolated from the gas phase and passed into a liquid flow reactor so that the HCHO can undergo reaction in order to be detected. Within the reactor the solution is mixed with 2,4-pentadione and ammonia to produce 3,5-diacetly-1,4-dihydrolutidine (DDL) in a Hantzsch cyclization reaction, Figure 1.11. The DDL produced absorbs light at 410 nm and fluoresces strongly at ~510 nm.

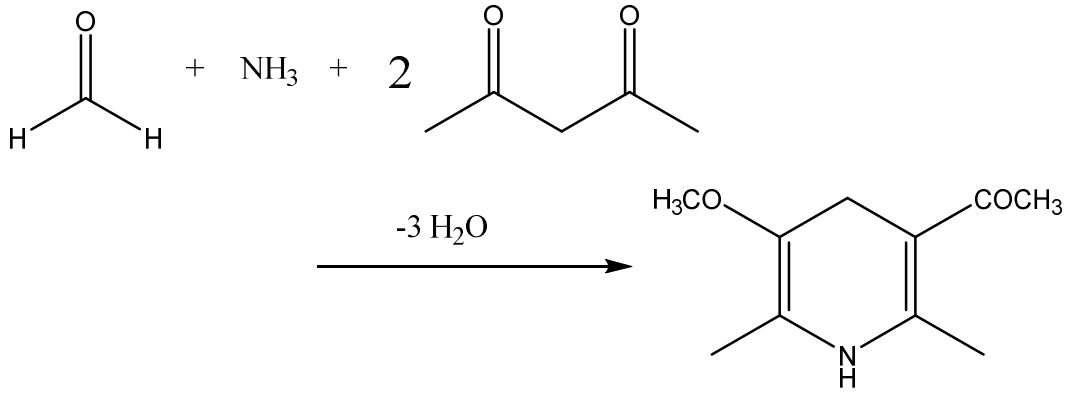

Figure 1.11: Liquid phase Hantzsch cyclization reaction utilised in the Hantzsch Fluorimetry method for the measurement of HCHO.

Upon exit from the liquid flow reactor the solution is irradiated with 410 nm radiation typically from a phosphor coated mercury lamp. The intensity of the resulting fluorescence is recorded using a detector such as a PMT and is proportional to the level of HCHO that existed in the gas that was sampled by the instrument. It is necessary to calibrate systems that use the Hantzsch Fluorimetery

method to measure HCHO. Calibrations are performed by using liquid standards containing a known quantity of HCHO in place of aqueous sulphuric acid in the stripping coil and monitoring the instrument response.

1.9.3 Other methods and intercomparisons

There are many non-spectroscopic methods that have been reported in the literature for the measurement of gas phase HCHO and an in depth discussion of all is beyond the scope of this work. A comprehensive review of techniques for detecting gas phase HCHO can be found in Chung et al. (2013). Non-spectroscopic measurements of HCHO reported include those by gas chromatography (GC), high performance liquid chromatography (HPLC) and ion chromatography (IC) (Dumas, 1982, Mann and Grayeski, 1987, Lorrain et al., 1981, Hunter et al., 1998). Measurements have also been reported using a polarographic technique (Septon and Ku, 1982).

There are numerous intercomparisons of instrumentation, and methods used for the measurement of HCHO in the atmosphere. One of the most thorough of such is that reported by Hak et al. (2005) where four methods were compared in urban air at a site in Milan, Italy. The techniques used were LP-DOAS (1 instrument), Hantzsch Fluorimetry (5 instruments), HPLC (1 instrument) and IR absorption (1 instrument). During the comparison period up to 13 ppb of HCHO were observed and the measurements made using the DOAS, Hantzsch Fluorimetry and IR absorption instruments were all in agreement to within ±11 %. Measurements made using the HPLC instrument were up to 25 % lower. More recently an intercomparison study was reported by Kaiser et al. (2014) for measurements made using a LIF type instrument (similar to that described in Chapter 2 of this thesis) and a Hantzsch Fluorimetry type instrument. During this study gas from an atmospheric simulation chamber was simultaneously analysed by both instruments under a range of conditions. The measurements were shown to correlate well ($R^2 > 0.997$) and agree to within the uncertainties that were associated with each technique.

1.10 Review of ground-based formaldehyde measurements

Measurements of gas phase HCHO have been reported in the literature from a wide variety of atmospheres ranging from those heavily influenced by biogenic emissions to those heavily influenced by anthropogenic emissions, and those influenced by a

mixture of emissions. In this section a selection of measurements in different atmospheres of gas phase HCHO from the literature are discussed.

A typical example of a biogenically influenced atmosphere, within which HCHO measurements have been reported in the literature, is that of a forest. A variety of levels of HCHO have been observed in forested atmospheres, example observations from two such studies are summarised in Table 1.5.

Campaign	Dates	Technique	Location	Maximum [HCHO]	Reference
OP3	April/May 2008 June/July 2008	LP-DOAS MAX-DOAS	Sabah, Borneo, Malaysia	4.5 ppb	MacDonald et al. (2012)
BEARPEX	September/October 2007	QCLS	Sierra Nevada, California, US	20 ppb	Choi et al. (2010)

Table 1.5: HCHO observations from two field campaigns in forest atmospheres reported in the literature.

Choi et al. (2010) reported measurements from the Biosphere Effects on Aerosols and Photochemistry Experiment (BEARPEX) at an elevated site on the western slope of the Sierra Nevada Mountains in California. The measurements were made using a quantum cascade laser spectrometer (QCLS). The level of HCHO was found to increase sharply at sunrise and peak around midday on hotter days and decrease through the afternoon hours into the evening. The cause of this was concluded to be a combination of high photochemical activity and emission of biogenic VOCs which could be photo-chemically processed to HCHO. The maximum level of HCHO detected was 20 ppb.

MacDonald et al. (2012) reported measurements made using both LP-DOAS and MAX-DOAS from a rainforest in the Sabah region of Malaysian Borneo during the OP3 campaign in 2008. Measurements were made for two intensive periods during this campaign; the first was in April and May and the second in June and July. The LP-DOAS and MAX-DOAS measurements were typically in good agreement and for both sets of measurements the level of HCHO was seen to peak at around midday, which was likely attributable to increased photo-oxidation of biogenic VOCs such as isoprene. The maximum level of HCHO observed was 4.5 ppb.

HCHO has been extensively studied in atmospheres influenced by anthropogenic emissions, such as those in urban locations. There are many urban measurements of HCHO reported in the literature so a selection of examples are reviewed here. Most measurements reported for urban atmospheres were conducted using an HPLC

technique where HCHO in ambient air was derivatised in a sampling cartridge which was then analysed at a later date. There are also a number of examples of measurements which have been made using the Hantzsh Fluorimetry technique. Most observations are typically in the range 1-10 ppb, Table 1.6 summarises the results from eleven studies.

Dates	Technique	Location	Average [HCHO]	Reference
October 1986	HPLC	Sao Paulo, Brazil	9.4 ppb	Grosjean et al. (1990)
June/July 1988				
July 1988				
Septermber 1987	HPLC	Rio de Janeiro, Brazil	4.2 ppb	Grosjean et al. (1990)
September 1988	HPLC	Salvador, Brazsil	10.4 ppb	Grosjean et al. (1990)
September 1993	HPLC	Los Angeles, California, US	5.3 ppb	Grosjean et al. (1996)
October 1984	HPLC	Los Angeles, California, US	0.8 ppb	Kawamura et al. (2000)
July-August 1998	HPLC	Las Vegas, Nevada, US	0.26 ppb (summer)	Jing et al. (2001)
November-February 1999			0.79 ppb (winter)	
1999-2001	HPLC	Elizabeth, New Jersey, US	5.3 ppb (spring)	Liu et al. (2006)
			3.9 ppb (summer)	
			4.7 ppb (autumn)	
			5.7 ppb (winter)	
June/July 1999	Hantzsch	Nashville, Tennessee, US	4.1	Dasgupta et al. (2005)
August 1999	Hantzsch	Atlanta, Georgia, US	8.0	Dasgupta et al. (2005)
August/September 2001	Hantzsch	Houston, Texas, US	4.5	Dasgupta et al. (2005)
June/July 2002	Hantzsch	Philadelphia, Pennsylvania, US	3.1	Dasgupta et al. (2005)

Table 1.6: Summary of HCHO observations from eleven field campaigns in urban atmospheres reported in the literature.

Grosjean et al. (1990) reported measurements from three urban locations in Brazilian cities; Sao Paulo, Rio de Janeiro and Salvador. The average levels measured were 9.4, 4.2 and 10.4 ppb, respectively. Additionally there have been many studies of ambient HCHO in large US cities. Grosjean et al. (1996) and Kawamura et al. (2000) reported an average level of 5.3 and 0.8 ppb, respectively, in Los Angeles. Jing et al. (2001) reported summer and winter measurements from a site in Las Vegas, 0.26 and 0.79 ppb on average, respectively. An extensive set of measurements spanning over two complete years was reported by Liu et al. (2006) from residential areas in Elizabeth, New Jersey, US. The seasonal average values ranged from 3.9 ppb in summer to 5.7 ppb in winter. Dasgupta et al. (2005) reported

measurements made using Hantzsch Fluorimetry from a further four US cities. Average values measured in Nashville, Atlanta, Houston and Philadelphia were 4.1, 8, 4.5 and 3.1 ppb, respectively. Measurements of HCHO at an urban background site in York are presented in Chapter 5 of this thesis.

Further to studies of forested and urban atmospheres, there are numerous examples of HCHO measurements reported in the literature that do not fit either category. Such as those made a rural locations where there is a mixture of anthropogenic and biogenic influence, and also coastal locations where clean marine air could be influenced by anthropogenic and biogenic emissions. Table 1.7 summarises results from studies of HCHO in ambient air in seven such atmospheres.

Campaign	Dates	Technique	Location	Average [HCHO]	Reference
SOS	July/Augst 1991 June 1992	HPLC	George Smith State Park, Geogia, US	3.6 ppb (1991) 3.1 ppb (1992)	Lee et al. (1995)
SCAPE	September 1990	HPLC	Shenandoah National Park, Virginia, US	1.0 ppb	Munger et al. (1995)
-	January/February 1980	HPLC	Juelich, North Rhine-Westphalia, Germany	0.3 ppb	Lowe and Schmidt (1983)
PRIDE-PRD	July 2006	MAX-DOAS	Guangzhou, Guandong, China	7 ppb	Li et al. (2013)
-	November/December 2003	HPLC	Cape Grim, Australia	~0.4 ppb	Ayers et al. (1997)
TORCH-2	May 2004	Hantzsch Fluorimetry	Weybourne, Norfolk, UK	~0.8 ppb	Lee et al. (2009)
-	November-June 2006	LP-DOAS	Sao Vicente, Cape Verde	~0.5 ppb	Mahajan et al. (2011)

Table 1.7: Summary of HCHO observations from four field campaigns in rural atmospheres and three field campaigns in coastal marine atmospheres.

Similar to urban environments a number of measurements have been made using the HPLC technique. Lee et al. (1995) reported average measured HCHO levels of 6.6 ppb in 1991 and 3.1 ppb in 1992 that were made as part of the Southern Oxidants Study (SOS) at a rural site in the George Smith State Park in Georgia, US. At another US rural site Munger et al. (1995) reported a 1 ppb average level of HCHO at the Shenandoah National Park, Virginia during the Shenandoah Cloud and Photochemistry Experiment (SCAPE). During the PRIDE-PRD campaign measurements were made at a rural location in the pearl river delta in China using the MAX-DOAS technique, the average level of HCHO detected was 7 ppb.

In addition to measurements made in rural atmospheres that are summarised in Table 1.7, results from three studies in coastal marine atmospheres are also summarised. The average levels of HCHO measured during these studies are lower than many of those quoted above in this section for other atmospheres, likely a result of marine air typically having a comparatively low loading of biogenic and anthropogenic emissions that can be photo chemically processed to produce HCHO. Ayers et al. (1997) reported an average level of HCHO measured using an HPLC technique of 0.4 ppb in a clean marine atmosphere at Cape Grim, Australia and Mahajan et al. (2011) reported an average level of HCHO measured by LP-DOAS of 0.5 ppb in clean marine air at site in Cape Verde. Observations from the TORCH-2 campaign reported by Lee et al. (2009) gave an average level of HCHO measured using Hantzsch Fluorimetry at a coastal site in Weybourne, Norfolk, UK of ~0.8 ppb. It is likely that this is higher than what has been reported at other coastal sites as the waters local to the site in Weybourne contain many busy shipping lanes. Measurements of HCHO from the same site in Weybourne are presented in Chapter 6 of this work.

1.11 Project aims

The direct measurement of OH reactivity provides a valuable tool for assessing the state of our knowledge of OH sinks that are present in ambient air. OH reactivity is routinely estimated through calculation, and computer model simulation, where the resulting values are compared with those measured. It is often the case that measured OH reactivity exceeds the estimated OH reactivity, and the difference is commonly referred to as the 'missing' OH reactivity. Where there is significant 'missing' OH reactivity in a given air mass, it can be concluded that OH reactive species are present which have not been identified. This means for the air mass in question our knowledge of OH chemistry is incomplete and likely merits further study. In order to accurately quantify 'missing' OH reactivity, we have to first have confidence in our ability to measure OH reactivity. Three techniques for the measurement of OH reactivity are reported in the literature and each have various advantages and disadvantages, as described in Section 1.5. A major aim of this work was to assess the performance of the Leeds LFP-LIF instrument for the measurement of OH reactivity through participation in a series of inter-comparison experiments. Chapter 3 details results from these experiments where nine

instruments simultaneously measured the OH reactivity of a variety gases from a large atmospheric simulation chamber.

Another aim of this work was to develop a new instrument for the chemical identification of species that contribute to 'missing' OH reactivity. Chapter 4 details the design and characterisation of an OH flow reactor as a component of this new instrumentation. This instrumentation was utilised for the analysis of ambient air during a measurement campaign at an urban background site in York, UK. Aside from the development of the OH flow reactor, a major aim of this work was to measure OH reactivity using the Leeds LFP-LIF instrument during the same campaign, and compare observations with predicted values calculated using concentrations of co-measured sinks. The purpose of this was to conduct a detailed analysis of factors that drove changes observed in OH reactivity, and to quantify any 'missing' OH reactivity, thus giving potential for any observations made using the newly developed instrument to be analysed in context. A significant portion of this thesis is focussed on the measurement of HCHO. Another objective of the measurement campaign in York was to make the first ambient measurements of HCHO using a newly developed LIF instrument. The measurements of OH reactivity and HCHO from York are presented and discussed in Chapter 5.

Tropospheric ozone as a pollutant was discussed in Section 1.3 and is a topic central to the work presented in Chapter 6 of this thesis. Here results are presented from a measurement campaign at a site on the North Norfolk Coast, UK. The main objective of which, was to field test an instrument that has been recently developed by researchers at the University of Birmingham, for the direct measurement of the rate of ozone production in ambient air. The specific aims of this thesis in relation to this campaign were to co-measure OH reactivity and HCHO, and to interpret the resulting observations in the context of ozone production and complement the analysis of any direct measurements of ozone production rate.

1.12 References

AMEDRO, D., MIYAZAKI, K., PARKER, A., SCHOEMAECKER, C. & FITTSCHEN, C. 2012. Atmospheric and kinetic studies of OH and HO2 by the FAGE technique. *Journal of Environmental Sciences,* 24**,** 78-86.

ANDERSON, L. G., LANNING, J. A., BARRELL, R., MIYAGISHIMA, J., JONES, R. H. & WOLFE, P. 1996. Sources and sinks of formaldehyde and acetaldehyde: An analysis of Denver's ambient concentration data. *Atmospheric Environment,* 30**,** 2113-2123.

ATKINSON, R. 2007. Gas-phase tropospheric chemistry of organic compounds: a review. *Atmospheric Environment,* 41, Supplement**,** 200-240.

ATKINSON, R., BAULCH, D. L., COX, R. A., CROWLEY, J. N., HAMPSON, R. F., HYNES, R. G., JENKIN, M. E., ROSSI, M. J. & TROE, J. 2004. Evaluated kinetic and photochemical data for atmospheric chemistry: Volume I - gas phase reactions of O_x, HO_x, NO_x and SO_x species. *Atmos. Chem. Phys.,* 4**,** 1461-1738.

ATKINSON, R. & CARTER, W. P. L. 1984. Kinetics and mechanisms of the gas-phase reactions of ozone with organic compounds under atmospheric conditions. *Chemical Reviews,* 84**,** 437-470.

AYERS, G. P., GILLETT, R. W., GRANEK, H., DE SERVES, C. & COX, R. A. 1997. Formaldehyde production in clean marine air. *Geophysical Research Letters,* 24**,** 401-404.

BRUNE, W. H., BAIER, B. C., THOMAS, J., REN, X., COHEN, R. C., PUSEDE, S. E., BROWNE, E. C., GOLDSTEIN, A. H., GENTNER, D. R., KEUTSCH, F. N., THORNTON, J. A., HARROLD, S., LOPEZ-HILFIKER, F. D. & WENNBERG, P. O. 2016. Ozone production chemistry in the presence of urban plumes. *Faraday Discussions,* 189**,** 169-189.

CALPINI, B., JEANNERET, F., BOURQUI, M., CLAPPIER, A., VAJTAI, R. & VAN DEN BERGH, H. 1999. Direct measurement of the total reaction rate of OH in the atmosphere. *Analusis,* 27**,** 328-336.

CHANCE, K., PALMER, P. I., SPURR, R. J. D., MARTIN, R. V., KUROSU, T. P. & JACOB, D. J. 2000. Satellite observations of formaldehyde over North America from GOME. *Geophysical Research Letters,* 27**,** 3461-3464.

CHATANI, S., SHIMO, N., MATSUNAGA, S., KAJII, Y., KATO, S., NAKASHIMA, Y., MIYAZAKI, K., ISHII, K. & UENO, H. 2009. Sensitivity analyses of OH missing sinks over Tokyo metropolitan area in the summer of 2007. *Atmos. Chem. Phys.,* 9**,** 8975-8986.

CHOI, W., FALOONA, I. C., BOUVIER-BROWN, N. C., MCKAY, M., GOLDSTEIN, A. H., MAO, J., BRUNE, W. H., LAFRANCHI, B. W., COHEN, R. C., WOLFE, G. M., THORNTON, J. A., SONNENFROH, D. M. & MILLET, D. B. 2010. Observations of elevated formaldehyde over a forest canopy suggest missing sources from rapid oxidation of arboreal hydrocarbons. *Atmos. Chem. Phys.,* 10**,** 8761-8781.

CHUNG, P.-R., TZENG, C.-T., KE, M.-T. & LEE, C.-Y. 2013. Formaldehyde Gas Sensors: A Review. *Sensors (Basel, Switzerland),* 13**,** 4468-4484.

DASGUPTA, P. K., LI, J., ZHANG, G., LUKE, W. T., MCCLENNY, W. A., STUTZ, J. & FRIED, A. 2005. Summertime Ambient Formaldehyde in Five U.S. Metropolitan Areas: Nashville, Atlanta, Houston, Philadelphia, and Tampa. *Environmental Science & Technology,* 39**,** 4767-4783.

DI CARLO, P., BRUNE, W. H., MARTINEZ, M., HARDER, H., LESHER, R., REN, X., THORNBERRY, T., CARROLL, M. A., YOUNG, V., SHEPSON, P. B., RIEMER, D., APEL, E. & CAMPBELL, C. 2004. Missing OH Reactivity in a Forest: Evidence for Unknown Reactive Biogenic VOCs. *Science,* 304**,** 722-725.

DIGANGI, J. P., BOYLE, E. S., KARL, T., HARLEY, P., TURNIPSEED, A., KIM, S., CANTRELL, C., MAUDLIN III, R. L., ZHENG, W., FLOCKE, F., HALL, S. R., ULLMANN, K., NAKASHIMA, Y., PAUL, J. B., WOLFE, G. M., DESAI, A. R., KAJII, Y., GUENTHER, A. & KEUTSCH, F. N. 2011. First direct measurements of formaldehyde flux via eddy covariance:

implications for missing in-canopy formaldehyde sources. *Atmos. Chem. Phys.,* 11**,** 10565-10578.

DOLGOROUKY, C., GROS, V., SARDA-ESTEVE, R., SINHA, V., WILLIAMS, J., MARCHAND, N., SAUVAGE, S., POULAIN, L., SCIARE, J. & BONSANG, B. 2012. Total OH reactivity measurements in Paris during the 2010 MEGAPOLI winter campaign. *Atmos. Chem. Phys.,* 12**,** 9593-9612.

DUMAS, T. 1982. Determination of formaldehyde in air by gas chromatography. *Journal of Chromatography A,* 247**,** 289-295.

EDWARDS, P. M. 2011. *Tropospheric oxidation from the tropics to the poles.* PhD, University of Leeds.

EDWARDS, P. M., EVANS, M. J., FURNEAUX, K. L., HOPKINS, J., INGHAM, T., JONES, C., LEE, J. D., LEWIS, A. C., MOLLER, S. J., STONE, D., WHALLEY, L. K. & HEARD, D. E. 2013. OH reactivity in a South East Asian tropical rainforest during the Oxidant and Particle Photochemical Processes (OP3) project. *Atmos. Chem. Phys.,* 13**,** 9497-9514.

EERDEKENS, G., YASSAA, N., SINHA, V., AALTO, P. P., AUFMHOFF, H., ARNOLD, F., FIEDLER, V., KULMALA, M. & WILLIAMS, J. 2009. VOC measurements within a boreal forest during spring 2005: on the occurrence of elevated monoterpene concentrations during night time intense particle concentration events. *Atmos. Chem. Phys.,* 9**,** 8331-8350.

ESPERE. 2017. *ESPERE Climate Encyclopaedia* [Online]. 2017].

EUROPEAN ENVIRONMENT AGENCY, E. 2008. Air pollution harms human health and the environment. *In:* AGENCY, E. E. (ed.) *Air pollution.* Copenhagen: European Environment Agency.

FINLAYSON-PITTS, B. J. & PITTS, J. N. 2000. *Chemistry of the upper and lower atmosphere,* California, Academic Press.

FRIED, A., CRAWFORD, J., OLSON, J., WALEGA, J., POTTER, W., WERT, B., JORDAN, C., ANDERSON, B., SHETTER, R., LEFER, B., BLAKE, D., BLAKE, N., MEINARDI, S., HEIKES, B., O'SULLIVAN, D., SNOW, J., FUELBERG, H., KILEY, C. M., SANDHOLM, S., TAN, D., SACHSE, G., SINGH, H., FALOONA, I., HARWARD, C. N. & CARMICHAEL, G. R. 2003. Airborne tunable diode laser measurements of formaldehyde during TRACE-P: Distributions and box model comparisons. *Journal of Geophysical Research: Atmospheres,* 108**,** n/a-n/a.

FRIED, A. & RICHTER, D. 2006. Infrared Absorption Spectroscopy. *In:* HEARD, D. E. (ed.) *Analytical techniques for atmopspheric measurement.* Oxford: Blackwell.

FRIED, A., SEWELL, S., HENRY, B., WERT, B. P., GILPIN, T. & DRUMMOND, J. R. 1997. Tunable diode laser absorption spectrometer for ground-based measurements of formaldehyde. *Journal of Geophysical Research: Atmospheres,* 102**,** 6253-6266.

GOLDSTEIN, A. H. & GALBALLY, I. E. 2007. Known and Unexplored Organic Constituents in the Earth's Atmosphere. *Environmental Science & Technology,* 41**,** 1514-1521.

GROSJEAN, D., MIGUEL, A. H. & TAVARES, T. M. 1990. Urban air pollution in Brazil: Acetaldehyde and other carbonyls. *Atmospheric Environment. Part B. Urban Atmosphere,* 24**,** 101-106.

GROSJEAN, E., GROSJEAN, D., FRASER, M. P. & CASS, G. R. 1996. Air Quality Model Evaluation Data for Organics. 2. C1−C14 Carbonyls in Los Angeles Air. *Environmental Science & Technology,* 30**,** 2687-2703.

HAK, C., PUNDT, I., TRICK, S., KERN, C., PLATT, U., DOMMEN, J., ORDÓÑEZ, C., PRÉVÔT, A. S. H., JUNKERMANN, W., ASTORGA-LLORÉNS, C., LARSEN, B. R., MELLQVIST, J., STRANDBERG, A., YU, Y., GALLE, B., KLEFFMANN, J., LÖRZER, J. C., BRAATHEN, G. O. & VOLKAMER, R. 2005. Intercomparison of four different in-situ techniques for ambient formaldehyde measurements in urban air. *Atmos. Chem. Phys.*, 5**,** 2881-2900.

HANSEN, R. F., GRIFFITH, S. M., DUSANTER, S., RICKLY, P. S., STEVENS, P. S., BERTMAN, S. B., CARROLL, M. A., ERICKSON, M. H., FLYNN, J. H., GROSSBERG, N., JOBSON, B. T., LEFER, B. L. & WALLACE, H. W. 2013. Measurements of total hydroxyl radical reactivity during CABINEX 2009; Part 1: Field measurements. *Atmos. Chem. Phys. Discuss.*, 13**,** 17159-17195.

HANSEN, R. F., GRIFFITH, S. M., DUSANTER, S., RICKLY, P. S., STEVENS, P. S., BERTMAN, S. B., CARROLL, M. A., ERICKSON, M. H., FLYNN, J. H., GROSSBERG, N., JOBSON, B. T., LEFER, B. L. & WALLACE, H. W. 2014. Measurements of total hydroxyl radical reactivity during CABINEX 2009; Part 1: field measurements. *Atmos. Chem. Phys.*, 14**,** 2923-2937.

HARD, T. M., O'BRIEN, R. J., COOK, T. B. & TSONGAS, G. A. 1979. Interference suppression in HO fluorescence detection. *Appl. Opt.*, 18**,** 3216-3217.

HEARD, D. E. Field measurements of tropospheric OH and HO_2 radicals: Comparisons with model calculations, novel chemical mechanisms, and technique development. International Global Atmospheric Chemistry 2012, 2012 Beijing.

HEARD, D. E., CARPENTER, L. J., CREASEY, D. J., HOPKINS, J. R., LEE, J. D., LEWIS, A. C., PILLING, M. J., SEAKINS, P. W., CARSLAW, N. & EMMERSON, K. M. 2004. High levels of the hydroxyl radical in the winter urban troposphere. *Geophysical Research Letters,* 31**.**

HEARD, D. E. & PILLING, M. J. 2003. Measurement of OH and HO2 in the Troposphere. *Chemical Reviews,* 103**,** 5163-5198.

HOLLOWAY, A. M. & WAYNE, R. P. 2010. *Atmospheric Chemistry,* Cambridge, RSC Publishing.

HOTTLE, J. R., HUISMAN, A. J., DIGANGI, J. P., KAMMRATH, A., GALLOWAY, M. M., COENS, K. L. & KEUTSCH, F. N. 2008. A Laser Induced Fluorescence-Based Instrument for In-Situ Measurements of Atmospheric Formaldehyde. *Environmental Science & Technology,* 43**,** 790-795.

HUNTER, M. C., BARTLE, K. D., LEWIS, A. C., MCQUAID, J. B., MYERS, P., SEAKINS, P. W. & VAN TILBURG, C. 1998. The Use of the Helium Ionization Detector for Gas Chromatographic Monitoring of Trace Atmospheric Components. *Journal of High Resolution Chromatography,* 21**,** 75-80.

IARC 2006. *IARC Working Group on the Evaluation of Carcinogenic Risk to Humans. Formaldehyde, 2-Butoxyethanol and 1-tert-Butoxypropan-2-ol,* Lyon, IARC.

INGHAM, T., GODDARD, A., WHALLEY, L. K., FURNEAUX, K. L., EDWARDS, P. M., SEAL, C. P., SELF, D. E., JOHNSON, G. P., READ, K. A., LEE, J. D. & HEARD, D. E. 2009. A flow-tube based laser-induced

fluorescence instrument to measure OH reactivity in the troposphere. *Atmos. Meas. Tech. Discuss.,* 2**,** 621-657.

JACOB, D. J. 1999. *Introduction to atmospheric chemistry,* New Jersey, Princeton University Press.

JEANNERET, F., KIRCHNER, F., CLAPPIER, A., VAN DEN BERGH, H. & CALPINI, B. 2001. Total VOC reactivity in the planetary boundary layer 1. Estimation by a pump and probe OH experiment. *J. Geophys. Res.,* 106**,** 3083-3093.

JENKIN, M. E., SAUNDERS, S. M. & PILLING, M. J. 1997. The tropospheric degradation of volatile organic compounds: a protocol for mechanism development. *Atmospheric Environment,* 31**,** 81-104.

JING, L., STEINBERG, S. M. & JOHNSON, B. J. 2001. Aldehyde and monocyclic aromatic hydrocarbon mixing ratios at an urban site in Las Vegas, Nevada. *J Air Waste Manag Assoc,* 51**,** 1359-66.

JOHNSTON, H. S. & GRAHAM, R. 1974. Photochemistry of NOx and HNOx Compounds. *Canadian Journal of Chemistry,* 52**,** 1415-1423.

KADEN, D. A., MANDIN, C., G.D, N. & WOLKOFF, P. 2010. Formaldehyde. *WHO Guidelines for Indoor Air Quality: Selected Pollutants.* Geneva: World Health Organisation.

KAISER, J., LI, X., TILLMANN, R., ACIR, I., HOLLAND, F., ROHRER, F., WEGENER, R. & KEUTSCH, F. N. 2014. Intercomparison of Hantzsch and fiber-laser-induced-fluorescence formaldehyde measurements. *Atmos. Meas. Tech.,* 7**,** 1571-1580.

KAISER, J., WOLFE, G. M., BOHN, B., BROCH, S., FUCHS, H., GANZEVELD, L. N., GOMM, S., HÄSELER, R., HOFZUMAHAUS, A., HOLLAND, F., JÄGER, J., LI, X., LOHSE, I., LU, K., PRÉVÔT, A. S. H., ROHRER, F., WEGENER, R., WOLF, R., MENTEL, T. F., KIENDLER-SCHARR, A., WAHNER, A. & KEUTSCH, F. N. 2015. Evidence for an unidentified non-photochemical ground-level source of formaldehyde in the Po Valley with potential implications for ozone production. *Atmos. Chem. Phys.,* 15**,** 1289-1298.

KATO, S., SATO, T. & KAJII, Y. 2011. A method to estimate the contribution of unidentified VOCs to OH reactivity. *Atmospheric Environment,* 45**,** 5531-5539.

KAWAMURA, K., STEINBERG, S. & KAPLAN, I. R. 2000. Homologous series of C1–C10 monocarboxylic acids and C1–C6 carbonyls in Los Angeles air and motor vehicle exhausts. *Atmospheric Environment,* 34**,** 4175-4191.

KELLY, T. J. & FORTUNE, C. R. 1994. Continuous Monitoring of Gaseous Formaldehyde Using an Improved Fluorescence Approach. *International Journal of Environmental Analytical Chemistry,* 54**,** 249-263.

KELLY, T. J., SMITH, D. L. & SATOLA, J. 1999. Emission Rates of Formaldehyde from Materials and Consumer Products Found in California Homes. *Environmental Science & Technology,* 33**,** 81-88.

KIM, S., GUENTHER, A., KARL, T. & GREENBERG, J. 2011. Contributions of primary and secondary biogenic VOC to total OH reactivity during the CABINEX (Community Atmosphere-Biosphere INteractions Experiments)-09 field campaign. *Atmos. Chem. Phys,* 11**,** 8613-8623.

KOVACS, T. A. & BRUNE, W. H. 2001. Total OH Loss Rate Measurement. *Journal of Atmospheric Chemistry,* 39**,** 105-122.

KOVACS, T. A., BRUNE, W. H., HARDER, H., MARTINEZ, M., SIMPAS, J. B., FROST, G. J., WILLIAMS, E., JOBSON, T., STROUD, C., YOUNG, V.,

FRIED, A. & WERT, B. 2003. Direct measurements of urban OH reactivity during Nashville SOS in summer 1999. *J. Environ. Monit.,* 5**,** 68-74.

KRUPA, S. V., NOSAL, M. & LEGGE, A. H. 1998. A numerical analysis of the combined open-top chamber data from the USA and Europe on ambient ozone and negative crop responses. *Environmental Pollution,* 101**,** 157-160.

LEE, J. D., YOUNG, J. C., READ, K. A., HAMILTON, J. F., HOPKINS, J. R., LEWIS, A. C., BANDY, B. J., DAVEY, J., EDWARDS, P., INGHAM, T., SELF, D. E., SMITH, S. C., PILLING, M. J. & HEARD, D. E. 2009. Measurement and calculation of OH reactivity at a United Kingdom coastal site. *Journal of atmospheric chemistry,* 64**,** 53-76.

LEE, Y.-N., ZHOU, X. & HALLOCK, K. 1995. Atmospheric carbonyl compounds at a rural southeastern United States site. *Journal of Geophysical Research: Atmospheres,* 100**,** 25933-25944.

LEE, Y. N., ZHOU, X., KLEINMAN, L. I., NUNNERMACKER, L. J., SPRINGSTON, S. R., DAUM, P. H., NEWMAN, L., KEIGLEY, W. G., HOLDREN, M. W., SPICER, C. W., YOUNG, V., FU, B., PARRISH, D. D., HOLLOWAY, J., WILLIAMS, J., ROBERTS, J. M., RYERSON, T. B. & FEHSENFELD, F. C. 1998. Atmospheric chemistry and distribution of formaldehyde and several multioxygenated carbonyl compounds during the 1995 Nashville/Middle Tennessee Ozone Study. *Journal of Geophysical Research: Atmospheres,* 103**,** 22449-22462.

LEWIS, A. C., CARSLAW, N., MARRIOTT, P. J., KINGHORN, R. M., MORRISON, P., LEE, A. L., BARTLE, K. D. & PILLING, M. J. 2000. A larger pool of ozone-forming carbon compounds in urban atmospheres. *Nature,* 405**,** 778-781.

LI, X., BRAUERS, T., HOFZUMAHAUS, A., LU, K., LI, Y. P., SHAO, M., WAGNER, T. & WAHNER, A. 2013. MAX-DOAS measurements of NO_2, HCHO and CHOCHO at a rural site in Southern China. *Atmos. Chem. Phys.,* 13**,** 2133-2151.

LIU, W., ZHANG, J., KWON, J., WEISEL, C., TURPIN, B., ZHANG, L., KORN, L., MORANDI, M., STOCK, T. & COLOME, S. 2006. Concentrations and source characteristics of airborne carbonyl compounds measured outside urban residences. *J Air Waste Manag Assoc,* 56**,** 1196-204.

LORRAIN, J. M., FORTUNE, C. R. & DELLINGER, B. 1981. Sampling and ion chromatographic determination of formaldehyde and acetaldehyde. *Analytical Chemistry,* 53**,** 1302-1305.

LOU, S., HOLLAND, F., ROHRER, F., LU, K., BOHN, B., BRAUERS, T., CHANG, C. C., FUCHS, H., HÄSELER, R. & KITA, K. 2010. Atmospheric OH reactivities in the Pearl River Delta - China in summer 2006: measurement and model results. *Atmos. Chem. Phys,* 10**,** 11243-11260.

LOWE, D. C. & SCHMIDT, U. 1983. Formaldehyde (HCHO) measurements in the nonurban atmosphere. *Journal of Geophysical Research: Oceans,* 88**,** 10844-10858.

MAAS, R. & GREENFELT, P. E. 2016. *Towards Cleaner Air. Scientific Assessment Report,* Oslo, United Nations Economic Commission for Europe.

MACDONALD, S. M., OETJEN, H., MAHAJAN, A. S., WHALLEY, L. K., EDWARDS, P. M., HEARD, D. E., JONES, C. E. & PLANE, J. M. C. 2012. DOAS measurements of formaldehyde and glyoxal above a south-east Asian tropical rainforest. *Atmos. Chem. Phys.,* 12**,** 5949-5962.

MAHAJAN, A. S., WHALLEY, L. K., KOZLOVA, E., OETJEN, H., MENDEZ, L., FURNEAUX, K. L., GODDARD, A., HEARD, D. E., PLANE, J. M. C.

& SAIZ-LOPEZ, A. 2011. DOAS observations of formaldehyde and its impact on the HOx balance in the tropical Atlantic marine boundary layer. *Journal of Atmospheric Chemistry,* 66**,** 167-178.

MANN, B. & GRAYESKI, M. L. 1987. New chemiluminescent derivatizing agent for the analysis of aldehydes and ketones by high-performance liquid chromatography with peroxyoxalate chemiluminescence. *Journal of Chromatography A,* 386**,** 149-158.

MAO, J. Q., REN, X. R., CHEN, S. A., BRUNE, W. H., CHEN, Z., MARTINEZ, M., HARDER, H., LEFER, B., RAPPENGLUCK, B., FLYNN, J. & LEUCHNER, M. 2010. Atmospheric oxidation capacity in the summer of Houston 2006: Comparison with summer measurements in other metropolitan studies. *Atmospheric Environment,* 44**,** 4107-4115.

MCGRATH, J., MAULDIN, L. & KOSCIUCH, E. OH and OH Reactivity Measurements during the OASIS Campaign at Barrow, Alaska. Americal Geophysical Union, Fall Meeting 2009, 2009 San Francisco.

MCGRATH, J. A. 2010. *Measurements of hydroxyl radical reactivity using a chemical ionization mass spectrometry technique.* PhD, University of Colarado at Boulder.

MICHOUD, V., HANSEN, R. F., LOCOGE, N., STEVENS, P. S. & DUSANTER, S. 2015. Detailed characterizations of the new Mines Douai comparative reactivity method instrument via laboratory experiments and modeling. *Atmos. Meas. Tech.,* 8**,** 3537-3553.

MILFORD, J. B., GAO, D., SILLMAN, S., BLOSSEY, P. & RUSSELL, A. G. 1994. Total reactive nitrogen (NO y) as an indicator of the sensitivity of ozone to reductions in hydrocarbon and NO x emissions. *Journal of Geophysical Research: Atmospheres,* 99**,** 3533-3542.

MÖHLMANN, G. R. 1985. Formaldehyde Detection in Air by Laser-Induced Fluorescence. *Applied Spectroscopy,* 39**,** 98-101.

MUNGER, J. W., JACOB, D. J., DAUBE, B. C., HOROWITZ, L. W., KEENE, W. C. & HEIKES, B. G. 1995. Formaldehyde, glyoxal, and methylglyoxal in air and cloudwater at a rural mountain site in central Virginia. *Journal of Geophysical Research: Atmospheres,* 100**,** 9325-9333.

NAZAROFF, W. W. & WESCHLER, C. J. 2004. Cleaning products and air fresheners: exposure to primary and secondary air pollutants. *Atmospheric Environment,* 38**,** 2841-2865.

NÖLSCHER, A. C., SINHA, V., BOCKISCH, S., KLÜPFEL, T. & WILLIAMS, J. 2012a. A new method for total OH reactivity measurements using a fast Gas Chromatographic Photo-Ionization Detector (GC-PID). *Atmos. Meas. Tech. Discuss.,* 5**,** 3575-3609.

NÖLSCHER, A. C., WILLIAMS, J., SINHA, V., CUSTER, T., SONG, W., JOHNSON, A. M., AXINTE, R., BOZEM, H., FISCHER, H., POUVESLE, N., PHILLIPS, G., CROWLEY, J. N., RANTALA, P., RINNE, J., KULMALA, M., GONZALES, D., VALVERDE-CANOSSA, J., VOGEL, A., HOFFMANN, T., OUWERSLOOT, H. G., VILÃ -GUERAU DE ARELLANO, J. & LELIEVELD, J. 2012b. Summertime total OH reactivity measurements from boreal forest during HUMPPA-COPEC 2010. *Atmos. Chem. Phys.,* 12**,** 8257-8270.

O'BRIEN, R. J. & HARD, T. M. 1993. Tropospheric hydroxyl radical. *In:* NEWMAN, L. (ed.) *Measurement challenges in atmospheric chemistry.* 1 ed. Washington: American Chemical Society.

PALMER, P. I., JACOB, D. J., CHANCE, K., MARTIN, R. V., SPURR, R. J. D., KUROSU, T. P., BEY, I., YANTOSCA, R., FIORE, A. & LI, Q. 2001. Air mass factor formulation for spectroscopic measurements from satellites: Application to formaldehyde retrievals from the Global Ozone Monitoring Experiment. *Journal of Geophysical Research: Atmospheres,* 106**,** 14539-14550.

PALMER, P. I., JACOB, D. J., FIORE, A. M., MARTIN, R. V., CHANCE, K. & KUROSU, T. P. 2003. Mapping isoprene emissions over North America using formaldehyde column observations from space. *Journal of Geophysical Research: Atmospheres,* 108**,** n/a-n/a.

REN, X., BRUNE, W. H., MAO, J., MITCHELL, M. J., LESHER, R. L., SIMPAS, J. B., METCALF, A. R., SCHWAB, J. J., CAI, C., LI, Y., DEMERJIAN, K. L., FELTON, H. D., BOYNTON, G., ADAMS, A., PERRY, J., HE, Y., ZHOU, X. & HOU, J. 2006a. Behavior of OH and HO2 in the winter atmosphere in New York City. *Atmospheric Environment,* 40, Supplement 2**,** 252-263.

REN, X., BRUNE, W. H., OLIGER, A., METCALF, A. R., SIMPAS, J. B., SHIRLEY, T., SCHWAB, J. J., BAI, C., ROYCHOWDHURY, U., LI, Y., CAI, C., DEMERJIAN, K. L., HE, Y., ZHOU, X., GAO, H. & HOU, J. 2006b. OH, HO2, and OH reactivity during the PMTACS-NY Whiteface Mountain 2002 campaign: Observations and model comparison. *J. Geophys. Res,* 111**,** D10S03.

REN, X., EDWARDS, G. D., CANTRELL, C. A., LESHER, R. L., METCALF, A. R., SHIRLEY, T. & BRUNE, W. H. 2003a. Intercomparison of peroxy radical measurements at a rural site using laser-induced fluorescence and Peroxy Radical Chemical Ionization Mass Spectrometer (PerCIMS) techniques. *J. Geophys. Res.,* 108**,** 4605.

REN, X., HARDER, H., MARTINEZ, M., LESHER, R. L., OLIGER, A., SHIRLEY, T., ADAMS, J., SIMPAS, J. B. & BRUNE, W. H. 2003b. HO_x concentrations and OH reactivity observations in New York City during PMTACS-NY2001. *Atmospheric Environment,* 37**,** 3627-3637.

REN, X., HARDER, H., MARTINEZ, M., LESHER, R. L., OLIGER, A., SIMPAS, J. B., BRUNE, W. H., SCHWAB, J. J., DEMERJIAN, K. L., HE, Y., ZHOU, X. & GAO, H. 2003c. OH and HO2 Chemistry in the urban atmosphere of New York City. *Atmospheric Environment,* 37**,** 3639-3651.

REN, X., OLSON, J. R., CRAWFORD, J. H., BRUNE, W. H., MAO, J., LONG, R. B., CHEN, Z., CHEN, G., AVERY, M. A., SACHSE, G. W., BARRICK, J. D., DISKIN, G. S., HUEY, L. G., FRIED, A., COHEN, R. C., HEIKES, B., WENNBERG, P. O., SINGH, H. B., BLAKE, D. R. & SHETTER, R. E. 2008. HOx chemistry during INTEX-A 2004: Observation, model calculation, and comparison with previous studies. *Journal of Geophysical Research: Atmospheres,* 113**,** n/a-n/a.

REN, X. R., BRUNE, W. H., CANTRELL, C. A., EDWARDS, G. D., SHIRLEY, T., METCALF, A. R. & LESHER, R. L. 2005. Hydroxyl and peroxy radical chemistry in a rural area of Central Pennsylvania: Observations and model comparisons. *Journal of atmospheric chemistry,* 52**,** 231-257.

SADANAGA, Y., YOSHINO, A., KATO, S. & KAJII, Y. 2005. Measurements of OH Reactivity and Photochemical Ozone Production in the Urban Atmosphere. *Environmental Science & Technology,* 39**,** 8847-8852.

SADANAGA, Y., YOSHINO, A., KATO, S., YOSHIOKA, A., WATANABE, K., MIYAKAWA, Y., HAYASHI, I., ICHIKAWA, M., MATSUMOTO, J.,

NISHIYAMA, A., AKIYAMA, N., KANAYA, Y. & KAJII, Y. 2004a. The importance of NO2 and volatile organic compounds in the urban air from the viewpoint of the OH reactivity. *Geophys. Res. Lett.,* 31**,** L08102.

SADANAGA, Y., YOSHINO, A., WATANABE, K., YOSHIOKA, A., WAKAZONO, Y., KANAYA, Y. & KAJII, Y. 2004b. Development of a measurement system of OH reactivity in the atmosphere by using a laser-induced pump and probe technique. *Review of Scientific Instruments,* 75**,** 2648-2655.

SALTHAMMER, T., MENTESE, S. & MARUTZKY, R. 2010. Formaldehyde in the Indoor Environment. *Chemical Reviews,* 110**,** 2536-2572.

SANDER, S. P., FRIEDL, R. R., GOLDEN, D. M., KURYLO, M. J., HUIE, R. E., ORKIN, V. L., MOORTGAT, G. K., RAVISHANKARA, A. R., KOLB, C. E., MOLINA, M. J. & FINLAYSON-PITTS, B. J. 2003. Chemical kinetics and photochemical data for use in atmospheric studies. *JPL Publication,* 02-25.

SAUNDERS, S. M., JENKIN, M. E., DERWENT, R. G. & PILLING, M. J. 2003. Protocol for the development of the Master Chemical Mechanism, MCM v3 (Part A): tropospheric degradation of non-aromatic volatile organic compounds. *Atmospheric Chemistry and Physics,* 3**,** 161-180.

SEPTON, J. C. & KU, J. C. 1982. Workplace air sampling and polarographic determination of formaldehyde. *Am Ind Hyg Assoc J,* 43**,** 845-52.

SHIRLEY, T. R., BRUNE, W. H., REN, X., MAO, J., LESHER, R., CARDENAS, B., VOLKAMER, R., MOLINA, L. T., MOLINA, M. J., LAMB, B., VELASCO, E., JOBSON, T. & ALEXANDER, M. 2006. Atmospheric oxidation in the Mexico City metropolitan area (MCMA) during April 2003. *Atmospheric Chemistry and Physics,* 6**,** 2753-2765.

SILLMAN, S. 1999. The relation between ozone, NOx and hydrocarbons in urban and polluted rural environments. *Atmospheric Environment,* 33**,** 1821-1845.

SILLMAN, S. & HE, D. 2002. Some theoretical results concerning O3-NOx-VOC chemistry and NOx-VOC indicators. *Journal of Geophysical Research: Atmospheres,* 107**,** ACH 26-1-ACH 26-15.

SINHA, V., WILLIAMS, J., CROWLEY, J. N. & LELIEVELD, J. 2008. The Comparative Reactivity Method – a new tool to measure total OH Reactivity in ambient air. *Atmos. Chem. Phys.,* 8**,** 2213-2227.

SINHA, V., WILLIAMS, J., DIESCH, J. M., DREWNICK, F., MARTINEZ, M., HARDER, H., REGELIN, E., KUBISTIN, D., BOZEM, H., HOSAYNALI-BEYGI, Z., FISCHER, H., ANDRÃ©S-HERNÃ¡NDEZ, M. D., KARTAL, D., ADAME, J. A. & LELIEVELD, J. 2012. Constraints on instantaneous ozone production rates and regimes during DOMINO derived using in-situ OH reactivity measurements. *Atmos. Chem. Phys.,* 12**,** 7269-7283.

SINHA, V., WILLIAMS, J., LELIEVELD, J., RUUSKANEN, T. M., KAJOS, M. K., PATOKOSKI, J., HELLEN, H., HAKOLA, H., MOGENSEN, D. & BOY, M. 2010. OH reactivity measurements within a boreal forest: evidence for unknown reactive emissions. *Environmental science & technology,* 44**,** 6614-6620.

SMITH, G. P. & CROSLEY, D. R. 1990. A photochemical model of ozone interference effects in laser detection of tropospheric OH. *Journal of Geophysical Research: Atmospheres,* 95**,** 16427-16442.

SMITH, S. C. 2007. *Atmospheric measurements of OH and HO_2 using the FAGE technique: Instrument development and data analysis.* PhD, University of Leeds.

STONE, D., WHALLEY, L. K. & HEARD, D. E. 2012. Tropospheric OH and HO2 radicals: field measurements and model comparisons. *Chemical Society Reviews,* 41**,** 6348-6404.

STONE, D., WHALLEY, L. K., INGHAM, T., EDWARDS, P. M., CRYER, D. R., BRUMBY, C. A., SEAKINS, P. W. & HEARD, D. E. 2016. Measurement of OH reactivity by laser flash photolysis coupled with laser-induced fluorescence spectroscopy. *Atmos. Meas. Tech.,* 9**,** 2827-2844.

TAATJES, C. A., SHALLCROSS, D. E. & PERCIVAL, C. J. 2014. Research frontiers in the chemistry of Criegee intermediates and tropospheric ozonolysis. *Physical Chemistry Chemical Physics,* 16**,** 1704-1718.

UHDE, E. & SALTHAMMER, T. 2007. Impact of reaction products from building materials and furnishings on indoor air quality—A review of recent advances in indoor chemistry. *Atmospheric Environment,* 41**,** 3111-3128.

WALLINGTON, T. J. 1986. Kinetics of the gas phase reaction of OH radicals with pyrrole and thiophene. *International Journal of Chemical Kinetics,* 18**,** 487-496.

WAYNE, R. P. 2000. *Chemistry of Atmospheres,* New York, Oxford University Press.

WHALLEY, L. K., EDWARDS, P. M., FURNEAUX, K. L., GODDARD, A., INGHAM, T., EVANS, M. J., STONE, D., HOPKINS, J. R., JONES, C. E., KARUNAHARAN, A., LEE, J. D., LEWIS, A. C., MONKS, P. S., MOLLER, S. J. & HEARD, D. E. 2011. Quantifying the magnitude of a missing hydroxyl radical source in a tropical rainforest. *Atmos. Chem. Phys.,* 11**,** 7223-7233.

WHALLEY, L. K., STONE, D., BANDY, B., DUNMORE, R., HAMILTON, J. F., HOPKINS, J., LEE, J. D., LEWIS, A. C. & HEARD, D. E. 2016. Atmospheric OH reactivity in central London: observations, model predictions and estimates of in situ ozone production. *Atmos. Chem. Phys.,* 16**,** 2109-2122.

WOOD, E. C. & COHEN, R. C. 2006. Fluorescence Methods. *In:* HEARD, D. E. (ed.) *Analytical techniques for atmospheric measurement.* Oxford: Blackwell.

WORLD HEALTH ORGANISATION, W. 2005. Air Quality Guidelines Global Update 2005.

YANG, Y., SHAO, M., WANG, X., NÖLSCHER, A. C., KESSEL, S., GUENTHER, A. & WILLIAMS, J. 2016. Towards a quantitative understanding of total OH reactivity: A review. *Atmospheric Environment,* 134**,** 147-161.

YASSAA, N., SONG, W., LELIEVELD, J., VANHATALO, A., BÄCK, J. & WILLIAMS, J. 2012. Diel cycles of isoprenoids in the emissions of Norway spruce, four Scots pine chemotypes, and in Boreal forest ambient air during HUMPPA-COPEC-2010. *Atmos. Chem. Phys.,* 12**,** 7215-7229.

YOSHINO, A., NAKASHIMA, Y., MIYAZAKI, K., KATO, S., SUTHAWAREE, J., SHIMO, N., MATSUNAGA, S., CHATANI, S., APEL, E., GREENBERG, J., GUENTHER, A., UENO, H., SASAKI, H., HOSHI, J.-Y., YOKOTA, H., ISHII, K. & KAJII, Y. 2012. Air quality diagnosis from comprehensive observations of total OH reactivity and reactive trace species in urban central Tokyo. *Atmospheric Environment,* 49**,** 51-59.

YOSHINO, A., SADANAGA, Y., WATANABE, K., KATO, S., MIYAKAWA, Y., MATSUMOTO, J. & KAJII, Y. 2006. Measurement of total OH reactivity

by laser-induced pump and probe technique - comprehensive observations in the urban atmosphere of Tokyo. *Atmospheric Environment,* 40**,** 7869-7881.

ZANNONI, N., GROS, V., LANZA, M., SARDA, R., BONSANG, B., KALOGRIDIS, C., PREUNKERT, S., LEGRAND, M., JAMBERT, C., BOISSARD, C. & LATHIERE, J. 2016. OH reactivity and concentrations of biogenic volatile organic compounds in a Mediterranean forest of downy oak trees. *Atmos. Chem. Phys.,* 16**,** 1619-1636.

Chapter 2 - Experimental Methods

2.1 Overview

The first part of this chapter (Section 2.2) describes a LFP-LIF instrument used for the measurement of OH reactivity in the atmosphere. The exploitation of this instrument during two field campaigns is described in Chapters 5 and 6 and observations are also presented. In Chapter 3 measurements are presented from an inter-comparison study where multiple instruments utilising a range of techniques were used to measure OH reactivity. The second part of this chapter (Section 2.3) describes a new LIF instrument for the measurement of HCHO, this instrument was first used in the laboratory in experiments to characterise an OH flow reactor as part of a new instrument for the identification of 'missing' OH reactivity (Chapter 4). The first deployments of the HCHO LIF instrument to the field are detailed in Chapters 5 and 6 where observations are also presented.

2.2 Measurement of OH reactivity

2.2.1 Instrument overview and principle of operation

The measurements of OH reactivity presented in this work were all made using the Leeds laser flash photolysis coupled with laser induced fluorescence (LFP-LIF) instrument. Light from a 266 nm laser is pulsed through a flow tube to photolyse ozone and produce $O(^1D)$ and $O_2(^1\Delta_g)$ (Matsumi and Kawasaki, 2003), R 2.1. The $O(^1D)$ produced subsequently reacts with water vapour to produce two molecules of OH, R 2.2.

$$O_3 + h\nu_{(266\,nm)} \rightarrow O(^1D) + O_2(^1\Delta_g) \qquad \textbf{R 2.1}$$

$$O(^1D) + H_2O \rightarrow + 2OH \qquad \textbf{R 2.2}$$

Following its production, in addition to physical losses, the OH is lost to reaction with any sinks that are present in the air that was sampled. This loss is observed in

real-time as a LIF signal from a FAGE cell for OH detection. The decay signal recorded is used to determine the OH reactivity of the sample through analysis of the exponent of the best fitting exponential decay function to the signal. Specific details regarding the determination of a raw OH loss rate ($k'_{OH(raw)}$) from a decay signal are presented in Section 2.1.7. To determine k'_{OH} from $k'_{OH(raw)}$ it is necessary to subtract a loss rate of OH due to physical processes occurring within the flow tube of the instrument, mainly diffusion of OH out of the photolysed volume sampled and wall loss. Specific details regarding the determination of $k'_{OH(physical)}$ are presented in Section 2.1.10.

When the LFP-LIF instrument was used to measure OH reactivity in the field for this work, levels of ambient ozone and water vapour were always sufficient to generate sufficient OH, via R2.1 and R2.2 for the instrument to operate. However, it is necessary to introduce ozone and water vapour in laboratory experiments, as these are not present in zero air or VOC standards, by irradiating some synthetic air with UV light and also passing some air through a water bubbler, to entrain water vapour. Irradiation of the air with UV light results in the production of ozone through photolysis of dioxygen, and subsequent reaction of oxygen atoms formed with dioxygen, R 2.3 and R 2.4.

$$O_2 + h\nu \rightarrow O(^3P) + O(^3P) \qquad \textbf{R 2.3}$$

$$O(^3P) + O_2 + M \rightarrow O_3 + M \qquad \textbf{R 2.4}$$

Figure 2.1 shows a schematic diagram of the Leeds laser flash photolysis instrument. The key features of the current configuration are labelled, however, it should be noted that the instrument was continually developed through the course of this work. Where measurements are described in later chapters a specific instrument configuration is referred to. Details of each configuration are provided in Section 2.2.8. In all configurations of the instrument ambient air is drawn through a stainless steel flow tube at ~0.14 m s^{-1} using a scroll pump, and the pressure inside flow tube is monitored using a pressure transducer (MKS 120AD). The 266 nm light is provided at a pulse repetition frequency of 1 Hz at 80 mJ, specific details of the laser used for this are provided in Section 2.1.3. The 266 nm light enters the flow tube via a fused silica window to produce a column of OH that is assumed to be radially uniform in concentration and generated through R 2.1 and R 2.2 as described above.

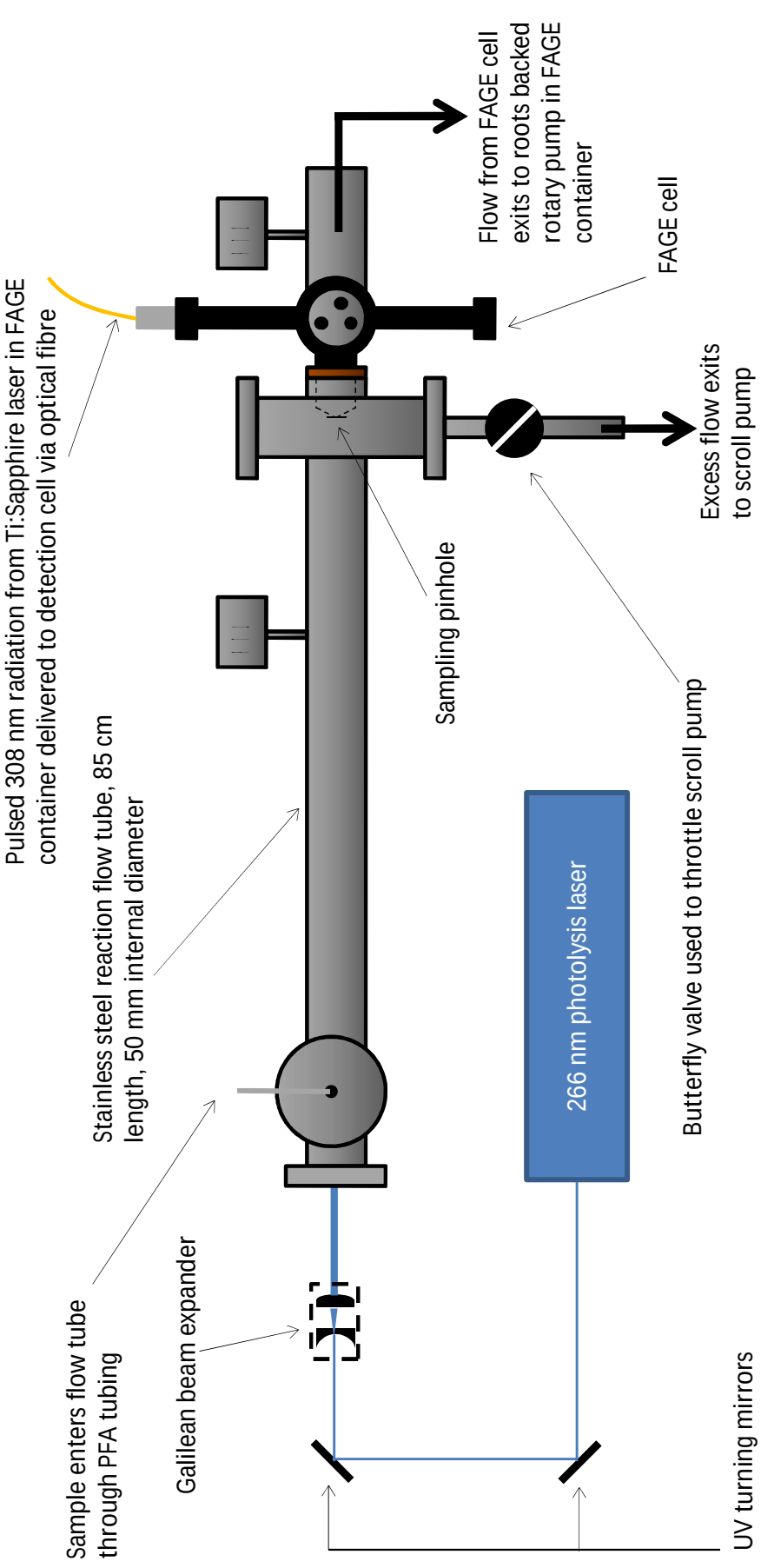

Figure 2.1: Schematic diagram of the Leeds laser flash photolysis instrument (not to scale). PT1 stands for pressure transducer 1 (MKS 120AD). PT2 stands for pressure transducer 2 (SENSOTEC 27806-017A).

The flow tube, FAGE cell and 266 nm laser head of the LFP-LIF instrument were securely fixed to an aluminium table top for all measurements of OH reactivity reported in this work, which was either kept on the roof of the FAGE container, inside the FAGE container or inside the laboratory. Figure 2.2 illustrates how the 266 nm laser, the flow tube, and the optics used to deliver 266 nm light into it were arranged on the table top.

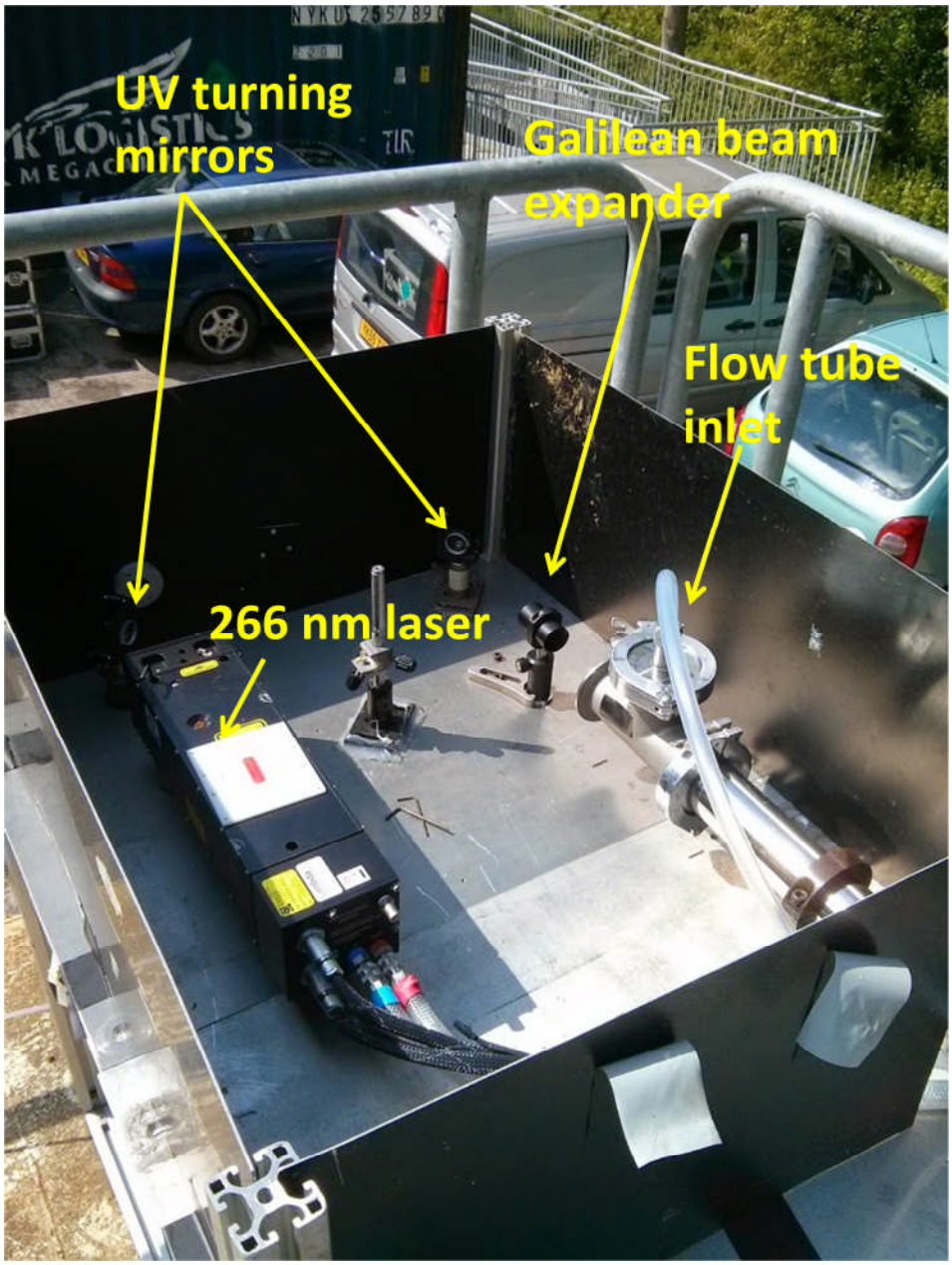

Figure 2.2: Photograph showing the 266 nm laser, and the optics used to deliver 266 nm light into the flow tube (also shown) of the LFP-LIF OH reactivity instrument. The components are shown fixed to an aluminium table top which can either be kept on the roof of the FAGE container for field measurements, or inside for laboratory measurements.

2.2.2 The Leeds FAGE container

The ground based FAGE instrument is housed within a shipping container that has been converted into a mobile laboratory, thus enabling easy transportation for *in situ* RO_x concentration and total OH reactivity measurements in a range of environments worldwide. The layout of the container, and the instrumentation used for the quantification of OH and HO_2 are summarised in Figure 2.3.

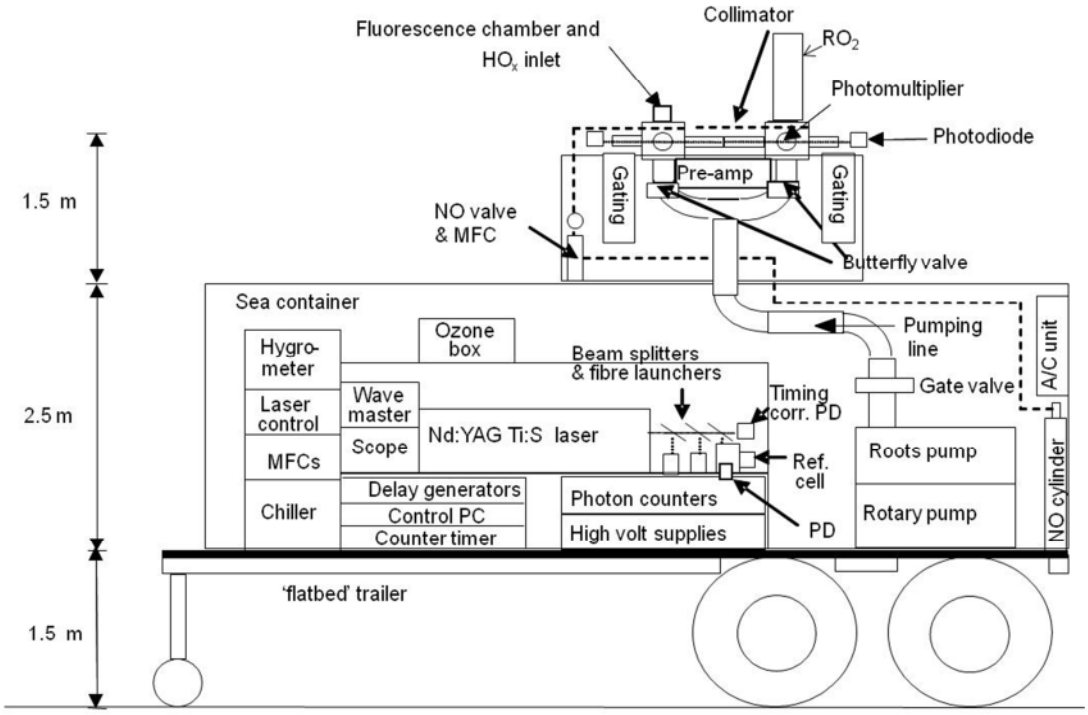

Figure 2.3: Diagram illustrating the key features of the Leeds FAGE shipping container, not to scale. Taken from Whalley et al. (2010).

Within the container electrical power is supplied to all apparatus, except for the vacuum system, via several uninterruptable power supplies (UPS). The vacuum system (roots backed by rotary pumps) is used to provide low pressure (~2 Torr each) to the two fluorescence cells shown on the roof, the reference cell and the cell of the laser flash photolysis OH lifetime instrument for measuring total OH reactivity (not shown here). The laser produces low energy high PRF UV light at 308 nm for OH detection by FAGE (the system is described in detail in section 2.2.2.). Optical fibre launchers (Elliot Gold) are used in conjunction with partially reflecting UV mirrors (beam splitters) to distribute 308 nm radiation from the optical bench to the various detection cells and the reference cell. The remaining laser power exiting the reference cell is monitored by a photodiode (New focus 2032) and

used in the normalisation of OH signals. Details of the laser wavelength drift correction system, detection and data acquisition systems, and the calibration system are all given in later sections.

2.2.3 The 266 nm photolysis laser

A Quantel USA CFR 200 lamp pumped solid state laser is used to produce 266 nm radiation for OH production (through R2.1 and R2.2) in the LFP-LIF instrument. The schematic diagram in Figure 2.4 summarises the key optical components of this laser and the delivery of 266 nm light to the flow tube of the instrument.

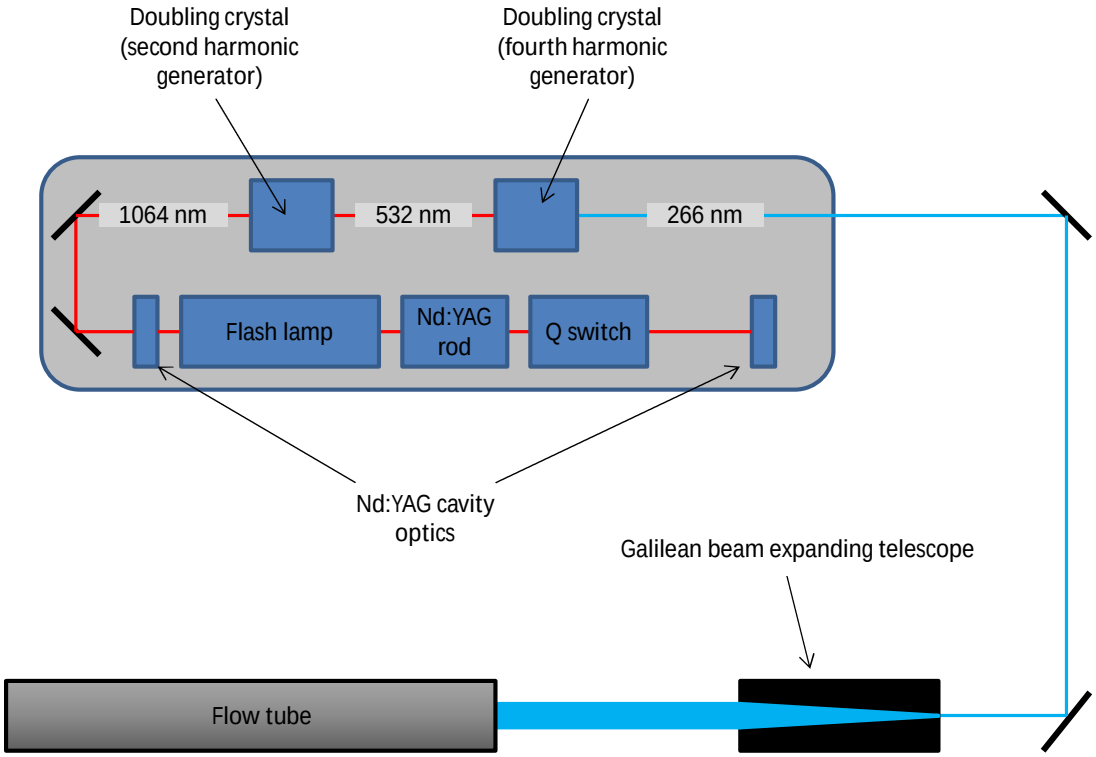

Figure 2.4: Schematic of the Quantel USA CFR 200 lamp pumped solid state laser used in the University of Leeds flash photolysis instrument for OH lifetime. The path of the beam within the laser head is for illustrative purposes only. Detail of the flow tube is shown in Figure **2.1**.

In order to generate the 266 nm light, pulsed infra-red (1064 nm) radiation is produced using an optical cavity which houses a flash lamp, Nd:YAG rod and Q-switch containing a $LiNbO_3$ crystal. The flash lamp is used to pump the Nd:YAG rod with broadband IR radiation, causing excitation of Neodymium ions and consequently allowing the creation of a population inversion. As relaxation occurs from the excited state, photons are emitted from the Nd:YAG rod into the cavity where they are attenuated by the Q-switch. When the population inversion becomes

sufficient, the Q-switch is turned on and radiation within the cavity is no longer attenuated; it becomes available to stimulate the Nd:YAG rod and cause mass release of photons through relaxation of the Neodymium ion population inversion. The result is a large pulse of laser radiation at 1064 nm. Subsequently this pulse is passed through two doubling crystals to generate fourth harmonic ultra violet radiation at 266 nm which is outputted by the laser head. This light is delivered to the flow tube of the instrument via a Galilean beam expanding telescope which expands the beam diameter to ~10 mm. The beam expander consisted of a fused silica plano concanve lens (F = -30 mm, D = 25.4 mm, LC4252, ThorLabs) and a fused silica plano convex lens (F = 50 mm, D = 25.4 mm, LA4148, ThorLabs) which were housed in a lens tube (SM1M20, ThorLabs) and separated by 20 mm. The laser head is powered and controlled by an Integrated Cooler and Electronics unit (ICE^{450}) and is securely attached to the instrument bench top by three metal supports.

2.2.4 The flow tube and FAGE cell

The flow tube has been designed so that when the instrument is in operation it contains a laminar flow profile within, which is essential as the diameter of the flash photolysis laser pulse (~10 mm) is much less than the diameter of the flow tube (~50 mm). If the flow profile was non-laminar, the rates of OH diffusion in and out of the column of generated OH would be higher due to turbulence, and consequently also the value of $k'_{OH(zero)}$. In a laminar flow regime there is a velocity gradient acting radially across the flow tube meaning that molecules further away from the centre move slower meaning that diffusion of OH out of the photolysed volume is slower. The distribution of flow velocities across the flow velocities is currently uncharacterised and should be studied in future characterisation experiments. However, the Reynolds number (R_e) for flow within the tube is ~450, corresponding to laminar flow, R_e is calculated using E 2.4.

$$R_e = \frac{\rho v D}{\mu} \qquad \textbf{E 2.1}$$

ρ is the density of gas flowing through the tube, v is the mean velocity of the gas (~0.14 m s^{-1}), D is the diameter of the flow tube and μ is the dynamic viscosity of the gas. E 2.4 shows that R_e is independent of length of the flow tube.

The cell of the LFP-LIF OH reactivity instrument, shown in Figure 2.5 detects OH using the FAGE technique, as described in Section 1.3. It is constructed from a 15 cm cube of black anodised aluminium. Holes have been machined through each face to produce a cavity inside and to allow the fitting of the sampling inlet, photomultiplier tube, side arms, reflector and connection to the vacuum pump. The inlet shown here was used in configuration 1 of the LFP-LIF OH reactivity instrument.

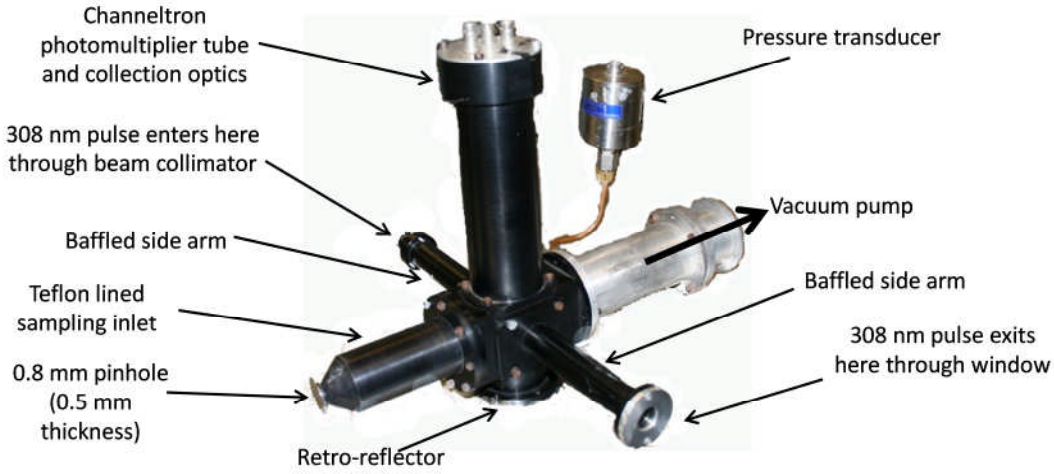

Figure 2.5: Labelled photograph of the FAGE fluorescence cell of the LFP-LIF OH reactivity instrument.

In all instrument configurations a collimator (Oz Optics, HPUCO-23A-308-M-25PQ) is used to deliver the 308 nm beam from the optical fibre to the baffled side entrance arm. The baffles within the side arms and the black anodised coating are used to reduce scatter of the 308 nm beam, thus minimising the background signal observed by the detector.

Fluorescence photons are detected perpendicular to the axis of the laser using a gated channeltron photomultiplier (CPM, Perkin Elmer C934P). A description of the method used for gating the CPM and recording a LIF signal is presented in Section 2.2.6. Fluorescence photons are focussed onto the photocathode of the CPM by a series of optics. First in the series was a biconvex collimating lens (Melles-Griot, focal length = 50 mm at λ = 546.1, diameter = 50 mm) which was followed by a narrow band UV interference filter (Barr Associates Inc, 308 nm). Finally the fluorescence was delivered to the CPM by two plano-convex focusing lenses (UGQ Optics Ltd, focal length = 75 mm at λ = 250 nm, diameter = 50 mm). To boost the

fluorescence signal a retro-reflector (CVI Optics fused silica plano concave spherical mirror, high UV reflectance coating) is used to maximise the photons that are focussed onto the CPM photocathode.

It is not essential to know the sensitivity of this detection cell when measuring total OH reactivity, but with better sensitivity, the signal to noise ratio for the decay measured after each photolysis pulse will be improved. When the signal to noise ratio is maximised OH decay signals can be integrated over a shorter period of time, improving the time resolution for measurements of total OH reactivity. For example, in urban atmospheres, the loading of VOCs, and consequently the OH reactivity, can change rapidly. For example in London spikes in OH reactivity of up to ~ 60 s^{-1} have been observed over the course of a ~5 minutes (Whalley et al., 2016). Therefore it is important that changes in OH reactivity are observable on the shortest timescale possible in order to fully investigate any potential sources.

2.2.5 The 308 nm detection laser

A solid state Nd:YAG pumped Ti:Sapphire laser is used to produce 308 nm UV light for the detection of OH in the FAGE cell of the LFP-LIF OH reactivity instrument. A Photonics Industries DS-532-18 Nd:YAG laser was used to pump the Ti:Sapphire cavity for this. Inside the laser head broadband near IR laser radiation at >30 W from diodes is used to pump a Q-switched Nd:YAG rod cavity with an intra-cavity doubling crystal. Green light at 532 nm (~10 W) with a PRF of 5 kHz exits this cavity and subsequently the Nd:YAG laser head. The green light is focussed and guided to a cavity containing a Ti:Sapphire crystal that is pumped to produce near IR radiation in the range 690 – 1000 nm. A series of prisms is then used to expand the beam onto a rotatable diffraction grating, the angle of which is used to tune the wavelength of the near IR beam to 924 nm which exits the Ti:Sapphire cavity with a power of ~1.6 W. Following this the beam is refocused and a portion is frequency doubled by a second harmonic generator (SHG) crystal to produce 462 nm radiation; this is then sum frequency mixed in a third harmonic generator (THG) crystal with residual 924 nm radiation to produce 308 nm radiation at ~80 mW. The schematic in Figure 2.6 illustrates the key optical components of the 308 nm laser used for OH detection in the FAGE cell of the LFP-LIF OH reactivity instrument.

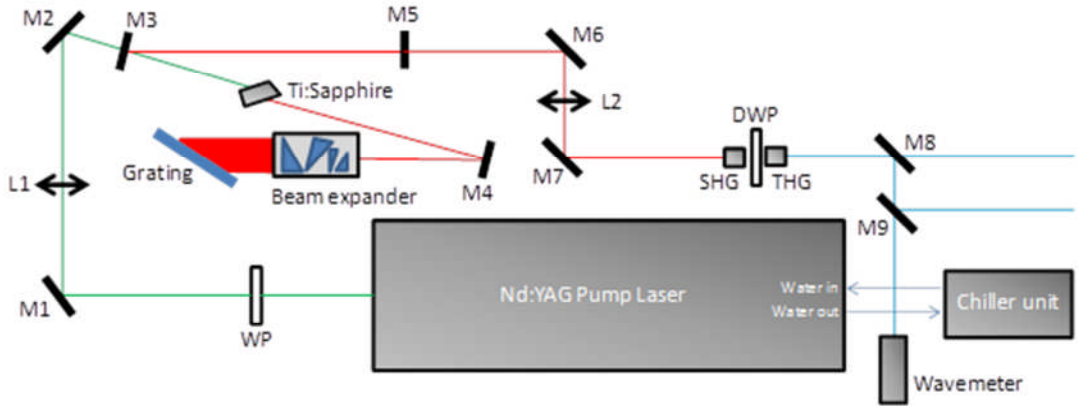

Figure 2.6: Schematic of the Nd:YAG (DS-532-18) pumped Ti:Sapphire detection laser of the Leeds ground based FAGE instrument. M1 and M2 are 532 nm turning mirrors; M3 and M4 are input couplers (high transmittance at 532 nm and high reflectance and 924 nm; M5 is an output coupler; M6 and M7 are 924 nm turning mirrors; M8 and M9 are 308 nm turning mirrors; L1 and L2 are focussing lenses; WP is a half waveplate at 532 nm; DWP is a half / full waveplate at 462 / 924 nm; SHG and THG are second and third harmonic generators (both Cesium Lithium Borate crystals).

The wavelength of the 308 nm laser described above is grating tuned to ensure that the LIF response from OH is maximised; this is achieved through the use of a reference cell (kept at ~2 Torr). A small flow of ambient air is pumped through a water bubbler to this reference cell where there is a hot wire filament supplied with 5 V at a current of 5 A. Thermolysis of water vapour results in OH production at levels several orders of magnitude higher than what is often present in ambient air. The reference cell is fitted with a CPM and gating (Section 2.2.6) is not required as the OH signal is large compared to the scattered light signal. Diffraction tuning of the 308 nm laser wavelength is achieved by rotating the diffraction grating within the Ti:Sapphire cavity using a computer controlled stepper motor. This enables a range of wavelengths in the 308 nm region to be systematically swept. The FAGE data collection software monitors the reference cell OH signal detected by the CPM during this process. The wavelength of blue light exiting the Ti:Sapphire laser is monitored using a Coherent Wavemaster 33-2650, with 1 pm accuracy. After the range of wavelengths has been swept, the position of the diffraction grating is readjusted automatically so that the OH signal detected in the reference cell is again at its maximum (within 95 %). When the diffraction grating resides in this position the wavelength of the 308 nm laser is considered to be ‘online’. The wavelength is fixed online for a pre-set period of time during which it is possible to record OH decay signals. The process of sweeping the wavelength and recording OH signal is

repeated continuously during field measurements of ambient OH. The time over which OH signal is measured can be adjusted, however this is typically ~5 minutes. A signal is also recorded for a shorter period of time when the laser is not at the correct wavelength to measure OH. This signal is due to laser background scatter and can be subtracted from ambient measurements, and is typically 1-2 counts per mW of laser light. Images of a reference cell and a typical sequence for the reference cell signal are shown in Figure 2.7

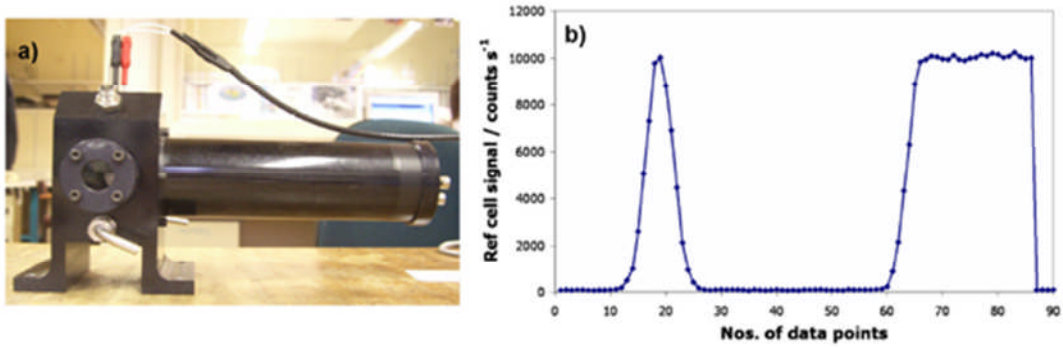

Figure 2.7: a) photograph of the reference cell used in the Leeds ground based FAGE instrument. b) a typical reference cell signal over time. Taken from (Smith, 2007)

2.2.6 Data acquisition

Two delay generators are used in the control system for the Leeds flash photolysis OH reactivity instrument, because during the measurement of a single OH decay, the OH detection timings are on a much smaller scale (200 μs between laser pulses) than the photolysis pulse and data collection timings (which occur every 1 s). t_0 is externally set by the delay generator that triggers the 308 nm laser.

A SRS (SRS-DG535) delay generator is used to control processes involved in OH detection during decays. Figure 2.8 illustrates the processes that are implemented by this delay generator for measurement following a single pulse of the 308 nm probe laser.

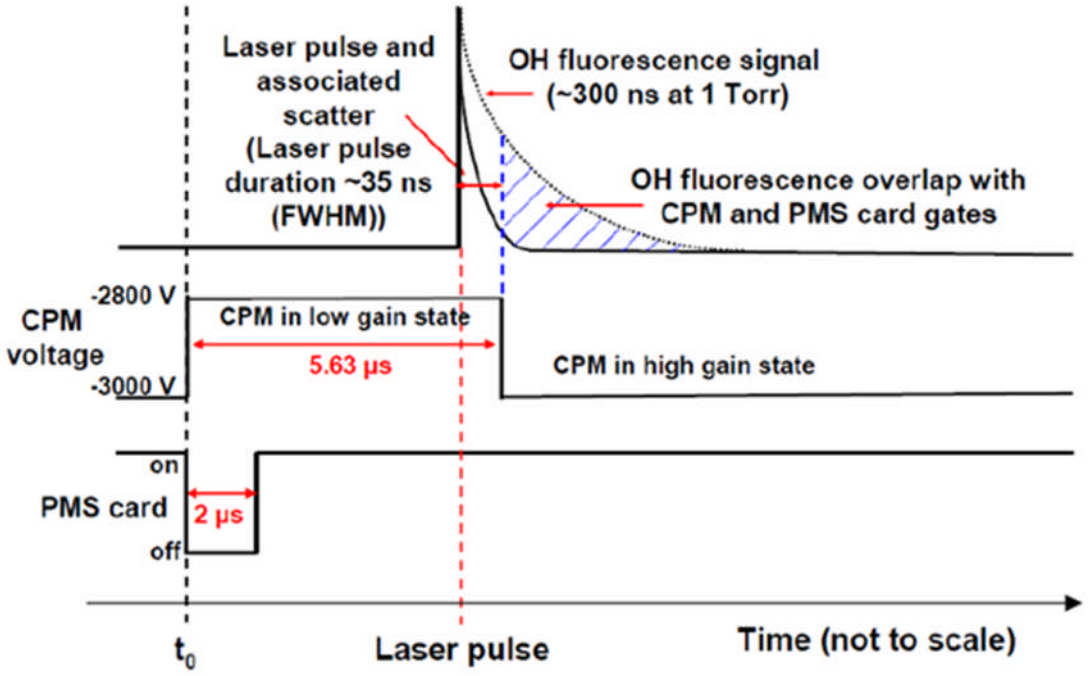

Figure 2.8: Schematic diagram to show timings controlled by the SRS delay generator for channel photomultiplier (CPM) and PMS card gating in the detection of the OH laser induced fluorescence. The fluorescence detected is indicated by the blue hatched region. Taken from Edwards (2011).

The CPM detector is held in a low gain state until after a pulse from the Ti:Sapphire laser (described in Section 2.2.5) and any associated scatter has decayed. The CPM is then switched to a high gain state by a gating box to record the LIF signal from the photolytically generated OH radicals. The processes depicted in Figure 2.8 are repeated every 200 μs (for each probe pulse) and these individual measurements of OH LIF signal can be used to construct an OH chemical decay following each photolysis laser pulse. One decay is recorded for each pulse of 266 nm light and the individual decay signals are summed over a set period of time before being written into memory on the instrument computer.

A Berkeley Nucleonics Corporation (BNC-555) delay generator is used to control the frequency of photolysis laser pulses and also the data collection cycles for each OH decay measured. Figure 2.9 illustrates the processes that are controlled by this delay generator.

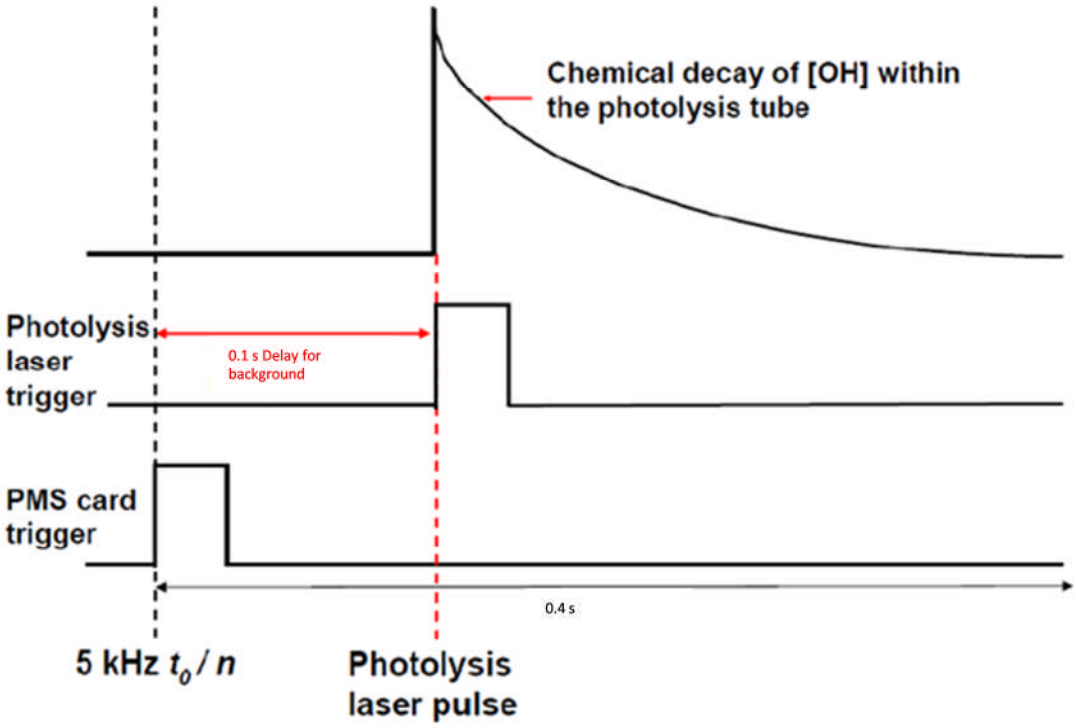

Figure 2.9: Schematic diagram to show timings of the photolysis laser and PMS card triggers controlled by the BNC delay generator. Adapted from Edwards (2011).

At the beginning of each decay measurement a photon counter card (Becker and Hickl, PMS200A) in the computer of the LFP-LIF instrument is triggered to start collecting data. The photolysis laser is delayed for 0.1s after this to allow for measurement of the background signal detected by the cell. The PMS card continues to record data for 0.3 s after this. The processes depicted in Figure 2.9 are repeated for each measurement of OH decay signals. The residence time of the gas within the flow tube is ~4 seconds meaning that during operation of the LFP-LIF instrument that same sample of gas is irradiated with 266 nm light multiple times. Tests where the repetition rate of the 266 nm laser was varied have shown that measurements are not impacted by the number of times the gas sample has been irradiated (Stone et al., 2016).

2.2.7 Instrument configurations

As a result of continual development of the LFP-LIF OH reactivity instrument through the course of this work, it is necessary here to describe two different configurations in which it was operated. configuration 1 was used for the measurements presented in Chapter 5 from the York 2014 ‘missing’ OH reactivity campaign. configuration 2 was used for the measurements presented in Chapter 6

from the integrated chemistry of ozone in the atmosphere (ICOZA) campaign, and also for measurements presented in Chapter 3 from comparison experiments at the SAPHIR chamber.

The biggest difference between configurations 1 and 2 was the FAGE cell inlet and method for pumping excess gas from the flow tube. In configuration 1 the inlet used was shown already in Figure 2.5. The inlet was lined with a nylon insert to reduce wall loss of OH prior to detection. A stainless steel circular disk (0.5mm thick) was positioned at the end of the inlet and held in place by evacuating the cell with a seal made by a rubber O-ring, this contained the sampling pinhole (0.8 mm diameter). The excess gas was removed by the scroll pump via a tube of the same dimensions as the flow tube however 50 cm in length. In configuration 2 a new inlet for the FAGE cell was fitted and the method for pumping out excess gas from the flow tube was changed as shown in Figure 2.10. In configuration 2 the gas exits radially compared to configuration 1 where it turned a corner (as shown in Figure 2.1). The pinhole (0.8 mm diameter) of the inlet was attached to a new flange which was fixed directly to the body of the FAGE cell. A short tube protruded from the FAGE cell and terminated in a KF50 flange which was connected to the end of the flow tube. The flange fixed to the FAGE cell had eight equally spaced holes perpendicular to the axis of the sampling pinhole to pump out excess gas from the flow tube. From these eight holes ~30 cm long ¼" internal diameter Teflon tubes were connected to a small metal chamber which connected to the scroll pump in order to pull gas through the flow tube.

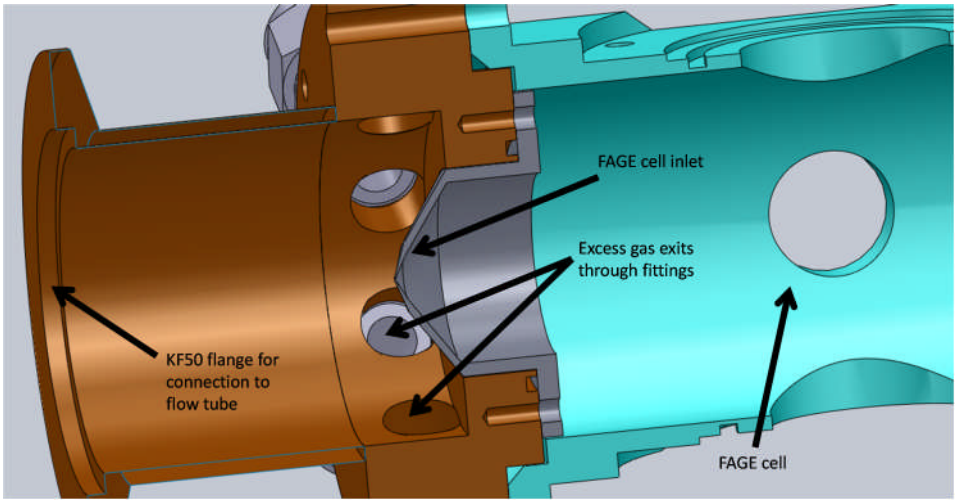

Figure 2.10: Cutaway scale diagram of the redesigned inlet attached to the FAGE cell of the LFP-LIF OH reactivity instrument. Provided by Dr. Trevor Ingham.

The system for pumping out excess gas radially around the pinhole was implemented as an attempt to achieve single exponential decaying OH signal. The new design was based on the hypothesis that the bi-exponential decays observed with the instrument in configuration 1 (discussed in Section 2.2.8) could have been due to turbulence in the flow sampled as it exited the flow tube by turning a corner. It was found that upon installation of the redesigned FAGE cell inlet single exponential OH signal decays were observed. Section 2.2.8 describes the methods used for determining $k'_{OH(raw)}$ values from OH decays recorded by the LFP-LIF instrument when operated in configurations 1 and 2.

2.2.8 Determination of $k'_{OH(raw)}$

As described above in Section 2.2.7 the LFP-LIF instrument was operated in one of two configurations for each set of OH reactivity measurements presented in this work. The profile of the OH LIF decay signals varied between these configurations. When the instrument was operated in configuration 1, all decays recorded exhibited two exponentially decaying components as the decays were bi-exponential. A rapid decrease in signal by a factor of ~2 in the first 0.05 s of the decay, followed by a decay in signal at a rate which varied with the OH reactivity of the gas sampled. The precise reason for the fast component at the beginning of the decays is unknown. It is, however, not exclusive to the Leeds LFP-LIF instrument. Sadanaga et al. (2004) reported such behaviour in their instrument. It is postulated that the reason for such behaviour of the Leeds LFP-LIF instrument in configuration 1 was somehow related to how the gas was sampled into the FAGE cell at the end of the reaction flow tube. Owing to time constraints prior to the deployment of the instrument (in configuration 1) for the York 2014 'missing' OH reactivity campaign (Chapter 5) it was not possible to fully investigate the cause of the bi-exponential decays described here. For OH decays recorded by the LFP-LIF instrument in configuration 1 a bi-exponential decaying (E 2.2) function was fitted in order to extract a value for $k'_{OH(raw)}$ following some processing of the decay signal.

$$\frac{(S_{OH})_t}{(S_{OH})_0} = C\exp\left(-k'_{OH(fast)}\right) + (1-C)\exp(-k'_{OH(raw)}) \qquad \textbf{E 2.2}$$

Each decay signal outputted by the LFP-LIF instrument was processed and a curve was fitted using an analysis program written in Python 2.7 and utilised the Scipy, Numpy and Matplotlib modules for ease of construction (McKinney, 2012, Walt et

al., 2011, Hunter, 2007). As 308 nm light for the detection of OH had a PRF of 5 kHz the time between pulses was 200 µs, photons were counted in 50 µs bins. Considering that the fluorescence lifetime of OH in a FAGE cell is on the order of a few 100 ns it is the case that between each photon counting bin where OH fluorescence signal is detected, there are three photon counting bins where no OH fluorescence signal is detected. Figure 2.11 summarises the timing of the OH fluorescence and non-fluorescence photon counting bins as they are recorded in the signal array that is outputted by the LFP-LIF instrument. Three bins containing no fluorescence signal are shown for every bin containing fluorescence signal.

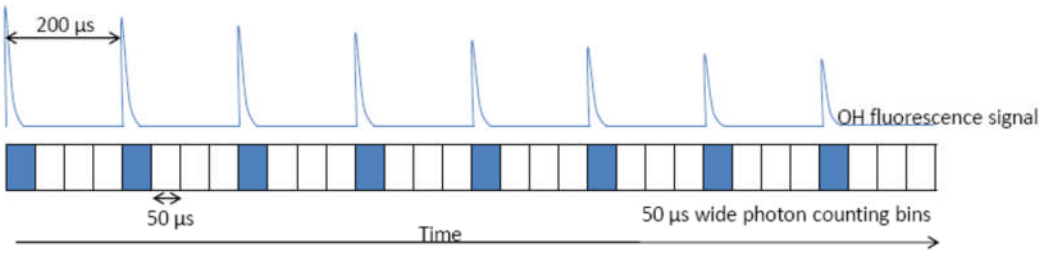

Figure 2.11: Schematic to represent the timing of the array of photon counting bins used to record OH decays in the LFP-LIF OH reactivity instrument. Blue blocks represent bins where photons from OH fluorescence are recorded (fluorescence bins) and clear blocks represent bins where OH fluorescence is not recorded (non-fluorescence bins). The OH LIF signal is seen to decay with time. Taken from Edwards et al (2011).

The analysis program removed the non-fluorescence photon counting bins from the data to obtain a signal containing only that of OH fluorescence. Every five elements in this array was then summed and assigned the time of the first element included in the sum in order to reduce noise in the signal. The resulting signal was averaged between 0.00005 and 0.09905 s to obtain a value for the background signal which was subsequently subtracted from each value. The function given in E 2.2 was fitted to the resulting background subtracted decay using a Levenberg-Marquardt algorithm between the time corresponding to the highest signal and the end of the decay. The analysis program outputs an image of the plotted background subtracted signal and the function fitted to the data to allow visual inspection of the quality of the fitted function. An example of such an image is shown in Figure 2.12.

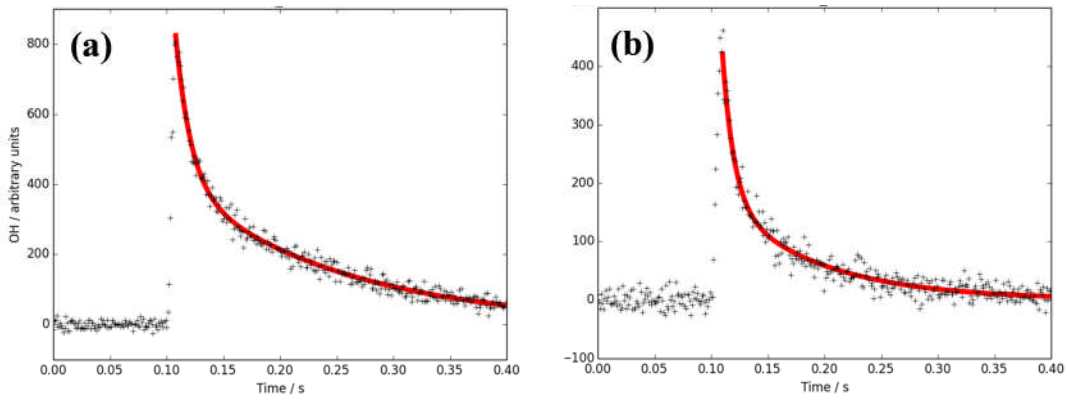

Figure 2.12: Examples of bi-exponential decays recorded by the LFP-LIF OH reactivity instrument whilst operated in configuration 1. The red lines are representative of the best fitted bi-exponential decay function (E 2.2) to the data. (a) $k'_{OH(raw)}$ = 6.8 (± 0.1) s^{-1} (b) $k'_{OH(raw)}$ = 11.7 (± 0.6) s^{-1}.

The parameters from the fitted function (E 2.2)were also outputted by the analysis program in addition to their 1 σ statistical uncertainties. The value of $k'_{OH(raw)}$ could then be used to determine k'_{OH} through the subtraction of $k'_{OH(physical)}$ as described in Section 2.1.10.

Upon return of the LFP-LIF instrument from the York 2014 'missing' OH reactivity campaign the inlet of the FAGE cell was redesigned in an attempt to eliminate the presence of $k'_{OH(fast)}$ in the OH decay signals and improve the sensitivity for OH detection. The redesigned inlet is described in Section 2.2.7 and was used in configurations 2 of the instrument. The signals recorded by the LFP-LIF instrument in configuration 2 consisted of only one exponentially decaying component. Therefore, it was possible to determine a $k'_{OH(raw)}$ value from these decays using a single exponential decay function, E 2.3.

$$\frac{(S_{OH})_t}{(S_{OH})_0} = \exp(-k'_{OH(raw)}t) \qquad \textbf{E 2.3}$$

An analysis program written in python very similar to that described above was used to determine $k'_{OH(raw)}$ values from the OH decays signal recorded by the LFP-LIF instrument in configuration 2. The process for fitting the function was identical except that in this case the portion of the decay signal that was fitted to could be adjusted. The start time for the fitting was chosen so that it was at the beginning of the decay signal and the end time was chosen so that data close to the background level did not influence the fit. Figure 2.13 shows two examples of a single-exponential decay recorded by the instrument and a fitted single exponential-decay

function. The $k'_{OH(raw)}$ values determined through fitting the single exponential functions to signals recorded by the LFP-LIF instrument in configuration 2 are used to determine k'_{OH} through subtraction of $k'_{OH(physical)}$ as described in Section 2.1.10.

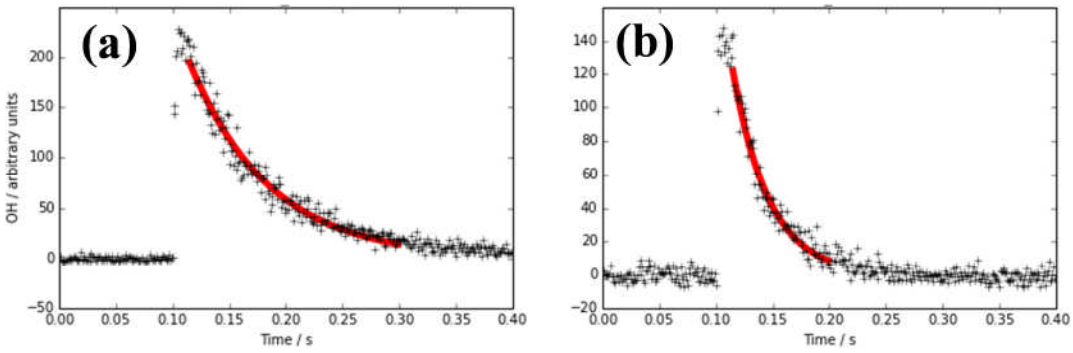

Figure 2.13: Examples of single exponential decays recorded by the LFP-LIF OH reactivity instrument whilst operated in configuration 2 or 3. The red lines are representative of the best fitted single exponential decay function (E 2.3) to the data. (a) $k'_{OH(raw)}$ = 14.2 (± 0.3) s^{-1} (b) $k'_{OH(raw)}$ = 31.2 (± 0.9) s^{-1}.

2.2.9 Measurement validation with standard gases

In order to validate the OH loss rates measured configuration 1, k_{OH+CO} was measured by the addition of known quantities of CO to the flow entering the instrument in a laboratory experiment. Synthetic air (BTCA) from a cylinder was flowed into the instrument in place of ambient air. A Hg(Ar) pen ray lamp (Lot-Oriel, LSP035) and water bubbler were used to add ozone and water vapour to the flow entering the instrument. A CO cylinder and additional mass flow controller were used to vary the mixing ratio of CO entering the flow tube, a schematic diagram of the experimental set-up is shown in Figure 2.14.

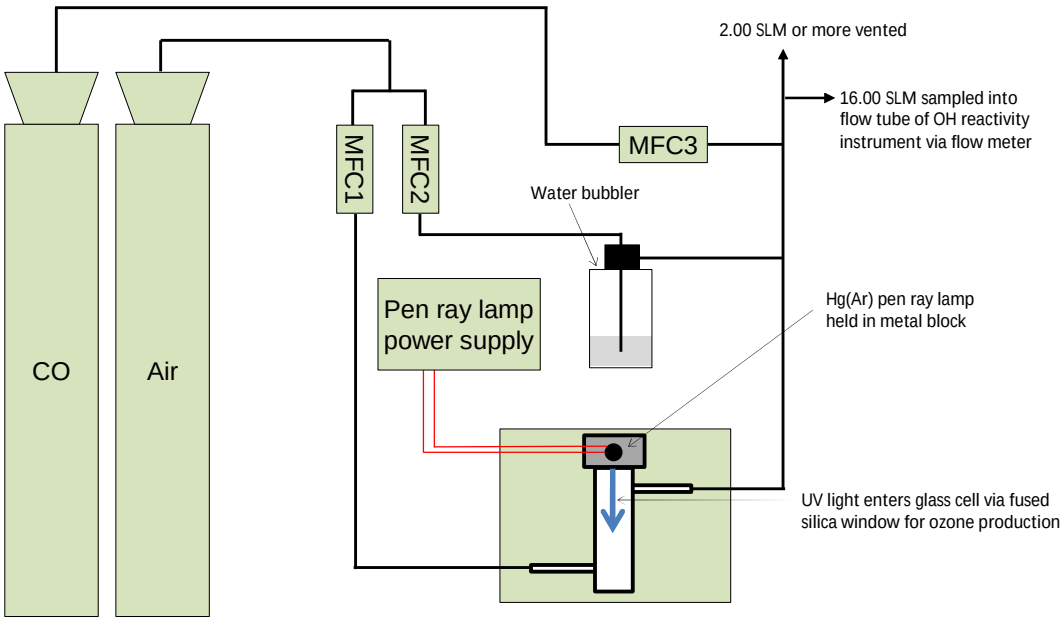

Figure 2.14: Schematic diagram to summarise the experimental set-up used for the measurement of k_{OH+CO} with the laser flash photolysis total OH reactivity instrument.

17.00 SLM of zero air were flowed through a water bubbler and mixed with 1.00 SLM of zero air that had been irradiated with a Hg(Ar) pen ray lamp (operated at ~8 mA) for ozone production (by R 2.3 and R 2.4); the resulting flow contained ozone at ~30 ppb. A flow from the CO cylinder (ranging between 0 and 20 sccm) was mixed into the bulk flow so that the mixing ratio of CO in the flow to the reactivity instrument could be varied between 0 and ~6200 ppb. This flow correlated to a range of [CO] within the flow tube of 0 to ~ 1.5 x 10^{14} molecule cm^{-3} when the measured pressure in the flow tube (~730 Torr) and assumed temperature (298 K) are taken into account. As [CO] within the flow tube was increased, it could be seen by inspection of the OH decay profiles, that the loss rate of OH increased. The Python analysis program described in Section 2.1.7 was used to extract a value of $k'_{OH(raw)}$ from each OH decay recorded as [CO] was varied in the flow tube. The values obtained were plotted against [CO] to produce a bimolecular plot which is shown in Figure 2.15, the gradient of which is equal to the measured bimolecular rate coefficient for the reaction of OH + CO.

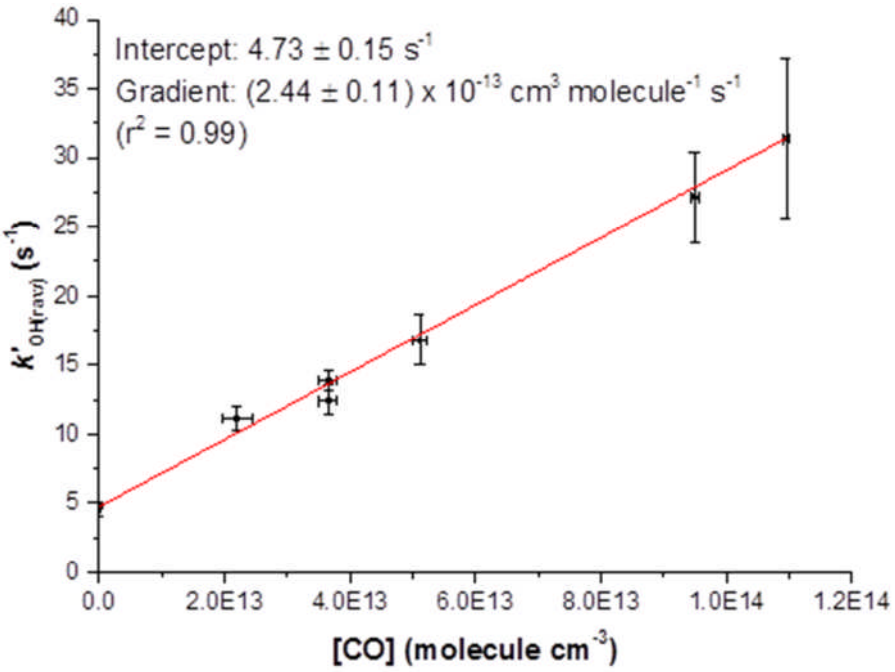

Figure 2.15: Bimolecular plot produced using OH loss rates measured using the LFP-LIF instrument in configuration 1 as the concentration of CO in the flow tube was varied. The gradient is equal to $k_{OH + CO}$,(2.44 ± 0.11) × 10^{-13} cm^3 $molecule^{-1}$ s^{-1}.

The value of $k_{OH + CO}$ measured using the LFP-LIF instrument was (2.44 ± 0.11) × 10^{-13} cm^3 $molecule^{-1}$ s^{-1}, this agrees well with the literature value (2.25± 0.5) × 10^{-13} cm^3 $molecule^{-1}$ s^{-1}) (Atkinson et al., 2004) for $k_{OH + CO}$ at 730 Torr to within the observed uncertainty. The highest value of $k'_{OH(raw)}$ recorded during this experiment was 39.4 s^{-1}. Therefore it can be concluded that OH decays recorded by the instrument in configuration 1 could be used with confidence to determine OH reactivity whilst sampling ambient air when the value of $k'_{OH(raw)}$ extracted was less than ~50 s^{-1}, such as those presented in Chapter 5.

In order to assess the validity of loss rates measured by the LFP-LIF instrument in configuration 2, $k_{OH + CH4}$ was measured in the same way as $k_{OH + CO}$ was measured for configuration 1 (Stone et al., 2016). A bimolecular plot is shown in Figure 2.16.

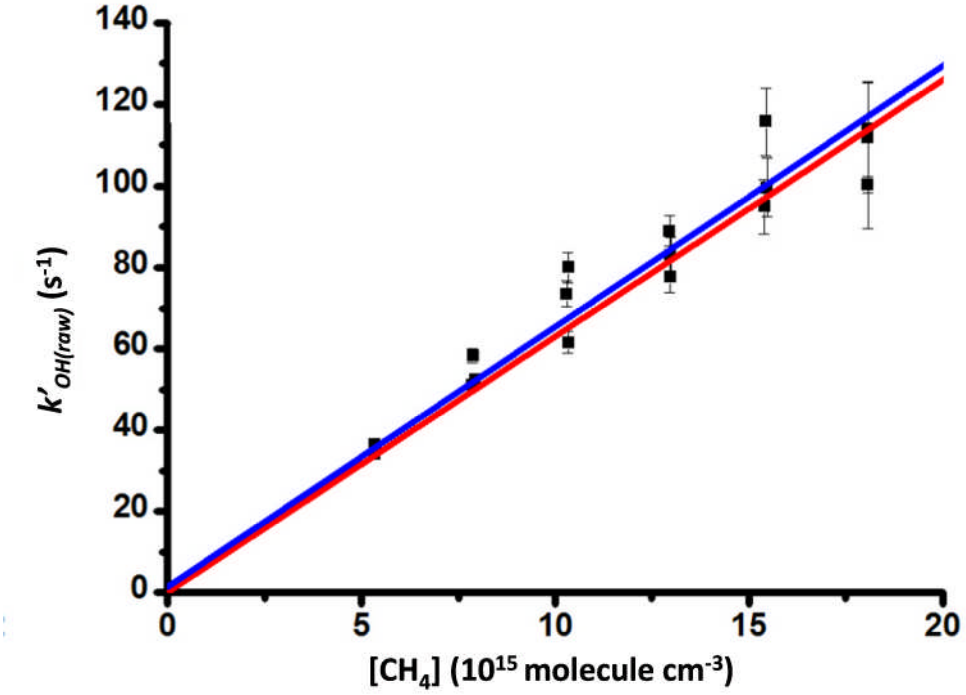

Figure 2.16: Bimolecular plot produced using OH loss rates measured using the LFP-LIF instrument in configuration 2 as the concentration of CH_4 in the flow tube was varied. The gradient is equal to $k_{OH + CH4}$, (6.4 ± 0.6) × 10^{-15} cm^3 $molecule^{-1}$ s^{-1}. The blue line represents the line of best fit (least squares) to the measured loss rates and the red line represents the literature value: (6.4± 1.2) × 10^{-15} cm^3 $molecule^{-1}$ s^{-1} (Atkinson et al., 2004) . Adapted from Stone et al. (2016).

The value of $k_{OH + CH4}$ measured using the LFP-LIF instrument was (6.4 ± 0.6) × 10^{-15} cm^3 $molecule^{-1}$ s^{-1}, this agrees well with the literature value (6.4± 1.2) × 10^{-15} cm^3 $molecule^{-1}$ s^{-1} (Atkinson et al., 2004). These results confirm that OH decays recorded by the instrument in configuration 2, such as those presented in Chapters 3 and 6, can be used with confidence to determine OH reactivity whilst sampling ambient air when the value of $k'_{OH(raw)}$ extracted was as high as ~120 s^{-1}.

2.2.10 Determination of physical loss rate of OH

To obtain a measurement of k'_{OH} from $k'_{OH(raw)}$, determined through fitting an exponentially decaying function (E2.2 or E2.3, Section 2.1.7) to an OH signal recorded by the LFP-LIF instrument, it is necessary to subtract a value for $k'_{OH(physical)}$. This section provides details on how $k'_{OH(physical)}$ was determined for each configuration of the instrument.

In principle, if moist synthetic air (free from OH reactive impurities) contained sufficient water vapour and ozone to generate sufficient OH to observe an OH

decay, and was supplied to the instrument, the $k'_{OH(raw)}$ value (minus a very small (<0.01 s^{-1}) contribution from the reaction between OH and O_3) determined would equal $k'_{OH(physical)}$. When a supply of synthetic air containing OH reactive impurities is used in the measurement of $k'_{OH(physical)}$, the value determined would be artificially high. If such a value was subtracted from $k'_{OH(raw)}$ the value determined in ambient air k'_{OH} would be artificially low, and consequently any 'missing' OH reactivity would be underestimated. To successfully determine $k'_{OH(physical)}$ for each configuration it was necessary to have access to very high purity synthetic air so that any chemical contribution to the loss rates observed is minimal. It is also imperative that the water in the bubbler used to humidify the flow to the instrument is as pure as possible.

At the beginning and end of the deployment of the LFP-LIF instrument for the York 2014 'missing' OH reactivity campaign (where the instrument was operated in configuration 1), BTCA synthetic air was used in an attempt to determine $k'_{OH(physical)}$. Values of $k'_{OH(raw)}$ determined from OH decays in synthetic BTCA air from a cylinder are referred to as $k'_{OH(zero)}$ in this work. The schematic diagram in Figure 2.17 summarises the experimental set-up that was used for this.

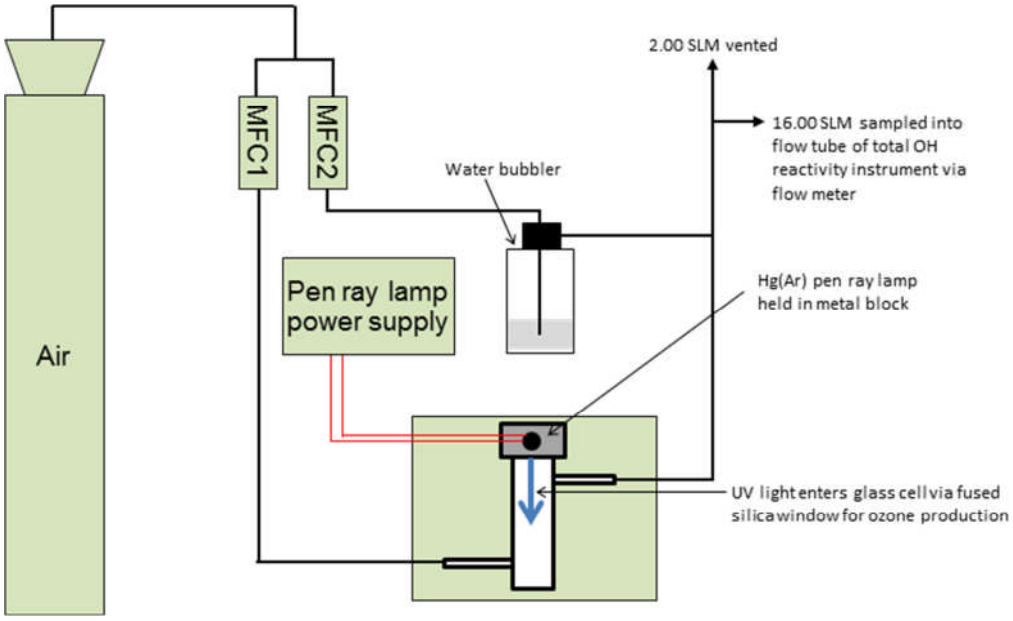

Figure 2.17: Diagram to summarise the experimental set-up used for the measurement of $k'_{OH(zero)}$ whilst the LFP-LIF OH reactivity instrument was operated in configuration 1

1 SLM of zero air was passed through a glass cell and irradiated via a fused silica window with UV radiation from a Hg(Ar) pen ray lamp (Lot-Oriel, LSP035)

operated at 8.2 mA for the production of ozone. It was mixed with 17 SLM from the same cylinder that had passed through a water bubbler so that 18 SLM in total were available to the instrument. An ozone analyser (Thermo Electron Corporation 49C) was used to measure that the flow contained ~30 ppb of ozone. The scroll pump used to draw gas through the flow tube of the instrument was throttled using a butterfly valve until the flow meter indicated that 16 SLM were entering the instrument. $k'_{OH(zero)}$ values were determined through fitting a bi-exponentially decaying function as described in Section 2.1.7, all of these values are plotted in Figure 2.18.

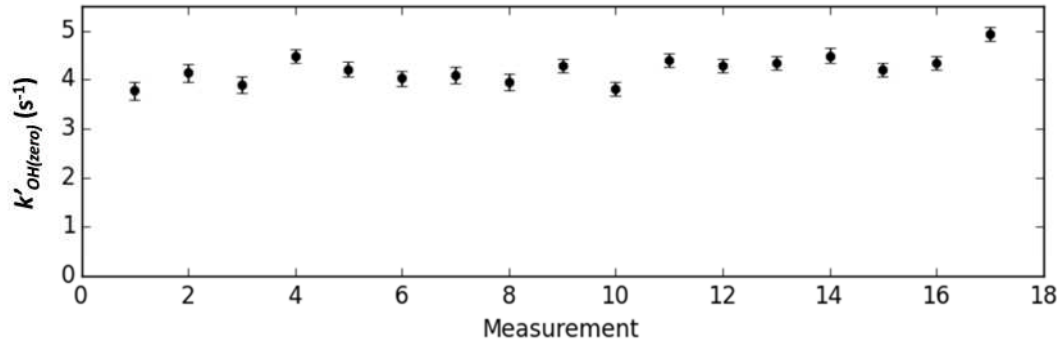

Figure 2.18: Measurements of the loss rate of OH in synthetic air ($k'_{OH(zero)}$) measured during the York 2014 'missing' OH reactivity campaign where the LFP-LIF instrument was operated in configuration 1. The y error bars represent the 1σ standard deviation in the value of $k'_{OH(zero)}$ as determined from the covariance matrix associated with the bi-exponential decay function fitted to the decay data, outputted by the scipy optimize function.

The average $k'_{OH(zero)}$ recorded was 4.22 ± 0.29 s^{-1} (1σ standard deviation). It is known that there are impurities (CO, NO_x and unspecified VOCs) present in BTCA synthetic air cylinders and only upper limits regarding these are available from the manufacturer (BOC, 2016). It is also possible that there could be OH reactive impurities present in the water used to humidify the flow to the instrument. Therefore, it was not possible to say with certainty what portion of the average zero loss rate in the BTCA synthetic air could be attributed to chemical impurities.

Measurements of $k'_{OH(zero)}$ were made before and after the ICOZA campaign for which the LFP-LIF instrument was deployed in configuration 2. The method used was very similar to that described above. However, in this case 1 SLM of synthetic air was irradiated with the pen ray lamp and mixed with 15 SLM that was humidified with the water bubbler. There was no vent in the system prior to the gas

entering the instrument as for configuration 1 of the instrument. In this case all 16 SLM entered the instrument and the pressure of the flow tube was monitored whilst the butterfly valve that throttled the scroll pump was adjusted until a stable pressure of ~760 Torr was achieved. The average (from six measurements prior to deployment and two post deployment) $k'_{OH(zero)}$ value determined for ICOZA was 5.22 ± 0.21 s^{-1} (1σ standard deviation).

Access to a very clean synthetic air supply at the SAPHIR chamber, during an OH reactivity comparison campaign (Chapter 3), provided a valuable opportunity to investigate the magnitude of any contribution from impurities in synthetic air to the $k'_{OH(zero)}$ values determined for configurations 1 and 2 of the LFP-LIF instrument. The synthetic air supply at SAPHIR was generated through the boil off of liquid nitrogen and oxygen (80% and 20%, respectively). It is assumed that this air was the purest that had ever been available for use in experiments to determine the true value of $k'_{OH(physical)}$, equal to the $k'_{OH(raw)}$ determined from an OH decay recorded in this zero air. The instrument was operated in configuration 2 when these measurements were made and the method for measurement was identical to that used for measurements of $k'_{OH(zero)}$ before and after the ICOZA campaign, except in this case the SAPHIR synthetic air supply was used in place of a cylinder. The OH signal was found to decay significantly slower in this case than in the pre and post-ICOZA measurements, visual inspection of the signal revealed that the signal decay was so slow that there was still evidence of a decay in the period during which the background signal is recorded prior to the triggering of the 266 nm photolysis pulse. A result of this was that it was not possible to use the method for extracting a $k'_{OH(raw)}$ as described in Section 2.1.7, as subtracting a background from the decays that included a contribution from OH LIF is not appropriate. Instead the back ground signal was determined separately through operation of the instrument, in the absence of 266 nm light, for one measurement cycle of an OH decay. This was subtracted from the OH decays recorded in the SAPHIR synthetic air to obtain a background subtracted signal, the natural logarithm of which was taken and a straight line was fitted so that a loss rate could be extracted. An example of such a signal used to determine $k'_{OH(physical)}$ is shown in Figure 2.19.

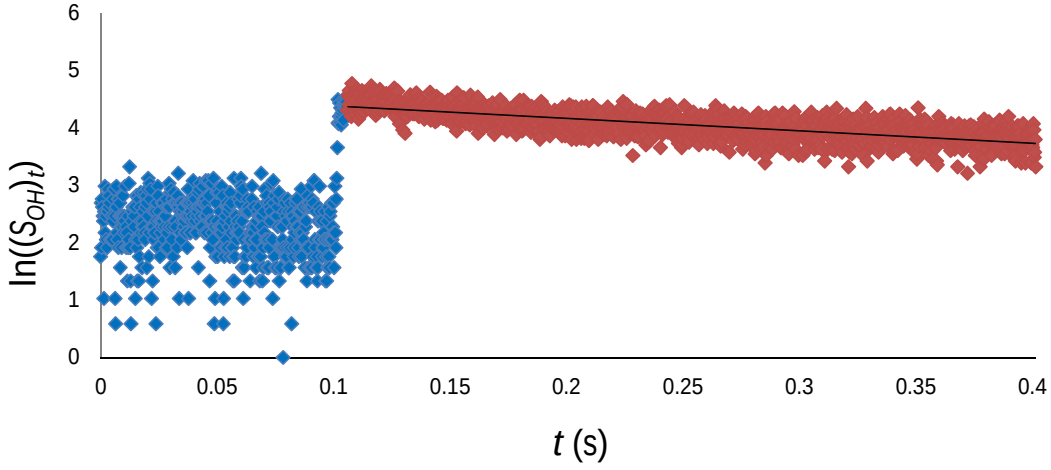

Figure 2.19: Example OH decay signal recorded in very clean synthetic air (produced by boil-off of liquid nitrogen and oxygen) at the SAPHIR chamber. $k'_{OH(physical)}$ = 2.18 s^{-1}.

The value of $k'_{OH(physical)}$ for the LFP-LIF instrument when operated in configuration 2 was determined as the average of five individual $k'_{OH(physical)}$ measurements. This was 2.25 ± 0.21 s^{-1} (1σ standard deviation) and is the value which was subtracted from the ambient measurements made during ICOZA (Chapter 6).

The value for $k'_{OH(physical)}$ that was subtracted from the measurements made during ICOZA was not appropriate for subtraction from the measurements made during the York 2014 'missing' OH reactivity campaign. The reason for this is that during ICOZA the instrument was operated in the same configuration as it was during the experiments with the SAPHIR synthetic air supply. During the ambient measurements in York the instrument was operated in configuration 1 where the inlet of the FAGE cell and method of removing excess gas from the flow tube were very different and would very likely have had an impact on the loss rate of OH due to physical processes occurring within the flow tube. For the purpose of determining $k'_{OH(physical)}$ for the instrument in configuration 1, it was assumed that the level of OH reactive impurities that were present in the flow to the instrument during the measurement of $k'_{OH(zero)}$ for the instrument in both configurations were the same. It is very likely that this was the case as laboratory measurements have shown there to be little variation in the value of $k'_{OH(zero)}$ measured with different cylinders of BTCA synthetic air and water (always from the same sources) used in the bubbler. The difference between $k'_{OH(zero)}$ for configuration 2 (5.22 ± 0.21 s^{-1}, average of measurements pre and post-ICOZA deployment) and $k'_{OH(physical)}$ measured with the

SAPHIR synthetic air supply was assumed to be equivalent to the contribution from OH reactive impurities to $k'_{OH(zero)}$ that was measured at the beginning and end of the measurements in York. This difference was subtracted from $k'_{OH(zero)}$ for configuration 1 (4.22 ± 0.28 s^{-1}, average of measurements at the beginning and end of measurements in York) to determine $k'_{OH(physical)}$ for configuration 1. The value determined was 1.25 ± 0.42 s^{-1} and this was subtracted from all of the ambient measurements from the York 2014 'missing' OH reactivity campaign presented in Chapter 5.

2.2.11 Effect of NO recycling

Stone et al. (2016) reported a modelling study on the potential interferences from OH recycling, at elevated NO levels, on measurements of k'_{OH}. OH decays in the LFP-LIF instrument were simulated under a range of conditions. Whilst it is an advantage of the LFP-LIF technique that the method used for the generation of OH does not also generate HO_2 (as in the TOHLM technique), it is possible for HO_2 to be generated within the instrument from the reaction of OH and CO. It is also possible for RO_2 radicals to be generated from the reactions between OH and VOCs. Any HO_2 or RO_2 generated within the instrument has the potential produce recycled OH when NO is present in the gas sampled (as described in Section 1.2.1). If the rate of recycled OH production was very high it is possible that OH signals recorded by the LFP-LIF instrument could be artificially raised at longer decay times. It was concluded by Stone et al. (2016) that the LFP-LIF instrument does not suffer from any significant interference resulting from production of HO_2 and RO_2 within the instrument.

2.3 Measurement of formaldehyde

2.3.1 Instrument overview and principle of operation

The methodology for the detection of HCHO with the Leeds LIF instrument is based on that outlined by Hottle et al. (2008). Gas is sampled into a low pressure aluminium cell (Section 2.2.3) and UV radiation from a fibre laser (Section 2.2.2) is used to excite HCHO in the $5_{0,5} \leftarrow 5_{1,4}$ rotational transition of the 4 $A^1A_2 \leftarrow X^1A_1$ vibronic band at 353.370 nm. Resulting photons from broadband fluorescence of HCHO are detected orthogonal to the path of the laser beam, the count rate of which (Section 2.2.5) is proportional to concentration of HCHO in the gas sampled. A

calibration factor determined experimentally (Section 2.2.7) is used to determine the concentration of HCHO in the gas sampled.

The HCHO LIF instrument is relatively compact and the majority of components are contained within one shock insulated 19” rack housed within a plastic gasket sealed case with removable side panels for easy transportation. Figure 2.20 shows the arrangement of the key components within the case.

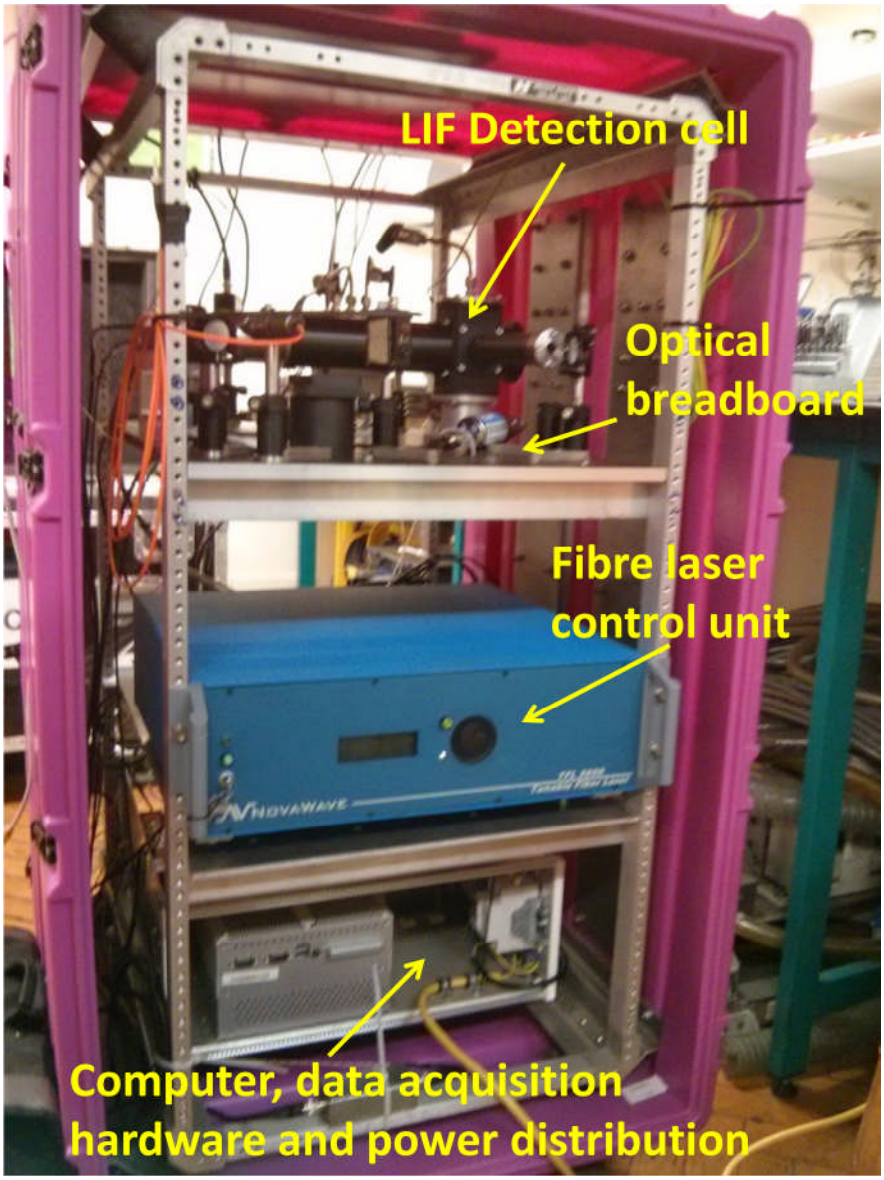

Figure 2.20: Photograph showing the arrangement of key componenets (labelled) of the HCHO LIF instrument within the 19” rack.

The case is shown with both side panels removed, however, when fitted, a computer fan was situated in the bottom of back panel to draw air into the case which exited through a hole in the top of the front panel; this was to prevent overheating of the

laser, computer and other components. A hole (50 mm diameter) was in the centre of the back panel to allow gas lines and cables to enter whilst the case is sealed. A 19" rack enclosure at the bottom of the rack contained a computer and other data acquisition hardware, and above this was the control unit of the fibre laser which was also housed within a 19" rack enclosure. Fixed as a shelf in the top of the rack was an optical breadboard, to which the fibre laser head was fixed in addition to all other optical components and the detection cell and a reference cell. The HCHO LIF instrument was developed through the course of this work and consequently it is necessary that each configuration used to obtain measurements presented in this work is described. Details of three configurations are provided in Section 2.3.6 which differed only with regards to the layout and contents of the optical breadboard.

2.3.2 The 353 nm detection laser

UV radiation from a pulsed (300 kHz) tuneable fibre laser (TFL3000, Novawave) was then used to excite HCHO in the LIF instrument described here. The majority of the optical components of this laser are built into the control unit which is housed inside a 19" rack enclosure, this is connected to the laser head via an optical fibre. Figure 2.21 summarises the key optical components housed within the laser control unit and laser head.

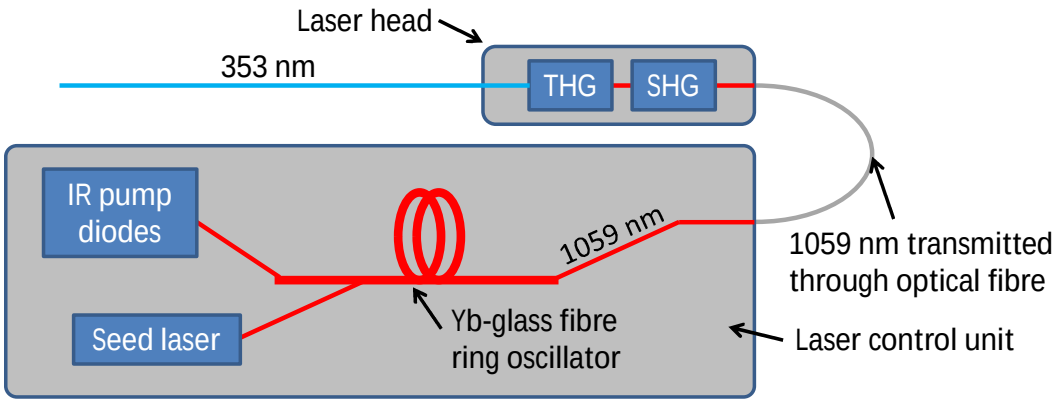

Figure 2.21: Schematic diagram to illustrate the key processes occurring within the tuneable fibre laser used to excite HCHO. SHG: second harmonic generating crystal, THG: third harmonic generating crystal.

The operating principle of the fibre laser for the generation of UV light differs considerably from that of a Ti:Sapphire laser (Section 2.2.5). In the fibre laser, a Yb-doped glass fibre laser is used as a cavity and main oscillator where laser excitation

can occur. The Yb-doped glass fibre cavity is bonded directly to an optical fibre which transmits radiation from broadband IR pump diodes. A second optical fibre bonded to the main oscillator is used to transmit radiation from an IR (1059 nm) seed laser diode, The specific wavelength outputted is controlled through adjustment of the current supplied to the seed diode and is controlled through the application of an analogue voltage to the laser control unit. The radiation from the seed diode is amplified by the main oscillator to output ~1W of 1059 nm radiation which is delivered to the laser head via an optical fibre. Inside the laser head this is tripled by sum frequency mixing using a second harmonic generating crystal and a third harmonic generating crystal. Following this 353 nm UV light exits the laser head, in addition to some excess green light (second harmonic).

2.3.3 The detection cell

The main body of the detection cell of the HCHO LIF instrument was very similar in design to that of the LFP-LIF instrument (described in Section 2.1.3). There were, however, differences regarding the method for achieving low pressure in the cell and also for sampling air into it. The pressure inside the cell of the HCHO LIF instrument does not have to be as low as inside a FAGE cell for OH measurement, owing to the fluorescence lifetime being significantly longer for HCHO, and also that there is no need for gating of the detector as an off-resonant spectroscopic feature is used. Measurements of HCHO are typically made at cell pressures in the range 110 - 120 Torr. It is possible to achieve such a cell pressure using a scroll pump (Agilent Technologies, IDP3), as opposed to a roots backed rotary pump and pinhole that would be required for a FAGE cell. The diagram in Figure 2.22 illustrates the design of the HCHO detection cell.

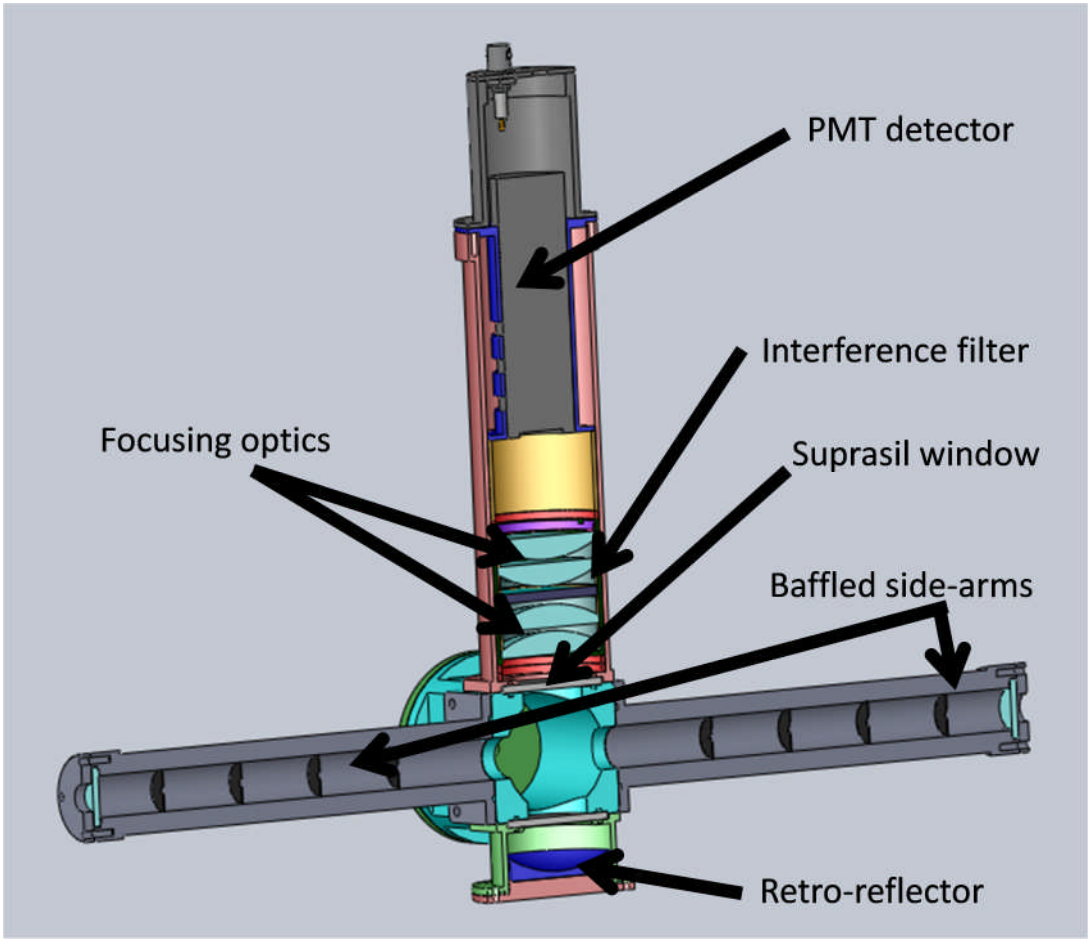

Figure 2.22: Cutaway scale diagram of the detection cell of the HCHO LIF instrument. Provided by Dr. Trevor Ingham.

The unit orthogonal to the baffled arms for the entry and exit of laser light housed the photo multiplier tube (PMT, Sens-Tech P25PC photodetector module), and also a set of optics to image photons from HCHO florescence onto the photocathode of this detector. Two plano-convex lenses (diameter = 50 mm, focal length = 52 mm) were used to collimate the fluorescence through an interference filter (Barr Associates, 390 – 550 nm) which was used to discriminate HCHO fluorescence photons from scatter at 353 nm. Following this a further two plano-convex lenses (diameter = 50 mm, focal length = 52 mm) were used to focus the filtered fluorescence signal onto the PMT photocathode. An uncoated circular Suprasil window between two o-rings was used to form an airtight seal between the unit housing the PMT and the LIF cell. A retro-reflector (CVI Optics fused silica plano-concave spherical mirror) was mounted directly opposite the PMT to deflect photons from HCHO fluorescence, which were emitted in the direction opposite to the detector, towards the detector to maximise sensitivity. The two cell faces orthogonal

to both the detection and laser axis were used for pumping out and sampling air into the cell, only one such face is visible in Figure 2.22.

2.3.4 The reference cell

A reference cell was developed to enable the automation of tuning the wavelength of the fibre laser to optimise the HCHO signal. The reference cell, as shown in Figure 2.23 was constructed from a block of 75 x 75 x 75 mm aluminium, into the centre of one face of which a hole, 30 mm in diameter, and 70 mm deep, was machined to form the inner walls. Two short cylindrical aluminium arms (30 mm maximum length, 15 mm OD) fitted with fused silica Brewster windows were used to allow laser light to enter and exit the cell. Three ¼" Swagelok fittings were attached to the top of the cell to allow gas flow in and out, and to enable a pressure sensor (26PCDFA1G, Honeywell) to be fitted. The diagram in Figure 2.23 illustrates the design of the reference cell of the HCHO LIF instrument.

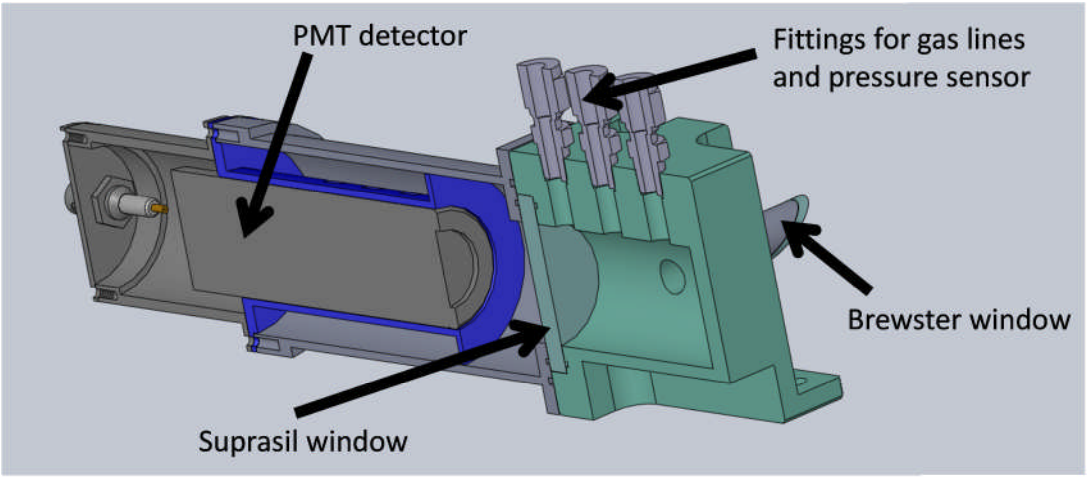

Figure 2.23: Cutaway scale diagram of the reference cell of the HCHO LIF instrument. Provided by Dr. Trevor Ingham.

The PMT housed in the detection arm of the reference cell was identical to that used in the main cell, the timings for measurement of the HCHO signal (Section 2.3.5) were also the same. However, no interference filter or focussing optics were used in the reference cell as achieving good sensitivity is not important. After exiting the main detection cell the laser light was directed by two UV turning mirrors into the reference cell. A high background signal (200,000 -300,000 count s^{-1}) was not positioned on the HCHO transition, as a result of laser scatter from the inner walls of the cell which did not have a black-anodised coating.

In order to scan the wavelength of the tuneable fibre laser and observe a resulting change in the reference cell signal representative of the rotational spectroscopic structure of HCHO, it was necessary to elevate the level of HCHO inside the reference cell to levels significantly higher than in ambient air. Depolymerisation of paraformaldehyde (SIGMA-ALDRICH, P6148, reagent grade, crystalline) using heat was chosen as a method to achieve this.

The two remaining ¼" Swagelok fittings of the reference cell were each connected to quarter-turn valves and both were set to their closed position. The line to the scroll pump, that was routinely used to evacuate the main detection cell, was connected to one of these valves. The remaining valve was connected to ~1 m length of ¼" internal diameter Teflon tubing, the other end of which was connected to a short piece of capped ¼" stainless steel tubing which contained a few granules of the crystalline paraformaldehyde (the HCHO reservoir). The valve to the scroll pump was partially opened and closed when the pressure within the reference cell was reduced to ~100 Torr. The HCHO reservoir was then heated with a heat gun for ~5 s whilst the valve connecting it to the reference cell was opened. This enabled gas phase HCHO formed by depolymerisation of paraformaldehyde to enter the reference cell; a pressure increase of ~50 Torr was observed. Following this the valve to the HCHO reservoir was closed and the valve to the scroll pump was partially opened until the pressure was again ~100 Torr. The resulting system was completely sealed and the level of HCHO in the gas phase was sufficient for the peak of the spectral line at 353.370 nm to be observed at ~400,000 count s^{-1} above the background. The signal from the new reference cell was used to automate the process of tuning the wavelength of the fibre laser on to the spectroscopic line at 353.370 nm so that HCHO could be measured in ambient air with the main detection cell. Further details of this process are provided in Section 2.3.5

2.3.5 Data acquisition

The master clock of the fibre laser was used to control timing for photon counting in the HCHO detector. For every pulse from the fibre laser a transistor-transistor logic (TTL) pulse was used to trigger a delay generator card in the computer. Upon receiving this trigger, the delay generator card waited 400 ns before providing a TTL pulse (1000 ns duration) to trigger a photon counting card that was operated in the 'multiscaler' mode (PMS400A, Becker and Hickl). After a further 200 ns elapsed

following the triggering of the photon counting card, another TTL pulse (200 ns duration) from the delay generator card was used to un-gate a channel on the photon counting card. Photons from laser induced fluorescence of HCHO were collected within these 200 ns. The fluorescence lifetime of HCHO is approximately 200 ns at ~120 Torr so this collection window should provide ample time for detection (Hottle et al., 2008). The schematic diagram in Figure 2.24 summarises the sequence of events that occurred during the measurement of the HCHO LIF signal that followed one pulse from the fibre laser.

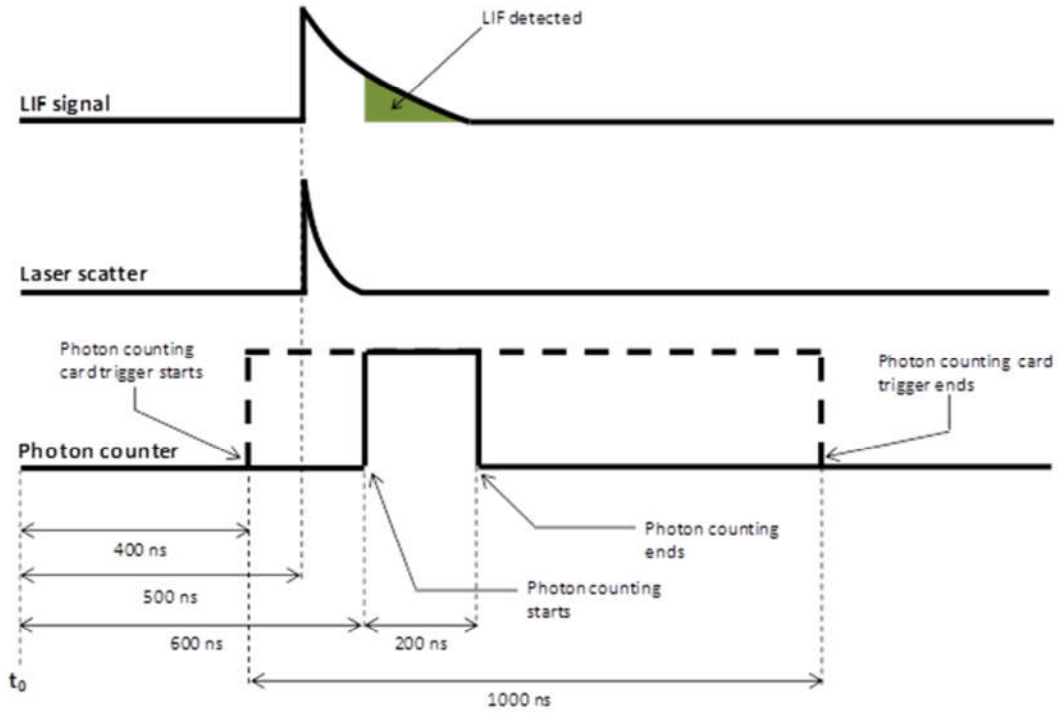

Figure 2.24: Schematic diagram to summarise the timings of the sequence of events for the measurement of the HCHO LIF signal following one pulse from the fibre laser. Diagram not to scale

It was necessary to trigger the photon counting card well in advance of the LIF signal as the PMS400A card has a 'dead time' of 50 ns between bins; i.e. if the card was triggered and un-gated simultaneously a maximum of 50 ns worth of LIF signal could be lost. Operating the photon counting card in multiscaler mode meant that the photons counted were logged as a function of time; the LIF signal recorded was outputted in count s^{-1}, where all of the photons that were detected in the 200 ns detection window (within 1 s) were summed. In order to determine the level of HCHO present in ambient air it is necessary to subtract a background signal from the signals described above. The background subtracted signal is equivalent to a

concentration of HCHO as governed by a calibration factor, details regarding the calibration of the HCHO LIF instrument are provided in Section 2.3.7.

The signal from the reference cell (described in Section 2.3.4) was used to automate the tuning of the wavelength of the fibre laser between that of the spectroscopic line of HCHO at 353.370 nm and a lower wavelength (353.360 nm) before the feature, referred to here as the 'offline' wavelength. There were four defined stages to this measurement cycle.

In the first stage a voltage was applied to the 'seed' laser diode of the tuneable fibre laser in order to increase its temperature by a small amount, which in turn resulted in an increase in wavelength from its starting ('offline') position. The wavelength of the fibre laser was increased by ~10 pm so that a peak corresponding to the HCHO rotational transition at 353.370 nm was observed in the reference cell signal. Following this the wavelength was decreased during the second stage until the reference cell signal was within 95 % of the maximum value observed during the first stage. This defined the start of the third stage where the wavelength was fixed for ten minutes whilst the 'online' HCHO signal from the main detection cell was recorded (1 s data). On completion of the third stage the wavelength was returned to its starting value and the 'offline' HCHO signal from the main detection cell was recorded for one minute. The plot in Figure 2.25 shows a typical reference cell signal that was observed during one measurement cycle.

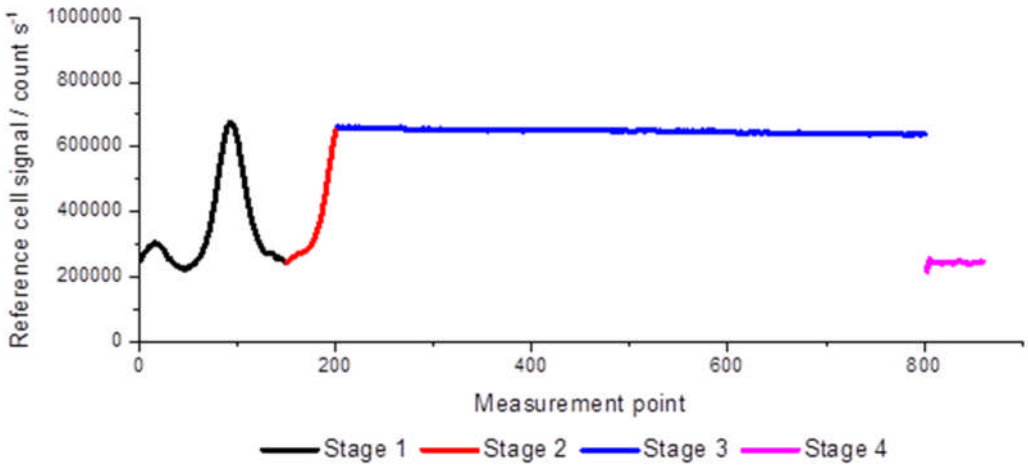

Figure 2.25: A typical reference cell signal observed during one complete measurement cycle of the LIF HCHO instrument. Time resolution between adjacent points is 1s.

For every measurement cycle each point in the 'online' and 'offline' signals from the main detection are normalised for laser power using a photodiode. The 'offline' normalised is averaged and subtracted from every online point to yield a signal that could be used in combination with a calibration factor to determine the concentration of gas phase HCHO in the gas sampled.

2.3.6 Instrument configurations

Due to continual development of the HCHO LIF instrument through the course of this work, it is necessary here to describe three different configurations in which it was operated. configuration 1 was used for the measurements presented in Chapter 4 where the instrument was used in experiments to characterise a newly developed OH flow reactor. configuration 2 was used for the ambient measurements presented in Chapter 5 from the York 2014 'missing' OH reactivity campaign. configuration 3 was used for the ambient measurements presented in Chapter 6 from the ICOZA campaign. The main difference between the configuration 1, and configurations 2 and 3 was the layout of the optical breadboard and the maximum laser power that was available for use. The only difference between configurations 2 and 3 was the amount of laser power that was available for use.

In configuration 1 there was no reference cell in operation to automate the measurement process. In the OH reactor characterisation experiments described in Chapter 4, the wavelength of the fibre laser was tuned between the online and offline position manually. The signal from the main cell was monitored whilst laboratory air was sampled and the wavelength was increased by ~10 pm (through increasing the temperature of the seed diode) from the starting value. Due to there being ~20 mW of UV laser power available and the relatively high level of HCHO in the laboratory air sampled (5 ppb) it was possible to see the main spectroscopic feature at 353.370 nm clearly peaking at ~1000 count s^{-1} above the background (~150 count s^{-1}). As the level of HCHO in the laboratory air was fairly constant, it was possible to stop and restart the wavelength scan so that it could be stopped again when the signal had returned to its maximum value. The instrument was considered 'online' for measurements when in this state. Figure 2.26 summarises the set-up of the optical components of the HCHO LIF instrument when operated in configuration 1.

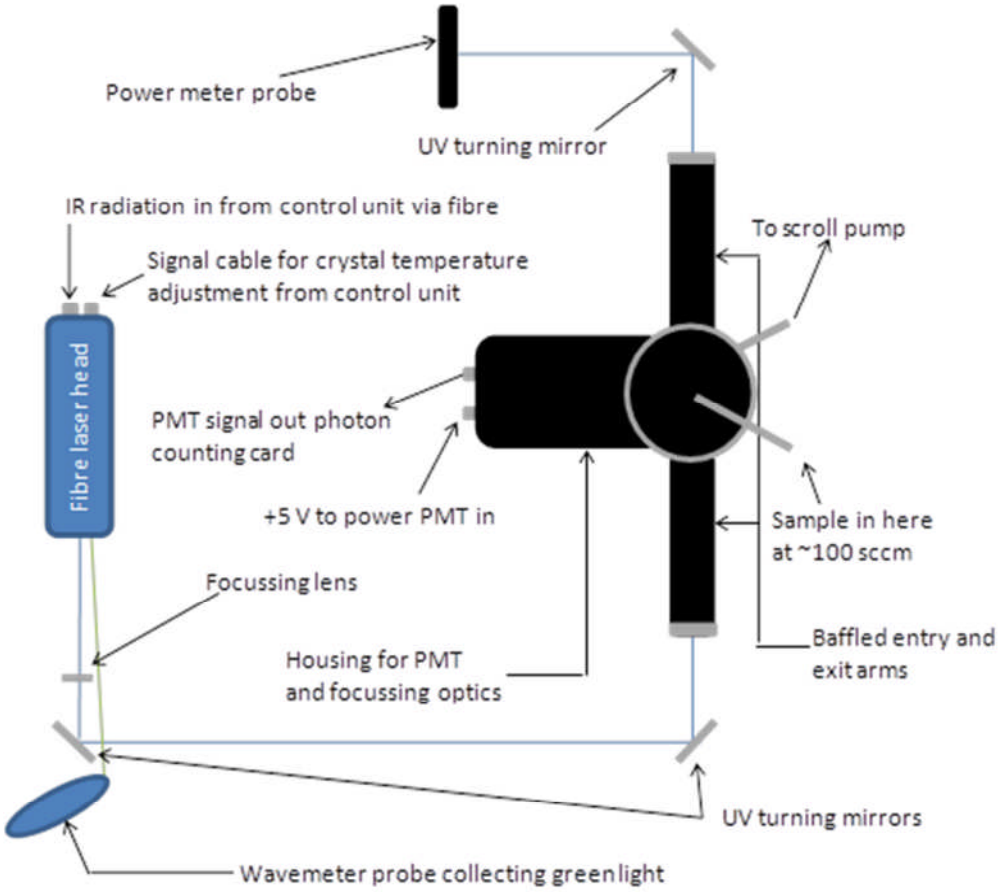

Figure 2.26: Schematic diagram to summarise the key features of the optical set-up and the detection cell used in configuration 1of the LIF HCHO detector. Diagram not to scale.

UV radiation exited the fibre laser head and was directed into the entry arm of the detection cell by two UV turning mirrors. Upon exiting the detection cell a third UV turning mirror was used to direct the laser beam onto a power meter probe so that the power could be tuned and monitored without disruption of the measurement of HCHO. Excess green light from the fibre laser head was directed into a wave meter probe so that the wavelength could be monitored as a proxy for the wavelength of the UV light.

Following the completion of the OH reactor characterisation experiments described in Chapter 4, problems were encountered with the fibre laser of the HCHO LIF instrument. On return to the manufacturers it was determined that the optical fibre used to deliver IR radiation to the laser head had become burned. This was repaired, however, to prevent reoccurrence of this problem it was advised that the laser outputted a maximum of 10 mW UV light. When the laser was re-integrated into the rack of the HCHO LIF instrument a reference cell was also installed to enable the

automation of tuning the wavelength and data acquisition. Figure 2.27 summarises the set-up of the optical components of the HCHO LIF instrument when operated in configuration 2.

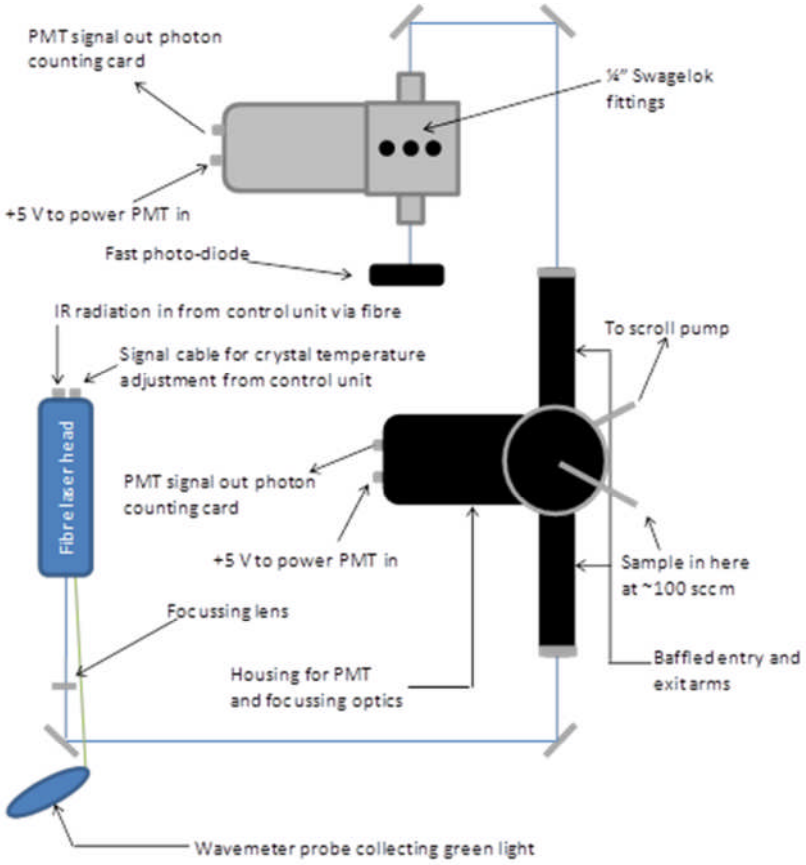

Figure 2.27: Schematic diagram to summarise the key features of the optical set-up and the detection cell used in configuration 2 (and also configuration 3, see below) of the LIF HCHO detector. Diagram not to scale.

The optical set-up of configuration 2 was the same as it was in configuration 1 prior to where the UV light exited the main detection cell. Upon exit from the main detection cell the UV light was redirected by two turning mirrors through the reference cell, upon exit from which it was terminated onto the active-area of a fast photodiode. The signal from the photodiode was used to record laser power so that the LIF signals recorded from the main detection cell could be normalised for laser power in mW.

configuration 3 of the HCHO LIF instrument was exactly the same as configuration 2 with regards to the optical components. However, the maximum UV laser power available in this configuration was ~6 mW following a second repair by the manufacturer which was necessary due to a burned crystal in the laser head. The

reduced laser power made it very difficult to calibrate the photodiode which previously measured laser power for normalising the LIF signal. Consequently, signals recorded by the HCHO LIF instrument in configuration 3 were normalised for laser power in V (the raw signal from the photodiode) rather than mW.

2.3.7 Calibration methods

As LIF is not an absolute method of measurement it is necessary to calibrate the HCHO LIF instrument so the LIF signals could be converted to concentrations using a calibration factor (C_{HCHO}). Two calibration methods were used in this work. In configurations 1 and 2 the instrument was calibrated using a method analogous to that used for calibrating a FAGE cell for OH detection, as described by Commane et al. (2010). However, in this case MeOH vapour was photolysed at 184.9 nm in a turbulent flow tube (termed the 'wand') for HCHO production rather than photolysis of H_2O vapour for OH production.

The aircraft FAGE instrument calibration 'wand' was used to calibrate the detection cell of the LIF HCHO instrument in configurations 1 and 2. 38 SLM of synthetic (BOC, BTCA) air were mixed with another 4 SLM that had passed through a MeOH bubbler. The mixture was flowed into the wand so that a known concentration of HCHO could be produced through MeOH photolysis by UV light from a Hg(Ar) pen ray lamp (Lot-Oriel, LSP035) at 184.9 nm in the presence of O_2, R 2.5.

$$MeOH + h\nu \xrightarrow{O_2} HCHO + HO_2 \qquad \textbf{R 2.5}$$

The level of HCHO produced was varied through adjustment of the current supplied to the Hg(Ar) pen ray lamp within the 'wand' in order to vary the flux of photons that irradiated the flow containing the MeOH vapour (F). This is determined as a function of lamp current separately in an experiment where NO is used as a chemical actinometer. The method for determining F as a function of lamp current is described in Commane et al. (2010) and the values used for the calibration of the HCHO LIF instrument in configuration 1 were provided by Dr. Trevor Ingham. The concentration of HCHO exiting the 'wand' was calculated using E 2.4.

$$[HCHO] = [MeOH]\sigma_{(184.9\,nm)MeOH}\emptyset_{HCHO}Ft \qquad \textbf{E 2.4}$$

[MeOH] is the concentration of methanol in the flow to the 'wand' (~3 x 10^{17} molecule cm^{-3}) calculated using the vapour pressure at the measured bubbler

temperature (~5 ºC), $\sigma_{(184.9\ nm)MeOH}$ is the absorption cross section of MeOH at 184.9 nm (6.65 x 10^{-19} cm^2 $molecule^{-1}$), Ø is the quantum yield of HCHO (assumed to be equal to 1 in air) and *t* is the irradiation time (0.008 s) that was calculated using the 'wand' dimensions and 42 SLM total flow rate.

The wavelength of the fibre laser was tuned to its 'online' value and the current supplied to the pen ray lamp in the 'wand' was varied between ~1.5 and 6.5 mA. HCHO LIF signals were recorded at five lamp currents, each for ~2 minutes. The averaged signals recorded for each lamp current were plotted against the corresponding lamp currents to produce a calibration plot as shown in Figure 2.28. The value for C_{HCHO} ((9.25 ± 13.1) × 10^{-9} count s^{-1} $molecule^{-1}$ cm^3) determined was used for the conversion of HCHO LIF signals to concentrations for the measurements presented in Chapter 4. This corresponds to a detection limit of ~54 ppt in 1 s for a signal to noise ratio of 1.

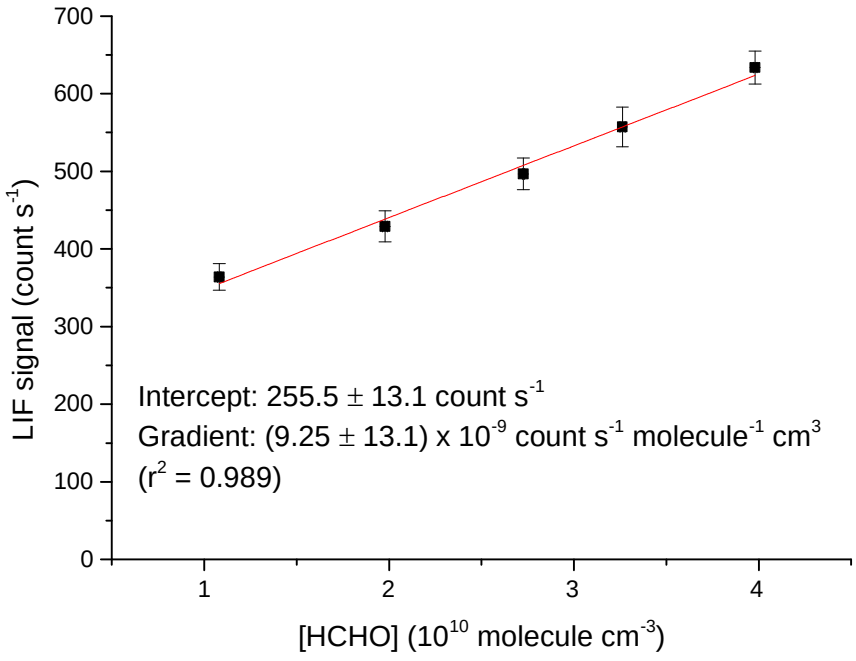

Figure 2.28: Results from the calibration of the LIF HCHO in configuration 1. The gradient of the line of best fit is equal to the sensitivity (C_{HCHO}) which is 9.25 x 10^{-9} count s^{-1} $molecule^{-1}$ cm^3. y-error bars represent ± 1σ standard deviation in the LIF signals recorded. It was not possible to determine x-error bars due to a number of parameters, such as flow rates, not being logged.

The instrument was calibrated using the same method when in configuration 2 during its deployment for the York 2014 'missing' OH reactivity campaign. The

ground based FAGE calibration wand was used for this and the experimental conditions were very similar to what is described above, however there were two differences. Firstly for the calibration in configuration 2 a total flow of 30 SLM of synthetic air was supplied to the 'wand' and all of this passed through the MeOH bubbler. The value of *t* used in the calculation of [HCHO] was also different (t = 0.012 s) as the dimensions of the ground based FAGE 'wand' were slightly different to the aircraft 'FAGE' wand and the total flow rate through the wand was different. The relationship between *F* and lamp current used for this 'wand' was supplied by Dr. Lisa Whalley. The LIF signals were also normalised for laser power in mW for calibrations in configuration 2 as this included a calibrated photodiode. The calibration plot for the HCHO LIF instrument in configuration 2 is shown in Figure 2.29. The value for C_{HCHO} ((1.46 ± 0.034) × 10^{-9} count s^{-1} mW^{-1} $molecule^{-1}$ cm^3) determined was used for the conversion of HCHO LIF signals to concentrations for the ambient measurements from York presented in Chapter 5. This corresponds to a limit of detection of ~81 ppt in 1 s for a signal to noise ratio of 1.

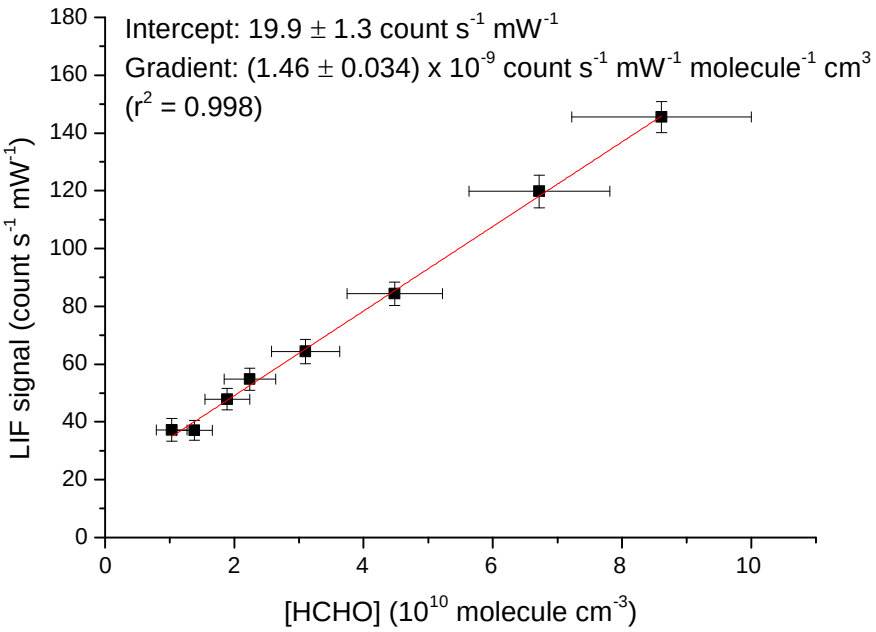

Figure 2.29: Results from the calibration of the LIF HCHO instrument during the York 2014 'missing' OH reactivity field campaign. The gradient of the line of best fit is equal to the sensitivity (C_{HCHO}) which is 1.46 × 10^{-9} count s^{-1} mW^{-1} $molecule^{-1}$ cm^3. y-error bars represent ± 1σ standard deviation in the LIF signals recorded. x-error bars represent the uncertainty in the calculated [HCHO] supplied to the instrument, as determined through propagation of the uncertainties in each parameter used to calculated [HCHO] using E 2.4.

It can be seen that the lines of best fit to the data in Figure 2.28 and Figure 2.29 both have positive y-intercepts. The reason for this is due to a constant background level of HCHO contaminant present in the flow from the MeOH bubbler in both case. Tests for both configurations of the instrument have shown that no LIF signal was observable above the background when neat synthetic air was sampled by the detection cell.

A permeation source of gas phase HCHO was used to calibrate the HCHO LIF instrument when operated in configuration 3. The main reason for this was that using the 'wand' calibration method described above can be challenging and time consuming in the field. The performance of pen ray lamps can also deteriorate rapidly, and if the value for *F* used is incorrect due to this, it may not be possible to rationalise any discrepancies between calibrations. For example, if the relationship between *F* and lamp current was determined at the beginning and end of a field campaign (it would not be practical to measure this regularly during the campaign), any differences might be difficult to reconcile. In this case it would be unknown if a change in C_{HCHO} was due to deterioration of the pen ray lamp or if it was a genuine change in sensitivity.

A commercial permeation tube source containing paraformaldehyde (Kintek Analytical) was used to provide gas phase HCHO at a known emission rate of 10 ng min^{-1} at 60 ˚C. The emission rate of the permeation tube source is checked gravimetrically periodically. During the calibration of the instrument in configuration 3 the permeation tube was contained in a stabilised oven (Kintek Analytical, temperature variation <±0.1 ˚C) at 60 ˚C. A constant flow of 75 SCCM of synthetic air (BOC, BTCA) was passed through the volume containing the permeation tube and this resulted in a known gas phase concentration of 2.67×10^{12} molecule cm^{-3} of HCHO (calculated using 10 ng min^{-1} emission rate) on exit. This flow was mixed with a larger flow from the same cylinder to dilute the HCHO before it was passed to the HCHO LIF instrument. The dilution flow was adjusted to change the level of HCHO in the flow to the instrument and was adjusted between 2 and 15 SLM to give a range in [HCHO] between ~1-9 × 10^{10} molecule cm^{-3}. Points for zero HCHO were measured using a neat flow of synthetic air. As discussed in Section 2.3.6 it was not possible to normalise the LIF signals recorded for laser power measured in mW owing to it being difficult to accurately measure the reduced power of the UV laser light following a repair. For the calibration of the instrument

in configuration 3, which was used for the ICOZA deployment (Chapter 6), signals are plotted in count s^{-1} V^{-1}. However, the laser power was very stable during ICOZA and it is estimated that the 'online' UV laser power was typically ~4 mW. Figure 2.30 shows the calibration plot that was determined for configuration 3 of the HCHO LIF instrument during its deployment for the ICOZA campaign.

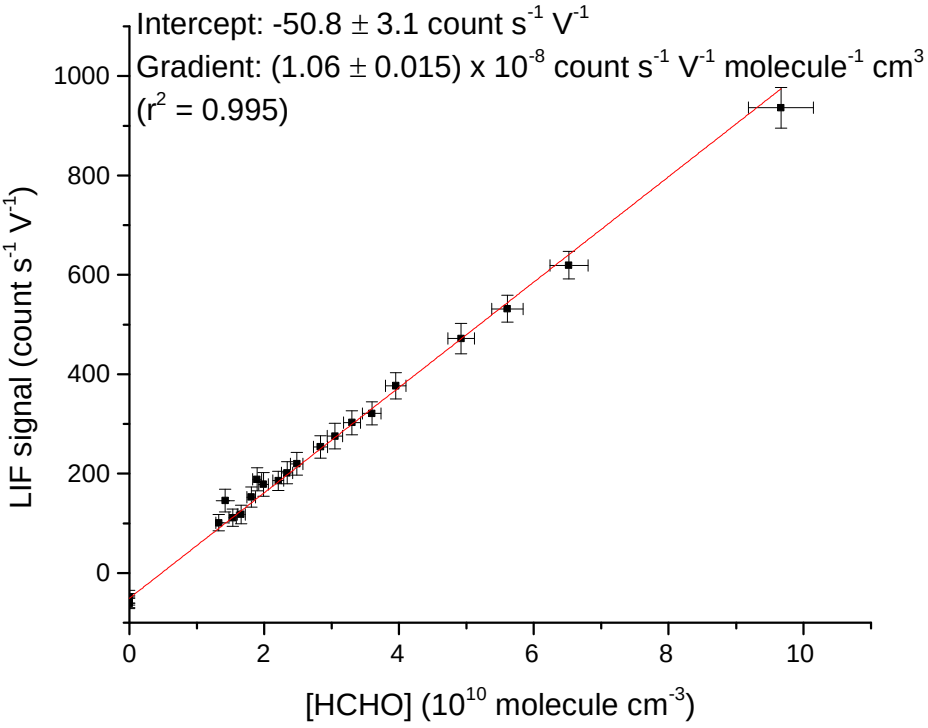

Figure 2.30: Results from the calibration of the LIF HCHO instrument during the ICOZA campaign. The gradient of the line of best fit is equal to the sensitivity (C_{HCHO}) which is 1.06 × 10^{-8} count s^{-1} V^{-1} $molecule^{-1}$ cm^3. y-error bars represent ± 1σ standard deviation in the LIF signals recorded. x-error bars represent the uncertainty in the calculated [HCHO] supplied to the instrument, as determined through propagation of the uncertainties in the flow of gas over the permeation source, and the dilution flow.

The HCHO LIF instrument was recalibrated at the end of the ICOZA campaign using the same method to check the stability of its sensitivity over time. This also provided a good opportunity to test for any dependency of the sensitivity of the instrument on cell pressure. During normal operation of the instrument the pressure of the main detection cell was ~115 Torr. However, this has been observed to drift by a few Torr over time. Each point in the calibration at the end of ICOZA was repeated three times, each at a different cell pressure (110, 115 and 120 Torr). Figure 2.31 shows the calibration plot that was determined for configuration 3 of the

HCHO LIF instrument at the end of the ICOZA campaign. The signals recorded for each concentration of HCHO did not vary significantly as the pressure of the detection cell was adjusted, indicating no quantifiable pressure dependency of C_{HCHO} in the range 110-120 Torr.

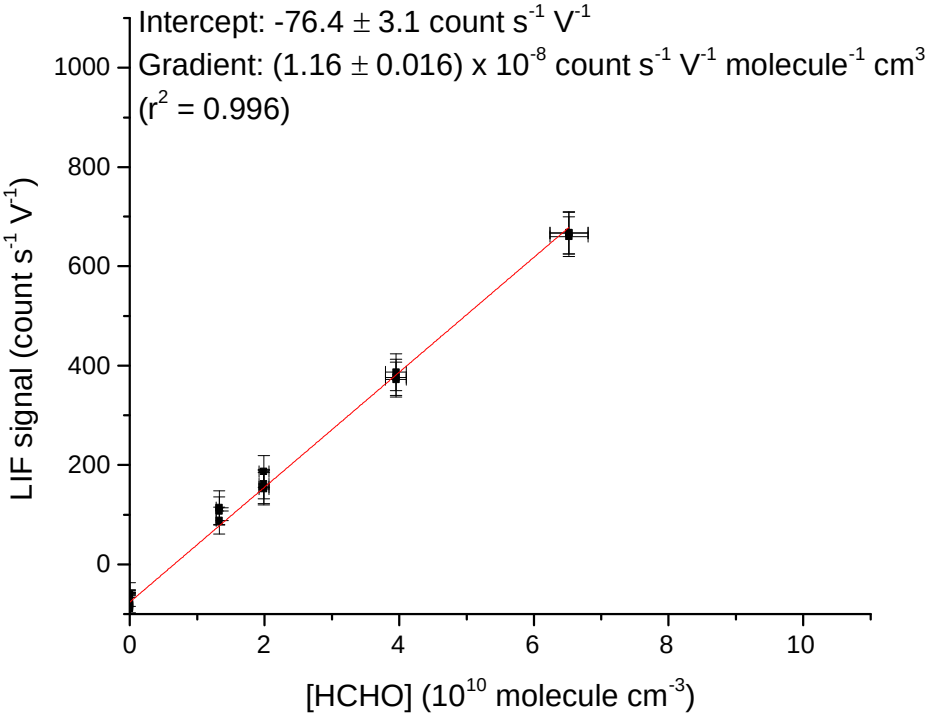

Figure 2.31: Results from the calibration of the LIF HCHO instrument at the end of the ICOZA campaign. The gradient of the line of best fit is equal to the sensitivity (C_{HCHO}) which is 1.16×10^{-8} count s^{-1} V^{-1} molecule^{-1} cm^3. Three points at each level of HCHO were recorded each at different cell pressures (110, 115 and 120 Torr). y-error bars represent ± 1σ standard deviation in the LIF signals recorded. x-error bars represent the uncertainty in the calculated [HCHO] supplied to the instrument, as determined through propagation of the uncertainties in the flow of gas over the permeation source, and the dilution flow.

It can be seen from Figure 2.30 and Figure 2.31 that both calibration plots show a small negative intercept, indicating that there was a negative signal differential when neat synthetic air was supplied to the instrument. This was not expected as in configurations 1 and 2 of the instrument this behaviour was not observed. It is likely that the cause of this was due to non-linearity between the response of the photodiode used to normalise the LIF signals and laser power.

Given the persistent presence of the negative intercept in the calibration plots it was used in the conversion of HCHO LIF signals to concentrations. This intercept and the C_{HCHO} values determined from both calibrations were very similar with only

minor (although slight larger than the quoted uncertainties) differences. The average intercept was used in combination with the average C_{HCHO} to convert the signals. This corresponded to a limit of detection of 46 ppt in 1 s for a signal to noise ratio of 1. All limits of detection for HCHO ($[HCHO]_{min}$) reported in this chapter were calculated using E 2.5. *SNR* is the signal to noise ratio, S_{back} is the background signal resulting from scattered light, t is the measurement period and m and n are the number of 'online' and 'offline' points, respectively.

$$[HCHO]_{min} = \frac{SNR}{C_{HCHO}} \sqrt{\frac{S_{back}}{t} + \left(\frac{1}{m} + \frac{1}{n}\right)} \qquad \textbf{E 2.5}$$

To visually demonstrate the signal to noise ratios that are typically observed by the HCHO LIF instrument, two example signals are shown in Figure 2.32. These were recorded during the first calibration of the ICOZA campaign (shown in Figure 2.30). Both signals shown demonstrate that in each case the HCHO signals recorded ('online' shown in green) are clearly distinguishable from the background signals ('offline' shown in red).

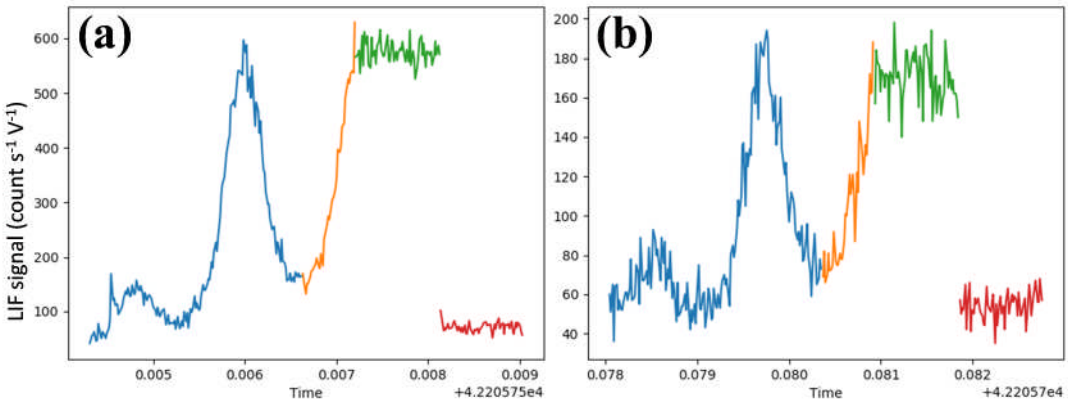

Figure 2.32: Example signals recorded by the HCHO LIF instrument. 1 s data are shown and signals are normalised for laser power as recorded in V by a photo-diode. Each plot shows a complete measurement cycle; blue signal is recorded as the laser wavelength is scanned over the spectroscopic feature, orange signal is recorded as the laser wavelength scan is reversed, green signal is recorded during the 'online' period and red signal is recorded during the 'offline' period. (a) shows a signal where a relatively high concentration of HCHO (~6×10^{10} molecule cm^{-3}) was supplied to the instrument. (b) shows a signal where a relatively low concentration of HCHO (~2×10^{10} molecule cm^{-3}) was supplied to the instrument. Note: the range of the y-axis is different for each plot.

2.4 Summary

In this chapter two field instruments have been described, details regarding their principle of operation, data acquisition method, and component parts are presented. A LFP-LIF instrument for the measurement of OH reactivity is described in Section 2.2. Observations of OH reactivity made using this instrument, in ambient air at an urban background site in York, UK and a coastal site in Norfolk, UK are presented in Chapters 5 and 6 of this thesis, respectively. Observations of OH reactivity made using this instrument, during an inter-comparison study at the SAPHIR chamber are presented in Chapter 3. The LFP-LIF instrument has been continually developed through the course of this work and as a result its configuration has changed between the studies described in Chapters 3, 5 and 6. Two configurations of the LFP-LIF instrument are described in Section 2.2.7, configuration 1 was used for measurements in York and configuration 2 was used for measurements in Norfolk and at the SAPHIR chamber. Section 2.2.9 details the determination of the loss rate of OH due to physical process within the flow tube for each configuration of the LFP-LIF instrument, this was 1.25 ± 0.42 s^{-1} for configuration 1 and 2.25 ± 0.21 s^{-1} for configuration 2.

In Section 2.3 of this chapter details of an LIF instrument for the detection of gas phase HCHO are presented. The instrument was used in laboratory measurements of HCHO that are presented in Chapter 4, it was used to make measurements of HCHO in ambient air in York and Norfolk, simultaneous to the deployment of the LFP-LIF instrument. Similar to the LFP-LIF instrument the HCHO LIF instrument was continually developed through the course of this work. Three configurations are described in Section 2.3.6. configuration 1 was used for the laboratory experiments in Chapter 4 and configurations 2 and 3 were used for the York and Norfolk deployments, respectively. Section 2.3.7 details two methods for the calibration of the instrument; one where a known quantity of HCHO is produced through photolysis of MeOH for addition to the instrument, and one where a known quantity of OH is added to the instrument using a commercial permeation source. The first method was used to calibrate the instrument for the laboratory measurements presented in Chapter 4, and the measurements from York presented in Chapter 5. The second method was used to calibrate the instrument for the measurements from Norfolk presented in Chapter 6.

2.5 References

ATKINSON, R., BAULCH, D. L., COX, R. A., CROWLEY, J. N., HAMPSON, R. F., HYNES, R. G., JENKIN, M. E., ROSSI, M. J. & TROE, J. 2004. Evaluated kinetic and photochemical data for atmospheric chemistry: Volume I - gas phase reactions of Ox, HOx, NOx and SOx species. *Atmos. Chem. Phys.,* 4**,** 1461-1738.

BOC. 2016. *Automotive Speciality Gases* [Online]. BOC. Available: http://www.boconline.co.uk/en/industries/manufacturing/automotive/automotive-speciality-gases/automotive-speciality-gases.html 2016].

COMMANE, R., FLOQUET, C. F. A., INGHAM, T., STONE, D., EVANS, M. J. & HEARD, D. E. 2010. Observations of OH and HO2 radicals over West Africa. *Atmos. Chem. Phys.,* 10**,** 8783-8801.

EDWARDS, P. M. 2011. *Tropospheric oxidation from the tropics to the poles.* PhD, University of Leeds.

HOTTLE, J. R., HUISMAN, A. J., DIGANGI, J. P., KAMMRATH, A., GALLOWAY, M. M., COENS, K. L. & KEUTSCH, F. N. 2008. A Laser Induced Fluorescence-Based Instrument for In-Situ Measurements of Atmospheric Formaldehyde. *Environmental Science & Technology,* 43**,** 790-795.

HUNTER, J. D. 2007. Matplotlib: A 2D Graphics Environment. *Computing in Science & Engineering,* 9**,** 90-95.

MATSUMI, Y. & KAWASAKI, M. 2003. Photolysis of Atmospheric Ozone in the Ultraviolet Region. *Chemical Reviews,* 103**,** 4767-4782.

MCKINNEY, W. 2012. *Python for data analysis,* CA, O'Reilly Media Inc.

SMITH, S. C. 2007. *Atmospheric measurements of OH and HO_2 using the FAGE technique: Instrument development and data analysis.* PhD, University of Leeds.

STONE, D., WHALLEY, L. K., INGHAM, T., EDWARDS, P. M., CRYER, D. R., BRUMBY, C. A., SEAKINS, P. W. & HEARD, D. E. 2016. Measurement of OH reactivity by laser flash photolysis coupled with laser-induced fluorescence spectroscopy. *Atmos. Meas. Tech.,* 9**,** 2827-2844.

WALT, S. V. D., COLBERT, S. C. & VAROQUAUX, G. 2011. The NumPy Array: A Structure for Efficient Numerical Computation. *Computing in Science & Engineering,* 13**,** 22-30.

WHALLEY, L. K., STONE, D., BANDY, B., DUNMORE, R., HAMILTON, J. F., HOPKINS, J., LEE, J. D., LEWIS, A. C. & HEARD, D. E. 2016. Atmospheric OH reactivity in central London: observations, model predictions and estimates of in situ ozone production. *Atmos. Chem. Phys.,* 16**,** 2109-2122.

Chapter 3 - OH reactivity intercomparison

3.1 Overview of intercomparison

3.1.1 Aim of intercomparison

The field of OH reactivity measurements in the atmosphere has grown rapidly through the course of the last decade with several techniques to achieve such measurements reported. A detailed review of OH reactivity measurements in the literature is provided in Chapter 1. There are three techniques reported for the measurement of OH reactivity and these are the TOHLM (Kovacs and Brune, 2001), LFP-LIF (Sadanaga et al., 2004) and CRM (Sinha et al., 2008) methods. To date there is only one comparison of techniques for OH reactivity measurement reported in the literature. Hansen et al. (2015) reported a comparison of ambient measurements from a NO_x rich site situated on the campus of the University of Lille in Villeneuve d'Ascq, France for two weeks in October 2012. Measurements were made with a LFP-LIF instrument operated by researchers of the University of Lille and a CRM instrument operated by researchers of the Mines Douai National Graduate School of Engineering. The comparison showed that the CRM measurements under predicted OH reactivity by ~20 % as a result of direct photolysis of OH reactive species in the glass OH reactor of the instrument. Adjustment of the configuration of the OH reactor on completion of the ambient measurements was found to reduce this affect to a negligible level, highlighting the value of conducting comparative studies of OH reactivity instrumentation. The comparison also highlighted the importance of accurately determining $k'_{OH(physical)}$ for LFP-LIF instruments, as it was concluded that impurities in the zero air used to measure this likely inflicted a negative bias of ~2 s^{-1} on the measurements.

It was proposed at the first OH Reactivity Specialists Uniting Meeting (ORSUM) in October 2014 at the Max Planck Institute for Chemistry in Mainz, Germany, that a formal intercomparison of all techniques for the measurement of OH reactivity

would be beneficial to the community, where as many instruments as reasonably possible were deployed. It was decided at the ORSUM meeting that this study would take place at the Simulation of Atmospheric Photochemistry in a Large Reaction (SAPHIR) chamber at the Jülich Forschungszentrum. The study took place in October 2015 and included participation from 8 research groups operating a total of 9 instruments (1 TOHLM, 4 LFP-LIF and 4 CRM). The aim was to compare the performance of all instruments in a variety of simulated atmospheric compositions. This chapter summarises the study and presents some results from experiments where the chamber contained 'simple' OH reactive species (CO) and more complex OH reactive species; monoterpenes and real biogenic emissions from a plant chamber, SAPHIR-PLUS (Plant Chamber under SAPHIR). The author was responsible for measurements of OH reactivity made using the Leeds LFP-LIF instrument (described in Section 2.2) in these experiments. These measurements are identified as 'LIF-4' through the chapter. Measurements of OH reactivity reported by other participating institutions during these experiments are anonymised. However, the instruments used to make these measurements will be revealed in a future publication.

3.1.2 The SAPHIR chamber

The SAPHIR chamber is located at the Jülich Forschungszentrum, Germany, and is operated by researchers of the Institute of Chemistry and Dynamics of the Geosphere – Troposphere. The chamber is cylindrical in shape and the walls consist of double walled Teflon foil through which UV radiation from the sun is transmissible, allowing the sun to serve as a natural light source for the study of photo chemically initiated reactions. It is operated at 50 Pa above ambient pressure and a large louvre roof system allows the chamber to be blocked from sunlight to allow reactions to be studied in the dark. The total volume of the chamber is ~270 m^3 and more detailed descriptions can be found in Bohn et al. (2005), Rohrer et al. (2005) and Wegener et al. (2007). Figure 3.1 shows a photograph of the SAPHIR chamber exposed to sunlight with the louvre roof open.

SAPHIR is designed so that there is room for multiple shipping containers housing instrumentation to be positioned underneath. The advantage of this is that relatively short sampling lines can be used as they can pass through the floor of the chamber and be routed to instrumentation through the roof of a shipping container. There are

five inlet port panels in the floor of the chamber to allow for this, one of such is shown in Figure 3.2.

Figure 3.1: The SAPHIR chamber pictured with the louvre roof open to allow exposure to sunlight. Taken from (EUROCHAMP, 2016).

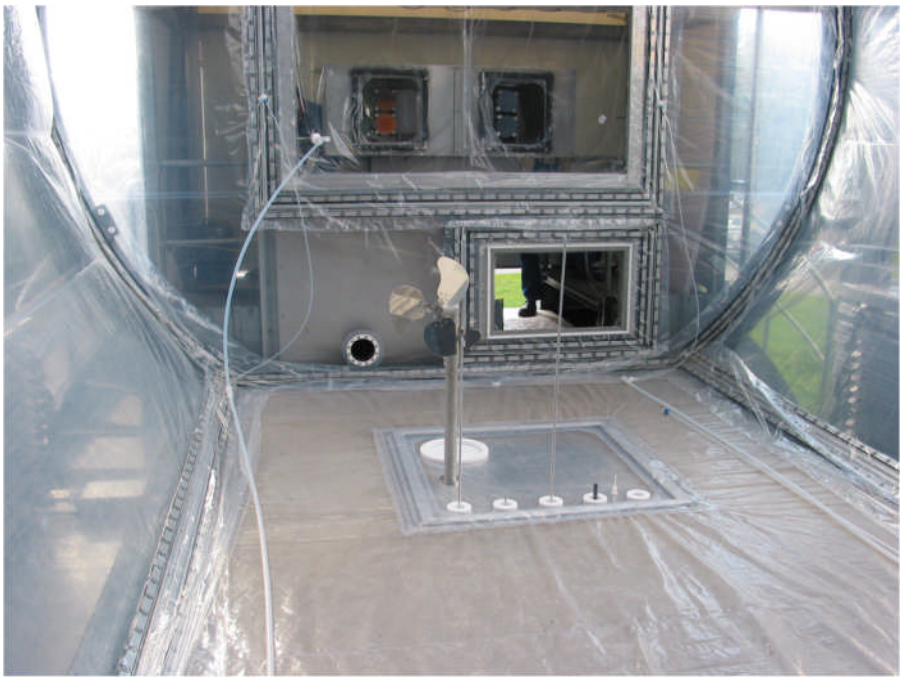

Figure 3.2: One of five inlet port panels in the floor of the SAPHIR chamber to allow gas samples to be transferred to instrumentation in shipping containers below. Taken from (EUROCHAMP, 2016).

3.1.3 Participating instrumentation

A total of 9 instruments were used for the measurement of OH reactivity during the comparison study at the SAPHIR chamber. The institutions which deployed these instruments are listed in Table 3.1 in addition to the measurement techniques used and appropriate references.

Institution	Technique	Reference
Penn State University (USA)	TOHLM	Kovacs and Brune (2001)
University of Leeds (UK)	LFP-LIF	Stone et al. (2016)
Jülich Forschungszentrum (FZJ) (Germany)	LFP-LIF	Lou et al. (2010)
Jülich Forschungszentrum (FZJ) (Germany)	LFP-LIF	Fuchs et al. (2016)
University of Lille (France)	LFP-LIF	Amedro et al. (2012)
Max Planck Institute for Chemistry (MPIC) (Germany)	CRM	Sinha et al. (2008)
Mines Douai National Graduate School of Engineering (France)	CRM	Michoud et al. (2015)
Laboratory of the Sciences of Climate and the Environment (LSCE) (France)	CRM	Zannoni et al. (2016)
Finnish Meteorological Institute (FMI) (Finland)	CRM	Not available

Table 3.1: Instruments for the measurement of OH reactivity used in the intercomparison study at the SAPHIR chamber in October 2015.

Each of the 9 instruments listed were housed in shipping containers below the chamber during the comparison study. The positioning of these containers is summarised by the diagram in Figure 3.3. Areas displayed in red are where containers were placed specifically for the OH reactivity comparison study described here, all other spaces shown were occupied by containers that were a permanent fixture at SAPHIR. The space labelled Leeds was occupied by the Leeds FAGE container and housed the Leeds LFP-LIF instrument which was operated in configuration 2 (described in Chapter 2) and shared an inlet port panel with the University of Lille LFP-LIF instrument. The method for sampling from SAPHIR with the Leeds LFP-LIF instrument is described in Section 3.2. In one of the containers adjacent to the Leeds FAGE container three CRM instruments were housed and all sampled from the same inlet port panel. To the other side of the Leeds FAGE container was a container which housed the Penn State TOHLM instrument which shared an inlet port panel with two Jülich Forschungszentrum LFP-LIF instruments which were operated from a container opposite. The LSCE

CRM instrument was operated from another container along with some instrumentation for ancillary measurements. These shared an inlet port panel with some GC instrumentation that were used to measure VOCs.

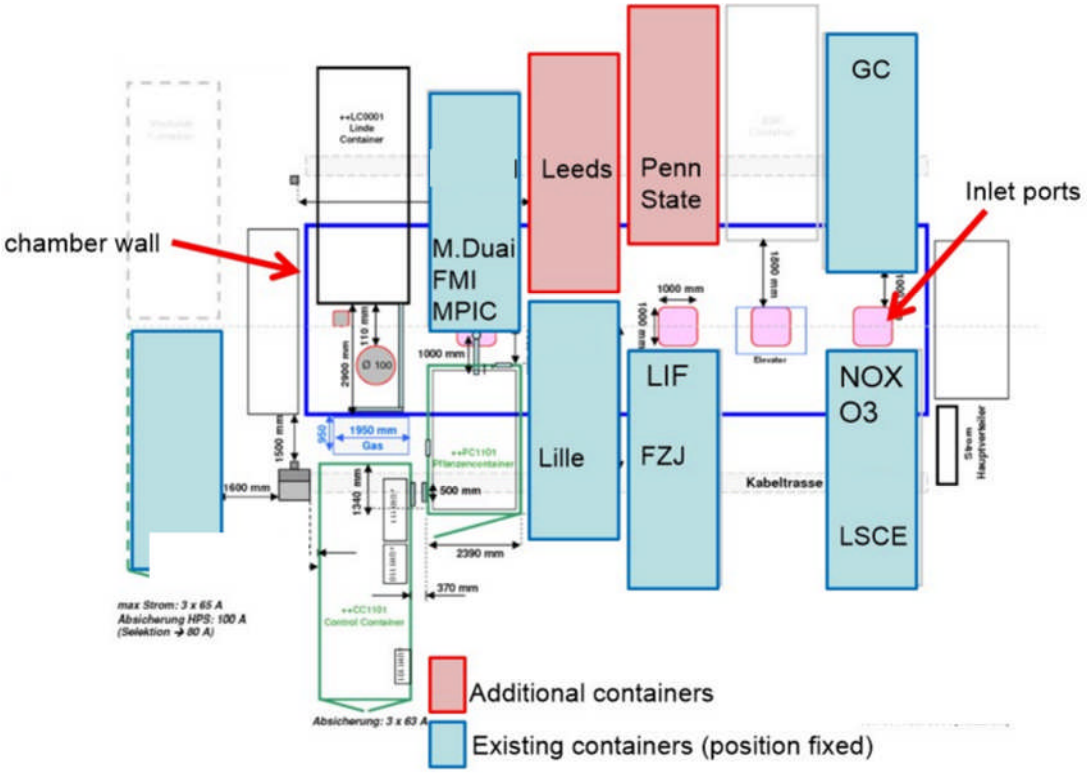

Figure 3.3: Diagram to show the placement of instrumentation within shipping containers below the SAPHIR chamber during the OH reactivity intercomparison study in October 2015. Areas shown in red were occupied by containers that were placed underneath the chamber for the purpose of the comparison. Areas shown in blue were occupied by containers that were a permanent fixture at SAPHIR. Provided by Dr. Hendrik Fuchs, Jülich Forschungszentrum.

3.2 Sampling method

The Leeds LFP-LIF instrument was operated in configuration 2 (as described in Section 2.2.7) from inside the Leeds FAGE container (described in Section 2.2.2). The container was positioned at SAPHIR such that ~1/3 of its roof area was covered and the main door was facing away from the chamber. The image shown in Figure 3.4 shows the position of the FAGE container at SAPHIR whilst measurements were made during the OH reactivity intercomparison.

Figure 3.4: Image showing the Leeds FAGE container at the SAPHIR chamber during the OH reactivity comparison in October 2015.

Owing to it being necessary to position the FAGE container beneath SAPHIR to minimise the length of the sampling line, it was not possible to position the instrument on the roof of the container as is usually the case for ambient measurements in the field. The components which would usually be fixed to a table top, were removed and fixed to a new aluminium panel in the same way as they had been fixed to the table top. This panel fitted to the top of the rack inside the FAGE container above the 308 nm detection laser as shown in Figure 3.5.

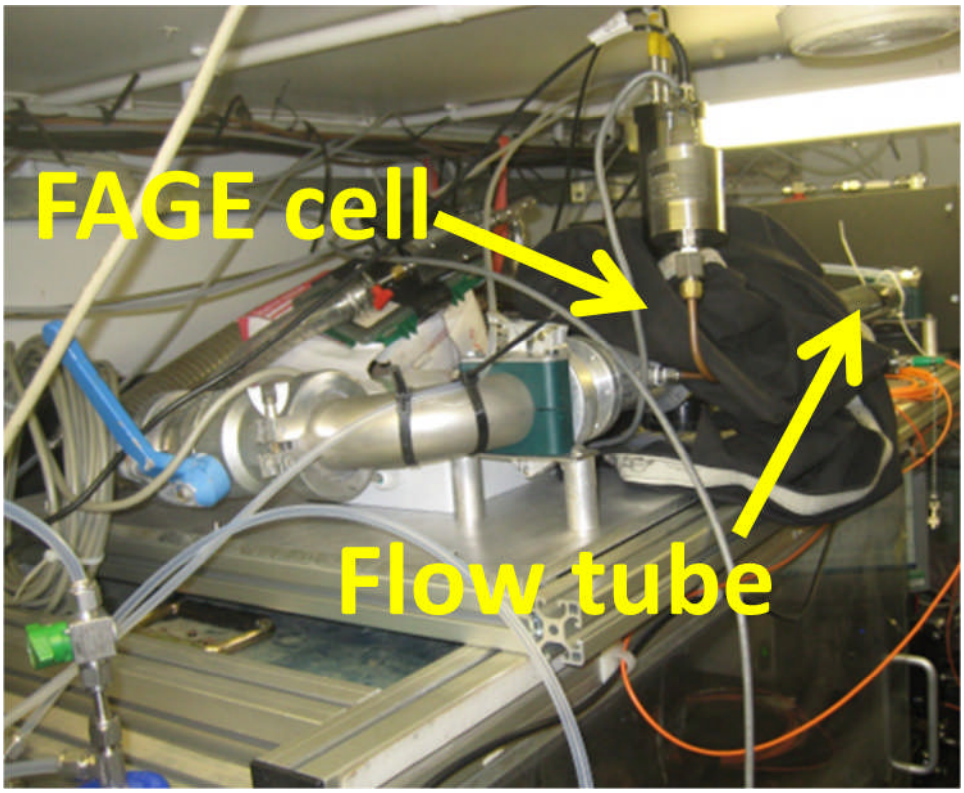

Figure 3.5: Photograph of the LFP-LIF instrument above the racking inside the FAGE container. Visible key features are labelled.

A PFA sampling line ~5 m in length (½" OD) connected the instrument to the inlet port panel (example shown in Figure 3.2) through which it protruded ~30 cm into the chamber. It was connected to the flow tube of the instrument via a ½" Swagelok t-piece where one of the connectors was reduced to ¼" Teflon tubing which in turn was connected to a ¼" valve. This valve was fitted to a glass cell where a flow of synthetic air could be irradiated with a Hg(Ar) pen ray lamp to generate ozone to be photolysed by 266 nm laser radiation in the flow tube of the instrument. In all experiments conducted during the comparison the chamber was humidified to a sufficient level for OH decays to be observed by all LFP-LIF instruments and in most experiments ozone was also added to the chamber for this. However, in some experiments such as those where monoterpenes and biogenic emissions were oxidised through ozonolysis, it was not possible for ozone to be in the chamber prior to the initiation of ozonolysis (through addition of ozone). During these experiments ozone was added to the gas sample prior to entrance to the flow tube using the system described above so that OH decays were observable. For this 1 SLM of synthetic air supplied locally at SAPHIR through the boil off of liquid nitrogen and

oxygen was irradiated in the glass cell and mixed with 15 SLM of gas sampled from the chamber. Measurements using an ozone analyser (Thermo Scientific) showed that this would result in ~60 ppb of ozone within the flow tube of the instrument, when the pen ray lamp was operated at 21 mA (max output). These conditions were the same for every experiment where the addition of ozone was necessary.

It was not practically feasible to routinely check the flow rate of the gas sample into the LFP-LIF instrument through periodically fitting the flow meter (MKS 179A, 0-20 SLM) to the sampling line, as is usually the case during ambient measurements. The sampling line had to remain connected to the chamber at all times. To enable constant monitoring of the flow of gas sampled it was necessary to first determine the flow rate into the FAGE cell. Experiments were conducted where the flow meter was fitted to the end of the ~5 m sampling line and the gas lines that are usually used for pumping excess gas out of the flow tube were capped. A flow rate of 3.6 SLM was measured and found to be stable over a range of FAGE cell pressures (1.1 – 4.8 Torr) whilst the flow tube pressure was stable at ~760 Torr. Upon connecting the sampling line to SAPHIR, the flow meter was fitted to the tubing to the scroll pump so that the flow rate of excess gas leaving the instrument could be monitored. During the intercomparison experiments the reading from the flow meter was continually monitored and the butterfly valve that was used to throttle the scroll pump was adjusted to maintain a flow of 12.4 SLM (16 SLM in total entering the flow tube).

During experiments where no ozone was added to the instrument (e.g. that described in Section 3.3.1), $k'_{OH(physical)}$ for the instrument in configuration 2 was subtracted directly from $k'_{OH(raw)}$ that was determined from the decay signals to obtain k'_{OH}. However, during experiments where it was necessary for ozone to be added (e.g. those described in Section 3.3.2) to the instrument, the $k'_{OH(raw)}$ determined from the decay signals were first adjusted according to the dilution by the ozone containing flow.

3.3 Results

3.3.1 Addition of CO

Several experiments were conducted during the OH reactivity intercomparison where known quantities of OH reactive species were added to SAPHIR to test and

compare the response of each instrument. The results from such an experiment with CO are presented here. Humidified synthetic air and ozone ~40 ppb were supplied to the chamber at the beginning of the experiment and ~ 1 hour elapsed before the first addition of ~2 ppb of CO was made. No further additions were made for ~1.5 hours to allow ample time for CRM instruments to obtain 3 or more measurements, as the time resolution for CRM instruments is significantly longer than for LIF type instruments. Following this, similar additions of CO were made to SAPHIR in the same way until a maximum level of ~35 ppm was reached. Figure 3.6 shows measurements of k'_{OH} that were reported for this experiment from each participating instrument. Measurements labelled as 'LIF-4' were made using the Leeds LFP-LIF instrument.

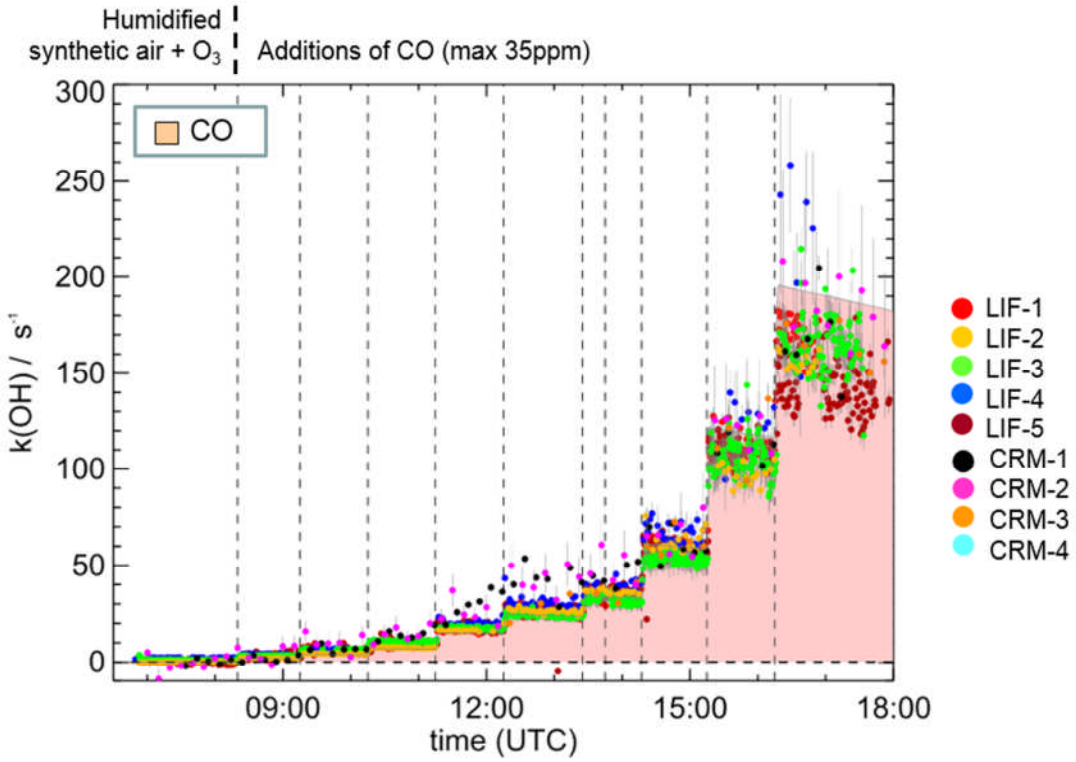

Figure 3.6: Time series of k'_{OH} measured in SAPHIR by nine instruments where known quantities of CO were supplied to the chamber in stepwise additions. Results are anonymised with techniques separated into two categories LIF and CRM where LFP-LIF and TOHLM measurements are both classified as LIF instruments. The shaded area is representative of the OH reactivity calculated to be attributable to the CO added. 'LIF-4' measurements were made using the Leeds LFP-LIF instrument. Provided by Dr. Hendrik Fuchs, Jülich Forschungszentrum.

The results show that the measurements made using the Leeds LFP-LIF ('LIF-4') instrument were in agreement with those made by other instruments in this

experiment, particularly the other LIF type instruments. Observations reported from all instruments followed the profile of the OH reactivity calculated to be attributable to the CO that was added to the chamber (shaded in pink). The agreement is shown to be particularly close when k'_{OH} is below ~100 s^{-1}. However, above this there is considerably more scatter between points for all instruments, indicating that measurements made by participating instruments may become less reliable above this threshold. This is true for the Leeds LFP-LIF measurements which show significantly more scatter following the final two additions of CO than for the rest of the experiment. However, the OH reactivity calculated using the CO concentration here is greater than 100 s^{-1}. This is far beyond (35 ppm) what is typically observed in ambient air for any environment, the scatter observed during this experiment should not significantly affect the precision of field measurements made using the Leeds LFP-LIF instrument.

The points representing measurements by the CRM instruments show more variation than the LIF measurements when k'_{OH} is below ~50 s^{-1}. The cause of this is likely that changes in pyrrole concentration which need to be quantified to determine k'_{OH} in CRM type instruments (described in Section 1.5.4), are subject to greater uncertainty at lower reactivities, owing to the changes in pyrrole concentration being closer to the limit of detection of the instrumentation used for detection.

3.3.2 Oxidation of monoterpenes and real biogenic emissions

To test the performance of the participating instruments with more complex gas mixtures some experiments were conducted with known quantities of monoterpenes, characteristic of biogenically influenced atmospheres, and also real biogenic emissions from plants. It was important to compare the performance of the instrumentation under such conditions as 'missing' OH reactivity is often postulated to be the result of undetected biogenic emissions, such as monoterpenes. Di Carlo et al. (2004) and Edwards et al. (2013) reported 'missing' reactivities as high as ~50 % from forest atmospheres where k'_{OH} was measured using the TOHLM technique. High 'missing' OH reactivity has also been reported from forest atmospheres using the CRM technique, for example Sinha et al. (2008) reported 65 % 'missing' reactivity and Nölscher et al. (2012) reported 68 % 'missing' reactivity. There are no observations of OH reactivity for a biogenically dominated environment reported in the literature from a LFP-LIF instrument at present. Although measurements in

forested environments reported in the literature for different techniques are from various locations, simultaneous measurements of OH reactivity have not been made in such an environment using more than one technique.

The first of these experiments described here involved stepwise addition of a mixture of monoterpenes (containing equal quantities of α-pinene, limonene and myrcene) to SAPHIR to cover a range of OH reactivities up to ~20 s^{-1}. Following this ozone was added to the chamber to initiate an ozonolysis reaction. Figure 3.7 shows measurements of k'_{OH} that were reported for this experiment from each participating instrument. Measurements labelled as 'LIF-4' were made using the Leeds LFP-LIF instrument.

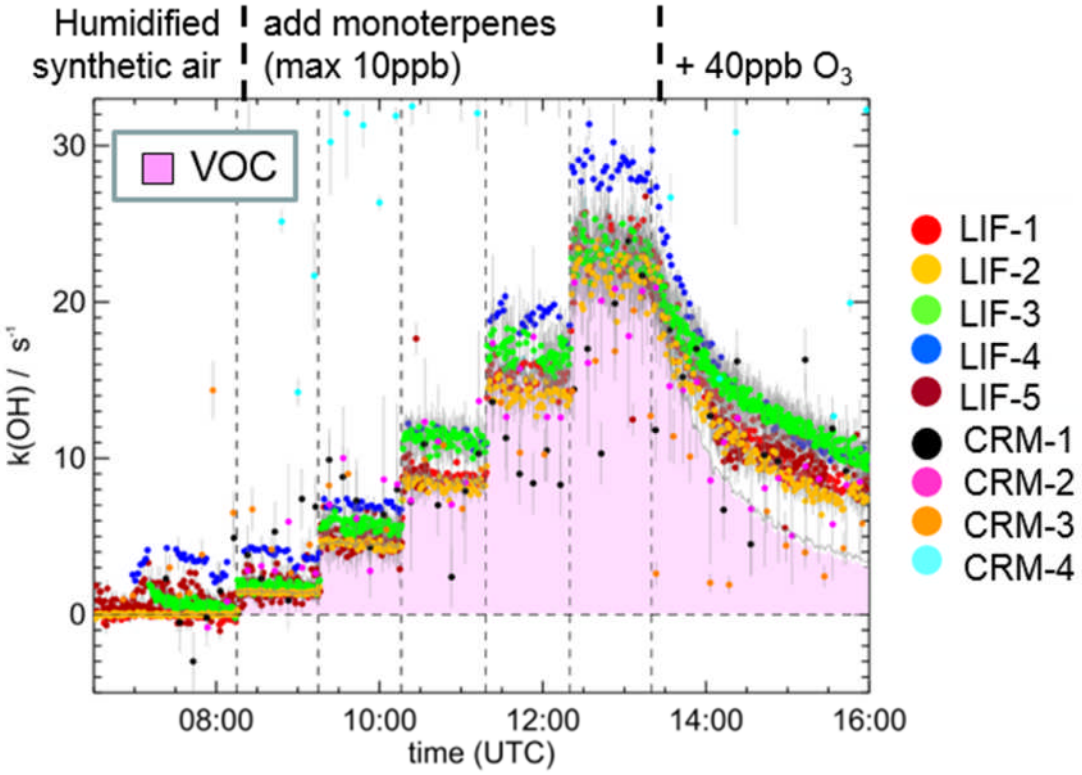

Figure 3.7: Time series of k'_{OH} measured in SAPHIR by nine instruments where known quantities of monoterpenes were supplied to the chamber in stepwise addition followed by the addition of ozone for the initiation of ozonolysis. Results are anonymised with techniques separated into two categories, LIF and CRM, where LFP-LIF and TOHLM measurements are classified as LIF instruments. The shaded area is representative of the OH reactivity calculated to be attributable to the monoterpenes added. 'LIF-4' measurements were made using the Leeds LFP-LIF instrument. Provided by Dr. Hendrik Fuchs, Jülich Forschungszentrum.

The results show that the measurements made using the Leeds LFP-LIF ('LIF-4') instrument tracked the profile of the measurements made with the other instruments

well, particularly the other LIF type instruments. However, they are typically offset by ~3-5 s^{-1} through the course of this experiment. It can be seen that in the 'zero' period (before the addition of any monoterpenes to SAPHIR) that there was some variability in the Leeds LFP-LIF measurements. The most probable explanation for this is that some OH reactive contaminants contributed to the OH reactivity that was measured. This experiment was the first of the intercomparison where it was necessary to add O_3 to the flow tube of the instrument, owing to it being absent from the chamber. It is possible that contaminants originated in the system used to supply O_3 to the instrument.

With the exception of the Leeds LFP-LIF instrument, which had a positive bias likely due to contaminants as discussed above, the LIF type instruments were in good agreement through the course of this experiment and tracked the profile of the calculated OH reactivity attributable to the monoterpenes well (shaded in blue). Measurements from the CRM instruments in this experiment are shown to be considerably more scattered than the LIF measurements and are typically lower. It is possible that these measurements could have underestimated k'_{OH} as a result of direct photolysis of VOCs within the glass OH reactors of these instruments.

The ozonolysis reaction was initiated at ~1330 and from this time the values of OH reactivity measured are shown to decrease gradually, as was the calculated OH reactivity attributable to the monoterpenes. However, the measurements decreased at a slower rate which would be expected in this scenario, when it is considered that OH reactive ozonolysis products that are OH reactive would have formed and these are not included in the calculated reactivity.

In the second experiment described here a plant chamber (SAPHIR PLUS) was used to supply real biogenic emissions to SAPHIR (Hohaus et al., 2016). Upon completion of humidification of SAPHIR at the beginning of the experiment at ~0800 a gas line was opened to allow the transfer of biogenic emissions from plants held within SAPHIR PLUS to SAPHIR. The transfer line was kept open until a maximum of ~6 ppb of emissions had been transferred. Following this, ozone was added to initiate ozonolysis of these emissions at ~1500. Figure 3.8 shows measurements of k'_{OH} that were reported for this experiment from each participating instrument. Measurements labelled as 'LIF-4' were made using the Leeds LFP-LIF instrument.

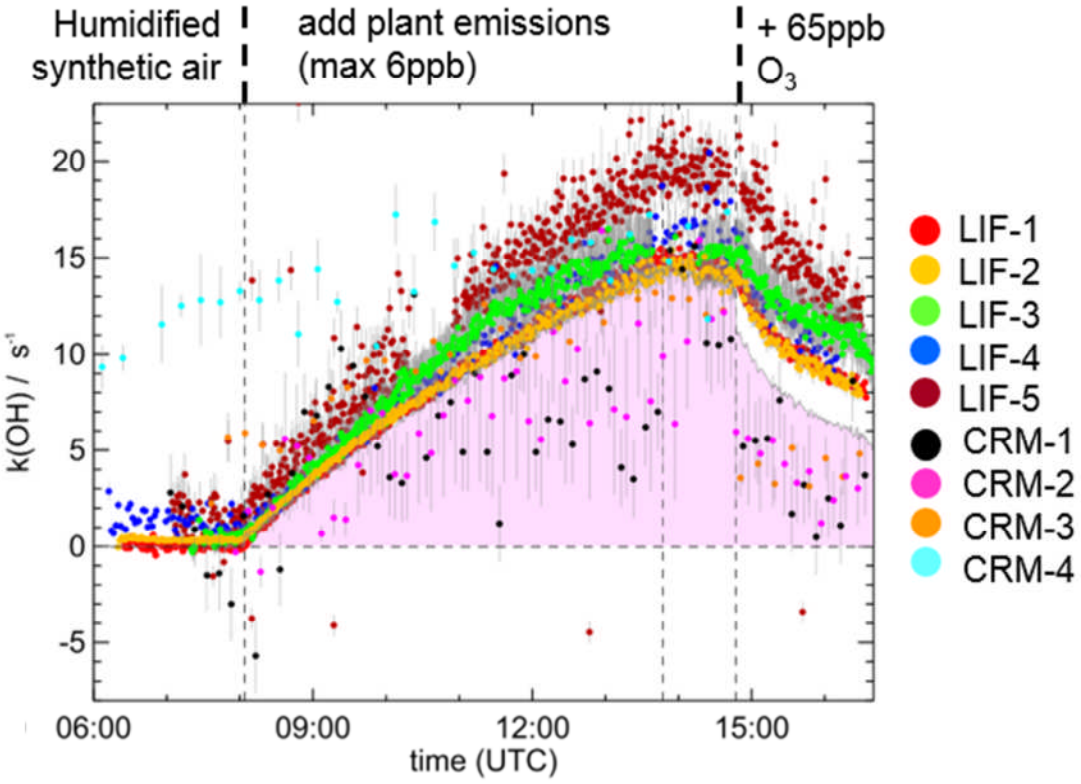

Figure 3.8: Time series of k'_{OH} measured in SAPHIR by nine instruments where real biogenic emissions were to the chamber from a plant chamber (SAPHIR PLUS). Results are anonymised with techniques separated into two categories, LIF and CRM, where LFP-LIF and TOHLM measurements are classified as LIF instruments. 'LIF-4' measurements were made using the Leeds LFP-LIF instrument. Provided by Dr. Hendrik Fuchs, Jülich Forschungszentrum.

It is shown again that the profile of the observations from most of the LIF type instruments are very similar (including those made using the Leeds LFP-LIF ('LIF-4') instrument) and that the most scatter is shown in the observations from CRM instruments. Many observations from CRM instruments are also lower than those from LIF type instruments and the OH reactivity calculated from monoterpene concentrations quantified by a proton transfer mass spectrometer (PTR-MS) and GC-FID. It is possible that these measurements were artificially low due to direct photolysis of OH reactive species within the glass reactors of the CRM instruments. Both the measurements and the calculated reactivity decrease upon addition of ozone to SAPHIR indicating that biogenic emissions from SAPHIR PLUS were removed through ozonolysis reactions. Following the addition of ozone there is also a significant discrepancy between the measured and calculated OH reactivities.

Similar to the previous experiment this is likely due to the formation of OH reactive ozonolysis products that were not measured.

3.3.3 Correlations

In total during the OH reactivity comparison at SAPHIR 10 experiments were conducted, anonymised results from three of these are presented and discussed above. The measurements made using the Leeds LFP-LIF instrument are identified as 'LIF-4'. Results from all experiments undertaken, and a thorough comparison of the measurements from each instrument will form the basis of a future publication. Each experiment conducted fitted into one of two categories. In some experiments known quantities of relatively 'simple' (e.g. CO and CH_4) OH reactive species were added to SAPHIR and no reaction was initiated. In contrast, in other experiments more complex mixtures of OH reactive species were added and ozonolysis reactions were initiated through the addition of ozone, or the chamber contents was photochemically processed through exposure to sunlight.

In experiments where the concentrations of 'simple' OH reactive species added to SAPHIR were known, it was possible to examine the relative relationships between the response of each participating instrument and the calculated k'_{OH}. Whilst full results for only one such experiment are presented above (Figure 3.6), the relationship between measured and calculated OH reactivity for all of these experiments combined is summarised by Figure 3.9. A graph is shown for measured OH reactivity from each instrument that participated versus calculated OH reactivity.

The results show that there was strong correlation between the measurements of OH reactivity that were made using the Leeds LFP-LIF instrument and the OH reactivity calculated from measured OH sinks ($R^2 = 0.97$). The correlation between measured and calculated reactivity was typically stronger for LIF type instruments than the CRM instruments (0.97 vs 0.59 average R^2). It is also shown that the majority of instruments slightly over predicted the calculated OH reactivity, this is possibly because only OH reactive species that were intentionally added to the chamber were included in the calculation of k'_{OH}. It is likely that there were OH reactive impurities present in the chamber that contributed to the measured values.

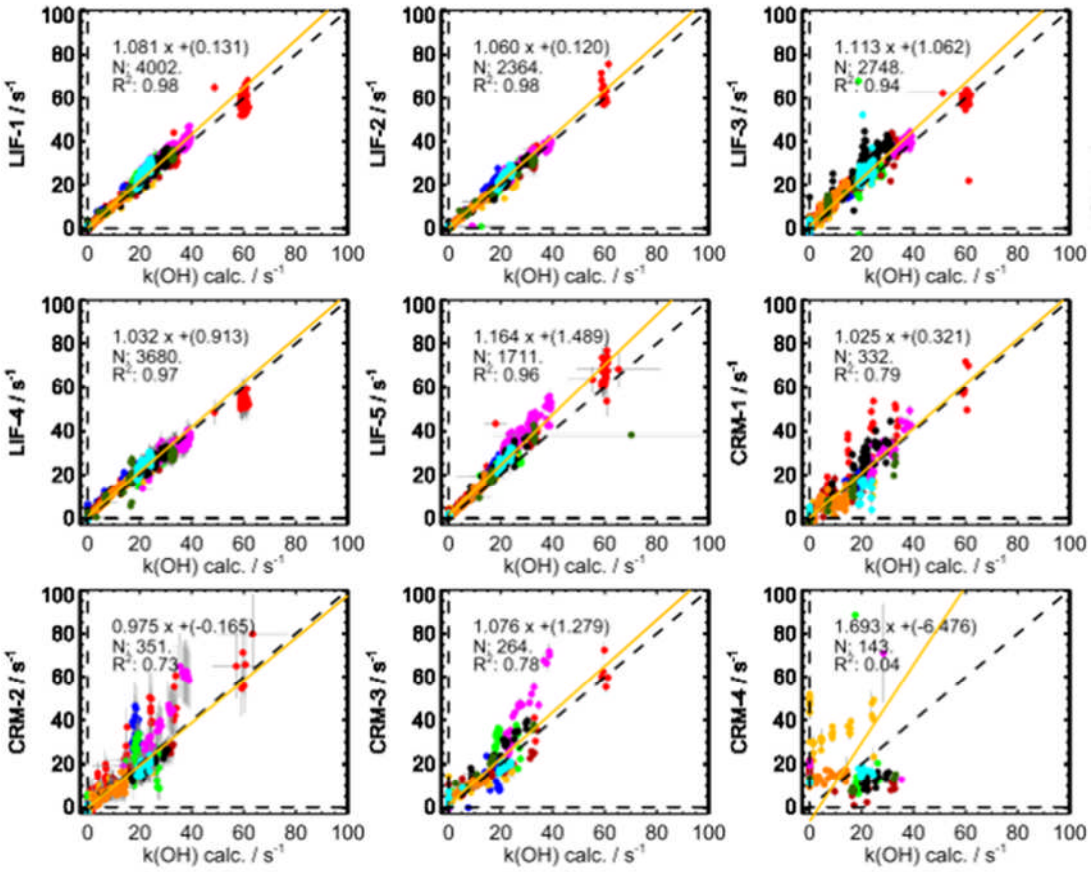

Figure 3.9: Graphs which summarise the relationship between measured and calculated k'_{OH} from all experiments conducted during the OH reactivity comparison at SAPHIR where 'simple' OH reactive species were added to the chamber and no reaction was initiated. Each colour used for the points plotted represent data from a different experiment. 'LIF-4' is identified as the Leeds LFP-LIF instrument. Provided by Dr. Hendrik Fuchs, Jülich Forschungszentrum.

In experiments such as those described in Section 3.3.2 where more 'complex' OH reactive monoterpenes were added to SAPHIR, the overall response of each instrument was compared. It was not possible for the complete inventory of emissions from SAPHIR PLUS to be characterised in one of the experiments to enable reliable calculation of OH reactivity. Therefore, it was decided that the response of each instrument would be compared to a reference instrument. LIF-1 was chosen as this made observations of k'_{OH} that were the least scattered. Figure 3.10 shows data from the two experiments described in Section 3.3.2 for the other instruments plotted against those from LIF-1.

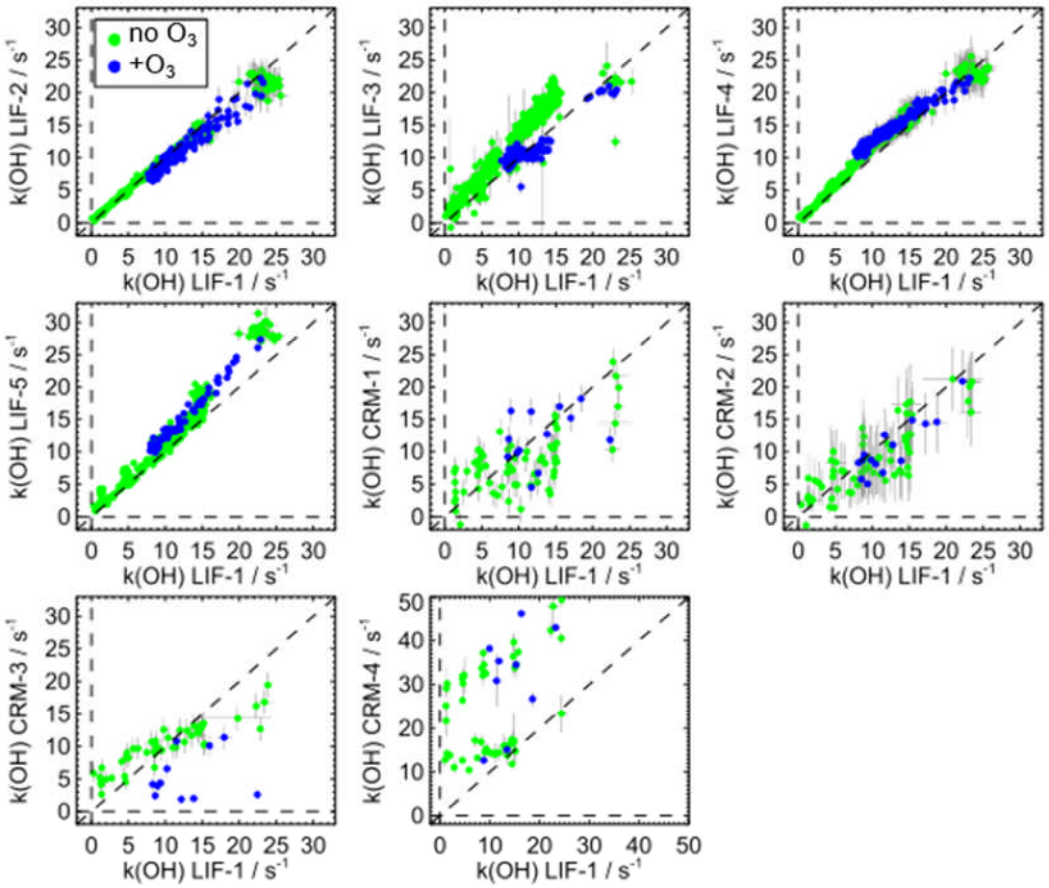

Figure 3.10: A summary of the relationship between measured k'_{OH} from each participating instrument and a reference instrument (LIF-1) for both experiments described in Section 3.3.2 where biogenic emissions were added to SAPHIR and an ozonolysis reaction was initiated. Green points represent data recorded prior to the addition of ozone. Blue points represent data after the addition of ozone. 'LIF-4' is identified as the Leeds LFP-LIF instrument. Provided by Dr. Hendrik Fuchs, Jülich Forschungszentrum.

Again it is shown that the measurements obtained using the LIF type instruments are considerably less scattered than those obtained using the CRM instruments. It can be seen that for most instruments the relationship (slope and scatter) demonstrates no difference in the presence and absence of ozone. However, there appears to be a distinct difference between data recorded by LIF-3. The reason for this is currently unclear and future analysis of these data will be presented in a future publication based on the results from the intercomparison.

3.4 Summary and conclusions

The Leeds LFP-LIF instrument for the measurement of OH reactivity was successfully deployed to the SAPHIR chamber at the Jülich Forschungszentrum,

Germany to take part in an intercomparison campaign. A total of nine instruments from eight different institutions were used for measurements (1 TOHLM, 4 LFP-LIF and 4 CRM). Ten experiments were conducted in total and results from three of these are presented in this chapter. In the first of these, known quantities of CO were added stepwise to SAPHIR whilst the response of each instrument was monitored. It was found that the measurements from all instruments tracked the calculated OH reactivity attributable to CO well. Significantly more scatter was observed for the CRM measurements during this experiment, particularly at lower k'_{OH}. It is likely this was due to corresponding smaller changes in pyrrole concentrations that needed to be observed, in order to successfully determine k'_{OH}, being closer to the limits of detection of instrumentation used for the measurement of pyrrole.

In the second two experiments described in this chapter mixtures of more complex OH reactive species were added to the chamber to simulate a biogenically influenced atmosphere. In the first of these a 1:1:1 mixture of α-pinene, limonene and myrcene was added to the chamber in stepwise additions until the OH reactivity reached ~20 s^{-1}. Following this an ozonolysis reaction was initiated and the measurements were all shown to decrease. It was shown in this experiment that observations from most instruments tracked the changes in calculated reactivity well and that again more scattered observations were reported from the CRM instruments. In the third experiment described in this chapter real biogenic emissions from a plant chamber (SAPHIR PLUS) were flowed into SAPHIR. The process took place over several hours until ~6 ppb total monoterpenes had been added, and the ozonolysis reaction was then initiated. For both experiments described where a biogenically influenced atmosphere was simulated it was found that CRM measurements had a tendency to be lower than the LIF type measurements. A possible explanation for this is that the more complex OH reactive species present were photolysed in the OH reactors of the CRM instruments leading to artificially low measurements, as was reported by Hansen et al. (2015).

It should be noted that the observations and comparisons presented in this chapter are preliminary and only the measurements from one of the LIF type instruments (LIF-4) is directly attributable to the author. A more in-depth analysis of all of the data will be conducted by researchers at Jülich Forschungszentrum in order to comprehensively examine the performance of each instrument, in the context of each experiment.

3.5 References

AMEDRO, D., MIYAZAKI, K., PARKER, A., SCHOEMAECKER, C. & FITTSCHEN, C. 2012. Atmospheric and kinetic studies of OH and HO2 by the FAGE technique. *Journal of Environmental Sciences,* 24**,** 78-86.

BOHN, B., ROHRER, F., BRAUERS, T. & WAHNER, A. 2005. Actinometric measurements of NO₂ photolysis frequencies in the atmosphere simulation chamber SAPHIR. *Atmos. Chem. Phys.,* 5**,** 493-503.

DI CARLO, P., BRUNE, W. H., MARTINEZ, M., HARDER, H., LESHER, R., REN, X., THORNBERRY, T., CARROLL, M. A., YOUNG, V., SHEPSON, P. B., RIEMER, D., APEL, E. & CAMPBELL, C. 2004. Missing OH Reactivity in a Forest: Evidence for Unknown Reactive Biogenic VOCs. *Science,* 304**,** 722-725.

EDWARDS, P. M., EVANS, M. J., FURNEAUX, K. L., HOPKINS, J., INGHAM, T., JONES, C., LEE, J. D., LEWIS, A. C., MOLLER, S. J., STONE, D., WHALLEY, L. K. & HEARD, D. E. 2013. OH reactivity in a South East Asian Tropical rainforest during the Oxidant and Particle Photochemical Processes (OP3) project. *Atmos. Chem. Phys. Discuss.,* 13**,** 5233-5278.

EUROCHAMP. 2016. *EUROCHAMP* [Online]. Available: www.eurochamp.com [Accessed].

FUCHS, H., TAN, Z., LU, K., BOHN, B., BROCH, S., BROWN, S. S., DONG, H., GOMM, S., HÄSELER, R., HE, L., HOFZUMAHAUS, A., HOLLAND, F., LI, X., LIU, Y., LU, S., MIN, K. E., ROHRER, F., SHAO, M., WANG, B., WANG, M., WU, Y., ZENG, L., ZHANG, Y., WAHNER, A. & ZHANG, Y. 2016. OH reactivity at a rural site (Wangdu) in the North China Plain: Contributions from OH reactants and experimental OH budget. *Atmos. Chem. Phys. Discuss.,* 2016**,** 1-30.

HANSEN, R. F., BLOCQUET, M., SCHOEMAECKER, C., LÉONARDIS, T., LOCOGE, N., FITTSCHEN, C., HANOUNE, B., STEVENS, P. S., SINHA, V. & DUSANTER, S. 2015. Intercomparison of the comparative reactivity method (CRM) and pump–probe technique for measuring total OH reactivity in an urban environment. *Atmos. Meas. Tech.,* 8**,** 4243-4264.

HOHAUS, T., KUHN, U., ANDRES, S., KAMINSKI, M., ROHRER, F., TILLMANN, R., WAHNER, A., WEGENER, R., YU, Z. & KIENDLER-SCHARR, A. 2016. A new plant chamber facility, PLUS, coupled to the atmosphere simulation chamber SAPHIR. *Atmos. Meas. Tech.,* 9**,** 1247-1259.

KOVACS, T. A. & BRUNE, W. H. 2001. Total OH Loss Rate Measurement. *Journal of Atmospheric Chemistry,* 39**,** 105-122.

LOU, S., HOLLAND, F., ROHRER, F., LU, K., BOHN, B., BRAUERS, T., CHANG, C. C., FUCHS, H., HÄSELER, R. & KITA, K. 2010. Atmospheric OH reactivities in the Pearl River Delta - China in summer 2006: measurement and model results. *Atmos. Chem. Phys,* 10**,** 11243-11260.

MICHOUD, V., HANSEN, R. F., LOCOGE, N., STEVENS, P. S. & DUSANTER, S. 2015. Detailed characterizations of the new Mines Douai comparative reactivity method instrument via laboratory experiments and modeling. *Atmos. Meas. Tech.,* 8**,** 3537-3553.

NÖLSCHER, A. C., WILLIAMS, J., SINHA, V., CUSTER, T., SONG, W., JOHNSON, A. M., AXINTE, R., BOZEM, H., FISCHER, H., POUVESLE, N., PHILLIPS, G., CROWLEY, J. N., RANTALA, P., RINNE, J., KULMALA, M., GONZALES, D., VALVERDE-CANOSSA, J., VOGEL,

A., HOFFMANN, T., OUWERSLOOT, H. G., VILÃ -GUERAU DE ARELLANO, J. & LELIEVELD, J. 2012. Summertime total OH reactivity measurements from boreal forest during HUMPPA-COPEC 2010. *Atmos. Chem. Phys.,* 12**,** 8257-8270.

ROHRER, F., BOHN, B., BRAUERS, T., BRÜNING, D., JOHNEN, F. J., WAHNER, A. & KLEFFMANN, J. 2005. Characterisation of the photolytic HONO-source in the atmosphere simulation chamber SAPHIR. *Atmos. Chem. Phys.,* 5**,** 2189-2201.

SADANAGA, Y., YOSHINO, A., WATANABE, K., YOSHIOKA, A., WAKAZONO, Y., KANAYA, Y. & KAJII, Y. 2004. Development of a measurement system of OH reactivity in the atmosphere by using a laser-induced pump and probe technique. *Review of Scientific Instruments,* 75**,** 2648-2655.

SINHA, V., WILLIAMS, J., CROWLEY, J. N. & LELIEVELD, J. 2008. The Comparative Reactivity Method – a new tool to measure total OH Reactivity in ambient air. *Atmos. Chem. Phys.,* 8**,** 2213-2227.

STONE, D., WHALLEY, L. K., INGHAM, T., EDWARDS, P. M., CRYER, D. R., BRUMBY, C. A., SEAKINS, P. W. & HEARD, D. E. 2016. Measurement of OH reactivity by laser flash photolysis coupled with laser-induced fluorescence spectroscopy. *Atmos. Meas. Tech.,* 9**,** 2827-2844.

WEGENER, R., BRAUERS, T., KOPPMANN, R., RODRÍGUEZ BARES, S., ROHRER, F., TILLMANN, R., WAHNER, A., HANSEL, A. & WISTHALER, A. 2007. Simulation chamber investigation of the reactions of ozone with short-chained alkenes. *Journal of Geophysical Research: Atmospheres,* 112**,** n/a-n/a.

ZANNONI, N., GROS, V., LANZA, M., SARDA, R., BONSANG, B., KALOGRIDIS, C., PREUNKERT, S., LEGRAND, M., JAMBERT, C., BOISSARD, C. & LATHIERE, J. 2016. OH reactivity and concentrations of biogenic volatile organic compounds in a Mediterranean forest of downy oak trees. *Atmos. Chem. Phys.,* 16**,** 1619-1636.

Chapter 4 - Development of an OH flow reactor

4.1 Motivation for the development of an OH flow reactor

A discussion of the concept of 'missing' OH reactivity is presented in Chapter 1, in addition to details of measurements reported in the literature where significant 'missing' OH reactivity has been observed. There is currently no method presented in the literature for the identification of species that contribute to 'missing' OH reactivity. However, Kato et al. (2011) reported a method to estimate the contribution from OH reactive species that were detectable, but not identifiable, to 'missing' OH reactivity. The study took the form of a relative rate experiment utilising gas chromatograph – flame ionisation detector (GC-FID) peaks. An OH flow reactor was coupled to a GC-FID instrument and ambient air was analysed where it had, and had not been, exposed to OH in a flow reactor. Figure 4.1 shows the schematic diagram in of the instrumental set-up used by Kato et al. (2011) in this study.

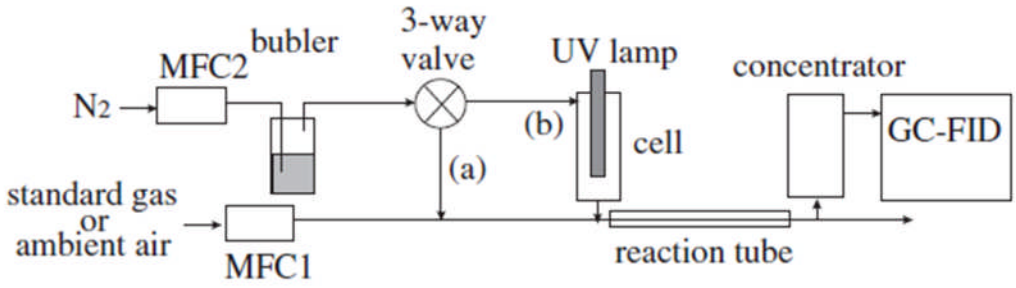

Figure 4.1: Schematic of the experimental set-up used by Kato et al. (2011) to estimate the contribution from unidentified VOCs to OH reactivity. (a) ambient air exposed to OH, (b) ambient air not exposed to OH. Taken from Kato et al. (2011).

The gas to be analysed (1 SLM, either from a standard gas mixture or ambient air) was mixed with nitrogen (1 SLM) which had been humidified using a water bubbler. This either had (OH formation) or had not (no OH formation) been exposed to UV

radiation from a UV lamp. When the humidified nitrogen flow was irradiated, OH was generated through photolysis of water vapour using the 184.9 nm spectral line from the UV lamp, R 4.1.

$$H_2O + h\upsilon_{(\sim 184.9\,nm)} \rightarrow OH + H \qquad \textbf{R 4.1}$$

Rate equations for the reaction of OH with identified (A_i) and unidentified (X_i) species can be expressed as shown in E 4.1 and E 4.2, respectively. k_{Ai} and k_{Xi} are bimolecular rate coefficients for the reaction of OH with A_i and X_i, respectively.

$$\frac{d[A_i]}{dt} = -k_{A_i}[OH][A_i] \qquad \textbf{E 4.1}$$

$$\frac{d[X_i]}{dt} = -k_{X_i}[OH][X_i] \qquad \textbf{E 4.2}$$

Both of these rate equations can be rearranged and integrated to obtain E 4.3 and E 4.4 below. $[A_i]_0$ and $[X_i]_0$ are the concentrations of the identified and unidentified species, respectively, which were determined from integration of peaks in the chromatogram of the sample which was not exposed to OH. $[A_i]_\infty$ and $[X_i]_\infty$ are the concentrations of the identified and the unidentified species, respectively, which again were determined from the chromatogram of the sample which was exposed to OH in the flow reactor.

$$\ln\left(\frac{[A_i]_0}{[A_i]_\infty}\right) = k_{A_i}\int [OH]\,\mathrm{d}t \qquad \textbf{E 4.3}$$

$$\ln\left(\frac{[X_i]_0}{[X_i]_\infty}\right) = k_{X_i}\int [OH]\,\mathrm{d}t \qquad \textbf{E 4.4}$$

In E 4.3 and E 4.4 the integral of [OH] with respect to time is a common factor, thus it was possible to use the relationship between $\ln([A_i]_0/[A_i]_\infty)$ and k_{Ai},to determine $\int$[OH]dt, and subsequently calculate bimolecular rate coefficients for the reaction between the unidentified species and OH. Assuming that VOCs present in the ambient air or standard gas flowed into the reactor were removed exclusively through their reaction with OH, relative rate theory dictates that the relationship should be linear. The relationship should also be unique to the composition of ambient air or standard gas sampled. Figure 4.2 shows the relationship between $\ln([A_i]_0/[A_i]_\infty)$ and k_{Ai} resulting from the analysis of a standard mixture containing 60 VOCs that was reported by Kato et al. (2011).

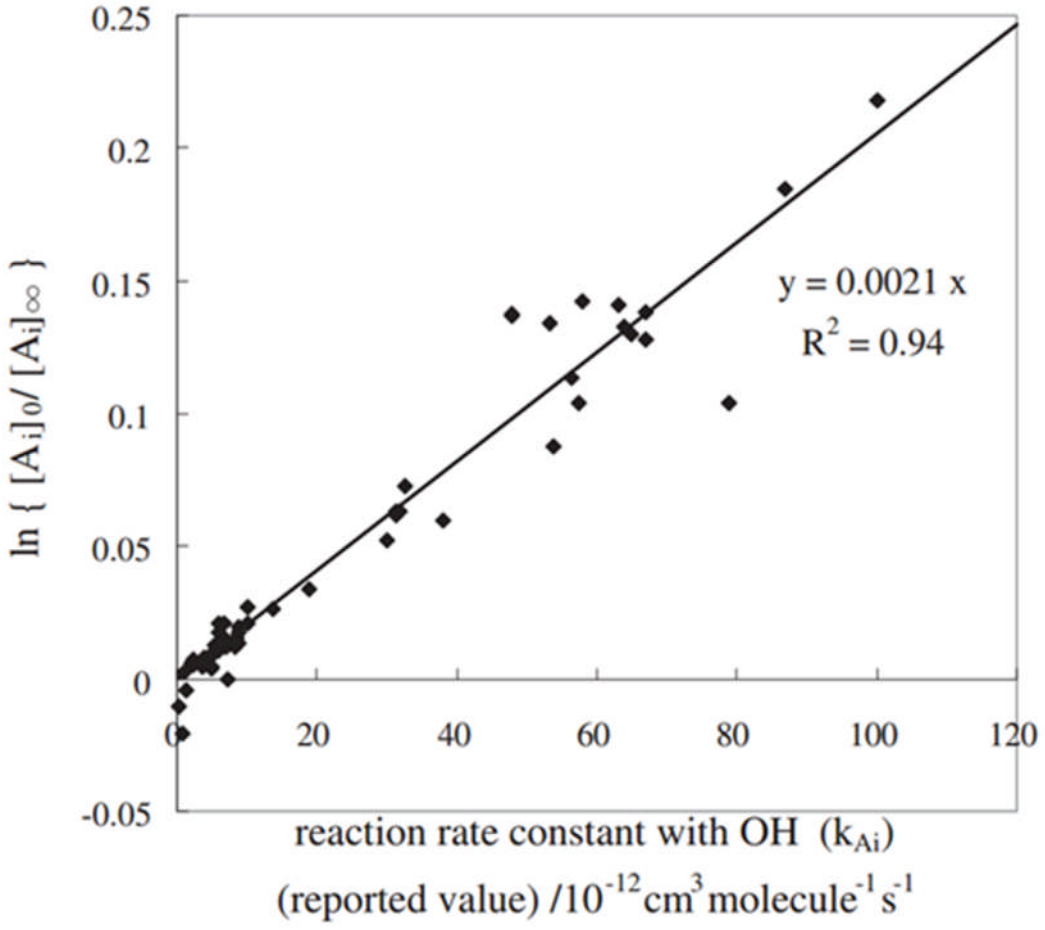

Figure 4.2: The natural logarithm of the ratio of the concentrations of known species (Ai) that have and have not been exposed to OH, respectively vs their literature rate coefficients for reaction with OH. The gradient is equal to the integral of [OH] with respect to time and is ~2×10^9 molecule cm^{-3} s. Taken from Kato et al. (2011).

The data exhibit a linear trend as is expected to be the case when E4.3 is considered. Owing to the linearity associated with the GC-FID technique, between the concentrations of species analysed, and their observed peak areas in the chromatograms, the argument of the logarithm in E 4.4 is equal to the ratio of peak areas for X_i. If the standard mixture contained unidentified OH reactive species, k_{Xi} values could have been determined using E4.4 and $\int$[OH]dt that was determined from the relationship between $\ln([A_i]_0/[A_i]_\infty)$ and k_{Ai}. Using this same method but with ambient air in place of the standard mix, Kato et al. (2011) reported that the relationship between $\ln([A_i]_0/[A_i]_\infty)$ and k_{Ai} could be used to determine $\int$[OH]dt over time in the field. This subsequently could be used in conjunction with E4.4 to determine k_{Xi} values for OH reactive species that were detectable but not identifiable in the field.

The retention times for the unidentified species in the chromatograms could be used to estimate their carbon number and subsequently response factors which were used to calculate estimated values for $[X_i]_0$. These could then be multiplied by corresponding k_{Xi} values (determined using the method outlined above), to obtain an estimate for the contribution from X_i to 'missing' OH reactivity in s^{-1}.

Kato et al. (2011) deployed the instrumentation described above for ambient measurements in urban Tokyo. A total of 28 unidentified species were found to contribute to 'missing' OH reactivity, they accounted on average for ~6 % of the total OH reactivity that was measured using a laser flash photolysis pump and probe instrument. However, the average 'missing' OH reactivity was ~20 % for the measurement period meaning that ~14 % of the total OH reactivity was still not accounted for by the identified and unidentified VOCs detected, or other routinely measured OH sinks (e.g. NO_x and CO). Whilst the study by Kato et al. (2011) broke new ground in the investigation of the source of 'missing' OH reactivity, no discoveries were reported relating to the chemical identities of X_i that were detected. The work detailed in this chapter aimed to address this through the development of a new instrument for the chemical identification of 'missing' OH reactivity.

The first sections details the design, characterisation, and predicted performance of the new OH flow reactor for use in a system similar to that reported by Kato et al. (2011), but with the capability to identify species that contributed to 'missing' OH reactivity. A gas chromatograph time of flight mass spectrometer (GC-TOF-MS) was used for this in the final version of the experimental set up to enable such identification. The final sections provide details of the resulting new instrument for the identification of species contributing to 'missing' OH reactivity and some preliminary observations from the analysis of ambient air during the York 2014 'missing' OH reactivity campaign.

4.2 Design process

The first prototype of the OH flow reactor consisted of a glass (borosilicate) flowtube (1 inch OD) within which a Hg(Ar) pen ray lamp was positioned. N_2, humidified using a water bubbler, was flowed through the tube over the lamp to produce OH through R3.1. Downstream from the lamp, ~5 cm, a flow of standard gas containing VOCs was introduced through a ¼ inch arm for the laboratory tests. If this design of OH reactor was deployed for ambient measurements, ambient air

would have been introduced here. Just after the point of this addition there was a ~45˚ bend in the flow tube, the purpose of this was to try to minimise exposure of UV light from the pen ray lamp to VOCs in the standard gas introduced to prevent their loss due to direct photolysis. For the system to be successful in a relative rate study VOCs must be lost exclusively to their reaction with OH and not photolysis. After passing through another ~20 cm of flow tube, where OH + VOC reactions could occur, the gas would be sampled for analysis. There was also a vent at the end of the system to allow excess gas to exit the system. This prototype design of the OH reactor was transported to the University of York where it was coupled with a GCxGC-TOF-MS instrument so that characterisation experiments could be conducted. Figure 4.3 summarises the key features of the glass OH flow reactor prototype.

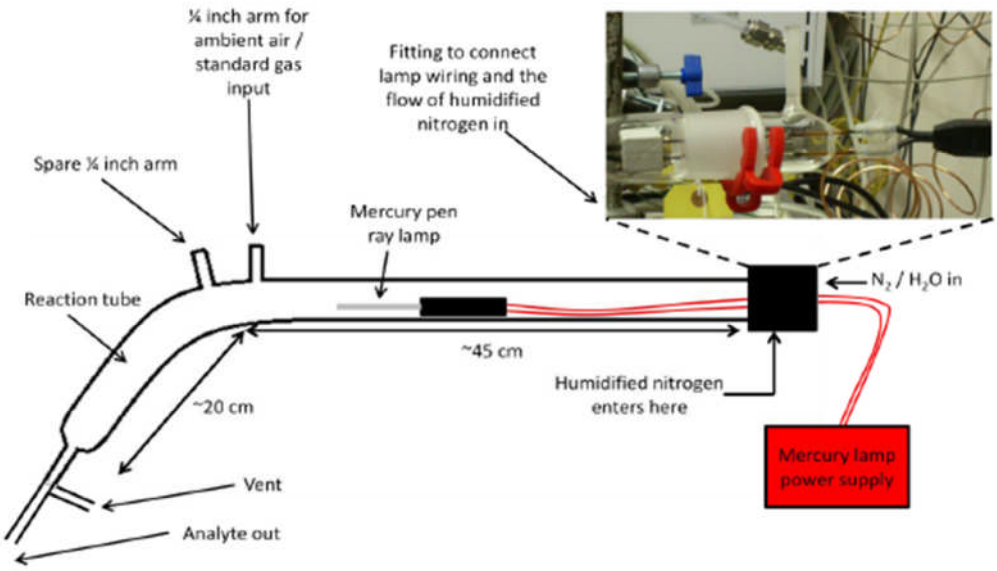

Figure 4.3: Schematic diagram showing the key features of a prototype glass (borosilicate) OH flow reactor that was interfaced with a GCxGC-TOF-MS instrument at the University of York for testing. Diagram not to scale.

Some characterisation experiments for the prototype glass OH flow reactor described above were conducted in which a national physical laboratories (NPL) mixture of 30 VOCs was flowed into the OH flow reactor in place of ambient air. The standard was flowed into the reaction flow tube and tests were first conducted to assess the efficiency of VOC removal. The outflow from the reactor was analysed by the GCxGC-TOF-MS instrument three times with the lamp on, and three times with the lamp off. Average peak areas for 19 VOCs that could be clearly resolved

for quantification are shown in Figure 4.4. All of the VOCs for which data were available were found to decrease when the pen ray lamp was switched on (OH generated), indicating that VOCs were being removed through their reaction with OH. Isoprene ($k_{OH+isoprene}$ = 1 × 10^{-10} cm^3 $molecule^{-1}$ s^{-1} at 298 K) (Atkinson et al., 2006) was removed to the greatest extent (~99 %) whereas benzene ($k_{OH+benzene}$ = 1.2 × 10^{-12} cm^3 $molecule^{-1}$ s^{-1} at 298 K) (Atkinson et al., 2006) was removed to the least extent (~28 %).

The decreases in the levels of the VOCs in the standard mixture that were observed upon exposure to OH were used to construct a plot of $\ln([A_i]_0/[A_i]_\infty)$ vs k_{Ai}, as shown Figure 4.5. A linear trend was found to exist, therefore indicating that the chromatographic peaks representing compounds for which data are plotted, decreased by quantities that scaled with their bimolecular rate coefficients for removal by OH (the basis of the relative rate method). If the only VOC removal process occurring within the reaction flow tube (when the pen ray lamp was switched on) by reaction with OH, the y intercept of the line best fit shown on Figure 4.5 would be expected to be zero. However, it is shown that there is an intercept (0.84); this indicates that there was another pathway for the loss of VOCs in the OH flow reactor other than removal by reaction with OH. It was concluded that the most likely reason for this was that a portion of the VOCs were removed through direct photolysis by stray UV light from the pen ray lamp that was used to generate OH.

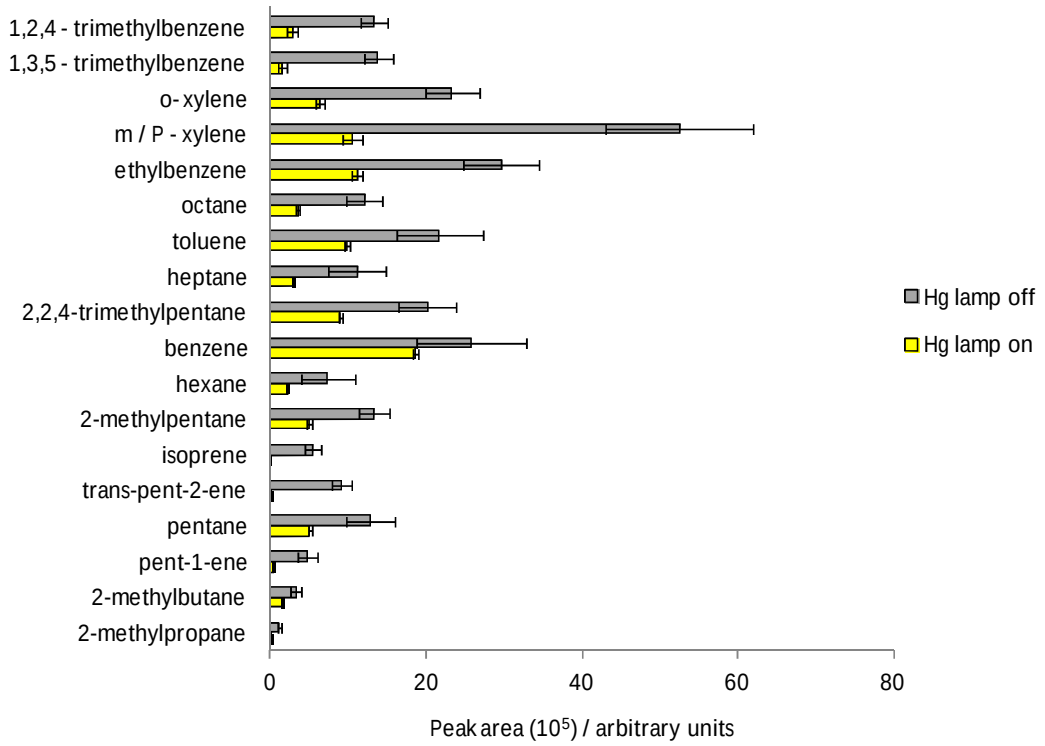

Figure 4.4: Chart to show differences in the concentrations of 18 VOCs with the Hg pen ray lamp off and on, (of the NPL 30 standard) detected in the outflow of the glass OH reactor prototype with the water bubbler present. The data shown are averaged values for three analyses. Error bars are the 1σ standard deviation of the peak areas determined from each analysis that were used to calculate the average values. Data supplied by Dr. Noelia Ramirez, University of York.

If the system consisting of the prototype glass OH flow reactor coupled to the GCxGC-TOF-MS instrument was deployed to the field for ambient measurements, it would have been necessary to construct a plot similar to that shown in Figure 4.5 for each sample of ambient air that was studied. Decreases observed in peaks for identifiable species would have been used to calculate $\ln([A_i]_0/[A_i]_\infty)$ and these would have been plotted against k_{Ai} values from the literature. $\int$[OH]dt would have been determined as the gradient the line of best fit to the points plotted and this would have been used to determine k_{Xi} values, and subsequently contributions to OH reactivity. The gradient of the line best fit shown on Figure 4.5 is not representative of $\int$[OH]dt if it is the case that VOCs were also lost via direct photolysis. $\ln([A_i]_0/[A_i]_\infty)$ values for each point plotted would have varied by different amounts depending on the absorption cross sections of the compound in question (over the spectral range of the pen ray lamp). For example, isoprene is known to absorb light at 184.9 nm, $\sigma = 1.3\times10^{-17}$ cm^2 molecule^{-1} (Martins et al., 2009). If some of the

isoprene were removed by direct photolysis, the data point representing isoprene would have influenced the value of ∫[OH]dt determined and consequently the k_{Xi} values calculated. Points representing other VOCs would also influence ∫[OH]dt in a similar way but to varying extents depending upon their absorption cross sections over the spectral range of the pen ray lamp. It was therefore necessary to study the extent to which VOCs were removed in the system by direct photolysis.

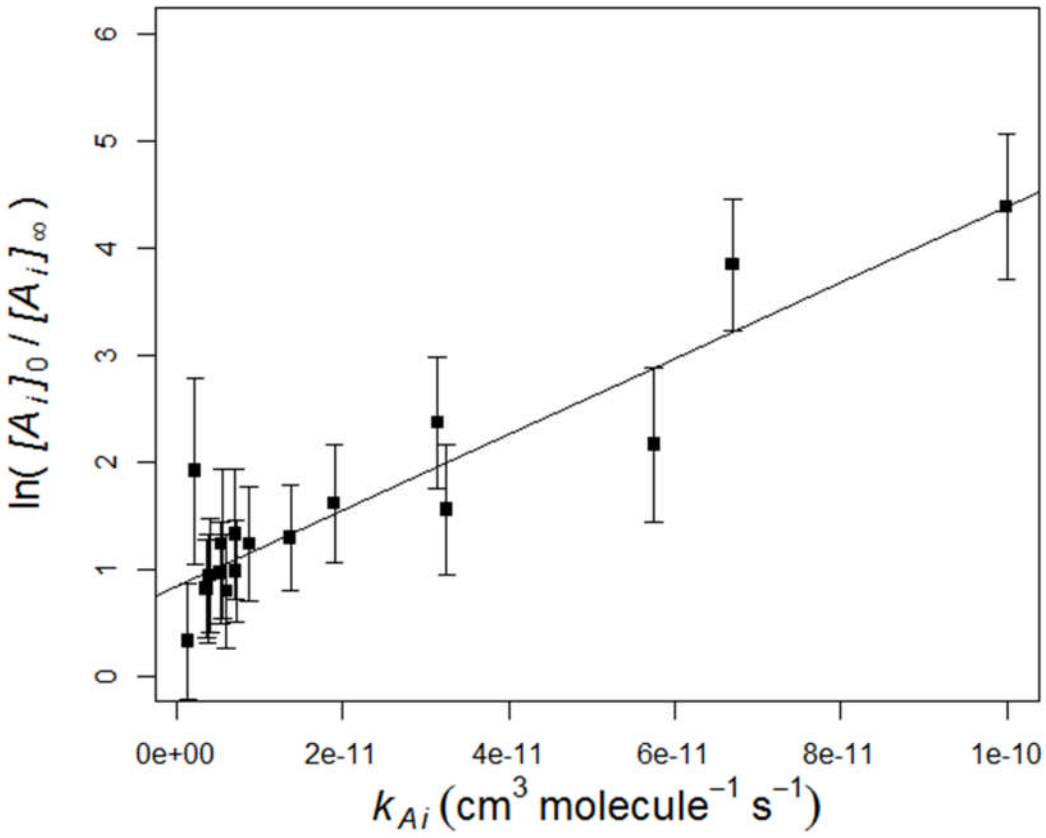

Figure 4.5: The natural logarithm of the ratio of concentrations of compounds within the NPL 30 standard VOC mix with the pen ray lamp of the prototype glass OH flow reactor switched off and on versus the bimolecular rate coefficient for the reactions of these species with OH. Y-error bars represent the uncertainty calculated through propagation of the 1 σ standard deviation of peak areas observed between analyses. Linear least squares gradient: 3.54×10^{10} molecule cm^{-3} s, intercept: 0.84, R^2: 0.85. Rate coefficients used are the same as those used by Kato et al. (2011). Raw data used to assemble plot supplied by Dr. Noelia Ramirez, University of York.

In order to assess whether or not VOCs were removed through direct photolyis in the prototype glass OH flow reactor, tests were conducted where the water bubbler was removed from the system (no OH generated). GCxGC-TOF-MS analyses were conducted with the pen ray lamp switched on, and switched off (three times each).

Figure 4.6 summarises the average peak areas for 18 of the 30 compounds in the NPL 30 standard, with and without the pen ray lamp switched on.

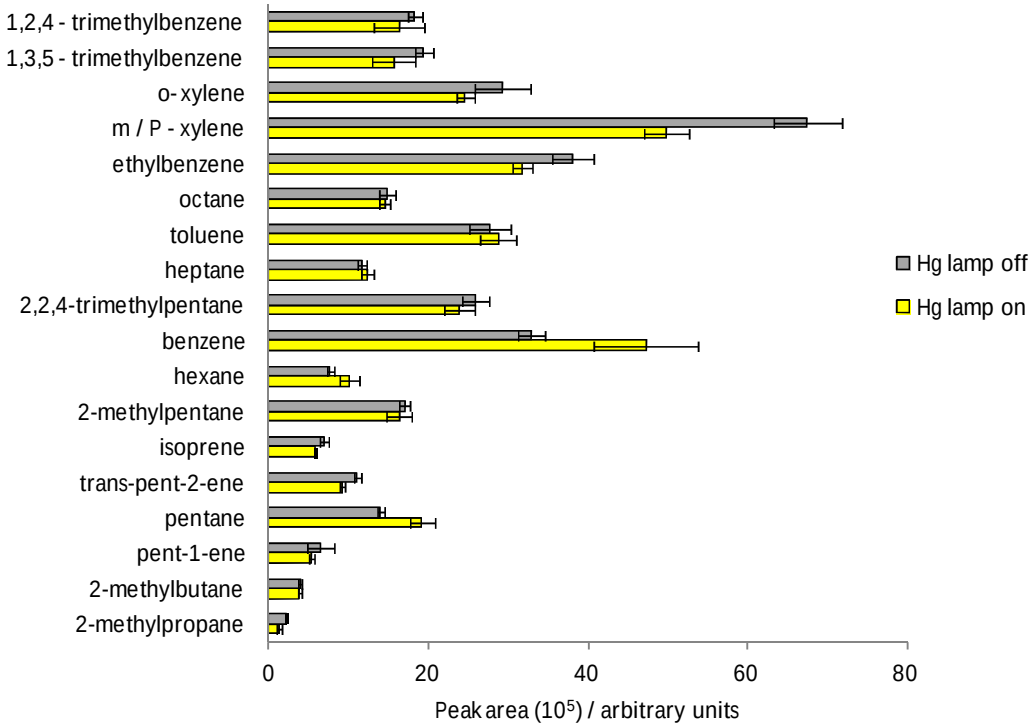

Figure 4.6: Chart to show differences in the concentrations of 18 VOCs with the Hg pen ray lamp off and on, (of the NPL 30 standard) detected in the outflow of the glass OH reactor prototype with no water bubbler present. The data shown are averaged values for three analyses. Error bars are the 1σ standard deviation of the peak areas determined from each analysis that were used to calculate the average values. Raw data supplied by Dr. Noelia Ramirez, University of York.

Peak areas were found to decrease for a significant portion of the VOCs for which data are shown when the pen ray lamp was switched on, supporting the hypothesis that direct photolysis was responsible for some of the decreases observed when OH was present. The photolysis testing also showed that peak areas increased for a small number of compounds, e.g. benzene and toluene. A cause for this could have been accumulation of these compounds on surfaces within the system over time on the glass walls, followed by subsequent desorption due to a heating effect (~3 ºC increase) from the lamp when switched on.

The OH flow reactor was redesigned to address the problem of direct photolysis of VOC's, and also to prevent heating of the system upon switching the lamp on which was shown to also influence changes in the levels of some species studied. The flow tube of the new OH flow reactor was constructed from aluminium box tubing and

contained a movable injector for the addition of ambient air (or standard gas) to a flow of nitrogen containing generated OH. This made it possible to adjust the distance between the flow mixing point and that of OH generation so that it could be optimised to prevent direct photolysis of VOC's, and also maximise their exposure to OH. Figure 4.7 summarises the key features of the redesigned OH flow reactor.

The end of the flow tube closest to the lamp was capped with a square piece of aluminium connected to a bored through Swagelok tee-piece via an NPT fitting to form a leak tight seal. The ¼" connector perpendicular to the flow tube was used to introduce humidified nitrogen for OH generation. The moveable injector entered the flow tube through the remaining fitting parallel to the flow tube and a Cajon type fitting formed a temporary leak tight seal. This enabled the position of the injector, and subsequently the mixing point of ambient air and the flow containing OH, to be adjusted. The moveable injector was constructed from ~30 cm of 1/8" (OD) stainless steel tubing (which is opaque to the UV light), the end of which was capped to allow ambient air to exit through four radial holes, all in the same plane and equally spaced, ~5 mm from the injector tip.

The Hg(Ar) pen ray lamp was housed within a block of aluminium independent to the flow tube where it was flushed with a small flow of nitrogen. This was done in order to minimise the heating effect induced by switching the lamp on that was shown to influence changes in the levels of some species in the previous design. A tightly packed block of ~40 small stainless steel tubes (1/8" OD, 0.15 mm wall thickness, 8 mm long) were used to collimate the UV light from the lamp before entry to the flow tube through a Suprasil window. The purpose of this was to reduce the divergence of light within the flow tube to ensure that the boundaries of the photolysis region for OH generation were well defined, in a similar way to the 'wand' HO_x calibration source. The redesigned OH flow reactor was characterised by experiments conducted using the fast response LIF HCHO detector described in Chapter 2. These experiments are described in addition to discussion of the results in Section 4.3.

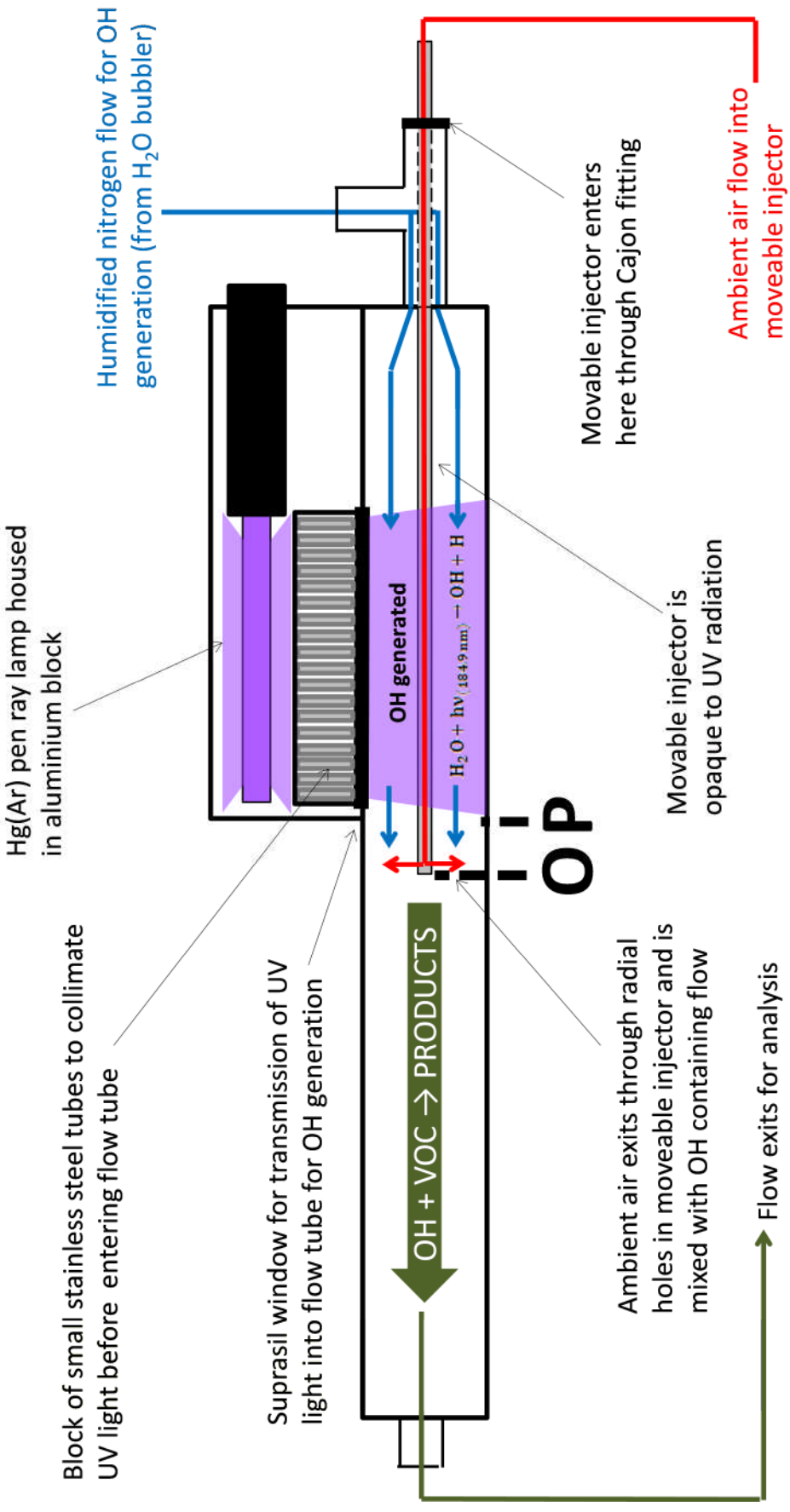

Figure 4.7: Schematic diagram to illustrate the key features of the redesigned OH flow reactor. Key features are labelled. Two positions for the injector tip are marked; O refers to the optimum position, and P refers to a non optimal position where the flow from the injector is irradiated meaning species present could be directly photolysed.

4.3 Characterisation

4.3.1 Methodology

Each GCxGC-TOF-MS analysis for the characterisation experiments described in Section 4.2 took ~90 minutes to complete, this made it very time consuming to assess the performance of the reactor and make an adjustment if necessary. It was decided that the redesigned OH flow reactor described at the end of Section 4.2 would be characterised in Leeds prior to interfacing with any instrumentation in York.

The OH flow reactor was characterised in Leeds using a fast response laser induced fluorescence (LIF) formaldehyde detector (described in Chapter 2, operated in configuration 1). HCHO production within the OH flow reactor was well suited for study in these characterisation experiments where methanol (MeOH) was flowed through the movable injector in place of ambient air (or standard VOC mixture). HCHO is useful to monitor as it is a product of both the direct photolysis of MeOH ($\sigma_{184.9\ nm(MeOH)}$ = (6.65 ± 0.33) x 10^{-19} cm^2 $molecule^{-1}$), and the reaction of MeOH with OH ($k_{MeOH + OH}$ = 9.10 × 10^{-13} cm^3 $molecule^{-1}$ s^{-1} at 298 K and 101 kPa) (R 4.2 and R 4.3) (Dillon et al., 2005, Picquet et al., 1998). Monitoring HCHO made it possible to assess whether or not species present in ambient air would be photolysed directly within the reaction flow tube, and also to investigate the extent to which they would be removed through reaction with OH.

$$MeOH + OH \xrightarrow{O_2} HCHO + HO_2 \qquad \textbf{R 4.2}$$

$$MeOH \xrightarrow{h\nu,\ O_2} HCHO + HO_2 \qquad \textbf{R 4.3}$$

It was expected that the performance of the reactor would differ depending on the flow rates of gases used. The [OH] available for reaction would be likely dependent upon the flow rate of humidified nitrogen, at lower flow rates more OH would be lost to the walls of the flow tube and impurities before mixing, at higher flow rates the residence time in the photolysis region may not be long enough for sufficient OH generation. Additionally, the optimum position of the movable injector would be dependent upon the flow rates as these would have played a role in governing the rate of diffusion of the flow from the injector tip into the photolysis region where OH is generated. The OH flow reactor was characterised under two sets of flow conditions. These were termed the 4.05 and 3.05 SLM conditions and are described

in detail in Section 4.3.2. In each case 1.05 SLM of synthetic air containing MeOH vapour was flowed through the moveable injector and mixed with either 2.00 or 3.00 SLM of nitrogen. The nitrogen was either humidified or, not humidified depending on the aim of the characterisation experiment.

HCHO was detected as a product of MeOH photolysis during experiments to optimise the position of the moveable injector to prevent direct photolysis of VOCs. All experiments for the optimisation of the injector position were conducted in the absence of OH (nitrogen not humidified). The experimental method is outlined in detail in Section 4.3.2 in addition to discussion of the results.

HCHO was detected as a product of the reaction between MeOH and OH. It was necessary to generate OH in these experiments (nitrogen humidified) so that the amount available for reaction at the flow mixing point (i.e. the injector tip) could be quantified. The experimental method is outlined in Section 4.3.3 in addition to discussion of the results. Characterisation experiments were also conducted where OH was generated in the reactor to determine its loss rate (to both the walls of the reactor and impurities in the gases used). The experimental method for this is outlined in Section 4.3.4 in addition to discussion of the results.

4.3.2 Optimisation of injector position

The results from the characterisation experiments of the prototype glass OH reactor described in Section 4.2 showed evidence for direct photolysis of VOC's within the flow tube. A moveable injector was incorporated into the redesigned OH flow reactor so that the distance between the introduction point for ambient air (or standard VOC mixture), and the irradiation zone for OH generation could be varied.

The position of the injector in the redesigned OH flow reactor was optimised for both the 4.05 and 3.05 SLM total flow conditions. In both cases 50 sccm of nitrogen was flowed through a MeOH bubbler (submersed in an ice bath to lower the MeOH vapour pressure), mixed with 1.00 SLM of synthetic air and introduced to the reactor via the moveable injector. This was mixed with either 3.00 or 2.00 SLM (for the 4.05 or 3.05 SLM conditions, respectively) of nitrogen in the flow tube containing generated OH; in all experiments the concentration of MeOH was in the order of 10^{16} molecule cm^{-3} (calculated using the MeOH vapour pressure at 0 °C). Figure 4.8 summarises the experimental set up that was used in experiments to optimise the position of the moveable injector.

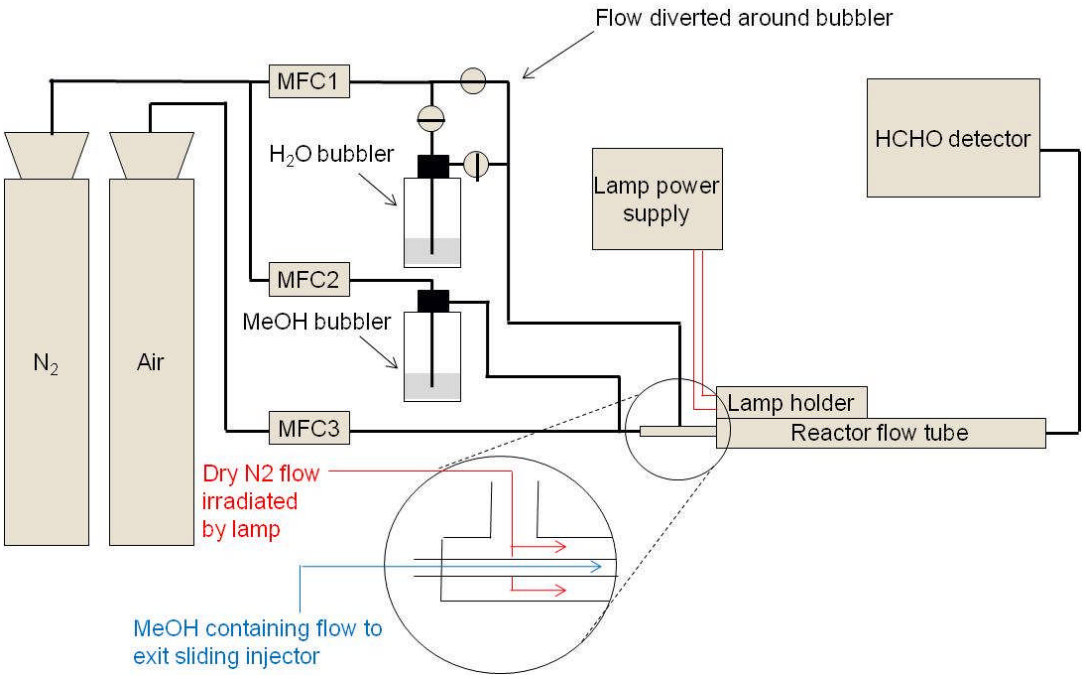

Figure 4.8: Schematic diagram to summarise the experimental set up used for optimising the position of the moveable injector within the OH flow reactor. The flow of nitrogen irradiated by the pen ray lamp was diverted around the water bubbler in this case to prevent the formation of OH.

In all OH reactor characterisation experiments it was not possible to eliminate a background HCHO signal within the system of ~1000 count s^{-1} (that was not formed from MeOH oxidation or photolysis). This was thought to be mainly due to HCHO present as an impurity in the MeOH bubbler and HCHO formed as a product from photolysis of impurities present in the N_2 cylinder following irradiation by the pen ray lamp. The direct contribution from the nitrogen and air cylinders was thought to be negligible as when gas from each was sampled by the HCHO detector no HCHO LIF signal was observable above the noise.

The injector was fully inserted into the reactor so that the distance between the flow mixing point and the edge of the Suprasil window (as shown in Figure 4.7) was ~6 cm. Following this the injector was withdrawn slowly and the HCHO signal was monitored; this remained constant until a rise was observed due to HCHO production from photolysis of MeOH (R 3.3). This position is labelled as 'P' in Figure 4.7. Following this the injector was pushed back the other way until the formaldehyde signal returned to its previous constant value. The resulting position was considered to be the optimum, as indicated by the 'O' label in Figure 4.7. Under the 4.05 and 3.05 SLM total flow regimes the optimum distances between the edge

of the Suprasil window and injector tip were ~1 and 2 cm, respectively. Thus suggesting that diffusion of the MeOH flow back into the photolysis region was enhanced as the total flow decreased, this observation also highlights the necessity of optimising the injector each time the flow conditions within the reactor are changed. It confirms that the optimum position of the injector is unique to the flow conditions. Figure 4.9 illustrates a typical profile for the formaldehyde signal observed during an injector optimisation experiment, the signals recorded at the 'O' and 'P' positions are indicated.

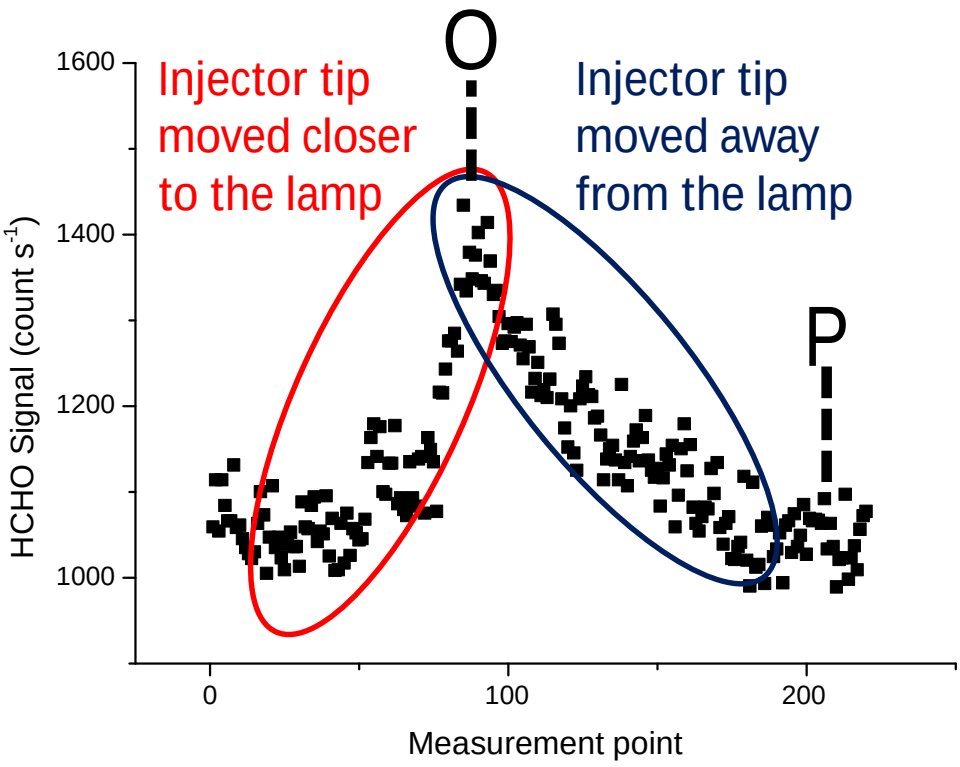

Figure 4.9: Example of an HCHO LIF signal resulting from MeOH photolysis, observed during an experiment to optimise the position of the movable injector within the redesigned OH flow reactor operated under the 4.05 SLM flow conditions.

4.3.3 Quantification of OH present at mixing point

Once the position of the moveable injector was optimised for a particular flow regime (so that it was sufficiently far away from the photolysis region as to avoid MeOH photolysis), the nitrogen flow was redirected through the water bubbler to enable OH production within the reactor. This made it possible to quantify the [OH] available for reaction with species present in the flow exiting the injector tip. This was achieved through the detection of HCHO formed from the reaction between

MeOH and OH (R 4.2). Figure 4.10 summarises the experimental set up that was used in these experiments that were conducted under both the 4.05 and 3.05 SLM flow conditions.

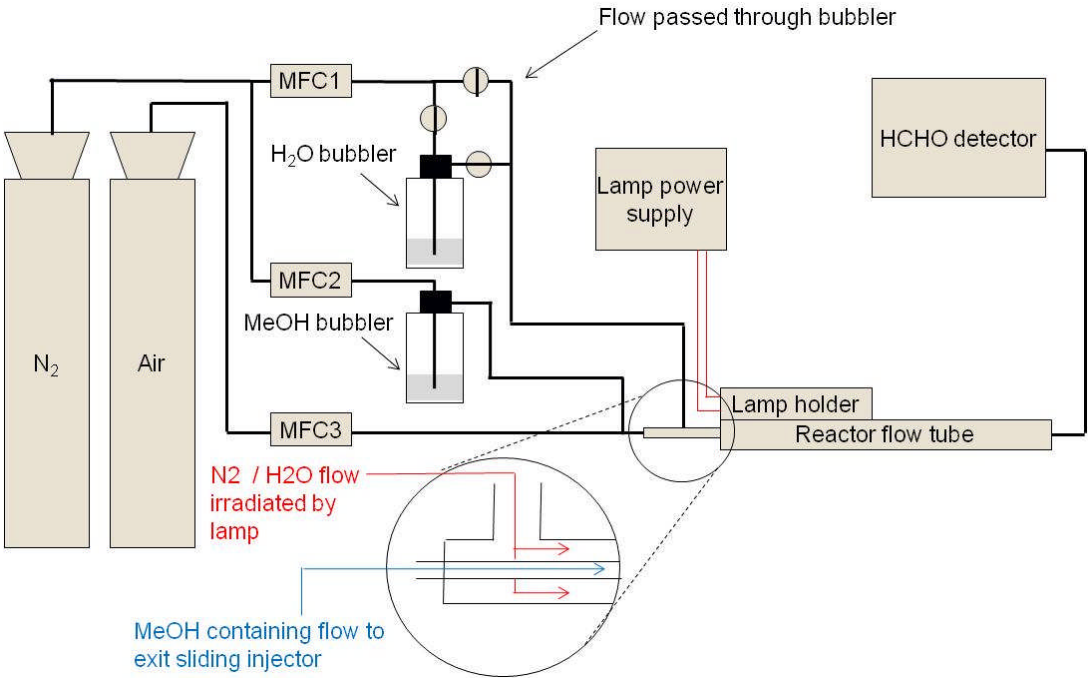

Figure 4.10: Schematic diagram to summarise the experimental set up used for quantifying [OH] present at the flow mixing point within the OH reactor. The flow of nitrogen irradiated by the pen ray lamp was passed through the water bubbler in this case to enable OH formation.

Upon passing the nitrogen flow through the water bubbler a significant increase in HCHO LIF signal was observed which then decreased over a period of a few minutes to reach a constant level. This was likely due to HCHO that had accumulated in the headspace of the water bubbler being flushed out. Once the signal stabilised, the injector was modulated between its optimum (where maximum OH oxidation took place without direct photolysis) and fully inserted position (all OH lost to walls of flow tube before mixing); a reproducible step change in the HCHO signal was observed. Figure 4.11 shows a typical HCHO signal that was observed during an experiment to quantify [OH] available for reaction.

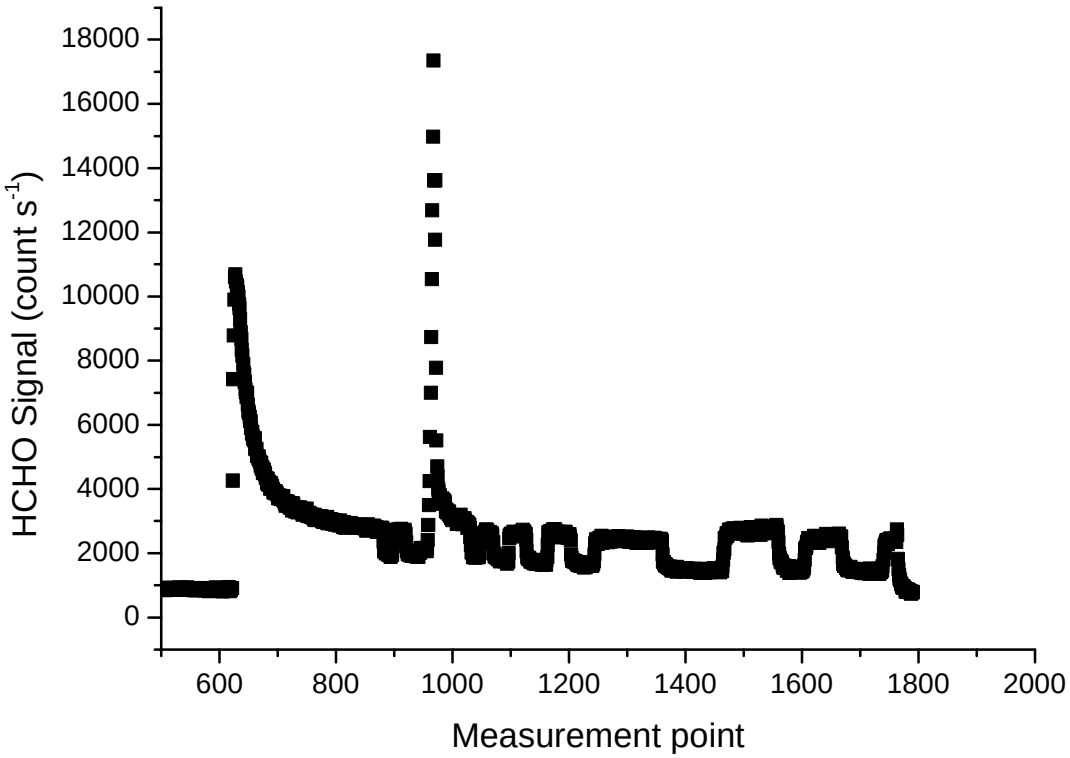

Figure 4.11: HCHO signal observed during an experiment to quantify [OH] available for reaction within the OH flow reactor under the 4.05 SLM total flow conditions. See text for details of changes in signal observed.

The sharp rise in HCHO signal following the redirection of the nitrogen flow through the water bubbler is shown just after measurement point 600 (each point is 1 second averaging). Following this the signal decreased to reach a near constant level at around measurement point 850. The signal at the constant level reached was in part due to HCHO production from the reaction of MeOH with OH. There was also a contribution from HCHO produced as an end product from the oxidation and photolysis of impurities present in the flow of humidified nitrogen used for OH generation. The step changes in signal as a result of modulation of the injector position can be seen from around measurement point 900 onwards. The sharp spike at around measurement point 950 was due to the injector being pulled back past the optimum position, thus resulting in high HCHO production from direct photolysis of MeOH, and also from increased exposure to OH due to there being less time for loss to walls and other impurities before mixing.

As MeOH was higher in concentration (in the order of 10^{16} molecule cm^{-3}) than the expected [OH] present at the mixing point (in the order of 10^{10} molecule cm^{-3}), it was assumed that each molecule of OH available for reaction produced one

molecule of HCHO. The change in [HCHO] represented by the step change in signal was calculated using a calibration determined for the HCHO detector. As MeOH was in such great excess ($k_{OH+MeOH}$[MeOH] >> k_{loss}), the [HCHO] change was assumed to be equal to the [OH] available for reaction with species in ambient air exiting the tip of the movable injector under the same flow conditions. Under the 4.05 and 3.05 SLM total flow conditions this was found to be 7.6 (± 4.0) x 10^{10} and 2.6 (± 1.5) x 10^{10} molecule cm^{-3}, respectively. The shorter residence time of the flow containing OH for the 4.05 SLM total flow conditions, likely contributed to the value measured being higher as there is less time for wall loss to occur in this case. The shorter distance between the injector tip and irradiated volume within the flow tube would have also had a similar effect on the residence time and wall loss.

4.3.4 Measurement of OH loss rate

By detecting HCHO in the outflow from the reactor at a range of sliding injector positions (between the optimum and fully inserted), it was possible to quantify the loss rate of OH in the reaction flow tube, k_{loss} (to both the walls and OH reactive impurities present) before mixing with the MeOH flow from the movable injector.

The OH loss rate in the reaction flow tube was measured under the 4.05 SLM total flow conditions described in Section 4.3.2 using the experimental set up shown in Figure 4.10. The injector was moved to its optimum position using the method outlined in Section 4.3.2 and HCHO was detected in the outflow from the reactor. The injector was then pushed inwards in 10 mm increments so that the distance between the flow mixing point and the photolysis region increased. Figure 4.12 shows the HCHO LIF signal that was recorded during the measurement of OH loss rate in the reaction flow tube.

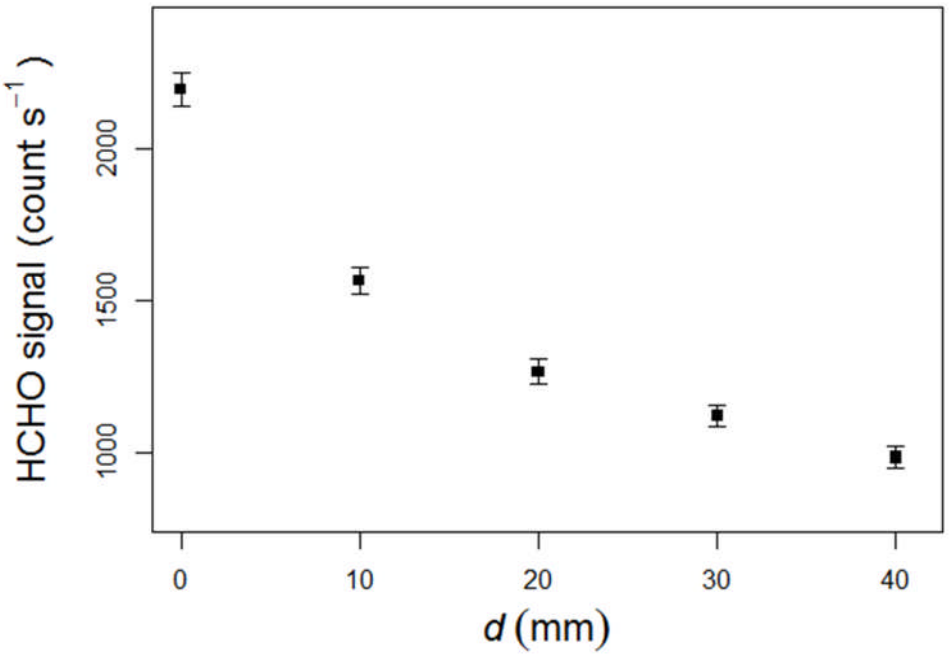

Figure 4.12: HCHO signal observed during the measurement of k_{loss} under the 4.05 SLM total flow conditions.

The data show that the HCHO signal decreased as *d* was increased, indicating that less OH was available for reaction when the flow mixing point was further away from that of OH generation. The HCHO signal at the optimum position (*d* = 0) was assumed to be equivalent to the starting concentration of OH before any losses occurred. It was assumed that the loss rate of OH within the flow tube before mixing was a first order process as given by, E 4.5.

$$\frac{d[OH]}{dt} = -k_{loss}[OH] \qquad \textbf{E 4.5}$$

E 4.5 was integrated between the residence time of OH in the flow tube before mixing where the injector was in its optimum position (*d* = 0 s), and the residence time in seconds before mixing following the movement of the injector (*t*) to give E 4.6.

$$\ln\left(\frac{[OH]_t}{[OH]_0}\right) = -k_{loss}t \qquad \textbf{E 4.6}$$

Assuming the change in HCHO signal observed was equivalent to the difference in [OH] available for reaction between different injector positions, E 4.7 could be used to determine the OH loss rate within the flow tube.

$$\ln\left(\frac{[HCHO]_t}{[HCHO]_0}\right) = -k_{loss}t \qquad \textbf{E 4.7}$$

The only term including HCHO concentrations in E 4.7 is the ratio of $[HCHO]_t$ to $[HCHO]_0$. Therefore it was not necessary to calculate the concentrations of HCHO detected at each injector position; the (background subtracted) signals alone were sufficient to calculate the ratio of $[HCHO]_t$ to $[HCHO]_0$.

A plot of $\ln([HCHO]_t/[HCHO]_0)$ vs *t* was constructed to determine the loss rate of OH to the walls of the flow tube, and to other impurities present in the humidified nitrogen flow for OH generation, this is shown in Figure 4.13.

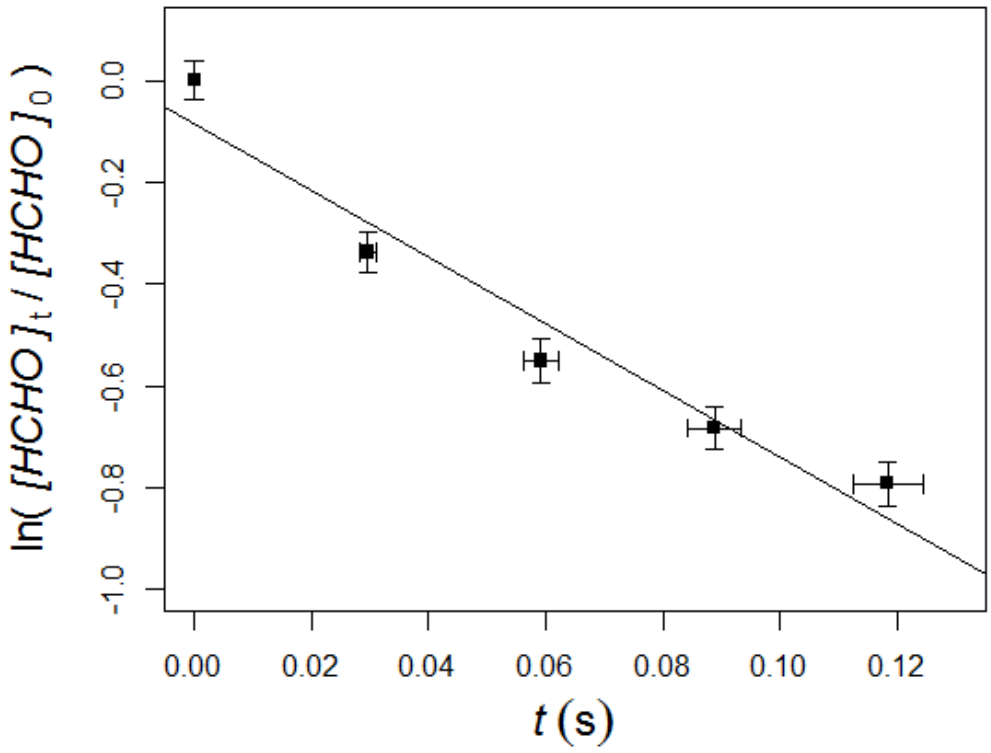

Figure 4.13: Plot of $\ln([HCHO]_t/[HCHO]_0)$ vs *t*. The gradient of the line of best fit (linear least squares) is equal to $-k_{loss}$ and the plot was constructed using data whilst the OH reactor was operated under the 4.05 SLM total flow conditions. Gradient: -6.57 ± 0.88 s^{-1}, intercept: 0.085 ± 0.06, R^2: 0.97.

The plot shows that the relationship between $\ln([HCHO]_t/[HCHO]_0)$ and *t* is not perfectly linear; some level of curvature is observed. The precise reason for this is uncertain, however is likely to be due to combination of two factors. The first of these is the self reaction of OH acting as another loss process. This is possible because the levels of OH generated in the OH reactor a relatively high (in the order

of 10^{10} molecule cm^{-3}). The second influencing factor is likely to be that the type of analysis used to determine the loss rate here, assumes that gas within the OH reactor is entrained within a 'plug' type flow. The flow within the OH reactor is almost certainly laminar, to improve the accuracy of this analysis, corrections for diffusion could be applied. However, due to time constraints such a correction was not investigated and a linear fit to the data was assumed to have a gradient approximately equal to $-k_{loss}$ for the purpose of assessing the potential performance of the OH reactor.

As described above, the gradient of the line of best fit shown in Figure 4.13 is assumed to be equal to $-k_{loss}$. The value for k_{loss} determined under the 4.05 SLM total flow conditions was 6.57 ± 0.88 s^{-1}, it was not possible to measure k_{loss} under the 3.05 SLM total flow conditions due to problems encountered with the fibre laser used in the HCHO detector. However, as the loss rate measured appears to be first order, it can be assumed that it would be the same under all flow conditions. During operation of the OH flow reactor where ambient air is flowed through the moveable injector, k_{loss} is competitive with k_{Ai} and k_{Xi}. Therefore it needs to be considered when determining the predicted effect on a real VOC mix. The value of k_{loss} determined here can be used in modelling studies to assess the potential performance of the redesigned OH flow reactor.

3.4 Simulated removal of VOCs

A zero dimensional chemical box model was constructed using Kintecus (Ianni, 2003) to crudely assess the potential performance of the redesigned OH reactor. The model was constructed such that it simulated the effect that the OH reactor could have on a standard mixture of 30 VOCs if flowed in through the sliding injector (where ambient air would be introduced in the field) under both the 4.05 and 3.05 SLM total flow conditions described in Section 4.3.1. A list of the compounds that were included in the model along with their respective bimolecular rate coefficients for reaction with OH used in the model are presented in Table 4.1.

OH Sink	$k_{sink + OH}$ (cm^3 $molecule^{-1}$ s^{-1}) at 298 K	Reference
Ethylene	8.8×10^{-12}	Sander et al. (2006)
Acetylene	8.3×10^{-13}	Sander et al. (2006)
Ethane	2.4×10^{-13}	Sander et al. (2006)
Propylene	3.0×10^{-11}	Atkinson et al. (2006)
Propane	1.1×10^{-12}	Sander et al. (2006)
iso-Butane	2.2×10^{-12}	Atkinson (1997)
1-Butene	3.1×10^{-11}	Atkinson (1997)
n-Butane	2.3×10^{-12}	Atkinson et al. (2006)
trans-2-butene	6.4×10^{-11}	Atkinson (1997)
cis-2-butene	5.6×10^{-11}	Atkinson (1997)
3-Methyl-1-butene	3.2×10^{-11}	Atkinson (1997)
iso-Pentane	3.7×10^{-12}	Atkinson (1997)
1-Pentene	3.1×10^{-11}	Atkinson (1997)
n-Pentane	4.0×10^{-12}	Atkinson (1997)
Isoprene	1.0×10^{-10}	Atkinson et al. (2006)
trans-2-Pentene	6.7×10^{-11}	Atkinson (1997)
cis-2-Pentene	6.5×10^{-11}	Atkinson (1997)
2-Methyl-2-butene	8.7×10^{-11}	Atkinson (1997)
2,2-Dimethylbutane	2.3×10^{-12}	Atkinson (1997)
Cyclopentene	6.7×10^{-11}	Atkinson (1997)
4-Methyl-1-pentene	3.8×10^{-11}	Grosjean and Williams (1992)
Cyclopentane	5.0×10^{-12}	Atkinson (1997)
2,3-Dimethylbutane	5.8×10^{-12}	Atkinson (1997)
2-Methylpentane	5.3×10^{-12}	Atkinson (1997)
3-Methylpentane	5.4×10^{-12}	Atkinson (1997)
2-Methyl-1-pentene	6.3×10^{-11}	Atkinson (1997)
n-Hexane	5.5×10^{-12}	Atkinson (1997)
trans-2-Hexane	4.8×10^{-11}	Atkinson (1994)
cis-2-Hexane	4.8×10^{-11}	Atkinson (1994)
Methylcyclopentane	8.8×10^{-12}	Atkinson (1994)

Table 4.1: List of 30 VOCs included in a Kintecus zero-dimensional chemical box model which was used to assess the potential performance of the redesigned OH flow reactor.

In all simulations the initial concentration of each species in the flow from the moveable injector was 1 ppb; this corresponded to the mix having an OH reactivity of 21.9 s^{-1} if sampled at 760 Torr and 298 K. Simulations lasted 2 seconds as this was found to be long enough for the concentration of each species to reach a constant level in all cases due to complete consumption of OH.

Two runs were executed using a starting value for [OH] that was determined to be available for reaction at the flow mixing point under the 4.05 SLM total flow conditions (7.6 x 10^{10} molecule cm^{-3}, Section 4.3). In the first run the measured value for k_{loss} (6.6 s^{-1}, Section 4.4) was not included in the model. However, it was included in the second run in order to assess the extent to which OH loss other than by reaction with sinks within the flow tube could affect the ability of the reactor to remove species present in ambient air through reaction with OH. The data outputted from the two simulations were used to calculate values for $\ln([A_i]_0/[A_i]_\infty)$ which were plotted against k_{Ai}, Figure 4.14.

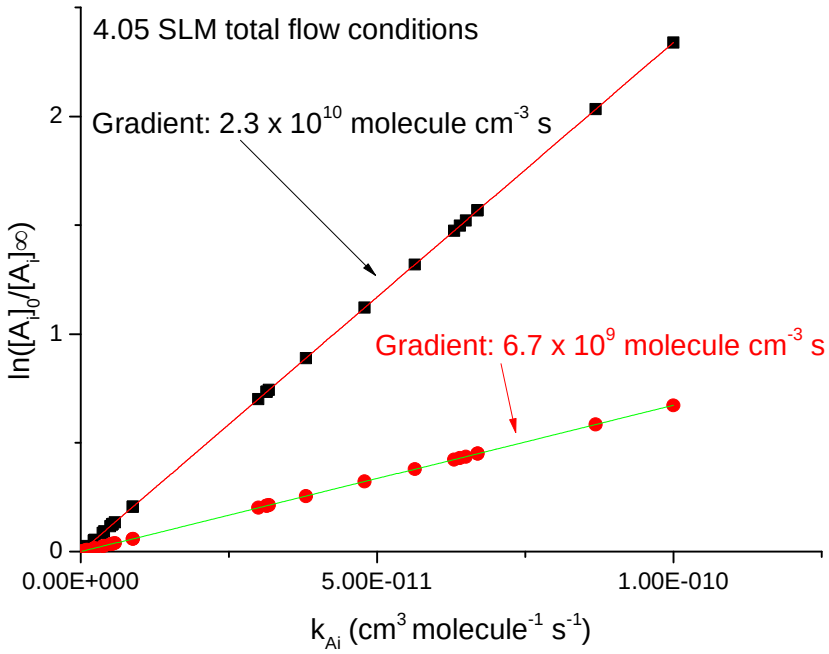

Figure 4.14: Plots of $\ln([A_i]_0/[A_i]_\infty)$ vs k_{Ai} produced using data outputted from a Kintecus model constructed to simulate the loss of 30 VOCs within the OH reactor. Data are shown for simulations where k_{loss} (loss to walls and reactions with impurities) was (plotted in red) and was not (plotted in black) included. The starting concentration of OH was 7.6 x 10^{10} molecule cm^{-3}.

By inspection of Figure 4.14 it can be seen that the gradient of the plot produced using data from the simulation, where wall loss was included, is lower than that where the wall loss was not included. This was expected as when OH is lost to processes other than reaction with species in the VOC mix, less would be available for reaction, therefore causing a reduction in [OH] integrated over reaction time which is equal to the gradient.

A further two model runs were executed using the value determined for [OH] available for reaction at the flow mixing point under the 3.05 SLM total flow conditions (2.6 x 10^{10} molecule cm^{-3}, Section 4.4). These were identical to the previous two runs except that the starting [OH] value was different. The data outputted were treated in the same way to produce two plots for for $\ln([A_i]_0/[A_i]_\infty)$ vs k_{Ai}, these are shown in Figure 4.15.

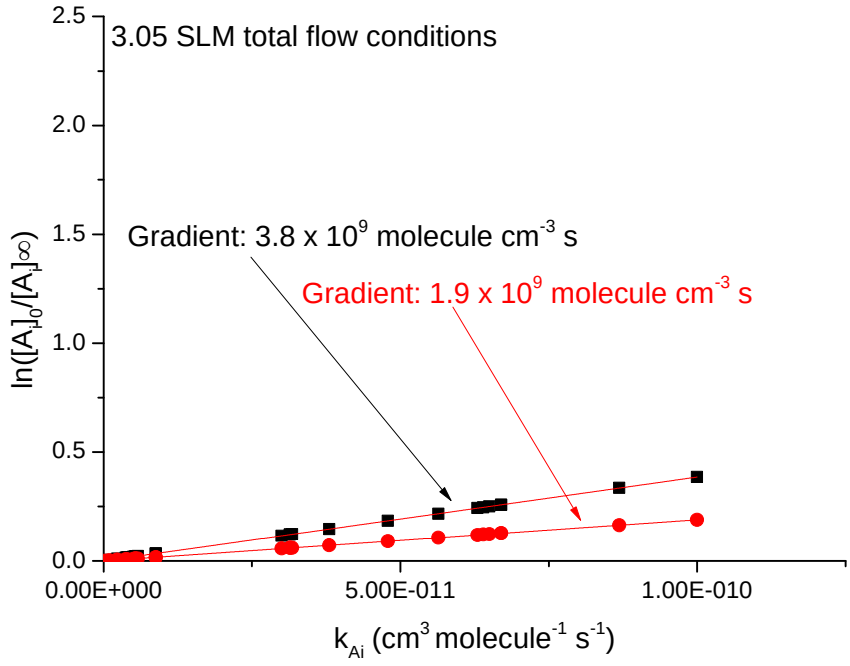

Figure 4.15: Plots of $\ln([A_i]_0/[A_i]_\infty)$ vs k_{Ai} produced using data outputted from a Kintecus model constructed to simulate the loss of 30 VOCs within the OH reactor. Data are shown for simulations where k_{loss} (loss to walls and reactions with impurities) was (plotted in red) and was not (plotted in black) included. The starting concentration of OH was 2.6 x 10^{10} molecule cm^{-3}.

Again it can be seen that the gradient of the plot produced using data where the 6.6 s^{-1} OH loss rate was included in the model is lower, however this was by a lesser amount than in the previous simulations (50 % lower as opposed to 71 % lower). This indicates that OH loss to the walls of the flow tube and impurities will impact the ability of the reactor to remove species present in ambient air most significantly when the initial [OH] available for reaction is higher. However, the gradient of the plot in Figure 4.14 where k_{loss} was included in the simulation is still greater than the gradient of both plots in Figure 4.15 where k_{loss} was included. Thus it can be concluded that operating the OH flow reactor under the 4.05 SLM total flow conditions will most likely result in the largest decreases in species present in ambient air due to reaction with OH.

In order to conduct a study similar to that reported by Kato et al. (2011), it is essential that decreases in concentrations of OH reactive species are observable for species where k_{Ai} is greater than ~10^{-12} cm^3 $molecule^{-1}$ s^{-1}. Candidate species for missing OH reactivity are thought to typically have k_{Ai} values above this threshold.

In the hypothetical example of measurements in an urban atmosphere showing evidence for 20 % average 'missing' OH reactivity with 15 s^{-1} average measured OH reactivity, it would be concluded that unmeasured sinks contributed 3 s^{-1} towards the measurements. In this case, if the average k_{Ai} value for the unmeasured sinks was significantly lower than 10^{-12} cm^3 $molecule^{-1}$ s^{-1} (e.g. 10^{-13} cm^3 $molecule^{-1}$ s^{-1}), their collective concentration would be 3 $\times 10^{13}$ molecule cm^{-3} (~1 ppm). Relative to the majority of other trace species that exist in the atmosphere, this level is very high. It would be unlikely that such levels would go undetected, especially when the diversity of instrumentation that are often deployed in OH reactivity studies is considered. If the average k_{Ai} value for the unmeasured sinks in this scenario was 10^{-12} cm^3 $molecule^{-1}$ s^{-1} their collective concentration would be 3 × 10^{12} molecule cm^{-3} (~100 ppb). $k_{toluene + OH}$ is ~5 × 10^{-12} cm^3 $molecule^{-1}$ s^{-1} so toluene is towards the lesser reactive end of the scale of species which would need to be removed by OH in the flow reactor by an observable quantity. Therefore it was an ideal candidate for study when assessing the suitability of the redesigned OH flow reactor for use in a study similar to Kato et al. (2011). The results from the model simulations described above (in the cases where k_{loss} was included) were used to predict changes that would be expected for the concentration of toluene under the same conditions. The predictions are summarised for the 4.05 and 3.05 SLM total flow conditions in Table 4.2, in addition to predictions for isoprene (which reacts much faster) for the purpose of comparison.

Totalflow conditions / SLM	Starting [OH] / molecule cm^{-3}	Predicted ∫[OH]dt / molecule cm^{-3} s	Predicted decrease in [isoprene] (%)	Predicted decrease in [toluene] (%)
4.05	7.6×10^{10}	6.7×10^{9}	49	4
3.05	2.6×10^{10}	1.9×10^{9}	17	1

Table 4.2: Summary of the predicted decreases that could be expected for isoprene and toluene if the total OH reactivity of ambient air sampled by the OH flow reactor had a total OH reactivity of 21.9 s^{-1}. Predicted values are shown for the operation of the OH flow reactor under both the 4.05 and 3.05 SLM total flow conditions.

The data presented in Table 4.2 show that operating the OH flow reactor under the 4.05 SLM total flow conditions should result in the largest decreases in concentration for toluene and isoprene. The predicted changes for both toluene and isoprene under the 4.05 SLM total flow conditions would be observable by the GC-TOF-MS (Agilent 7890 coupled with Markes BenchTOF) instrument at the University of York. However, the small decrease (1 %) in concentration predicted

for toluene under the 3.05 SLM total flow conditions would likely not be observable (Lidster, 2013).

It was decided that the OH flow reactor would be operated using the 4.05 SLM total flow conditions upon interfacing with a GC-TOF-MS instrument at the University of York to form a new instrument for identification of 'missing' OH reactivity. Section 4.5 provides details of the configuration and operation of the new instrument. The new instrument was successfully deployed during the York 2014 'missing' OH reactivity field campaign (Chapter 5) and some preliminary observations in ambient air from this campaign are presented in Section 4.6.

4.5 Coupling with GC-TOF-MS

The redesigned OH flow reactor described in Section 4.2 was successfully interfaced to a GC-TOF-MS instrument at the University of York to form a new instrument for the identification of 'missing' OH reactivity. The schematic in Figure 4.16 summarises the key features of the new system that incorporated the redesigned OH flow reactor described in Section 4.2.

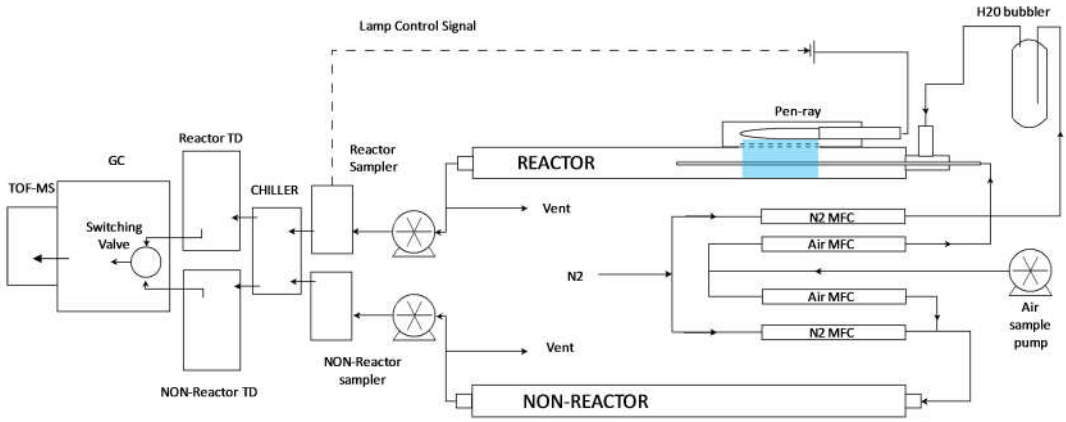

Figure 4.16: Schematic diagram to summarise the experimental set-up of the new instrument for the identification of 'missing' OH reactivity that was used for field measurements during the York 2014 'missing' OH reactivity campaign. Diagram provided by Dr. Richard Lidster, University of York.

The set-up consisted of two parallel sampling systems; one contained the OH flow reactor and the other contained a flow tube of the same dimensions where no OH was generated (no lamp, termed the non-reactor). The use of the parallel sampling system made it possible to conduct analyses of ambient air that had been sampled simultaneously. If analyses of sequentially sampled ambient air were conducted, as

by (Kato et al., 2011), it would be unknown whether or not a decrease in the concentration of a species detected was exclusively due to its removal by OH, (the decrease could be partly due to natural variation in the composition of the air mass sampled). The parallel sampling system used in the new instrument for the identification of 'missing' OH reactivity is thought to be the first of its kind as to the best knowledge of the author; no description of a similar system is available in the literature.

Ambient air was supplied to the set-up from a sampling manifold positioned on the roof of the Wolfson Atmospheric Chemistry Laboratories (WACL) building. A clean dry bellows pump was used to draw ambient air into the set-up and provide sufficient backing pressure to two MFCs (MKS, 0-1 SLM). The first of these was used to supply 1.00 SLM of ambient air to the OH flow reactor via the moveable injector and the second was used to supply 1.00 SLM of ambient air to the non-reactor. An additional two MFCs were used to supply nitrogen to the OH reactor and to the non-reactor at 3.00 SLM. The nitrogen flow to the reactor was humidified using a water bubbler to enable OH production, in the non-reactor case it was not humidified and served only to dilute the ambient sample by the same amount. Two sucking pumps were used to transfer gas from the reactor and non-reactor to their respective sampling units at ~2 SLM; the remaining flow in each case was vented to prevent over pressuring of the system.

Solenoid valves within the sampling units were used to control the timing for the trapping of samples from both the reactor and the non-reactor. Upon opening the valves, samples were simultaneously transferred to glass cold fingers submersed in an ethylene glycol cooling bath at -30 °C to 'freeze out' any water vapour present and prevent damage to the TOF-MS detector. Following the removal of water vapour, the samples from the reactor and the non-reactor were transferred to separate thermal desorption (TD) units for trapping. The sample lines from each TD unit were connected to the GC via a switching valve; this made it possible to sequentially desorb and analyse the two samples from the parallel system. Figure 4.17 shows the new instrument for the identification of 'missing' OH reactivity whilst in operation during the York 2014 'missing' OH reactivity field campaign, the key features are labelled.

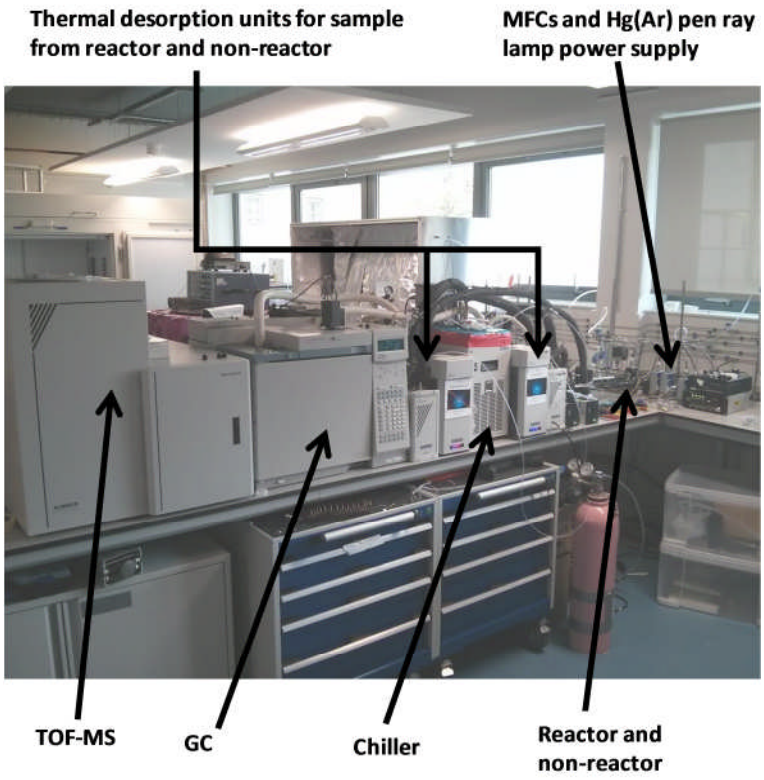

Figure 4.17: Photograph of the new instrument for the identification of 'missing' OH reactivity during the York 2014 'missing' OH reactivity field campaign. Key features are labelled.

Early testing of the two thermal desorption units with a neat flow from a VOC standard cylinder showed there to be a systematic offset in the level of each compound detected by GC-TOF-MS, i.e. the two systems were not equally efficient at trapping and desorbing species present in ambient air. It was necessary to quantify the difference in the concentration of all species detected due to this systematic offset in order identify compounds that were contributing to 'missing' OH reactivity. To achieve this, four GC-TOF-MS analyses were performed in every measurement cycle (two pairs of simultaneous samples from the parallel system).

The OH reactor was operated with the pen ray lamp switched off whilst the first two samples were trapped and desorbed sequentially onto the GC column. The differences in the peak areas between the two resulting chromatograms were representative of the difference in concentration due to the species specific systematic offset between the two TD units. Whilst the first two analyses were in progress, the pen ray lamp inside the OH reactor was switched on using an electromechanical relay which was triggered using a 'contact closure' from the sampling unit. Two more samples were then trapped and sequentially desorbed onto

the GC column upon completion of the first two analyses. In this case the differences in the peak areas observed between the two chromatograms were representative of the systematic offset between the two TD units, and any change due to removal via OH chemistry.

Data from multiple analyses where the lamp was switched off were used to construct a calibration plot for each identified species detected. These were used to estimate the contribution from the TD unit offset to the difference observed in the peak areas for identified species during analyses where the lamp was switched on. Therefore making it possible to quantify any change due to OH chemistry.

In order to use observations from the new instrument described here to determine rate coefficients for the reaction between unidentified species that contribute to 'missing' OH reactivity, it would first be necessary to examine the relationship between changes observed in peak areas for identifiable species and their bimolecular rate coefficients for reaction with OH. In the study reported by Kato et al. (2011) it was necessary to examine such a relationship for each sample of ambient air that was analysed. This was due to it not being possible to simultaneously trap samples of ambient air in their system. The capability of the instrumentation described in this chapter to simultaneously trap samples made it possible to use just one such relationship to calculate bimolecular rate coefficients for unidentified species.

3.6 Observations in ambient air

The new instrumentation was deployed for the first time during the York 2014 'missing' OH reactivity campaign in May / June 2014. Measurements of OH reactivity during this campaign are presented in Chapter 5 in addition to a detailed comparison with the levels calculated using the concentrations of co-measured identifiable sinks. It was determined that when OH reactivity was calculated using only data for identifiable sinks, the 'missing' OH reactivity on average for the campaign was 27 %. It is concluded in Chapter 5 that the majority of the 'missing' OH reactivity in York could be attributed to unidentified species that were measured with a GCxGC-FID instrument and also unmeasured products of photo-oxidation. Therefore, it was expected that the observations made using the instrumentation described in this chapter would only lead to the identification of a few species which

made minor contributions to the 'missing' OH reactivity. Figure 4.18 shows some data that were collected during the campaign in York for some identified species.

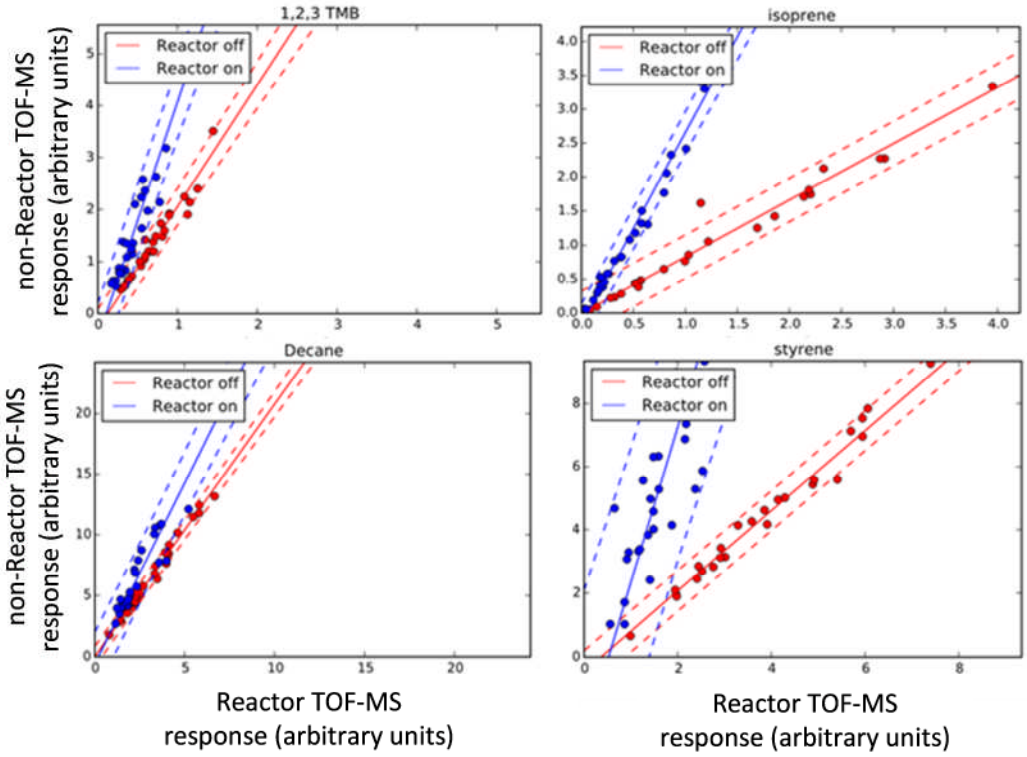

Figure 4.18: Relationships between GC-TOF-MS response for the Reactor and non-Reactor sampling systems, for four VOCs (1,2,3-trimethylbenzene, isoprene, decane and styrene), from analyses where the UV lamp in the OH flow reactor was switched off (no OH generated) and switched on (OH generated). Data shown are from the analysis of ambient air during the York 2014 'missing' OH reactivity campaign. Provided by Dr. Richard Lidster, University of York.

Each plot shows two sets of data for the linear relationship between responses for the two sampling systems (reactor and non-reactor), one where the lamp in the OH reactor switched off (red), and one with the lamp switched on (blue). The plots show that the relative responses for the two sampling systems vary considerably (shown through differences in the gradient of the red lines). The precise reason for there being such significant variation is unknown but is likely due to differences between the performance of thermal desorption unit in the two sampling systems. However, the data show that this species specific offset is systematic (because the red points exhibit linear behaviour) and so should not influence the measurements made, provided that the offset is accounted for through consideration of the ratio of the gradients as described in Section 4.5.

As described in Section 4.5 it is the relationship between the natural logarithms of the ratio of the gradients of line of best fits to these data sets and k_{Ai} values that can be used to determine ∫[OH]dt. Figure 4.19 shows this relationship that was determined through the analysis of ambient air during the campaign in York, ∫[OH]dt is 1.5×10^{10} molecule cm^{-3} s.

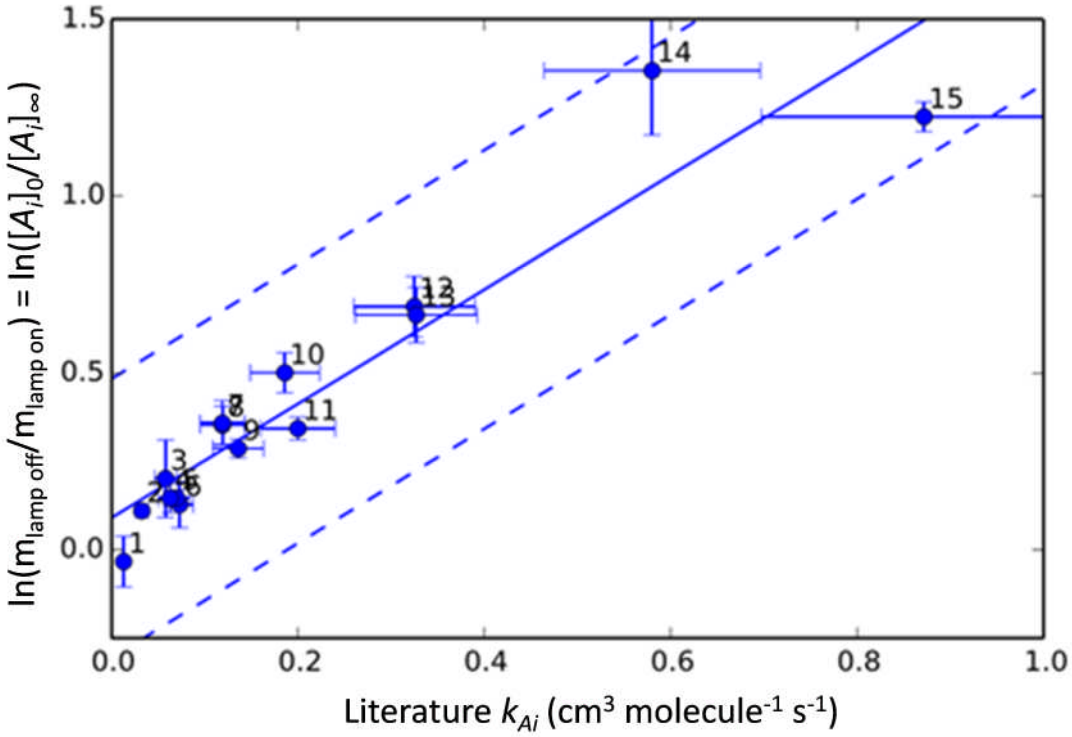

Figure 4.19: ln($m_{lamp\ off}$ / $m_{lamp\ on}$) vs literature rate coefficients for a selection of 15 VOCs measured in ambient air during the York 2014 'missing' OH reactivity campaign. Solid line represents the linear least squares fit to the data, gradient: 1.5×10^{10} molecule cm^{-3} s^{-1} (equal to ∫[OH]dt). Dashed lines represent 95 % confidence intervals. 1. benzene 2. toluene 3. propylbenzene 4.isopropylbenzene 5. ethylbenzene 6. *n*-heptane 7. decane 8. 2-ethyltoluene 9.o-xylene 10. 3-ethyltoluene 11. m/p-xylene 12. 1,2,4-trimethylbenzene 13. 1,2,3-trimethylbenzene 14. Styrene 15. Isoprene. Provided by Dr. Richard Lidster, University of York.

The data plotted show a linear trend, as is required to extract a ∫[OH]dt value. At present only limited ambient data (a few days) have been analysed from the new instrument described here. Full analysis of the ambient data for identifiable compounds will form the basis of future work in order to further populate Figure 4.19 and maximise the accuracy of ∫[OH]dt that is determined. A small number of peaks were also observed in the chromatograms that were not immediately identifiable, however, should be upon further analysis of the large amount of mass-

spectral data that were acquired (Lidster, 2013). Further work shall also include the determination of bimolecular rate coefficients for the reaction between these unidentified species and OH and also investigation of their chemical identity. Their contribution to 'missing' OH reactivity will be quantified.

4.7 Summary and conclusions

A new OH reactor has been designed and successfully characterised using a fast response LIF HCHO detector when operated using two sets of flow conditions (4.05 and 3.05 SLM total flow). Ambient air was introduced to the reactor via a moveable injector so that the distance between the point of flow mixing and irradiation of humidified nitrogen for OH generation could be adjusted. The position of the injector was optimised for each set of flow conditions to prevent direct photolysis of VOCs and to maximise their exposure to OH. The [OH] present at the point of mixing was also quantified for each flow condition and was found to be 7.6×10^{10} and 2.6×10^{10} molecule cm^{-3} for the 4.05 and 3.05 SLM conditions, respectively. The loss rate of OH within the reactor to the walls of the flow tube and impurities present in the gasses used was also measured to be 6.6 s^{-1}. A zero-dimensional chemical box model has been constructed to assess the effect that the OH reactor could have on the concentrations of VOCs in ambient air. It was concluded that it was necessary to operate the reactor using the 4.05 SLM total flow conditions in order for quantifiable decreases to be observed by GC-TOF-MS.

Following characterisation, the OH flow reactor was successfully interfaced with a GC-TOF-MS instrument at the University of York. The resulting set-up was a new instrument for the identification of 'missing' OH reactivity in the troposphere and has been deployed for field measurements during the York 2014 'missing' OH reactivity field campaign (19/05/2014 – 16/06/2014). Both identified and unidentified species were observed to decrease in concentration when ambient air was exposed to OH within the reactor, thus indicating a contribution from unidentified ('missing') sinks to total OH reactivity at the site. A large data set was generated, thorough analysis of which is required to fully understand the origin of any 'missing' OH reactivity. The new instrument described in this chapter shows potential as a valuable tool for investigating the source of 'missing' OH reactivity. It's deployment to environments with atmospheres know to have significant 'missing' OH reactivity, such as forests, should be considered in future.

4.8 References

ATKINSON, R. 1994. Gas phase tropospheric chemistry of organic compounds, Monograph 2. *Journal of Physical and Chemical Reference Data***,** 1-216.

ATKINSON, R. 1997. Gas-Phase Tropospheric Chemistry of Volatile Organic Compounds: 1. Alkanes and Alkenes. *Journal of Physical and Chemical Reference Data,* 26**,** 215-290.

ATKINSON, R., BAULCH, D. L., COX, R. A., CROWLEY, J. N., HAMPSON, R. F., HYNES, R. G., JENKIN, M. E., ROSSI, M. J., TROE, J. & SUBCOMMITTEE, I. 2006. Evaluated kinetic and photochemical data for atmospheric chemistry: Volume II – gas phase reactions of organic species. *Atmos. Chem. Phys.,* 6**,** 3625-4055.

DILLON, T. J., HOLSCHER, D., SIVAKUMARAN, V., HOROWITZ, A. & CROWLEY, J. N. 2005. Kinetics of the reactions of HO with methanol (210-351 K) and with ethanol (216-368 K). *Physical Chemistry Chemical Physics,* 7**,** 349-355.

GROSJEAN, D. & WILLIAMS, E. L. 1992. Environmental persistence of organic compounds estimated from structure-reactivity and linear free-energy relationships. Unsaturated aliphatics. *Atmospheric Environment. Part A. General Topics,* 26**,** 1395-1405.

IANNI, J. C. 2003. A Comparison of the Bader-Deuflhard and the Cash-Karp Runge-Kutta Integrators for the GRI-MECH 3.0 Model Based on the Chemical Kinetics Code Kintecus. *In:* BATHE, K. J. (ed.) *Computational Fluid and Solid Mechanics 2003.* Oxford: Elsevier Science Ltd.

KATO, S., SATO, T. & KAJII, Y. 2011. A method to estimate the contribution of unidentified VOCs to OH reactivity. *Atmospheric Environment,* 45**,** 5531-5539.

LIDSTER, R. 2013. *RE: Personal communication.*

MARTINS, G., FERREIRA-RODRIGUES, A. M., RODRIGUES, F. N., DE SOUZA, G. G. B., MASON, N. J., EDEN, S., DUFLOT, D., FLAMENT, J. P., HOFFMANN, S. V., DELWICHE, J., HUBIN-FRANSKIN, M. J. & LIMAO-VIEIRA, P. 2009. Valence shell electronic spectroscopy of isoprene studied by theoretical calculations and by electron scattering, photoelectron, and absolute photoabsorption measurements. *Physical Chemistry Chemical Physics,* 11**,** 11219-11231.

PICQUET, B., HEROUX, S., CHEBBI, A., DOUSSIN, J.-F., DURAND-JOLIBOIS, R., MONOD, A., LOIRAT, H. & CARLIER, P. 1998. Kinetics of the reactions of OH radicals with some oxygenated volatile organic compounds under simulated atmospheric conditions. *International Journal of Chemical Kinetics,* 30**,** 839-847.

SANDER, S. P., FRIEDL, R. R., GOLDEN, D. M., KURYLO, M. J., MOORTGAT, G. K., WINE, P. H., RAVISHANKARA, A. R., KOLB, C. E., MOLINA, L. T., FINLAYSON-PITTS, B. J., HUIE, R. E. & ORKIN, V. L. 2006. Chemical Kinetics and Photochemical Data for Use in Atmospheric Studies Evaluation Number 15. *JPL Publication,* 06-2.

Chapter 5 - York 2014 ‘missing’ OH reactivity campaign

5.1 Background to the York 2014 project

A substantial body of literature reports measurements of OH reactivity where comparisons have been drawn with those predicted either by calculations which use only the measured concentrations of OH sinks or by models where concentrations of VOC photo-oxidation products are predicted, and used to account for a portion of OH reactivity. A recurring theme is that measured OH reactivity almost always exceeds that predicted by a quantity known as the ‘missing’ OH reactivity. ‘Missing’ OH reactivity has been reported for environments ranging from the Borneo rainforest (~53 % missing, when comparing with a model prediction) (Edwards et al., 2013) to Urban Tokyo (~25 – 35 % missing, when comparing with a calculation) (Yoshino et al., 2012). A comprehensive summary of ‘missing’ OH reactivity reported in the literature is provided in Section 1.4. Kato et al. (2011) outlined a method for a relative rate study of GC-FID peaks representing OH reactive species in ambient air that either had, or had not, been exposed to OH, the aim of which was to determine the portion of ‘missing’ OH reactivity that could be accounted for by species that could be detected but not identified. The methodology is described in detail in Section 1.4.4 and detected approximately 4 % more of the measured OH reactivity during a campaign at an urban background site in Tokyo.

5.2 Aims

Presently, there is no method reported in the literature for the identification of the unidentified species that contribute to ‘missing’ OH reactivity, as reported by Kato et al. (2011). A key objective of the York 2014 ‘missing’ OH reactivity campaign was to address this. A new instrument was deployed alongside the Leeds laser flash

photolysis instrument for the measurement of OH reactivity, in addition to a very detailed suite of OH sink measurements to fully assess the nature of the OH sink at an urban background site. The new instrument was formed through the coupling of an OH flow reactor to a GC-TOF-MS system, details of the development are presented in Chapter 4 in addition to some preliminary observations.

In addition to OH reactivity, a measurement of formaldehyde (HCHO) can help when assessing the completeness of our knowledge of the OH sink in a given environment. HCHO is a final product from the photo-oxidation of almost all VOCs (Whalley et al., 2016). Comparison of measured and predicted values can reveal missing oxidation steps from a model or may point to a primary emission of HCHO (Kaiser et al., 2015). The LIF instrument for the measurement of HCHO, described in Chapter 2, was deployed for its first ambient measurements during the York 2014 'missing' OH reactivity campaign.

This chapter focusses on observations of OH reactivity and HCHO from the York 2014 'missing' OH reactivity campaign. An in depth analysis of the relationship between measured and predicted (calculated and modelled) OH reactivity is presented in addition to HCHO observations. The campaign took place in May / June 2014 on the campus of the University of York; the site, measurement suite and weather conditions are described in Section 5.3.

5.3 Site description, measurement suite and conditions

OH reactivity, radical and photolysis rate measurements were made from the roof of the FAGE container in a small car park next to the Wolfson Atmospheric Chemistry Laboratories (WACL), situated on the University of York campus in Heslington, York, UK (53° 56' N, 1° 02' W). The site was ~3 km south-east of the centre of York and ~2 km west of a major road (A64), there was also a small wooded area immediately to the east. This site was chosen as the air mass would likely be influenced by anthropogenic emissions from the centre of York and nearby roads, in addition to local biogenic emissions, all of which would likely include candidates for contributors to 'missing' OH reactivity. It was also directly adjacent to the WACL building from which a number of instruments to measure VOCs were operated. Figure 5.1 displays the location of the site at the WACL in relation to the centre of York and the A64.

The convenient location next to the WACL building made it possible to measure a large suite of VOCs and other species, including many which would not routinely be measured in the field due to logistical and technical limitations regarding instrumentation that can be operated with relative ease in the conventional laboratory setting. An example is the GC-TOF-MS system of the new instrument described in Chapter 4. The majority of other measurements were made from ambient air that had been sampled through a manifold mounted on the roof of the WACL building ~10 m south and ~5 m vertically higher than the inlets on the roof of the FAGE container. An exception to this was the measurement of HONO for which air was sampled from the roof of the nearby York GC container at approximately the same height as the FAGE container measurements and ~2 m away horizontally. Table 5.1 summarises the species / parameters measured, the location of sampling inlets / detectors, and the techniques used along with references to descriptions of the techniques.

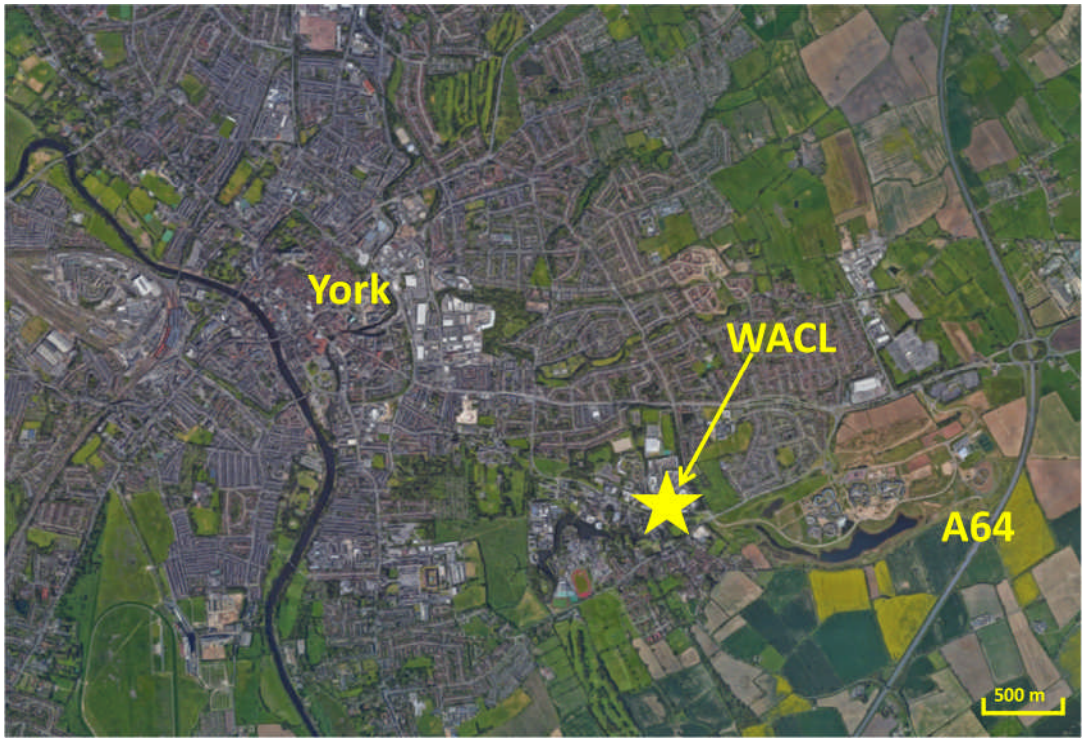

Figure 5.1: Satellite image showing the location (yellow star) of the measurement site at the WACL relative to the city centre of York and nearby major road (A64).

The Leeds FAGE container was positioned directly on the ground in close proximity to the WACL building; for all measurements made using the FAGE container instrumentation air was sampled from the container roof at a height of ~3 m. Figure

5.2 shows a photograph of the FAGE container at the measurement site during the campaign with the approximate locations of inlets / measurement points labelled.

Figure 5.2: Photograph of the Leeds FAGE container during the York 2014 'missing' OH reactivity campaign. Labels show the approximate locations of sampling inlets and points of measurement.

The weather conditions were dry for the majority of the campaign with periods of rainfall typically lasting no longer than a few hours. The average temperature was 14.9 ˚C and ranged from 6.7 to 24.9 ˚C with an average relative humidity of 43 % which ranged from 14 to 79 %. The wind speed did not exceed 2.2 m s^{-1} during the measurement period and the modal value recorded by the meteorological station was 0 m s^{-1}, indicating that air sampled at the various sampling locations could have been poorly mixed.

Measurement	Technique	Sample inlet	Reference
OH, HO_2, RO_2	Laser induced fluorescence spectroscopy (LIF)	FAGE container	Whalley et al. (2013)
OH reactivity	Laser flash photolysis coupled with laser induced fluorescence spectroscopy (LFP - LIF)	FAGE container	Stone et al. (2016)
HCHO	Laser induced fluorescence spectroscopy (LIF)	WACL manifold	This work
NO, NO_2	Chemiluminescence	FAGE container and WACL manifold	Weinheimer (2006)
O_3	UV absorption	FAGE container and WACL manifold	Heard et al. (2006)
CO	Hot mercuric oxide reduction coupled with UV detection	WACL manifold	Robbins et al. (1968)
HONO	Long path absorption photometry (LOPAP)	GC container	Heland et al. (2001)
Photolysis frequencies	Spectral radiometry	FAGE container	Hofzumahaus (2006)
$J(O^1D)$	Filter radiometry	FAGE container	Bohn et al. (2004)
NMHCs	Gas chromatography coupled with time of flight mass spectrometry (GC-TOF-MS)	WACL manifold	Lidster et al. (2014)
NMHCs	Gas chromatography coupled with flame ionisation detection (GC-FID)	WACL manifold	Dunmore et al. (2015)
NMHCs	Orthogonal gas chromatography coupled with flame ionisation detection (GCxGC-FID)	WACL manifold	Dunmore et al. (2015)

Table 5.1: Species / parameters measured during the York 2014 ‘missing’ OH reactivity campaign at the Wolfson Atmospheric Chemistry Laboratories.

5.4 OH reactivity

5.4.1 OH reactivity observations

The Leeds laser flash photolysis instrument for the measurement of OH reactivity was situated ~3 m above ground on the roof of the Leeds FAGE container for the duration of the measurement period. Measurements were made with the instrument in configuration 1 as described in Section 2.1.6. Figure 5.3 shows a photograph of the instrument at the measurement site whilst sampling ambient air.

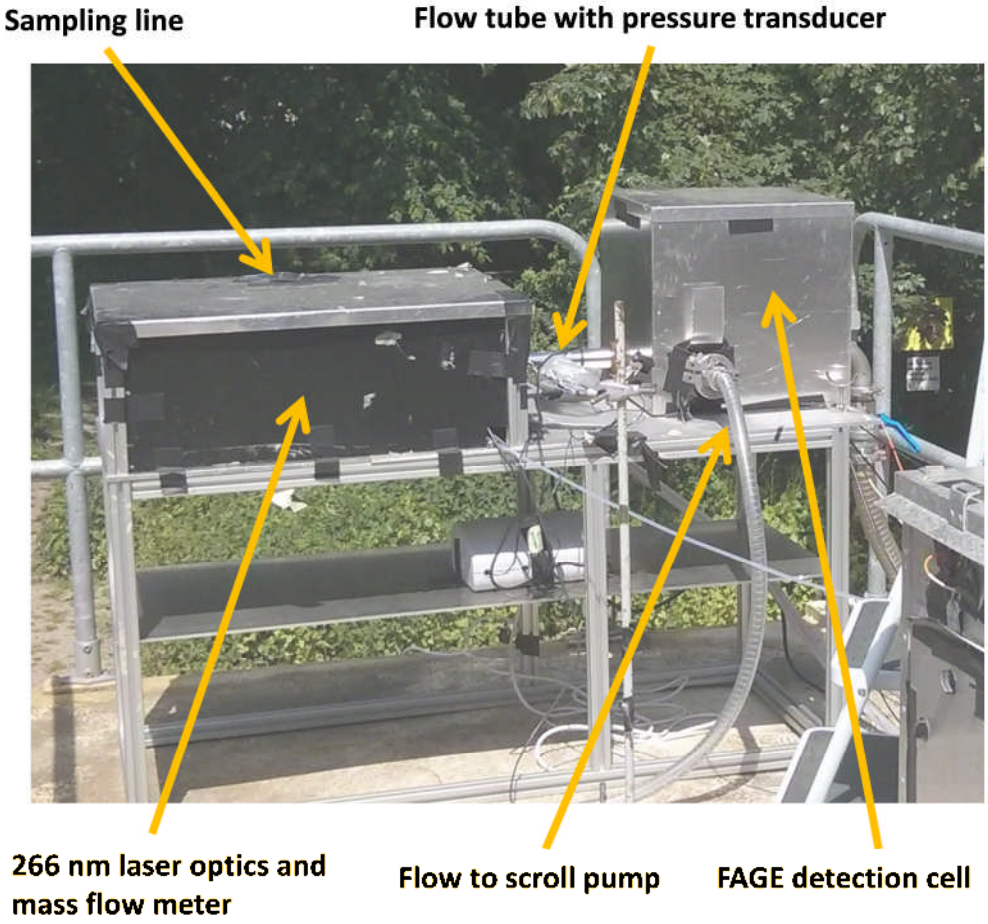

Figure 5.3: Image of the laser flash photolysis OH reactivity instrument whilst making measurements in ambient air during the York 2014 'missing' OH reactivity campaign, key features are labelled.

The scroll pump, photolysis laser control unit and the majority of the other electronic components of the instrument were housed inside the FAGE container. They were connected to the apparatus on the roof via long cables and tubing that were routed through a waterproof enclosure which housed the RO_x detection cells. A

10 m optical fibre was also routed through this enclosure to deliver 308 nm light for the detection of OH in the FAGE cell of the OH reactivity instrument.

Ambient levels of O_3 (15 – 30 ppb during the day) and water vapour (14 – 79 %) were high enough to form sufficient [OH] via photolysis of O_3 for a decay signal to be observed within ~1 minute. It was not necessary to add either O_3 or water vapour to the instrument for the duration of the campaign.

In order to extract a value for $k'_{OH(raw)}$ from OH decays observed whilst the instrument was in configuration 1 (as described in Section 2.2.7), a bi-exponential decay function (E2.2) was fitted to each decay. Following this, $k'_{OH(physical)}$, the loss rate of OH due to physical processes (diffusion and wall loss) in the flow tube was subtracted from each $k'_{OH(raw)}$ value. The value of $k'_{OH(physcal)}$ used was 1.25 s^{-1} and details of the determination of this value are reported in Section 2.1.8. The pressure within the flow tube of the OH reactivity instrument was slightly sub-ambient (by ~ 30 Torr) for the duration of the campaign, this meant that the concentration of OH sinks (in molecule cm^{-3}) in the flow tube were slightly lower than in the ambient air sampled. The result was that the OH loss rates, $k'_{OH(raw)}$ - $k'_{OH(physical)}$, were slightly lower than the actual loss rate of OH present in the ambient air sampled. To correct for this each $k'_{OH(raw)}$ - $k'_{OH(physical)}$ was multiplied by the ratio of the pressure of the ambient air sampled (P_{Amb}) to the pressure within the flow tube (P_{FT}), E5.1.

$$k'_{OH} = (k'_{OH(raw)} - k'_{OH(physical)}) \times \frac{P_{Amb}}{P_{FT}} \qquad \textbf{E5.1}$$

The laser flash photolysis OH reactivity instrument operated as intended for the majority of the campaign. The majority of gaps in the data recorded were as a result of intentionally switching off the instrument during planned breaks in the measurements.

OH reactivity was measured from 19/05/2014 to 16/06/2014 and all observations are displayed in the plots shown in Figure 5.4. Figure 5.4a shows the time series of OH reactivity plotted with error bars which represent the 1σ uncertainty (~±0.6 s^{-1} on average) determined through combining the uncertainties on the OH decay fits, the determination of $k'_{(physical)}$ and the correction for pressure described above. The measurements are re-plotted in Figure 5.4b with the omission of error bars for clarity. Values ranged from 2.8 to 17.4 s^{-1} and the mean average k'_{OH} was 6.3 s^{-1}.

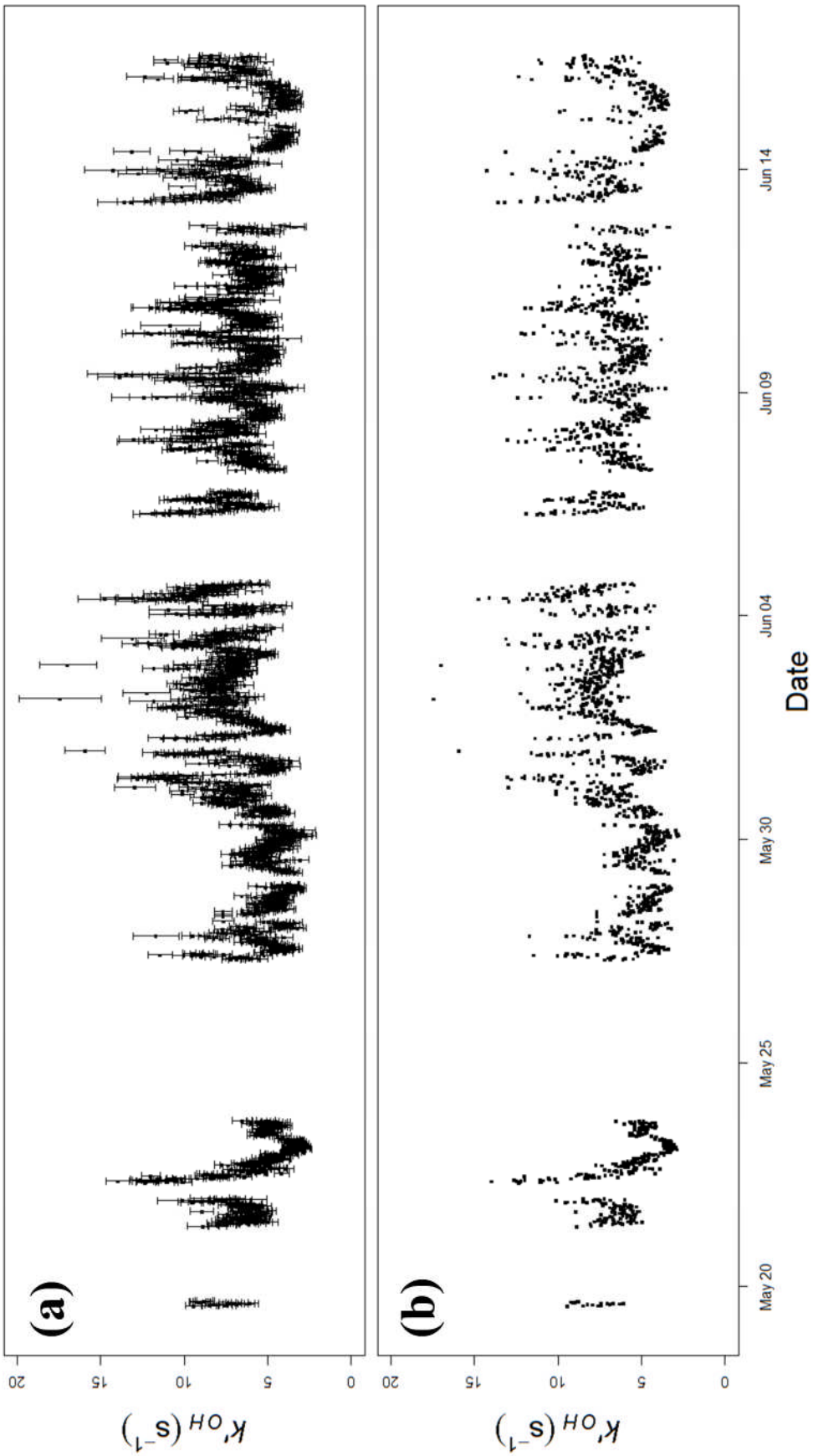

Figure 5.4: Time series of measured OH reactivity during the York 2014 'missing' OH reactivity campaign. (a) Data plotted with error bars representative of 1σ determined through combining the uncertainties from the decay fits, the determination of $k'_{OH(Zero)}$ and a correction for pressure. (b) data plotted without error bars for clarity.

5.4.2 Interpretation of OH reactivity observations

5.4.2.1 Diurnal behaviour

Owing to the location of the measurement site used for the York 2014 'missing' OH reactivity campaign being on a university campus, in close proximity to buildings and small roads, it is likely that locally emitted OH sinks would have momentarily affected the measured values of OH reactivity. Such species may not have accounted for a significant portion of the OH sink for the whole campaign, but may have done for a short period of time. In order to broadly examine nature of the OH sinks at the site, a diurnal profile for the 'average day' has been generated. All measurements of OH reactivity were averaged into 96 time bins with a mean value every 15 minutes using the 'timeAverage' function of the openair package in R (Carslaw and Ropkins, 2012, Carslaw, 2015), these data are plotted in Figure 5.5.

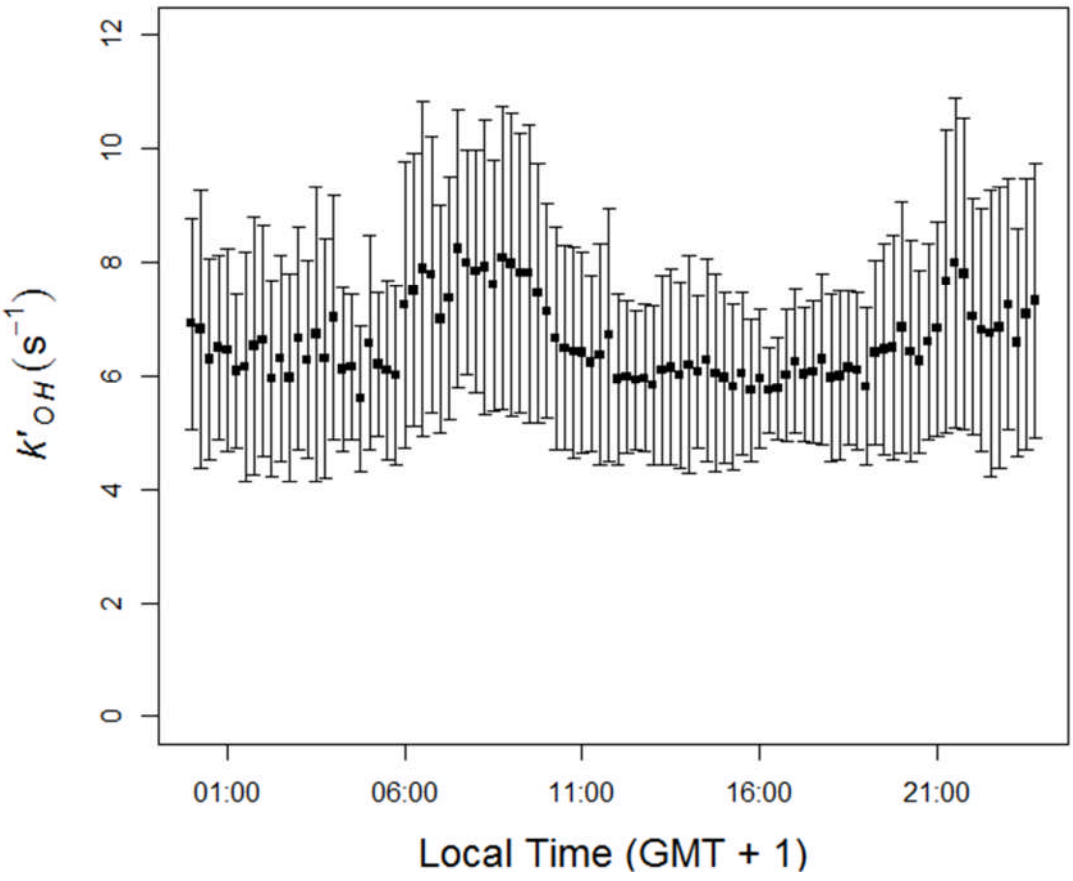

Figure 5.5: Diurnal profile of OH reactivity observed during the York 2014 'missing' OH reactivity campaign in 15 minute time bins. Error bars represent ± 1 σ standard deviation from the mean observation.

The profile of Figure 5.5 shows a rise in OH reactivity through the morning hours, starting at around 06:00 and reaching a maximum of ~8 s^{-1}. This is a typical feature of OH reactivity observations from environments where the air mass is significantly influenced by anthropogenic emissions at urban and urban background sites, in particular vehicular emissions. Diurnal morning rush hour peaks in OH reactivity were reported for measurements made in Mexico City (~120 s^{-1}), New York (~25 s^{-1}), Tokyo (~50 s^{-1}), Paris (~30 s^{-1}) and London (~27 s^{-1}) (Shirley et al., 2006, Ren et al., 2006a, Chatani et al., 2009, Dolgorouky et al., 2012, Whalley et al., 2016). In addition to diurnal morning rush hour peaks, evening rush hour peaks have also been reported. Strong diurnal evening rush hour peaks were reported for measurements in New York (~40 s^{-1}) and Tokyo (~35 s^{-1}) (Ren et al., 2006b, Chatani et al., 2009). Figure 5.5 shows a slight rise in OH reactivity from the afternoon into the night however there is no evidence of such a diurnal evening rush hour peak in the diurnal profile or in the data for individual days.

The maximum OH reactivity in the diurnal morning rush hour peak for the York measurements shown in Figure 5.5 is significantly lower than what has been reported at other locations listed above. York is a much smaller city than all of these, and the measurements were made on a University Campus near small roads which are less prone to morning congestion, this was most likely the main reason for the lower values measured. The close proximity of agricultural land also means that the cleaner less polluted air will have influenced the site more than if measurements were made closer to the city centre.

Brune et al. (2016) recently reported measurements of OH reactivity from the CalNex campaign at an urban background site in Bakersfield, CA, US. The site shared a number of similarities to the site at the WACL; both were car parks situated in close proximity to major roads (York ~2 km, CalNex ~0.8 km), and both were situated on the edge of cities in close proximity to agricultural land. The diurnal profile of the CalNex measurements did not show an evening rush hour peak. However, the values rose steadily through the night time hours (similar to those presented here) and stabilised in the early morning before steadily decreasing again through the daytime hours. This behaviour was attributed to differences in the height of the boundary layer between day time and night time. It is likely that the evening rise in diurnal OH reactivity observed in York was influenced by changes in the boundary layer height.

5.4.2.2 Correlations with other measurements

To further investigate the shape of the diurnal profile presented in Section 5.3.2.1, and the potential sources of sinks that influenced it, correlations between OH reactivity and other species measured were investigated. All correlations presented in this section were produced considering only measurements that were made from 31/05/2014 00:00:00 to 15/06/2014 07:45:00; from here on referred to as the comparison period. All measurements made during the campaign in York were merged into a single data set by Dr. Jenny Young so that a common time base was shared, with a measurement every 15 minutes during the comparison period. For species that were measured using GC techniques data were reported hourly. It followed that it was not possible to calculate concentrations for the 15 minute bins between the times at which data for GC measured species were reported. These data were estimated through linear interpolation between the 15 minute concentrations that were able to be determined. All of the correlations presented in this section were plotted using the merged data for the comparison period.

It was postulated in Section 5.3.2.1 that the diurnal morning peak in OH reactivity was a result of the morning 'rush hour' in traffic, which would indicate that vehicular emissions such as NO_x would have played a major role in influencing OH reactivity. NO_x observations from York are presented in Figure 4.6 and show that the levels of each species were often highest during the morning hours of each day. NO is shown to frequently rise to ~5 ppb and NO_2 is shown to frequently rise as high as 10 ppb. The correlation between OH reactivity and NO_x was investigated and the resulting plots are displayed in Figure 5.7.

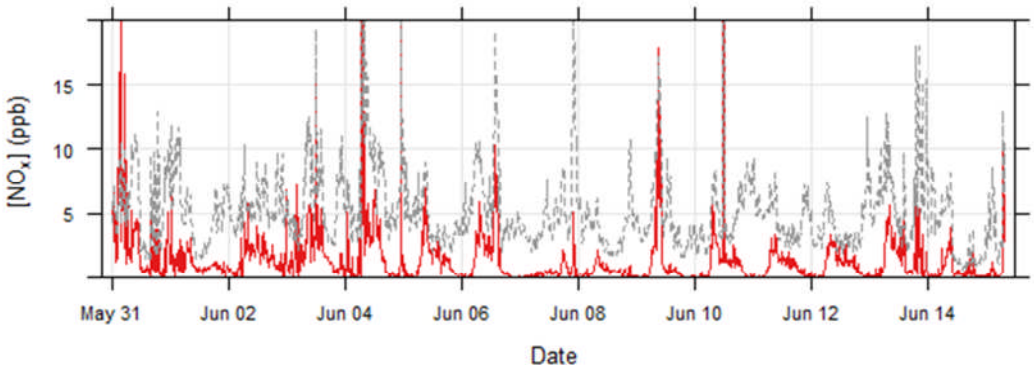

Figure 5.6: Observations of NO (red line) and NO_2 (grey dashed line) for the comparison period of the York 2014 'missing' OH reactivity campaign. Data are plotted at 15 minute time intervals.

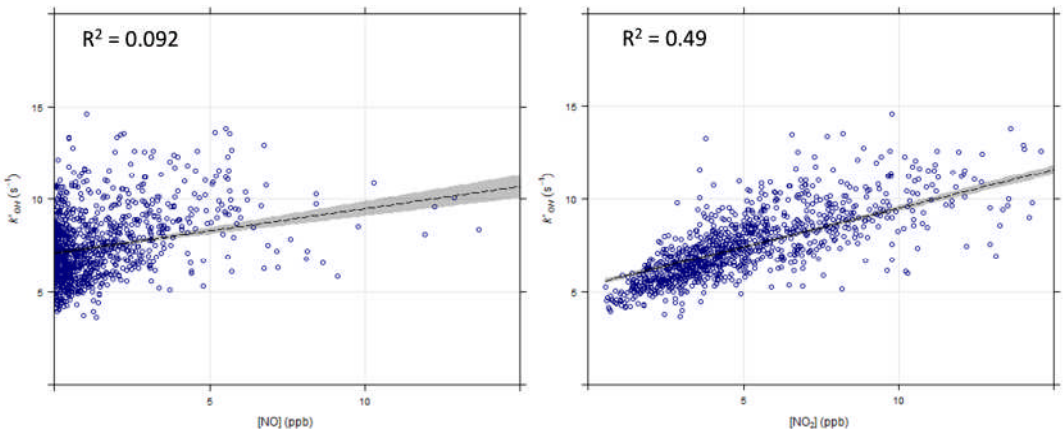

Figure 5.7: Plots of OH reactivity against both [NO] and [NO_2]. Data shown are 15 minute binned mean averages from measurements taken between 31/05/2014 00:00:00 – 15/06/2014 07:45:00 of the York 2014 'missing' OH reactivity campaign. The shaded areas represent the 95% confidence intervals from the linear fits (least squares).

It is shown that the correlation between OH reactivity and [NO_2] is stronger than it is with [NO] (R^2: 0.49 and 0.092, respectively). This difference in correlation strength is consistent with other observations of OH reactivity in atmospheres that are influenced by vehicular emissions. On average NO_2 often contributes more to OH reactivity than NO, and also is more dominant at driving change in OH reactivity. Two examples of this are measurements reported from Tokyo and London (Yoshino et al., 2006, Whalley et al., 2016). It follows from this that a stronger correlation between NO_2 and OH reactivity would be expected.

In addition to NO_x, correlations were examined for all other species that were measured. Figure 5.8 shows some examples for species where reasonable correlations were found. Correlations are shown for ethane, propane, propene and toluene; all of which are known vehicular emissions (Nakashima et al., 2012). The presence of these correlations further supports the hypothesis that vehicular emissions accounted for a significant portion of the OH sink in York.

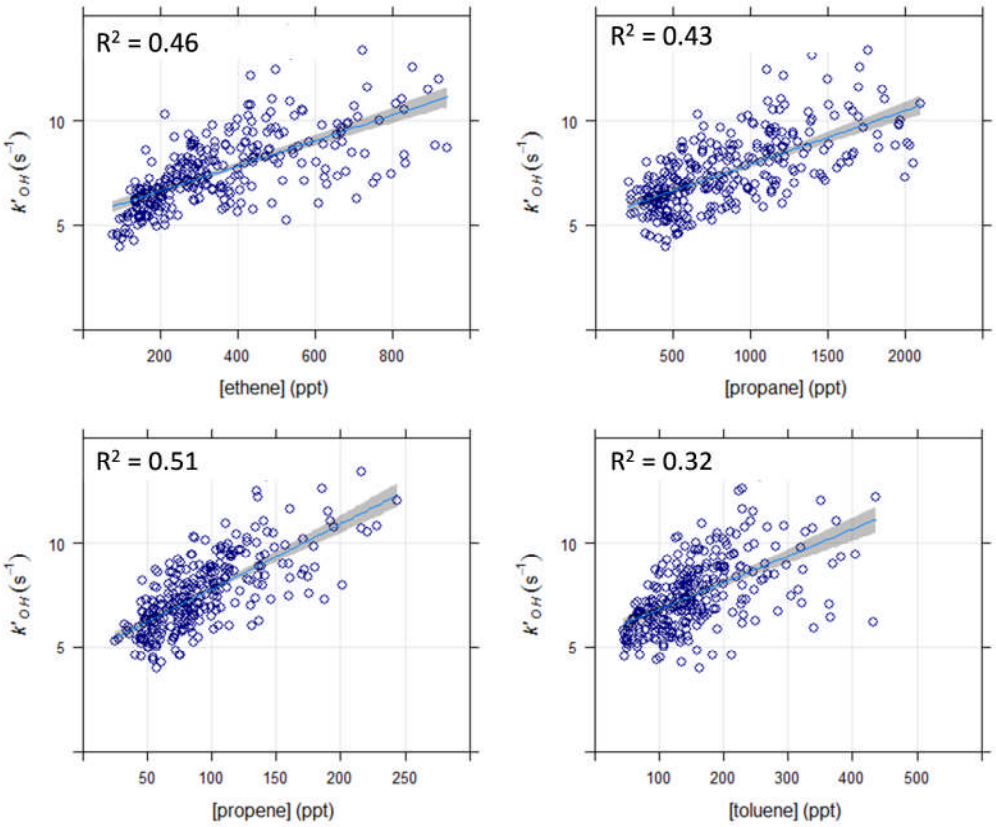

Figure 5.8: Plots of OH reactivity against [ethene], [propane], [propene] and [toluene]. Data shown are 15 minute binned mean averages from measurements taken between 31/05/2014 00:00:00 – 15/06/2014 07:45:00 of the York 2014 'missing' OH reactivity campaign. Data where VOC concentrations were estimated through linear interpolation have been excluded.. The shaded areas represent the 95% confidence intervals from the linear fits (least squares).

5.4.2.3 Calculation of OH reactivity

To examine the extent of the completeness of the suite of sinks measured during the campaign, the OH reactivity was calculated using the measured concentrations of sinks and corresponding bimolecular rate coefficients as in E1.3 (reproduced below). Sink concentrations in the merged 15 minute data set for the comparison period (described in Section 5.3.2.2) were used for this.

$$k'_{OH(calc)} = \sum_{j} k^{j}_{OH+Aj} [A_j] \qquad \textbf{E1.3}$$

The sinks which were used to calculate OH reactivity for the York 2014 'missing' OH reactivity campaign are summarise in Table 5.2. Each sink was also assigned to a class according to its functionality so that grouped contributions to calculated OH reactivity could be determined, these are also listed with their campaign average contributions. Details of the instrument used to measure each species are provided in addition to bimolecular rate coefficients. The values shown are those calculated at a temperature of 298 K and a pressure of 1 atmosphere. For the calculation of OH reactivity, the values used were determined using the temperature and pressure dependencies in conjunction with measured temperatures and pressures by the meteorological station that was positioned on the roof of the FAGE container. All expressions for rate coefficients were IUPAC recommended values taken from the Master Chemical Mechanism (MCM) v3.3 (Jenkin et al., 1997, Saunders et al., 2003) with the exception of 8 species (Cyclopentane, Isopentane, 2,2,4-Trimethylpentane, 4-Isopropyltoluene, Indane, *t*-Butylbenzene, 1,3-diethylbenzene, 1,4-Diethylbenzene), which were taken from the sources listed in the table caption as there was no data available in the MCM. The calculated OH reactivity is presented in Section 4.3.2.4 in addition to discussion of its relationship with the measured OH reactivity.

Sink	Class	$k_{sink + OH}$ (cm^3 $molecule^{-1}$ s^{-1})	Contribution to OH reactivity (s-1)	Instrument
O_3	O_3	7.3×10^{-14}	0.04	Thermo 49 Series
NO	NO	9.8×10^{-12}	0.38	Air Quality Design Inc. Chemiluminescence with LED NO_2 converter
NO_2	NO_2	9.9×10^{-12}	1.41	
CO	CO	2.3×10^{-13}	0.79	Ametek monitor
HONO	NO_z	6.0×10^{-12}	0.03	LOPAP
Methanol	Alcohols	9.0×10^{-13}	0.04	GC-FID
Ethane	Alkanes	2.4×10^{-13}	0.55	GC-FID
Propane		1.1×10^{-12}		GC-FID
Methylpropane		2.2×10^{-12}		GC-FID
Butane		2.4×10^{-12}		GC-FID
Pentane		4.0×10^{-12}		GC-FID
2-Methylpentane		5.3×10^{-12}		GC-FID
Hexane		5.5×10^{-12}		GC-FID
Heptane		7.0×10^{-12}		GC-FID
Octane		8.7×10^{-12}		GCxGC-FID
Nonane		1.0×10^{-11}		GCxGC-FID
Decane		1.1×10^{-11}		GCxGC-FID
Undecane		1.3×10^{-11}		GCxGC-FID
Dodecane		1.4×10^{-11}		GCxGC-FID
Cyclopentane [1]		5.0×10^{-12}		GC-FID
2-Methylbutane [2]		3.7×10^{-12}		GC-FID
2,2,4-Trimethylpentane [1]		3.3×10^{-12}		GCxGC-FID
Acetylene	Alkenes and Alkynes	7.5×10^{-13}	0.19	GC-FID
Ethene		7.8×10^{-12}		GC-FID
Propene		2.8×10^{-11}		GC-FID
trans-But-2-ene		6.4×10^{-11}		GC-FID
But-1-ene		3.1×10^{-11}		GC-FID
2-Methylprop-1-ene		5.1×10^{-11}		GC-FID
cis-But-2-ene		5.6×10^{-11}		GC-FID
trans-Pent-2-ene		6.7×10^{-11}		GC-FID
cis-Pent-2-ene		6.5×10^{-11}		GC-FID
Benzene	Aromatics	1.2×10^{-12}	0.53	GC-FID
Toluene		5.6×10^{-12}		GC-FID
Styrene		5.8×10^{-11}		GCxGC-FID
1,3-Dimethylbenzene		2.3×10^{-11}		GCxGC-FID
1,4-Dimethylbenzene		1.4×10^{-11}		GCxGC-FID
1,2-Dimethylbenzene		1.4×10^{-11}		GCxGC-FID
Ethylbenzene		7.0×10^{-12}		GCxGC-FID
Isopropylbenzene		6.3×10^{-12}		GCxGC-FID
Propylbenzene		5.8×10^{-12}		GCxGC-FID
1-Ethyl-3-methylbenzene		1.9×10^{-11}		GCxGC-FID
1-Ethyl-4-methylbenzene		1.2×10^{-11}		GCxGC-FID
1-Ethyl-2-methylbenzene		1.2×10^{-11}		GCxGC-FID
1,3,5-Trimethylbenzene		5.7×10^{-11}		GCxGC-FID
1,2,3-Trimethylbenzene		5.7×10^{-11}		GCxGC-FID
1,2,4-Trimethylbenzene		3.3×10^{-11}		GCxGC-FID
4-isopropyltoluene [3]		1.5×10^{-11}		GCxGC-FID
Indane [4]		1.9×10^{-11}		GCxGC-FID
t-butyl benzene [1]		4.5×10^{-12}		GCxGC-FID
1,3-diethyl benzene [5]		2.6×10^{-11}		GCxGC-FID
1,4-diethyl benzene [5]		1.6×10^{-11}		GCxGC-FID
α-Pinene	Biogenics	5.3×10^{-11}	0.32	GCxGC-FID
Limonene		1.6×10^{-10}		GCxGC-FID
Acetaldehyde	Carbonyls	1.5×10^{-11}	0.65	GCxGC-FID
Acetone		1.8×10^{-13}		GCxGC-FID
Formaldehyde		8.5×10^{-13}		LIF
1,3-Butadiene	Dialkenes	6.7×10^{-11}	0.21	GC-FID
Isoprene		1.0×10^{-10}		GC-FID

Table 5.2: OH sinks measured in York used in the calculation of OH reactivity. Species were assigned classes according to their functionality. Bimolecular rate coefficients for the reaction with OH at 298 K and 1 Atmosphere are shown, however pressure and temperature dependencies were used in the calculation of OH reactivity. Campaign average contributions to OH reactivity are also shown for each sink classification in addition to details of the instrument used for the measurement of each species. 1: Atkinson (2003) 2: Wilson et al. (2006) 3: Corchnoy and Atkinson (1990) 4: Kwok et al. (1997) 5: Carter (2010).

5.4.2.4 Measured and calculated OH reactivity

The values calculated using the 15 minute averaged sink concentrations are plotted in Figure 5.9, in addition to the measured values of k'_{OH} on the same time base. It can be seen that the profile of the calculated values tracks that of the measured values well for the majority of the comparison period, and that the measured values are typically slightly higher for the majority of the time. The results indicate that the identifiable OH sink measurements made during the campaign in York accounted for most, but not all of the OH reactivity that was measured. The correlation between the OH reactivity measured and calculated using concentrations of identifiable sinks, is presented in Figure 4.10. The majority of points plotted occupy the space below the 1:1 line representing 100% agreement, and above the boundary representing 50% underestimation by the calculation; the linear least squares gradient is 0.73. Therefore, it can be concluded that overall for the measurements in York, OH reactivity was under predicted when calculated using measured concentrations of identifiable sinks.

To gain further insight into periods of the campaign where there may have been 'missing' OH reactivity, the agreement between the measured and calculated values for individual days is considered. The plots in Figure 5.11 and Figure 5.12 compare measured and calculated OH reactivity for each day of the comparison period. In each plot the measured OH reactivity is represented by the red line and the calculated cumulative OH reactivity is represented by the top of the stacked structures. Each coloured band represents a contribution to calculated OH reactivity from groups of known measured OH sinks (summarised in Table 5.2) that were measured. The categories of OH sinks in order from the bottom of the stacked structures were: Dialkenes, Carbonyls, Biogenics, Aromatics, Alkenes and Alkynes, Alkanes, Alcohols, NO_2, NO and CO.

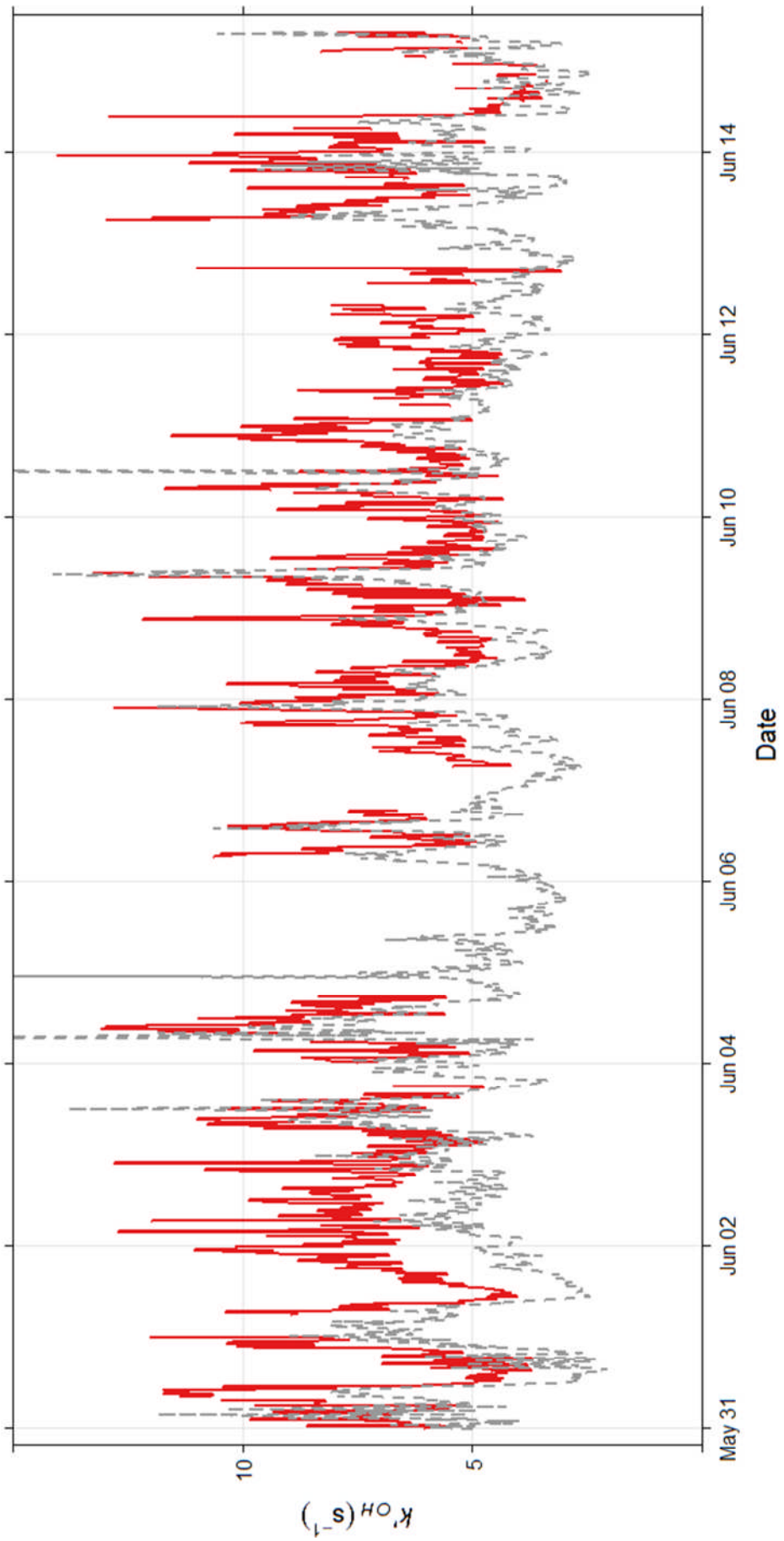

Figure 5.9: Measured OH reactivity (red line) and calculated OH reactivity (grey dashed line) for the comparison period of the York 2014 'missing' OH reactivity campaign. Data are plotted at 15 minute time intervals.

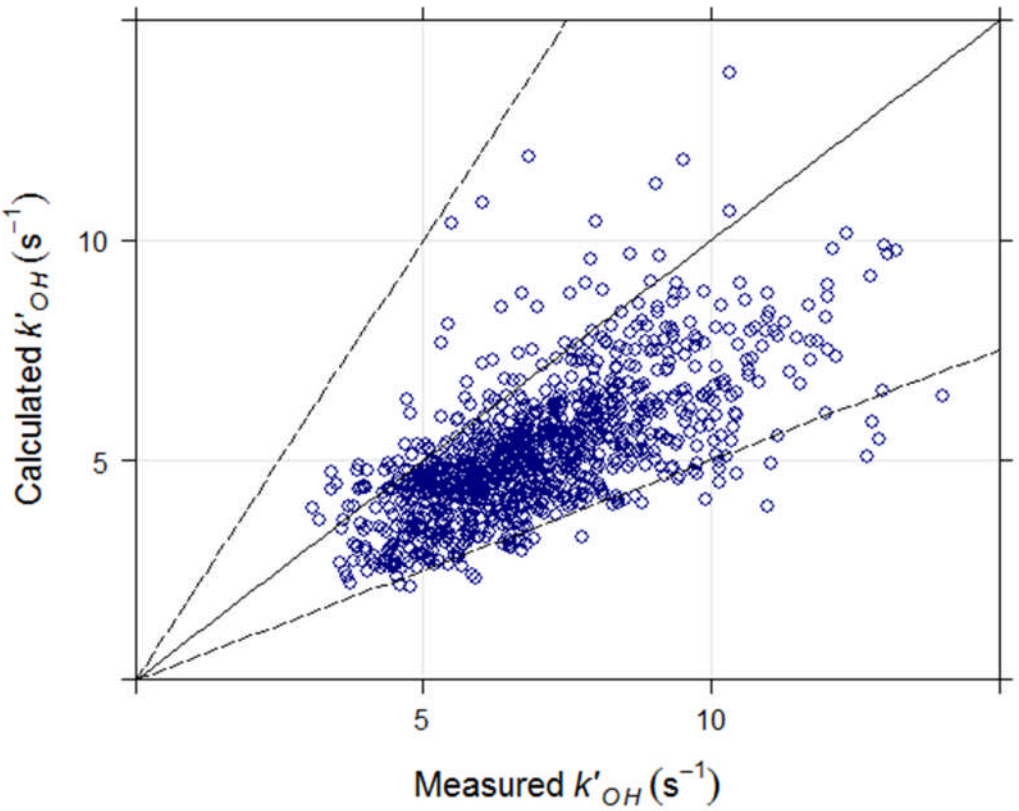

Figure 5.10: Correlation plot to show the relationship between measured and calculated OH reactivity during the York 2014 'missing' OH reactivity campaign. The solid line represents 1:1 agreement and the two dashed lines represent 50 % over or underestimation. Linear least squares gradient: 0.73, R^2:0.36.

It can be seen from Figure 5.11 and Figure 5.12 that the profile of the measured OH reactivity (red line) was typically higher than the calculated OH reactivity on all days shown. The difference is typically between 1 and 3 s^{-1} and is greatest towards the start of the comparison period (31/05/2014, 01/06/2014 and 02/06/2014) where the measured values are shown to be as much as a factor of two higher than the calculated values, e.g. late at night on 01/06/2014. The daily agreement between the measurements and calculations is discussed in more detail below.

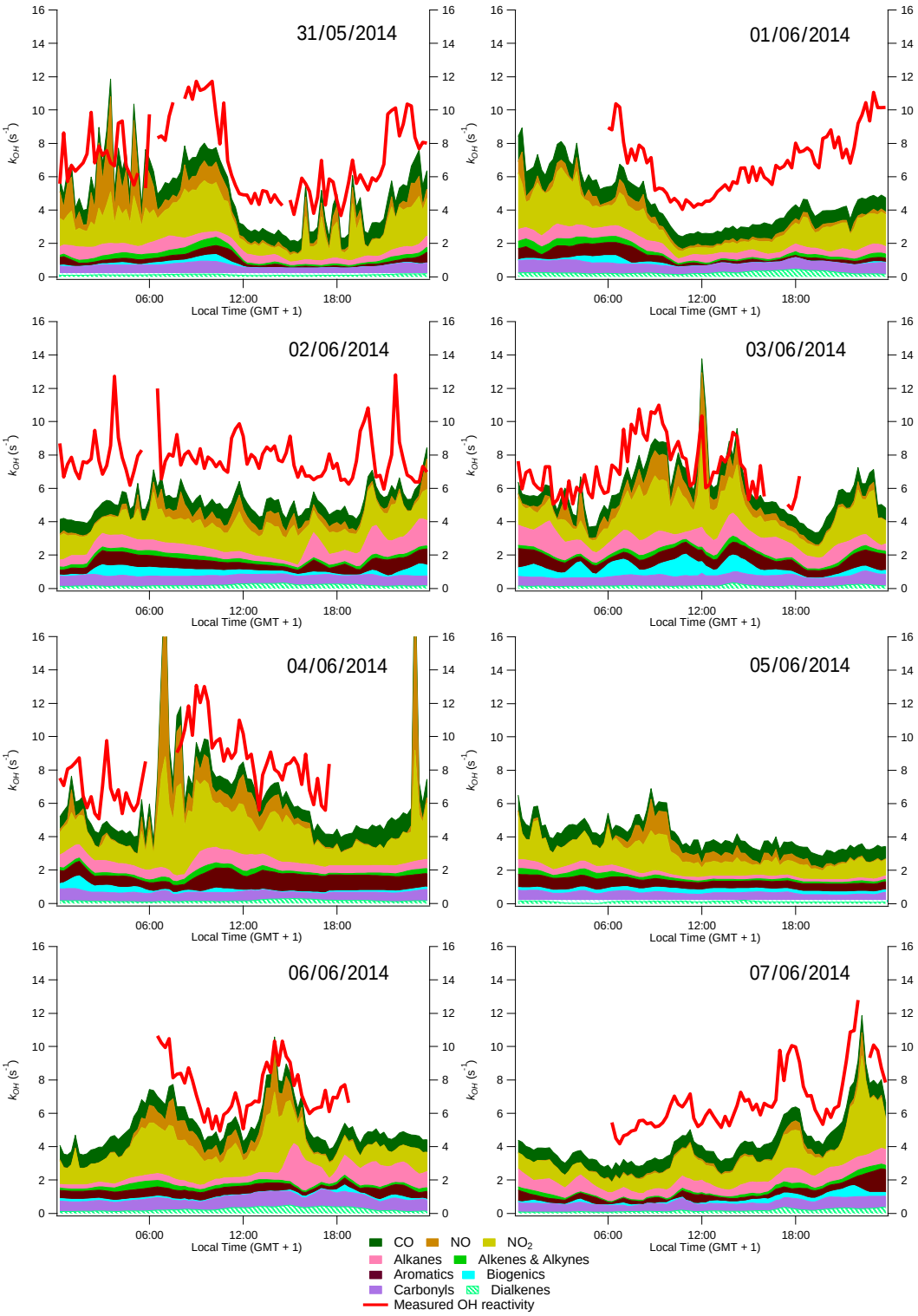

Figure 5.11: Daily comparisons (31st May -7th June 2014) of measured total OH reactivity (red line) with cumulative calculated OH reactivity (stacked coloured structures) from the comparison period of the York 2014 'missing' OH reactivity campaign. Calculated contributions for each OH sink classification were determined using data for all species measured that are summarised in Table 5.2.

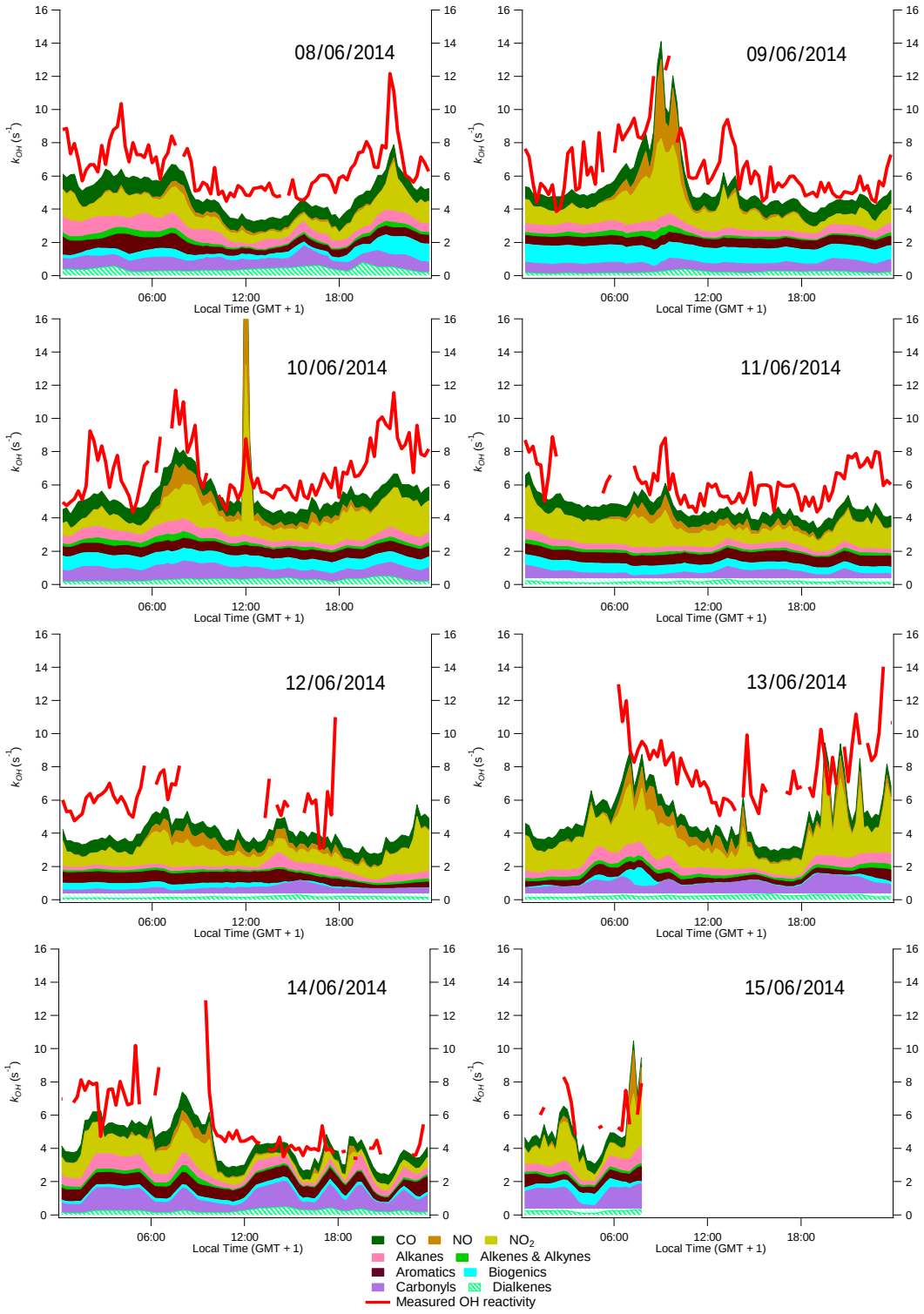

Figure 5.12: Daily comparisons (8th June -15th June 2014) of measured total OH reactivity (red line) with cumulative calculated OH reactivity (stacked coloured structures) from the comparison period of the York 2014 'missing' OH reactivity campaign. Calculated contributions for each OH sink classification were determined using data for all species measured that are summarised in Table 5.2.

Data for all days shown in Figure 5.11 and Figure 5.12 demonstrate that throughout the comparison period variations in OH reactivity were largely driven by NO_x emissions. The vertical width of the coloured bands representing NO and NO_2 both typically get wider when OH reactivity increases over a period of a few hours, and narrower when it decreases over a period of a few hours. This relationship is typically stronger for NO_2, an example of this is shown in the plot for 31/05/2014 where the measured and calculated OH reactivity are shown to both increase from ~0600 to peak at ~0900 before decreasing again. It can also be seen that often when there are sharp fluctuations in the contribution from NO_x, the same changes are not observed in the measured OH reactivity. Data from ~0000 – 0600 on 31/05/2014 demonstrate this as well as data at ~1200 on 03/06/2014 and 10/06/2014 where there are sharp spikes in the contribution from NO_x. As described in Section 4.2, ambient air was sampled from the roof of the FAGE container whereas the majority of OH sinks, such as NO_x, were measured from the WACL roof manifold. It is possible that the poor agreement between measured and calculated OH reactivity, where there are large rapid fluctuations in the contributions from NO_x, are a result of incomplete mixing of fresh emissions into the air mass sampled at the two inlets. The rapid fluctuations in the contribution from NO_x are likely due to local vehicular emissions from the carpark at the measurement site.

Contributions to OH reactivity from other classes of sink generally showed less variability through each day than NO_x, although on some days the contribution from other classes of compounds varies. Where VOC contributions were relatively large and variable, the calculated OH reactivity had a tendency to not track, be closer to, and sometimes exceed, the measurements. The data for 03/06/2014 demonstrate this where the contribution from biogenic species fluctuates through most of the day and the agreement is close. The agreement is also shown to be close after ~1000 on 14/06/2014 where after a reduction in the contribution from NO_x the contribution from carbonyls fluctuates, and the measured and calculated reactivity follow different profiles. The calculated values are shown to fluctuate by ~1.5 s^{-1} due to the carbonyl contribution which is not reflected in the measurements. Closer inspection of the data for individual species of carbonyls that were measured (acetaldehyde, acetone and formaldehyde) show that this variation is dominated by changes in the level of acetaldehyde. Acetaldehyde is known to be directly emitted from engine combustion and a wide range of industrial process (Ban-Weiss et al., 2008, Zavala et

al., 2009), and it is also known to be a direct emission from plants (Kreuzwieser et al., 1999, Fall, 2003). The different profiles for measured and calculated values on 14/06/2014 could be attributed to a very local source of acetaldehyde, from which a greater portion of emissions were sampled at the WACL roof manifold.

A very detailed suite of VOCs was measured during the campaign in York, many of which are not routinely measured in the field (e.g. the C8-12 alkanes, α-Pinene and Limonene). If a less detailed suite was measured there would have been a greater difference between measured and calculated OH reactivity values plotted in Figure and Figure . During the TORCH-2 campaign in Weybourne, the suite of VOCs measured was the same as those that were measured using the GC-FID instrument in York, the average missing OH reactivity was 40% when compared with the calculated values (Lee et al., 2009). Figure 4.13 shows an average diurnal (for data from the comparison period) of measured and calculated OH reactivity in York, where only concentrations of VOCs measured by the GC-FID measurements are included in the calculation.

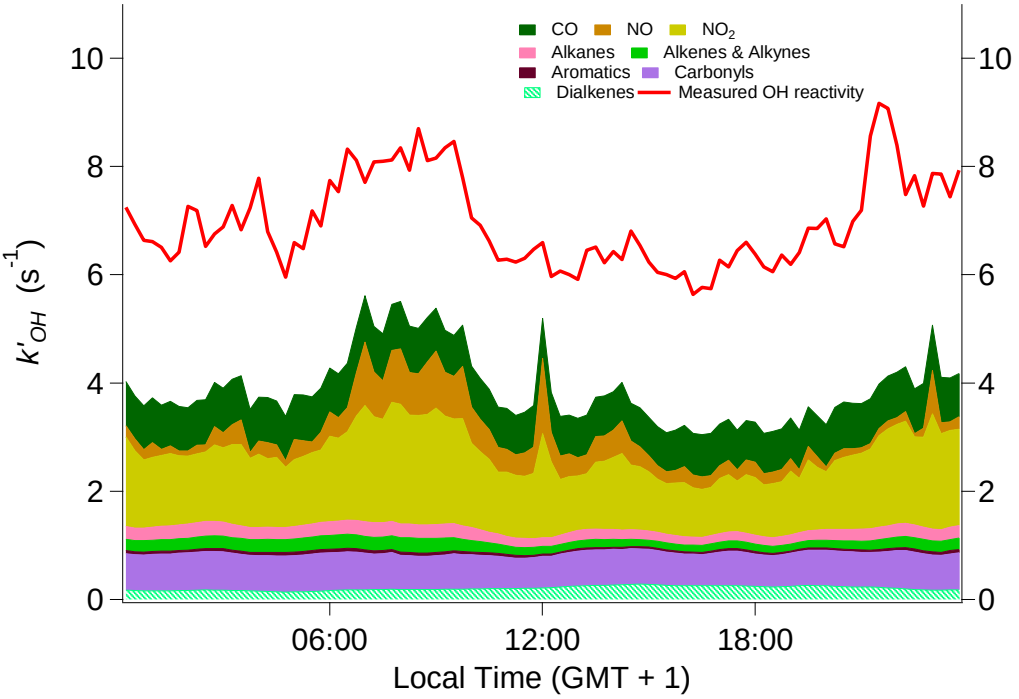

Figure 5.13: Diurnal profile of measured total OH reactivity (red line) with cumulative calculated OH reactivity (stacked coloured structures) for the comparison period (31/05/2014 00:00:00 to 15/06/2014 07:45:00) of the York 2014 'missing' OH reactivity campaign. Calculated contributions for each OH sink classification (not including CO, NO or NO_2) were determined using measurements of identifiable VOCs made using just the GC-FID system.

It is shown that there is a gap between the measured and calculated OH reactivity typically of ~3 s^{-1} throughout the course of the average day when the limited set of VOC measurements are used. The discrepancy was ~44 % of the measurements on average and if the only VOC measurements made in York were done so using the GC-FID system, this would have been reported as 'missing' OH reactivity. Also, if the VOC measurement suite used in York was available during the TORCH-2 campaign, there would have likely been less missing OH reactivity.

During the York 2014 'missing' OH reactivity campaign additional VOCs were also measured using the GCxGC-FID technique where it was possible to measure *n*-alkanes longer than *n*-octane up to *n*-dodecane and also substituted aromatics and biogenic species such as α-pinene and limonene. These additional species which are less regularly measured in the field, were included in the calculations of OH reactivity that are plotted in the above figures. Figure 5.14 shows an average diurnal (for data from the comparison period) of measured and calculated OH reactivity where these additional species are considered in the calculation.

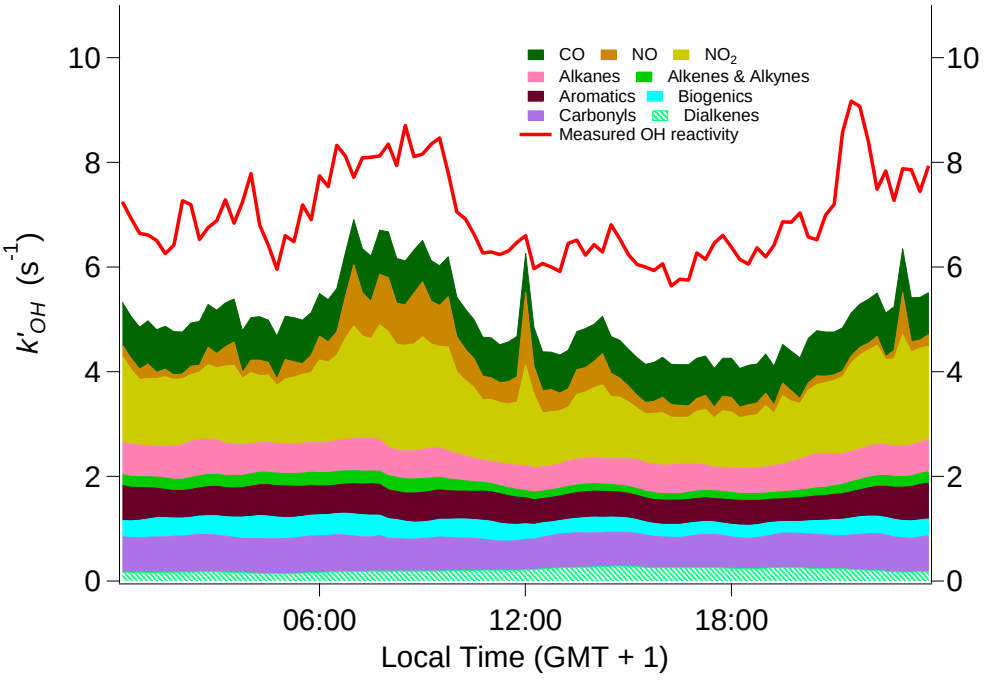

Figure 5.14: Diurnal profile of measured total OH reactivity (red line) with cumulative calculated OH reactivity (stacked coloured structures) for the comparison period (31/05/2014 00:00:00 to 15/06/2014 07:45:00) of the York 2014 'missing' OH reactivity campaign. Calculated contributions for each OH sink classification (not including CO, NO or NO_2) were determined using measurements of identifiable VOCs made using both the GC-FID and GCxGC-FID systems.

Not surprisingly, the difference between the measured and total calculated values is smaller here as concentrations of more sinks have been included in the calculation. The difference is typically ~2 s^{-1} and is ~27% of the measurements on average, meaning that the VOCs measured by the GCxGC-FID instrument accounted for ~17 % of the OH sink in York. Given the relatively conventional emission sources thought to have influenced the site such as traffic pollution and agricultural land, this observation is of wider importance.

Many studies in the literature conclude the presence of 'missing' OH reactivity from measurements made in a range of environments. Measurements in urban areas often show evidence for 'missing' OH reactivity, such as those reported from Nashville (~10 % missing) (Kovacs et al., 2003) and Paris (~54 % missing) (Dolgorouky et al., 2012). The additional VOCs that were measured by the GCxGC-FID instrument in York were not measured in these previous studies. Whalley et al. (2016) reported that when OH reactivity was modelled using measurements from central London, the predicted values rose from 67 % of the measurements, to within 15 % of the measurements with the inclusion of data for the same additional GCxGC-FID measured VOCs. Given this and the results presented here from the campaign in York, it is likely that if the additional species were measured in other studies in urban environments, such as those in Nashville and Paris, the 'missing' OH reactivity would have likely been significantly reduced. It should be noted that in the study reported by Whalley et al. (2016), predictions of OH reactivity were made using a computer model where contributions from oxidised intermediates were estimated, in addition to contributions from the measured OH sinks.

5.4.2.5 Accounting for 'missing' OH reactivity

In addition to the less commonly measured *n*-alkanes, substituted aromatics and biogenic species that were measured using the GCxGC-FID instrument, many unidentifiable VOCs were also detected. Peaks for these unidentified species were grouped according to their predicted functionality which is predicted by the space they occupy on the chromatograms. Grouped concentrations for each class of compound were then estimated. A detailed explanation of this process can be found in Dunmore et al. (2015) and the classes of unidentifiable VOCs were C9 aliphatics, C10 aliphatics, C11 aliphatics, C12 aliphatics, C13+ aliphatics, C4 substituted mono aromatics and monoterpenes. It is likely that the unidentified species contributed to

the ~27 % 'missing' OH reactivity that was observed in York. The estimated grouped concentrations were used in combination with estimated bimolecular rate coefficients for their reaction with OH, summarised in Table 5.2. Figure 5.15 shows a campaign average diurnal for measured and calculated OH reactivity where these are considered in the calculation of OH reactivity.

Sink	Class	$k_{sink + OH}$ (cm^3 $molecule^{-1}$ s^{-1})	Contribution to OH reactivity (s-1)	Instrument
C9 aliphatics	Alkanes	1.6×10^{-11}	0.53	GCxGC-FID
C10 aliphatics		1.3×10^{-11}		GCxGC-FID
C11 apliphatics		1.3×10^{-11}		GCxGC-FID
C12 aliphatics		1.4×10^{-11}		GCxGC-FID
C13+ aliphatics		1.6×10^{-11}		GCxGC-FID
C4 substituted monoaromatics	Aromatics	2.4×10^{-11}	0.09	GCxGC-FID
monoterpenes	Biogenics	5.3×10^{-11}	1.78	GCxGC-FID

Table 5.3: Unidentified groups of OH sinks measured in York. Grouped species were assigned classes according to their predicted functionality. With the exception of monoterpenes bimolecular rate coefficients shown are estimates at 300 K and 1 atmosphere taken from Carter (2010). No temperature or pressure dependencies were used for these grouped species when calculating their contribution to OH reactivity. The bimolecular rate coefficient shown for monoterpenes is assumed to be the same as that for α-Pinene as shown in Table 5.2. Campaign average contributions to OH reactivity are also shown for each sink classification in addition to details of the instrument used for the measurement of each species.

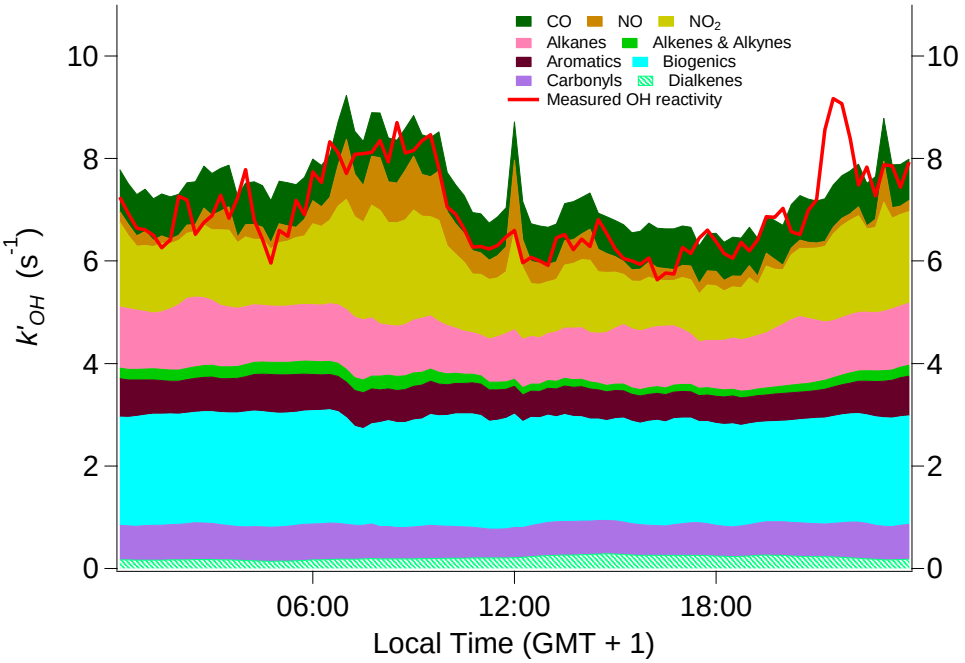

Figure 5.15: Diurnal profile of measured total OH reactivity (red line) with cumulative calculated OH reactivity (stacked coloured structures) for the comparison period (31/05/2014 00:00:00 to 15/06/2014 07:45:00) of the York 2014 'missing' OH reactivity campaign. Calculated contributions for each OH sink classification (not including CO, NO or NO_2) were determined using measurements of identifiable VOCs made using both the GC-FID and GCxGC-FID systems, and also grouped concentrations of unidentified VOCs detected by the GCxGC-FID system.

When grouped contributions for unidentified VOCs that were detected by the GCxGC-FID instrument are included in the calculation, the agreement between the measured and calculated profiles is much improved. There appears to be a slight over prediction of OH reactivity by the calculation, which is likely due to systematic uncertainty in the estimated concentrations of grouped VOCs, and that the bimolecular rate coefficients used to determine their contributions are estimates. The contribution from biogenics to calculated OH reactivity was shown to increase the most (by 1.78 s^{-1} on average), indicating that a large portion of the 'missing' OH reactivity in York was a result of unidentified primary biogenic emissions. It should be noted that the predictions of OH reactivity presented in this chapter are based on calculations that only take into account primary emissions. Products of VOC photo-oxidation are not considered. The enhanced agreement following inclusion of unidentifiable GCxGC-FID species in the calculation, as shown in Figure 5.14, is dissimilar to that reported for London by Whalley et al. (2016) where model generated intermediates were considered. Upon inclusion of unidentified GCxGC-FID species in this case the predictions were found to be within 6 % of the measurements. Considering the low wind speed in York (average of 0 m s^{-1} recorded by the meteorological station), and the relatively sheltered nature of the measurement site (next to the WACL building in a carpark), it is likely that primary emissions were more dominant in York than they were in London.

Figure 5.16 summarises the relationship between the measured diurnal profile and the three calculated diurnal profiles discussed above. In three scenarios the shape of the measured diurnal is reproduced well by the calculated diurnals. It is shown that for the two cases where OH reactivity is calculated using only concentrations of identifiable sinks, that the values typically do not agree with those measured, within the uncertainty determined as the 1σ daily variation. When the estimated contribution from the unidentifiable species is included, the values are increased to within the uncertainty of the measurements. However, it is not possible to know precisely the contribution from the unidentified species, as to do this would require knowledge of every species' individual concentration and bimolecular rate coefficient for its reaction with OH. It can only be concluded here that the unidentified species accounted for a portion of the 'missing' OH reactivity. It should be noted that the diurnal calculated OH reactivity including the unidentified species is subject to significant uncertainty. It was unexpected that inclusion of these species

would increase the calculated reactivity so that it matched the measurements considering that no unmeasured VOC products from the reactions of the measured sinks have yet been considered.

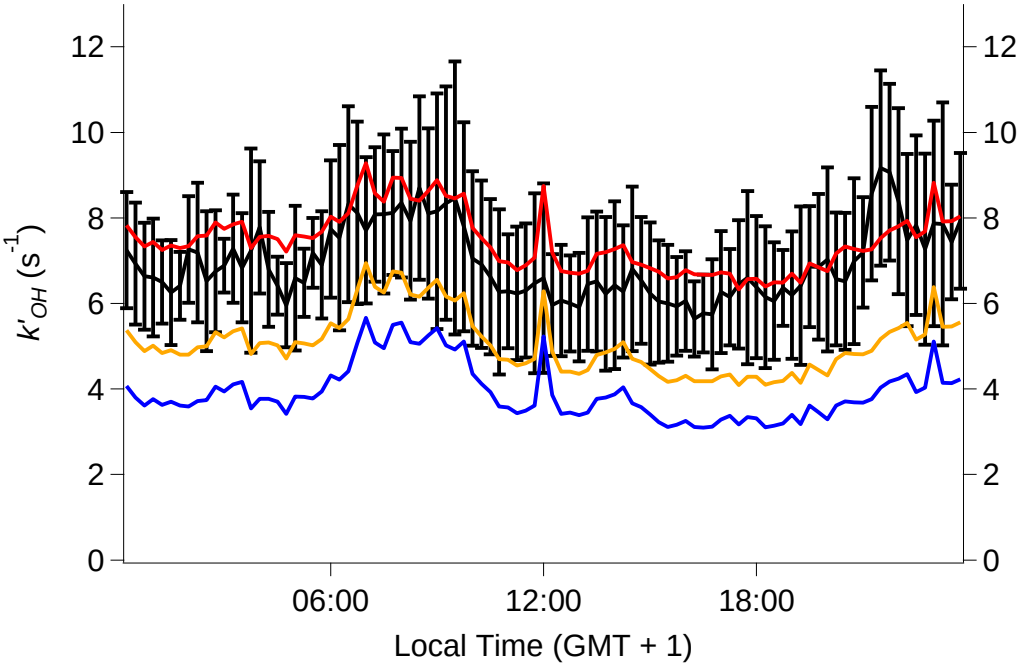

Figure 5.16: Diurnal profile of measured OH reactivity (black line), error bars represent the 1 σ variability of the measurements) and three scenarios for calculated OH reactivity. Blue line: calculated using VOC concentrations from GC-FID; orange line: same as for blue line with contribution from identifiable VOCs measured by GCxGC-FID; red line: same as for orange line with estimated contribution from unidentifiable species detected by the GCxGC-FID.

Many studies of OH reactivity reported in the literature use computer models where unmeasured products of the reactions between measured species and OH are considered as contributors to OH reactivity. To further investigate the OH reactivity observed during the York 2014 'missing' OH reactivity campaign, a zero dimensional chemical box modelling study was conducted by Dr. Jenny Young using the Master Chemical Mechanism (MCM). Figure 5.17 shows some model simulated diurnal profiles of OH reactivity alongside the measurements. For each of the three simulated diurnal profiles the model was run using standard MCM chemistry and unconstrained to HCHO, only measurements of OH sinks that could be identified were included. The three simulations differed in the deposition rate that was used for the intermediates generated. The results show that the model was

sensitive to deposition rate, as this was increased the agreement between the measured and predicted diurnals improved.

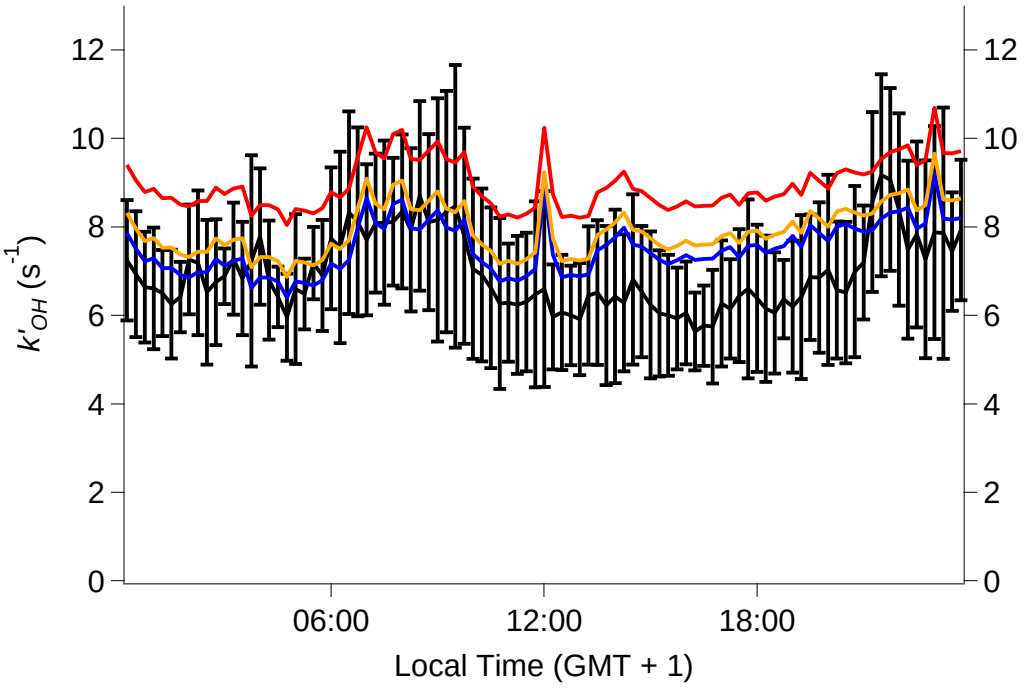

Figure 5.17: Diurnal profile of measured OH reactivity (black line), error bars represent the 1 σ variability of the measurements) and three predictions from three models (all unconstrained to HCHO with standard MCM chemistry). Red line: Deposition rate extended by 0.5 cm s^{-1}, Yellow line: Deposition rate extended by 0.8 cm s-1, Blue line: Deposition rate extended by 1.0 cm s^{-1}.

The shape of the model simulated diurnal profiles is similar to that of the measurements. However there is one key difference in the relationship between the calculation predictions and the model predictions. Figure 5.16 shows that the difference between the measurements and the predictions is roughly constant throughout the average day. However, Figure 5.17 shows more variation in the discrepancy which is shown to increase following the morning rush hour peak before decreasing again at nightfall. This may reflect uncertainties in the model treatment of boundary layer depth which influences the lifetime of model generated intermediates with respect to deposition.

The results presented in this section show that the missing OH reactivity observed in York can be accounted for when unidentified VOCs are included in the calculation of OH reactivity, and when a computer model is used to simulate OH reactivity by taking into account products of oxidation chemistry. However, both methods are

subject to significant uncertainty and may over predict the extra contributions. The grouped concentrations of unidentifiable VOCs are estimated as are the bimolecular rate coefficients for reaction with OH; predicted contributions from these species could potentially be subject to a systematic positive bias. The deposition rates for model generated intermediates, and the boundary layer depth, may not be representative of the real conditions at the time of the measurements. Intermediate species may be removed from the simulation too slowly resulting in their accumulation and subsequently over predicted contribution to OH reactivity. If both model generated intermediates and the unidentified grouped species were considered in the simulation of OH reactivity, this would over predict the measurements by a greater extent than is shown in Figure 5.16 and Figure 5.17.

5.5 Formaldehyde

5.5.1 Formaldehyde observations

Formaldehyde was measured during the York 2014 'missing' OH reactivity campaign using the new laser induced fluorescence instrument described in Section 2.3.6. The instrument was operated in configuration 2 and was housed inside a ground floor laboratory of the WACL building for the duration of the measurement period; ambient air was sampled from the roof manifold and passed through ~20 m of half inch OD Teflon tubing before reaching the instrument. The residence time of the gas in this tuning was ~2 s. Tests conducted by Dr. Trevor Ingham prior to deployment of the instrument, with tubing of dimensions, showed no evidence for loss of HCHO. Figure 5.18 shows the instrument during its deployment in York.

The York 2014 'missing' OH reactivity campaign was the first deployment of the HCHO instrument and as a safety precaution it was only operated during the daytime so that it could be closely monitored. The instrument operated successfully the majority of the time and near-continuous daytime measurements were recorded on twelve days. Measurements were made with 1 s time resolution and the instrument calibration factor, $(1.46 \pm 0.034) \times 10^{-9}$ count s^{-1} mW^{-1} $molecule^{-1}$ cm^3, determined using calibration method 1 as described in Section 2.3.7, was applied to the 1 s LIF signal differentials which were normalised for laser power. Figure 5.19 shows all of the 1 s HCHO data that were recorded in York.

Figure 5.18: Photograph of the HCHO instrument set up inside the WACL building during the York 2014 'missing' OH reactivity campaign.

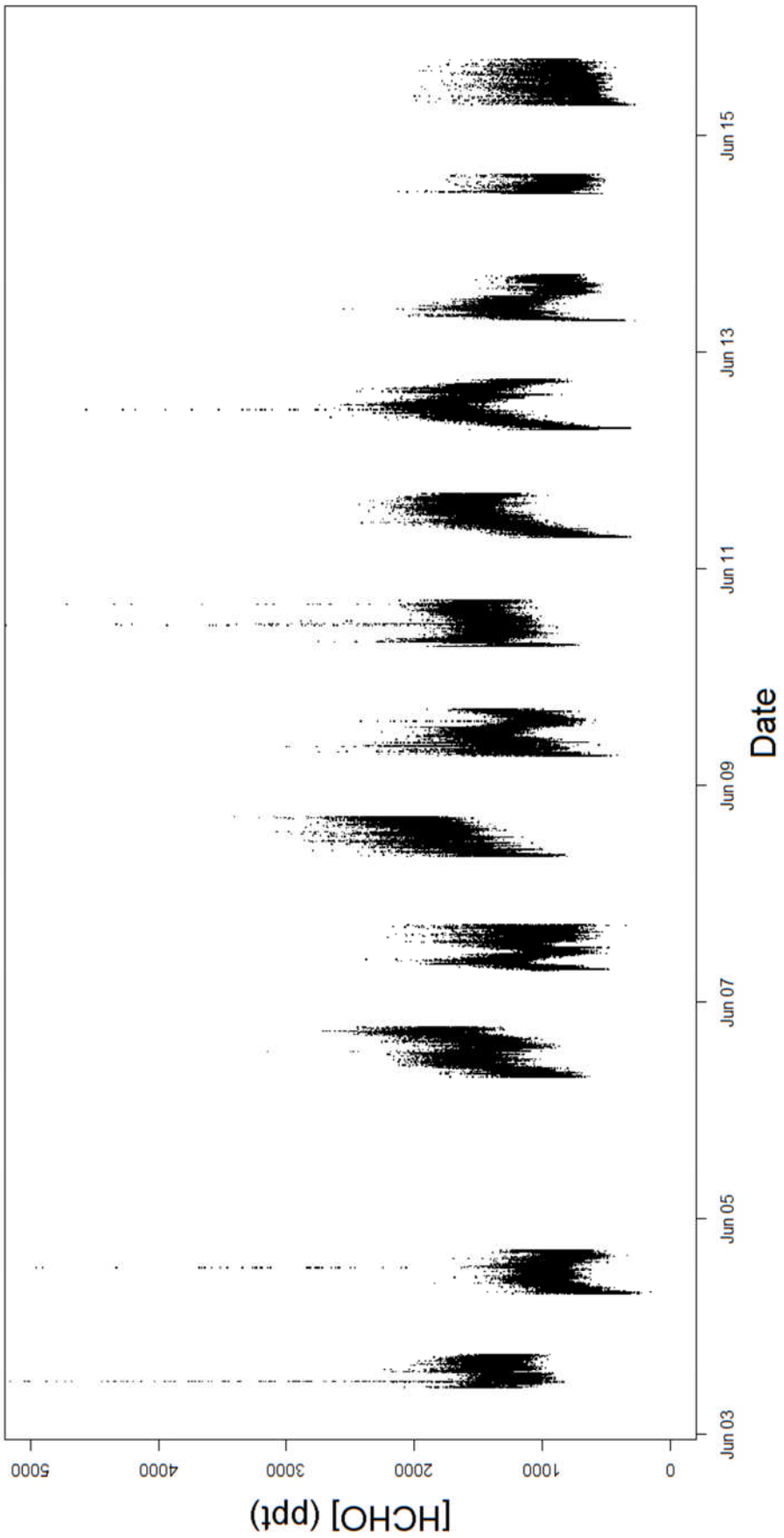

Figure 5.19: Time series of 1 second measurements of HCHO from the York 2014 'missing' OH reactivity campaign for days.

The results show that the level of daytime HCHO observed did not vary significantly from day to day, and the levels observed were typically between 0.5 and 2 ppb. The mean average level was ~1.3 ppb which is lower than other typical levels reported for urban areas in the literature. Dasgupta et al. (2005) reported average levels of 3.3, 7.9 and 2.3 ppb in Houston, Atlanta and Tampa, respectively. It is not surprising that the measurements made in York were lower than these as the measurements were not made in the city centre; the site was several miles away. The measurements made in Houston, Atlanta and Tampa were either taken in central, or heavily industrialised areas. High levels of HCHO are known to be emitted from vehicles as a result of incomplete fossil fuel combustion meaning that higher levels are to be expected in central urban and industrialised areas than in non-central urban background areas such as the measurement site in York (Anderson et al., 1996). Measurements reported from the Mexico City Metropolitan Area campaign (MCMA) were also unsurprisingly higher than the measurements in from York. Mean concentrations of ~8.2 and ~6.0 ppb were reported from two separate locations (Volkamer et al., 2005, Garcia et al., 2006, Grutter et al., 2005). Lee et al. (1998) also reported mean HCHO levels from 1995 measurements in Nashville to be ~4.2 ppb. Again it is not surprising that these measurements are significantly higher than recorded in York, considering the relative sizes of the cities. Considering that the OH reactivity reported from the MCMA campaign (~25 s^{-1} daytime) was also much higher than it was in York, the presence of more HCHO is to be expected as it is an end product of the photo-oxidative processing of VOCs (Shirley et al., 2006). It should be noted that here that the composition of the air mass in York is expected to be considerably different to the other locations mentioned above. All are much closer to the equator than York and are therefore typically subject to more regular and intense sunlight, meaning more rapid photo-chemical processing of VOCs leading to the production of HCHO is expected.

It can be seen in the complete 1 s time series shown in Figure 5.19 that there were sharp excursions in HCHO concentration on a number of days; the level of HCHO reaches as high as ~5 ppb before falling again in a matter of seconds. These events coincided with the arrival of vehicles (in most cases large trucks) to the car park at the measurement site (for example delivery of liquid N_2). Figure 5.20(a) shows all of the 1 s HCHO measurements from 04/06/2014 and an example of this behaviour is circled in red.

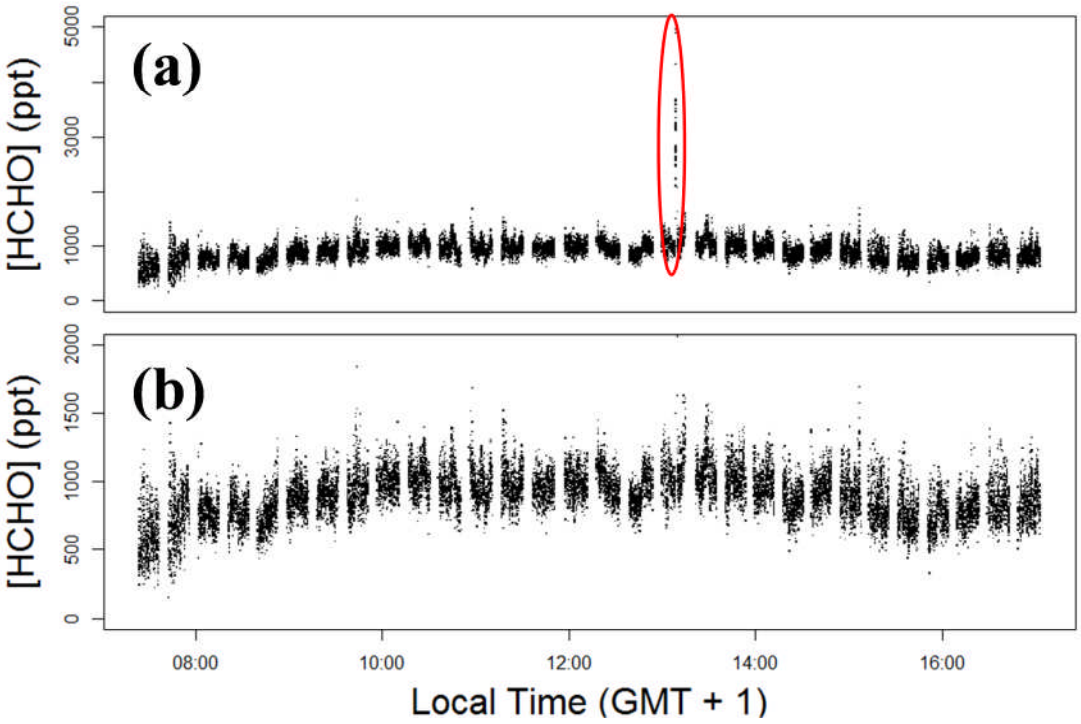

Figure 5.20: Observations of HCHO from 04/06/14 during the York 2014 'missing' OH reactivity campaign. (a) Data plotted with y-axis maximum of 5000 ppt to show example of a rapid excursion to high HCHO (circled in red). (b) Data plotted with y-axis maximum of 2000 ppt to show slower variation in HCHO.

The presence of these excursions in the 1 s data demonstrates an advantage of measuring atmospheric HCHO using a fast response LIF detector over other types of instruments with a slower response time. For example, if the measurements made during the campaign in York were made using the Hanzch Fluorimetry methodology, where measurements are typically made every minute, this behaviour would have not likely been observed. Figure 5.20(b) shows the same 1 s data set for 04/06/2014 as Figure 5.20(a) on a smaller scale so that more gradual changes in [HCHO] can be observed through the course of the day.

5.5.2 Interpretation of formaldehyde observations

5.5.2.1 Diurnal behaviour

It can be seen from Figure 5.19 that on the majority of days where formaldehyde was measured an increase was typically observed through the morning hours. An example of this is also clearly shown in Figure 5.20(b) where levels increased by ~500 ppt between 0800 and 1200. In order to broadly examine the variations in formaldehyde levels with respect to its chemistry, the data were processed in the same way as the OH reactivity data in order to produce a diurnal profile for the

'average day'. Measurements were averaged into 96 time bins with a mean value every 15 minutes; Figure 5.21 shows the diurnal profile obtained from all of the 1s data shown in Figure 5.19.

The diurnal profile shows an increase in HCHO through the morning hours which plateaus at ~1200. This behaviour is not surprising considering that HCHO is a major by-product of the photo oxidative processing of VOCs and can act as an overall tracer for VOC oxidation (DiGangi et al., 2011). It is likely that this rise is a result of an increased rate of production of OH as the sun rose leading to more rapid processing of VOCs to form HCHO. This is a common feature of HCHO measurements in environments with air masses characterised by a strong influence from anthropogenic emissions. Dasgupta et al. (2005) reported this feature in diurnal profiles resulting from measurements from Nashville, Atlanta, Philadelphia and Tampa.

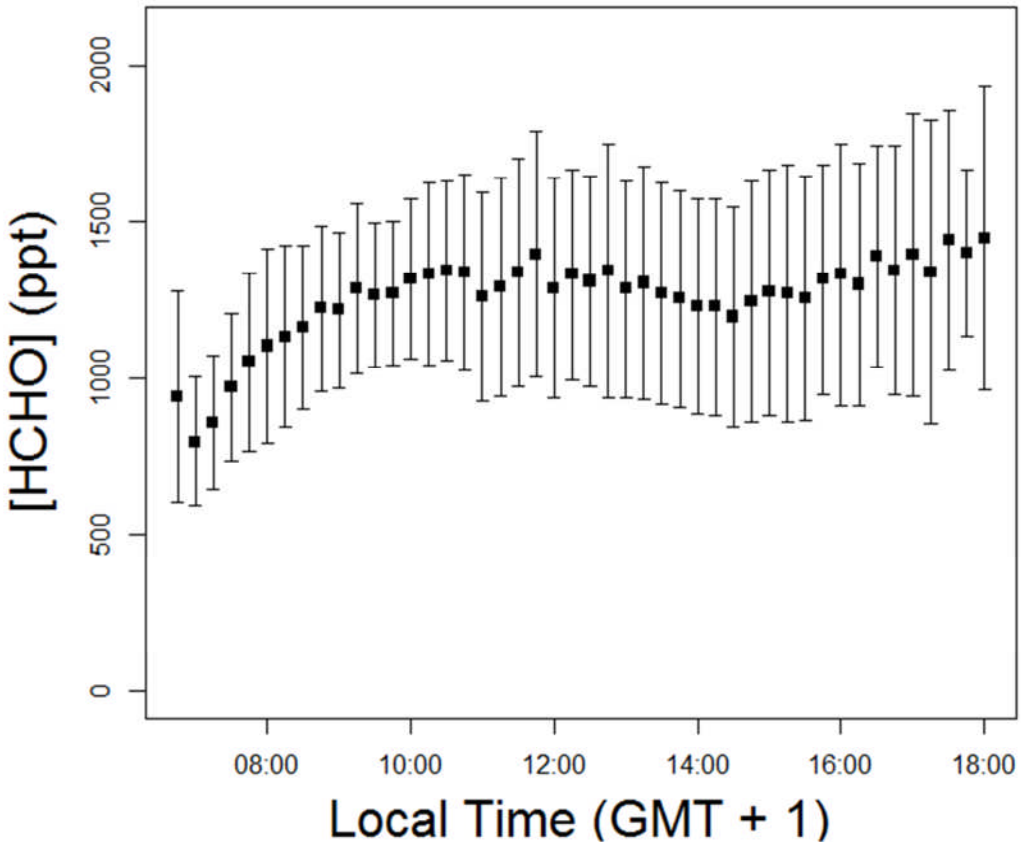

Figure 5.21: Diurnal profile of [HCHO] observed during the York 2014 'missing' OH reactivity campaign in 15 minute time bins. Error bars ± 1 σ standard deviation from the mean observation, and are a measure of the variability during a 15 minute time bin.

The behaviour exhibited by the diurnal profile is likely to have been driven by the photochemical processing of VOCs to produce HCHO. The change in the level of HCHO through the course of the average day is unlikely to have been driven by direct emissions as it does not vary in the same way as the contribution from NO_x to calculated OH reactivity. If the change was a result of direct emissions, a morning rush hour peak similar to the NO_x driven morning rush hour peak in OH reactivity would have likely been observed. To further investigate what contributed to the changes seen in HCHO, correlations with other species and parameters measured were examined.

5.5.2.2 Correlations with other measurements

The relationship between the level of HCHO and other species and parameters measured was examined to investigate any potential sources. Correlation plots to show the relationship between HCHO and NO_x are shown in Figure 5.22.

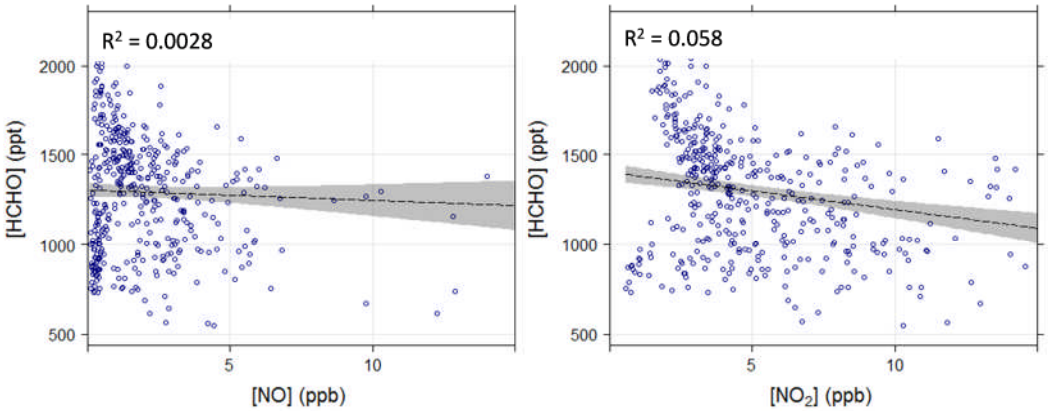

Figure 5.22: Plots of [HCHO] against both [NO] and [NO_2]. Data shown are 15 minute binned mean averages from measurements taken between 31/05/2014 00:00:00 – 15/06/2014 07:45:00 of the York 2014 'missing' OH reactivity campaign. The shaded areas represent the 95% confidence intervals from the linear fits (least squares).

It is shown that there are no correlations between HCHO and NO or NO_2. This is not surprising considering the shape of the diurnal profile which is characteristic of secondarily sourced HCHO. If direct HCHO sources were dominant in York some level of correlation would be expected here. The relationship between measured HCHO and all other measured species and parameters was examined, it was only possible to identify two weak correlations. These were with ambient air temperature, and the photolytic O^1D production rate ($J(O^1D)$), plots are shown in Figure 5.23.

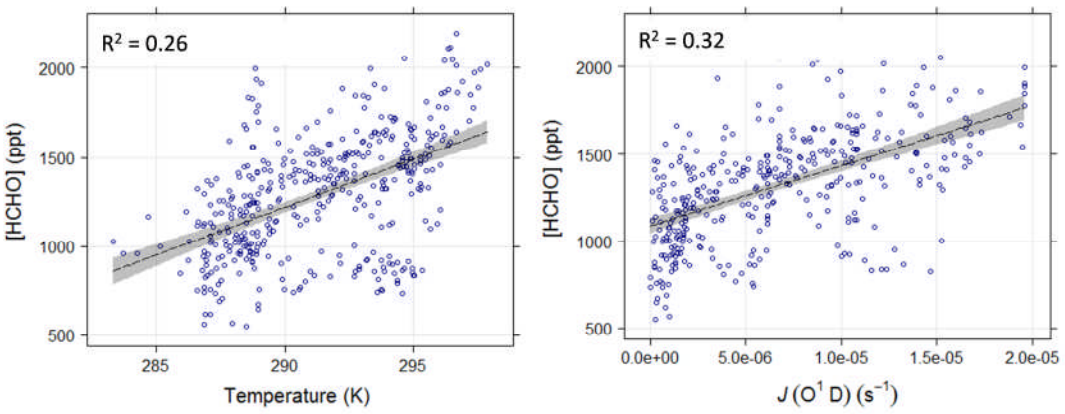

Figure 5.23: Plots of measured [HCHO] against both temperature and J(O1D). Data shown are 15 minute binned mean averages from measurements taken between 31/05/2014 00:00:00 – 15/06/2014 07:45:00 of the York 2014 'missing' OH reactivity campaign. The shaded areas represent the 95% confidence intervals from the linear fits (least squares).

It is to be expected that HCHO would correlate with both temperature and $J(O^1D)$, if its major source was secondary production. Higher $J(O^1D)$ is typically associated with elevated temperatures owing to there being more solar radiation available for photolysis and to heat the air mass. When there is a higher rate of O^1D production there is more rapid production of OH which ultimately leads to more rapid photo-oxidative processing of VOCs and subsequently more HCHO. Whilst these correlations are present, they are by no means strong and this is likely due to there being a contribution from locally produced HCHO and HCHO produced further afield which was transported to the site.

Given that the only measurements which showed correlation with the HCHO measurements were ambient air temperature and $J(O^1D)$, it can be concluded that that the dominant source of HCHO in York was secondary production from photo-oxidation. However, local sources of HCHO such as that from combustion engines, did contribute to the measurement for short periods of time.

5.6 Summary and conclusions

OH reactivity and formaldehyde observations from a site subject to significant influence from anthropogenic and biogenic emissions are presented. Measurements were made during the York 2014 'missing' OH reactivity campaign which took place in May / June 2014 at the University of York campus. The main objective for campaign was to test the operation of a new instrument for the identification of

species that contribute to 'missing' OH reactivity, alongside the laser flash photolysis instrument for the measurement of OH reactivity. Details of the new instrument are presented in Chapter 4. An additional aim was to field-test the Leeds LIF instrument for the measurement of formaldehyde; the ambient measurements presented here were the first to be made by it. Both instruments for the measurement of OH reactivity, and for the measurement of formaldehyde performed well for the majority of the campaign and there are few unplanned gaps in either set of data.

The mean average OH reactivity recorded was 6.3 s^{-1} which is lower than what has been reported in the literature for other studies where the air mass is largely characterised by anthropogenic emissions. It is concluded that the reason for the lower OH reactivity measurements presented here is that the site in York is roughly in as close proximity to agricultural land as it was to York city centre, meaning that less polluted air would have had a stronger influence, compared to studies where measurement sites were completely surrounded by urban development. OH reactivity was found to correlate well with NO_x and other anthropogenic emissions typical of vehicular exhaust.

OH reactivity was calculated using concentrations of known OH sinks that were measured at the same time. When concentrations for all of the identifiable sinks were included in the calculation, it was found that the values were typically lower than those measured by ~1 - 3 s^{-1}. On average for the comparison period of the campaign there was ~27 % 'missing' OH reactivity, with all measured identifiable OH sinks considered. A very detailed suite of VOCs were measured in York. When OH reactivity was calculated using only measured concentrations of VOCs which are routinely measured in the field (using GC-FID), the gap between the measured and calculated OH reactivity was significantly greater. If a typical set of VOC measurements were made in York it would have been concluded that on average there was 44 % 'missing' OH reactivity. The results from this study demonstrate the importance of measuring longer *n*-alkanes, substituted aromatics and biogenic species in this environment.

Discussion is given on the potential cause of the 'missing' OH reactivity. It was found that when a contribution to the calculated OH reactivity is estimated for grouped concentrations of unidentifiable species detected by the GCxGC-FID instrument, the two data sets are in close agreement. A zero-dimensional chemical

box modelling study also showed that the 'missing' OH reactivity could be accounted for by model-generated intermediates when the deposition rate is sufficient. However there is great uncertainty associated with both of these approaches. For the unidentified species both the concentrations and the rate coefficients are estimated and the model was shown to be sensitive to deposition rate. A portion of the 'missing' OH reactivity can likely be attributed to a combination of both the unidentified species, and products of photo-oxidation that were considered in the model. In addition to this it is possible that some currently unidentified species that were detected by the GC-TOF-MS system of the new instrument described in Chapter 4 could have also contributed. However, data from this instrument has not yet been analysed to quantify and identify any of these species.

The mean average level of formaldehyde observed was ~1.3 ppb which is lower than much of the literature based on studies in environments characterised by significant anthropogenic influence. Measurements were made only during the daytime owing to the need to closely monitor the instrument on its first deployment. The day time diurnal profile follows that typical of an environment where the dominant source is secondary formation from photo-oxidation of VOCs with a rise through the morning hours as the sun rises. Correlations of HCHO with temperature and $J(O^1D)$ support this and HCHO was not found to correlate with any other species or parameter measured. The advantage of the LIF technique for HCHO measurement is demonstrated by the presence of rapid excursions in the measurements that were synchronous with large vehicles entering the car park at the measurement site.

5.7 References

ANDERSON, L. G., LANNING, J. A., BARRELL, R., MIYAGISHIMA, J., JONES, R. H. & WOLFE, P. 1996. Sources and sinks of formaldehyde and acetaldehyde: An analysis of Denver's ambient concentration data. *Atmospheric Environment,* 30**,** 2113-2123.

ATKINSON, R. 2003. Kinetics of the gas-phase reactions of OH radicals with alkanes and cycloalkanes. *Atmos. Chem. Phys.*, 3**,** 2233-2307.

BAN-WEISS, G. A., MCLAUGHLIN, J. P., HARLEY, R. A., KEAN, A. J., GROSJEAN, E. & GROSJEAN, D. 2008. Carbonyl and Nitrogen Dioxide Emissions From Gasoline- and Diesel-Powered Motor Vehicles. *Environmental Science & Technology,* 42**,** 3944-3950.

BOHN, B., KRAUS, A., MÜLLER, M. & HOFZUMAHAUS, A. 2004. Measurement of atmospheric O3 → O(1D) photolysis frequencies using

filterradiometry. *Journal of Geophysical Research: Atmospheres,* 109**,** D10S90.

BRUNE, W. H., BAIER, B. C., THOMAS, J., REN, X., COHEN, R. C., PUSEDE, S. E., BROWNE, E. C., GOLDSTEIN, A. H., GENTNER, D. R., KEUTSCH, F. N., THORNTON, J. A., HARROLD, S., LOPEZ-HILFIKER, F. D. & WENNBERG, P. O. 2016. Ozone production chemistry in the presence of urban plumes. *Faraday Discussions,* 189**,** 169-189.

CARSLAW, D. C. 2015. *The openair manual - open-source tools for analysing air pollution data. Manual for version 1.1-4,* King's College London.

CARSLAW, D. C. & ROPKINS, K. 2012. openair - an R package for air quality data analysis. *Environmental Modelling and Software,* 27-28**,** 52-61.

CARTER, W. P. L. 2010. Development of the SAPRC-07 chemical mechanism. *Atmospheric Environment,* 44**,** 5324-5335.

CHATANI, S., SHIMO, N., MATSUNAGA, S., KAJII, Y., KATO, S., NAKASHIMA, Y., MIYAZAKI, K., ISHII, K. & UENO, H. 2009. Sensitivity analyses of OH missing sinks over Tokyo metropolitan area in the summer of 2007. *Atmos. Chem. Phys.,* 9**,** 8975-8986.

CORCHNOY, S. B. & ATKINSON, R. 1990. Kinetics of the gas-phase reactions of hydroxyl and nitrogen oxide (NO3) radicals with 2-carene, 1,8-cineole, p-cymene, and terpinolene. *Environmental Science & Technology,* 24**,** 1497-1502.

DASGUPTA, P. K., LI, J., ZHANG, G., LUKE, W. T., MCCLENNY, W. A., STUTZ, J. & FRIED, A. 2005. Summertime Ambient Formaldehyde in Five U.S. Metropolitan Areas: Nashville, Atlanta, Houston, Philadelphia, and Tampa. *Environmental Science & Technology,* 39**,** 4767-4783.

DIGANGI, J. P., BOYLE, E. S., KARL, T., HARLEY, P., TURNIPSEED, A., KIM, S., CANTRELL, C., MAUDLIN III, R. L., ZHENG, W., FLOCKE, F., HALL, S. R., ULLMANN, K., NAKASHIMA, Y., PAUL, J. B., WOLFE, G. M., DESAI, A. R., KAJII, Y., GUENTHER, A. & KEUTSCH, F. N. 2011. First direct measurements of formaldehyde flux via eddy covariance: implications for missing in-canopy formaldehyde sources. *Atmos. Chem. Phys.,* 11**,** 10565-10578.

DOLGOROUKY, C., GROS, V., SARDA-ESTEVE, R., SINHA, V., WILLIAMS, J., MARCHAND, N., SAUVAGE, S., POULAIN, L., SCIARE, J. & BONSANG, B. 2012. Total OH reactivity measurements in Paris during the 2010 MEGAPOLI winter campaign. *Atmos. Chem. Phys.,* 12**,** 9593-9612.

DUNMORE, R. E., HOPKINS, J. R., LIDSTER, R. T., LEE, J. D., EVANS, M. J., RICKARD, A. R., LEWIS, A. C. & HAMILTON, J. F. 2015. Diesel-related hydrocarbons can dominate gas phase reactive carbon in megacities. *Atmos. Chem. Phys.,* 15**,** 9983-9996.

EDWARDS, P. M., EVANS, M. J., FURNEAUX, K. L., HOPKINS, J., INGHAM, T., JONES, C., LEE, J. D., LEWIS, A. C., MOLLER, S. J., STONE, D., WHALLEY, L. K. & HEARD, D. E. 2013. OH reactivity in a South East Asian tropical rainforest during the Oxidant and Particle Photochemical Processes (OP3) project. *Atmos. Chem. Phys.,* 13**,** 9497-9514.

FALL, R. 2003. Abundant Oxygenates in the Atmosphere: A Biochemical Perspective. *Chemical Reviews,* 103**,** 4941-4952.

GARCIA, A. R., VOLKAMER, R., MOLINA, L. T., MOLINA, M. J., SAMUELSON, J., MELLQVIST, J., GALLE, B., HERNDON, S. C. & KOLB, C. E. 2006. Separation of emitted and photochemical formaldehyde

in Mexico City using a statistical analysis and a new pair of gas-phase tracers. *Atmos. Chem. Phys.,* 6**,** 4545-4557.

GRUTTER, M., FLORES, E., ANDRACA-AYALA, G. & BÁEZ, A. 2005. Formaldehyde levels in downtown Mexico City during 2003. *Atmospheric Environment,* 39**,** 1027-1034.

HEARD, D. E., READ, K. A., METHVEN, J., AL-HAIDER, S., BLOSS, W. J., JOHNSON, G. P., PILLING, M. J., SEAKINS, P. W., SMITH, S. C., SOMMARIVA, R., STANTON, J. C., STILL, T. J., INGHAM, T., BROOKS, B., DE LEEUW, G., JACKSON, A. V., MCQUAID, J. B., MORGAN, R., SMITH, M. H., CARPENTER, L. J., CARSLAW, N., HAMILTON, J., HOPKINS, J. R., LEE, J. D., LEWIS, A. C., PURVIS, R. M., WEVILL, D. J., BROUGH, N., GREEN, T., MILLS, G., PENKETT, S. A., PLANE, J. M. C., SAIZ-LOPEZ, A., WORTON, D., MONKS, P. S., FLEMING, Z., RICKARD, A. R., ALFARRA, M. R., ALLAN, J. D., BOWER, K., COE, H., CUBISON, M., FLYNN, M., MCFIGGANS, G., GALLAGHER, M., NORTON, E. G., O'DOWD, C. D., SHILLITO, J., TOPPING, D., VAUGHAN, G., WILLIAMS, P., BITTER, M., BALL, S. M., JONES, R. L., POVEY, I. M., O'DOHERTY, S., SIMMONDS, P. G., ALLEN, A., KINNERSLEY, R. P., BEDDOWS, D. C. S., DALL'OSTO, M., HARRISON, R. M., DONOVAN, R. J., HEAL, M. R., JENNINGS, S. G., NOONE, C. & SPAIN, G. 2006. The North Atlantic Marine Boundary Layer Experiment(NAMBLEX). Overview of the campaign held at Mace Head, Ireland, in summer 2002. *Atmos. Chem. Phys.,* 6**,** 2241-2272.

HELAND, J., KLEFFMANN, J., KURTENBACH, R. & WIESEN, P. 2001. A New Instrument To Measure Gaseous Nitrous Acid (HONO) in the Atmosphere. *Environmental Science & Technology,* 35**,** 3207-3212.

HOFZUMAHAUS, A. 2006. Measurement of Photolysis Frequencies in the Atmosphere. *In:* HEARD, D. (ed.) *Analytical Techniques for Atmospheric Measurement.* Blackwell Publishing Ltd.

JENKIN, M. E., SAUNDERS, S. M. & PILLING, M. J. 1997. The tropospheric degradation of volatile organic compounds: a protocol for mechanism development. *Atmospheric Environment,* 31**,** 81-104.

KAISER, J., WOLFE, G. M., BOHN, B., BROCH, S., FUCHS, H., GANZEVELD, L. N., GOMM, S., HÄSELER, R., HOFZUMAHAUS, A., HOLLAND, F., JÄGER, J., LI, X., LOHSE, I., LU, K., PRÉVÔT, A. S. H., ROHRER, F., WEGENER, R., WOLF, R., MENTEL, T. F., KIENDLER-SCHARR, A., WAHNER, A. & KEUTSCH, F. N. 2015. Evidence for an unidentified non-photochemical ground-level source of formaldehyde in the Po Valley with potential implications for ozone production. *Atmos. Chem. Phys.,* 15**,** 1289-1298.

KATO, S., SATO, T. & KAJII, Y. 2011. A method to estimate the contribution of unidentified VOCs to OH reactivity. *Atmospheric Environment,* 45**,** 5531-5539.

KOVACS, T. A., BRUNE, W. H., HARDER, H., MARTINEZ, M., SIMPAS, J. B., FROST, G. J., WILLIAMS, E., JOBSON, T., STROUD, C., YOUNG, V., FRIED, A. & WERT, B. 2003. Direct measurements of urban OH reactivity during Nashville SOS in summer 1999. *J. Environ. Monit.,* 5**,** 68-74.

KREUZWIESER, J., SCHNITZLER, J. P. & STEINBRECHER, R. 1999. Biosynthesis of Organic Compounds Emitted by Plants. *Plant Biology,* 1**,** 149-159.

KWOK, E. S. C., ATKINSON, R. & AREY, J. 1997. Kinetics of the gas-phase reactions of indan, indene, fluorene, and 9,10-dihydroanthracene with OH radicals, NO3 radicals, and O3. *International Journal of Chemical Kinetics,* 29**,** 299-309.

LEE, J. D., YOUNG, J. C., READ, K. A., HAMILTON, J. F., HOPKINS, J. R., LEWIS, A. C., BANDY, B. J., DAVEY, J., EDWARDS, P., INGHAM, T., SELF, D. E., SMITH, S. C., PILLING, M. J. & HEARD, D. E. 2009. Measurement and calculation of OH reactivity at a United Kingdom coastal site. *Journal of atmospheric chemistry,* 64**,** 53-76.

LEE, Y. N., ZHOU, X., KLEINMAN, L. I., NUNNERMACKER, L. J., SPRINGSTON, S. R., DAUM, P. H., NEWMAN, L., KEIGLEY, W. G., HOLDREN, M. W., SPICER, C. W., YOUNG, V., FU, B., PARRISH, D. D., HOLLOWAY, J., WILLIAMS, J., ROBERTS, J. M., RYERSON, T. B. & FEHSENFELD, F. C. 1998. Atmospheric chemistry and distribution of formaldehyde and several multioxygenated carbonyl compounds during the 1995 Nashville/Middle Tennessee Ozone Study. *Journal of Geophysical Research: Atmospheres,* 103**,** 22449-22462.

LIDSTER, R. T., HAMILTON, J. F., LEE, J. D., LEWIS, A. C., HOPKINS, J. R., PUNJABI, S., RICKARD, A. R. & YOUNG, J. C. 2014. The impact of monoaromatic hydrocarbons on OH reactivity in the coastal UK boundary layer and free troposphere. *Atmos. Chem. Phys.,* 14**,** 6677-6693.

NAKASHIMA, Y., TSURUMARU, H., IMAMURA, T., BEJAN, I., WENGER, J. C. & KAJII, Y. 2012. Total OH reactivity measurements in laboratory studies of the photooxidation of isoprene. *Atmospheric Environment,* 62**,** 243-247.

REN, X., BRUNE, W. H., MAO, J., MITCHELL, M. J., LESHER, R. L., SIMPAS, J. B., METCALF, A. R., SCHWAB, J. J., CAI, C., LI, Y., DEMERJIAN, K. L., FELTON, H. D., BOYNTON, G., ADAMS, A., PERRY, J., HE, Y., ZHOU, X. & HOU, J. 2006a. Behavior of OH and HO2 in the winter atmosphere in New York City. *Atmospheric Environment,* 40, Supplement 2**,** 252-263.

REN, X., BRUNE, W. H., OLIGER, A., METCALF, A. R., SIMPAS, J. B., SHIRLEY, T., SCHWAB, J. J., BAI, C., ROYCHOWDHURY, U., LI, Y., CAI, C., DEMERJIAN, K. L., HE, Y., ZHOU, X., GAO, H. & HOU, J. 2006b. OH, HO2, and OH reactivity during the PMTACS-NY Whiteface Mountain 2002 campaign: Observations and model comparison. *J. Geophys. Res,* 111**,** D10S03.

ROBBINS, R. C., BORG, K. M. & ROBINSON, E. 1968. Carbon Monoxide in the Atmosphere. *Journal of the Air Pollution Control Association,* 18**,** 106-110.

SAUNDERS, S. M., JENKIN, M. E., DERWENT, R. G. & PILLING, M. J. 2003. Protocol for the development of the Master Chemical Mechanism, MCM v3 (Part A): tropospheric degradation of non-aromatic volatile organic compounds. *Atmospheric Chemistry and Physics,* 3**,** 161-180.

SHIRLEY, T. R., BRUNE, W. H., REN, X., MAO, J., LESHER, R., CARDENAS, B., VOLKAMER, R., MOLINA, L. T., MOLINA, M. J., LAMB, B., VELASCO, E., JOBSON, T. & ALEXANDER, M. 2006. Atmospheric oxidation in the Mexico City metropolitan area (MCMA) during April 2003. *Atmospheric Chemistry and Physics,* 6**,** 2753-2765.

STONE, D., WHALLEY, L. K., INGHAM, T., EDWARDS, P. M., CRYER, D. R., BRUMBY, C. A., SEAKINS, P. W. & HEARD, D. E. 2016. Measurement

of OH reactivity by laser flash photolysis coupled with laser-induced fluorescence spectroscopy. *Atmos. Meas. Tech.,* 9**,** 2827-2844.

VOLKAMER, R., MOLINA, L. T., MOLINA, M. J., SHIRLEY, T. & BRUNE, W. H. 2005. DOAS measurement of glyoxal as an indicator for fast VOC chemistry in urban air. *Geophysical Research Letters,* 32**,** L08806.

WEINHEIMER, A. J. 2006. Chemical Methods: Chemiluminescence, Chemical Amplification, Electrochemistry, and Derivitization. *In:* HEARD, D. (ed.) *Analytical Techniques for Atmospheric Measurement.* Blackwell Publishing Ltd.

WHALLEY, L. K., BLITZ, M. A., DESSERVETTAZ, M., SEAKINS, P. W. & HEARD, D. E. 2013. Reporting the sensitivity of laser-induced fluorescence instruments used for HO2 detection to an interference from RO2 radicals and introducing a novel approach that enables HO2 and certain RO2 types to be selectively measured. *Atmos. Meas. Tech.,* 6**,** 3425-3440.

WHALLEY, L. K., STONE, D., BANDY, B., DUNMORE, R., HAMILTON, J. F., HOPKINS, J., LEE, J. D., LEWIS, A. C. & HEARD, D. E. 2016. Atmospheric OH reactivity in central London: observations, model predictions and estimates of in situ ozone production. *Atmos. Chem. Phys.,* 16**,** 2109-2122.

WILSON, E. W., HAMILTON, W. A., KENNINGTON, H. R., EVANS, B., SCOTT, N. W. & DEMORE, W. B. 2006. Measurement and Estimation of Rate Constants for the Reactions of Hydroxyl Radical with Several Alkanes and Cycloalkanes. *The Journal of Physical Chemistry A,* 110**,** 3593-3604.

YOSHINO, A., NAKASHIMA, Y., MIYAZAKI, K., KATO, S., SUTHAWAREE, J., SHIMO, N., MATSUNAGA, S., CHATANI, S., APEL, E., GREENBERG, J., GUENTHER, A., UENO, H., SASAKI, H., HOSHI, J.-Y., YOKOTA, H., ISHII, K. & KAJII, Y. 2012. Air quality diagnosis from comprehensive observations of total OH reactivity and reactive trace species in urban central Tokyo. *Atmospheric Environment,* 49**,** 51-59.

YOSHINO, A., SADANAGA, Y., WATANABE, K., KATO, S., MIYAKAWA, Y., MATSUMOTO, J. & KAJII, Y. 2006. Measurement of total OH reactivity by laser-induced pump and probe technique - comprehensive observations in the urban atmosphere of Tokyo. *Atmospheric Environment,* 40**,** 7869-7881.

ZAVALA, M., HERNDON, S. C., WOOD, E. C., JAYNE, J. T., NELSON, D. D., TRIMBORN, A. M., DUNLEA, E., KNIGHTON, W. B., MENDOZA, A., ALLEN, D. T., KOLB, C. E., MOLINA, M. J. & MOLINA, L. T. 2009. Comparison of emissions from on-road sources using a mobile laboratory under various driving and operational sampling modes. *Atmos. Chem. Phys.,* 9**,** 1-14.

Chapter 6 - Integrated Chemistry of Ozone in the Atmosphere campaign

6.1 Background to the ICOZA project

The atmospheric chemistry of ozone in the troposphere plays a key role in numerous processes relating to air quality and climate change as it is both a pollutant and a greenhouse gas. O_3 is a major constituent of photochemical smog and is a known respiratory irritant, exposure to excessive levels has been shown to be linked with increased mortality rates in a number of European cities; daily deaths have been shown to increase by 0.3 % per every ~5 ppb increase in O_3 exposure (World Health Organisation, 2005). In addition to this, tropospheric O_3 is damaging to crops; it can harm yields and reduce quality (Krupa et al., 1998). Tropospheric O_3 is often produced as a product from the photo-oxidative processing of VOCs in the presence of NO_x through the reaction of $O(^3P)$ with O_2, where $O(^3P)$ was formed from the photolysis of NO_2 that resulted from the reaction between NO and RO_2, or HO_2. This chapter focusses on the Integrated Chemistry of Ozone in the Atmosphere (ICOZA) campaign which took place at a site on the North Norfolk Coast, UK, in the summer of 2016. The focus of the ICOZA project was investigate O_3 production, through both its direct measurement, and the measurement of other species and parameters that relate to it.

6.2 Aims

Indirect approaches to determining the O_3 production regime and calculating O_3 production rate, such as those described Section 1.3, require accurate measurements of various species (NO_y, RO_x, VOCs), and good knowledge of physical parameters such as rate coefficients. This results in the indirect approaches being subject to significant uncertainty. The main aim of the ICOZA campaign was to directly

measure the O_3 production rate, and its response to changes in NO_x, and VOC levels, using a newly developed instrument deployed to a UK coastal site which is known to be regularly subject to the pollution outflow from London and continental Europe.

The new instrument was developed by the research group of Prof. William Bloss at the University of Birmingham and utilised a methodology known as the Perturbed Ozone Production Rate (POPR) approach. In this method ambient air is drawn into two transparent flow reactors, one of which transmits all wavelengths of UV-visible solar radiation that reach the earths surface (to allow photochemistry) and one which absorbs below ~400 nm (to stop photochemistry of NO_2). O_3 is measured in the flow from each reactor and is used to calculate the rate of *in situ* O_3 production by taking into account the residence time of the ambient air in the reactors. The measured O_3 production rate is perturbed by the addition of NO_x or VOCs before entry to the reactors to enable responses to be examined. A detailed description of the method can be found in Cazorla and Brune (2010).

An extensive suite of other species and parameters were co-measured to enable interpretation of the O_3 production rate. This chapter focusses on measurements of OH reactivity and HCHO that were made using the laser flash photolysis instrument and LIF instrument, respectively that are both described in Chapter 2.

6.3 Site description, measurement suite and conditions

During the ICOZA campaign all measurements were made at the University of East Anglia (UEA) managed Weybourne Atmospheric Observatory (WAO) on the North Norfolk coast, UK (52° 57' N, 1° 07' E). The main building at the observatory is a decommissioned second world war ammunitions store and houses a laboratory containing a variety of instrumentation for atmospheric measurement. It is built on land 16 m above sea level that declines gently towards a pebble beach that faces North. A detailed description of the WAO can be found in Penkett et al. (1999) and the geographical location of the site is shown by the satellite image in Figure 6.1.

Figure 6.1: Satellite image showing the location (yellow star) of the measurement site at the Weybourne Atmospheric Observatory during the ICOZA campaign.

The WAO was chosen for the ICOZA campaign owing to the variation in air masses it is regularly subjected to. It provided a strong opportunity to field test the University of Birmingham developed POPR instrument and to measure the *in situ* ozone production rates in polluted air masses subjected to varying degrees of photochemical ages and pollutant loadings. Previous measurement campaigns at the WAO have received photochemically aged air masses containing pollution from continental Europe in addition to lesser aged air masses from London and the rest of the UK, cleaner marine air from the North Sea also regularly reaches the site (Lee et al., 2009).

A large concreted area on the land adjacent to the WAO building provided ample space for the deployment of mobile laboratories from which measurements were also made during ICOZA. A van belonging to the University of Birmingham, the Leeds FAGE container and the Leicester container were deployed. The photograph in Figure 6.2 shows the positioning of the mobile laboratories relative to the WAO building. Table 6.1 summarises all of the measurements that were made during ICOZA, the locations of the inlets / measurement points and the techniques used.

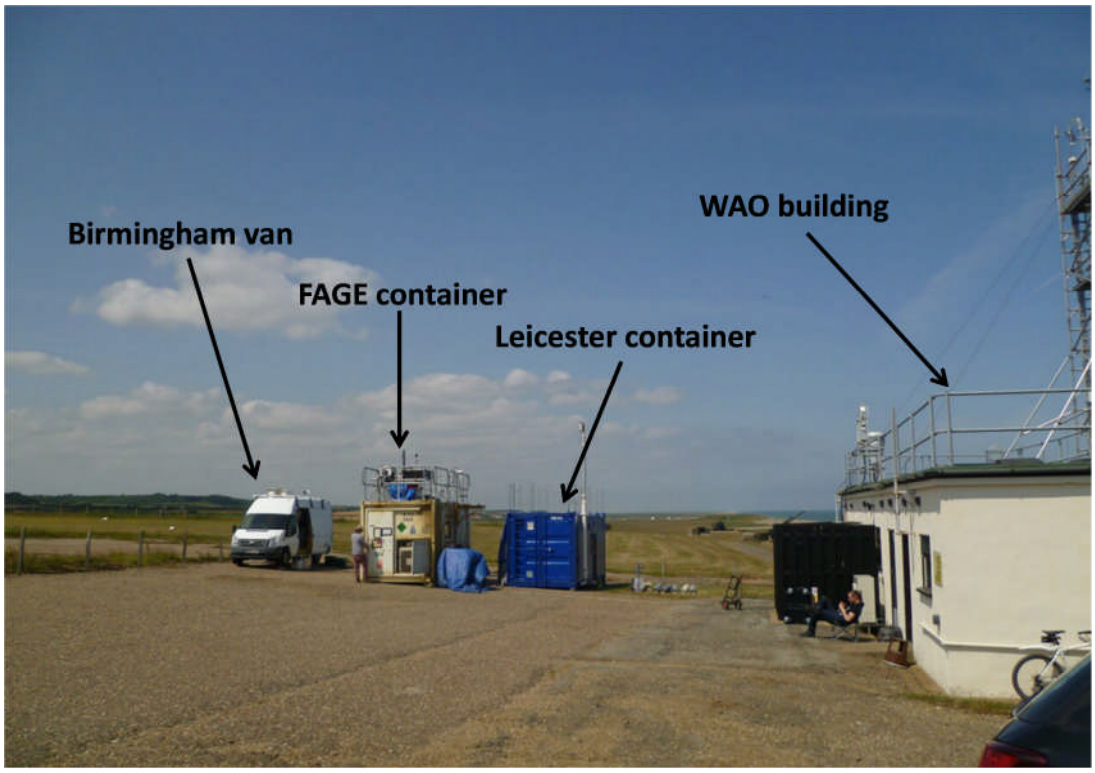

Figure 6.2: Photograph of the measurement site at the WAO where the Leeds FAGE container was situated for the ICOZA campaign.

For measurements that were made from the laboratory inside the WAO building, ambient air was either sampled via ~5 m of ¼" OD Teflon tubing from the roof or from a tower ~10 m above the roof. From the top of which, a glass manifold was used to circulate ambient air to the laboratory; this enabled subsequent samples of ambient air to taken by instruments.

Measurement	Technique	Sample inlet	Reference
OH, HO_2, RO_2	Laser induced fluorescence spectroscopy (LIF)	FAGE container	Whalley et al. (2013)
OH reactivity	Laser flash photolysis coupled with laser induced fluorescence spectroscopy (LFP - LIF)	FAGE container	Stone et al. (2016)
HCHO	Laser induced fluorescence spectroscopy (LIF)	WAO manifold	This work
Ozone production rate	Perturbed ozone production rate (POPR)	Birmingham van	Cazorla and Brune (2010)
NO, NO_2	Chemiluminescence	WAO roof	Weinheimer (2006)
NO_2	(CRDS)	Leicester container	Langridge et al. (2006)
O_3	UV absorption	WAO manifold	Heard et al. (2006)
CO	Hot mercuric oxide reduction coupled with UV detection	WAO manifold	Robbins et al. (1968)
HONO	Long path absorption photometry (LOPAP)	Birmingham van	Heland et al. (2001)
$ClNO_2$	Chemical Ionisation mass spectrometry (CIMS)	Leicester container	Bannan et al. (2015)
Photolysis frequencies	Spectral radiometry	FAGE container and Leicester container	Hofzumahaus (2006)
$J(O^1D)$	Filter radiometry	FAGE container	Bohn et al. (2004)
NMHCs	Gas chromatography coupled with flame ionisation detector (GC-FID)	WAO roof	-
NMHCs	Proton transfer mass spectrometer (PTR-MS)	WAO roof	Murphy et al. (2010)

Table 6.1: Species / parameters measured during the ICOZA campaign at the Weybourne Atmospheric Observatory (WAO)

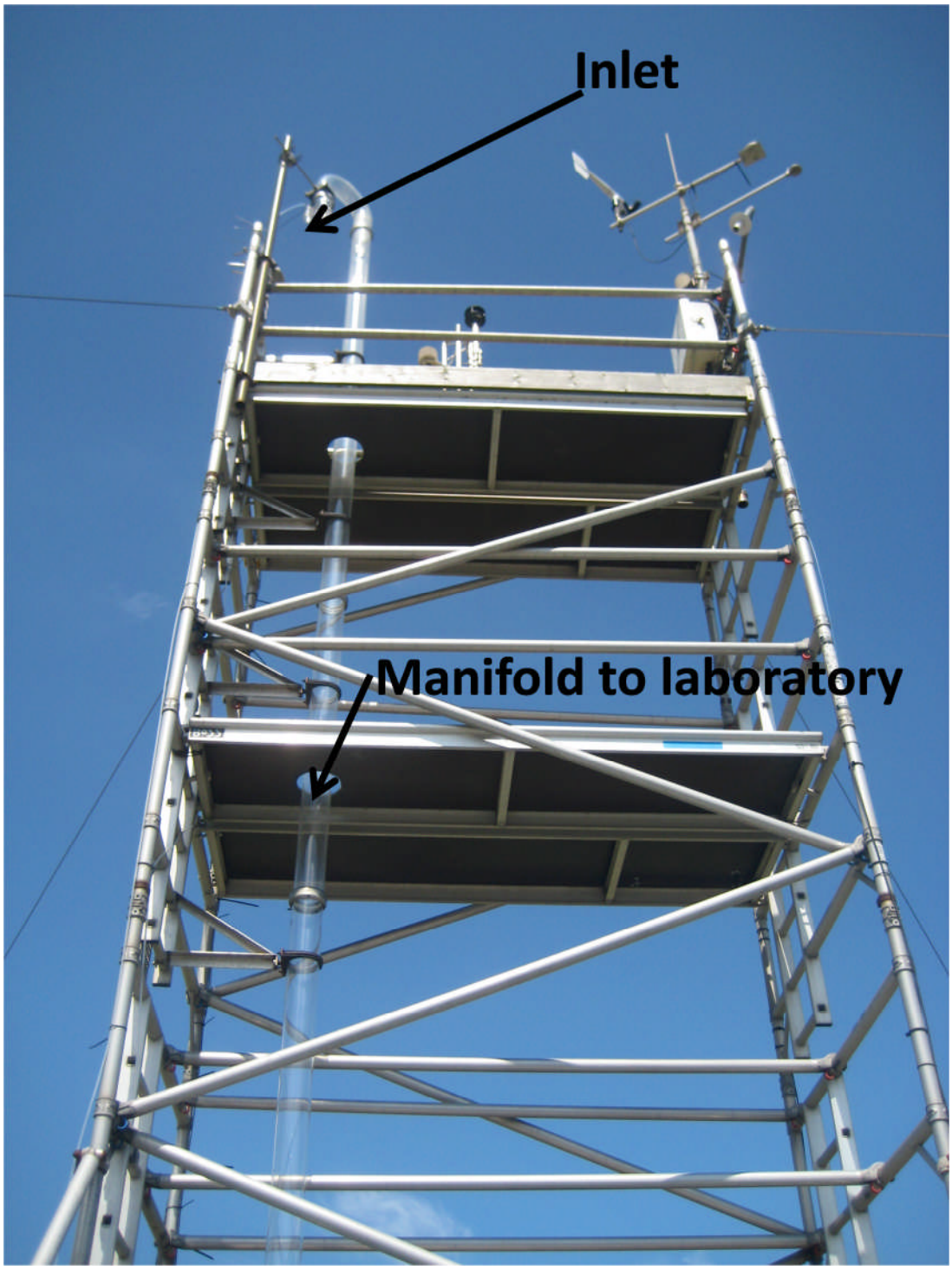

Figure 6.3: Photograph of the ~10m tower at the WAO where ambient air was sampled via a glass manifold (shown) to the laboratory for analysis.

The weather was very variable during the ICOZA campaign and ranged from a heat wave on 01/07/2015 to colder wetter days and night time thunderstorms. The average temperature was 16.3 ˚C and ranged from 9.4 to 29 ˚C with an average relative humidity of 75 % which ranged from 38 to 98 %. For most of the campaign the wind speed was typically below 10 m s^{-1} with a minimum of 0.3. m s^{-1}, higher wind speeds (18.3 m s^{-1} maximum) were observed on 25/07/2015 during and following a heavy thunderstorm. Figure 6.4 shows the variations in temperature, relative humidity and wind speed that were observed during the ICOZA campaign.

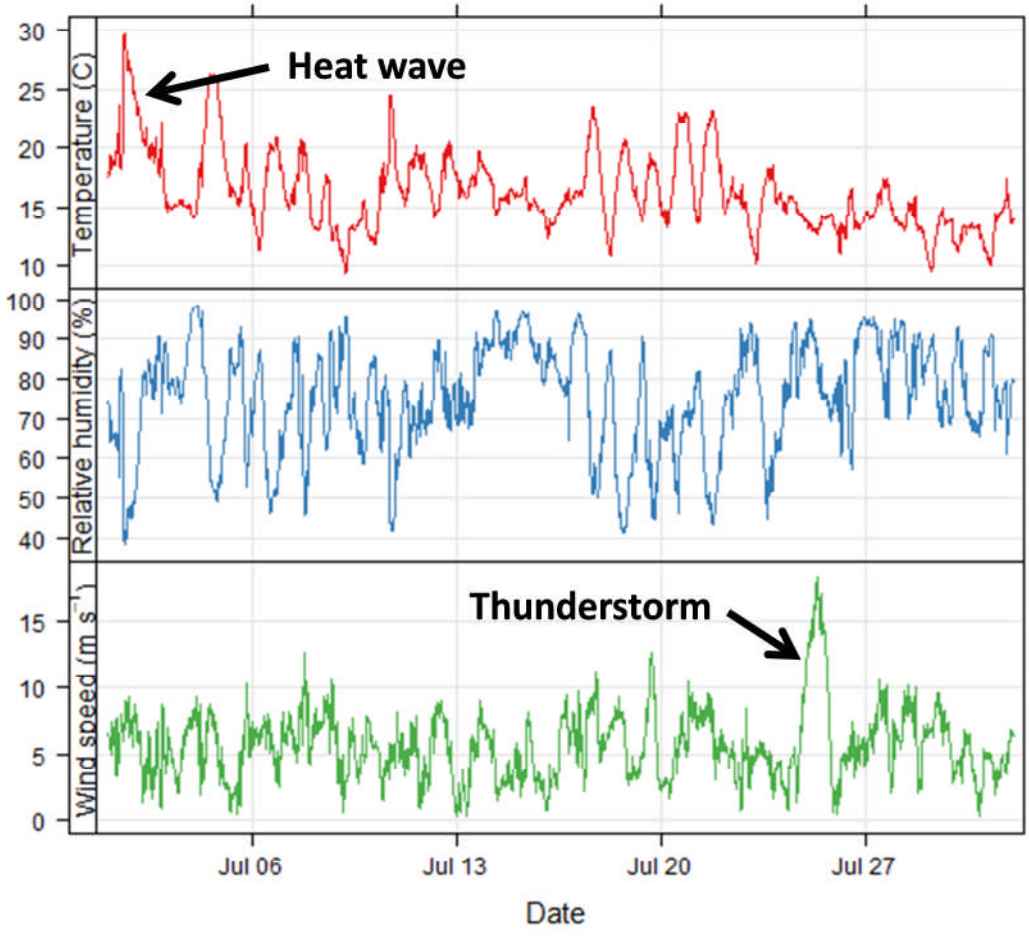

Figure 6.4: Time series of key meteorological parameters recorded by the Weybourne Atmospheric Observatory (WAO) meteorological station positioned at the top of the sampling tower. Key events are labelled.

6.4 OH reactivity

6.4.1 OH reactivity observations

The Leeds laser flash photolysis instrument for the measurement of OH reactivity was positioned ~3 m above ground on the roof of the Leeds FAGE container in a similar manner to during the York 2014 'missing' OH reactivity campaign (Chapter 4). The instrument was operated in configuration 2 as described in Section 2.2.7. The instrument operated well for the majority of the campaign with few unplanned gaps in the data. However, it was not possible to make measurements of OH reactivity during the final week of the campaign owing to problems encountered with the reference cell used to tune the wavelength of the 308 nm probe laser. Figure 6.5 shows the instrument whilst sampling ambient air during ICOZA with some key features labelled.

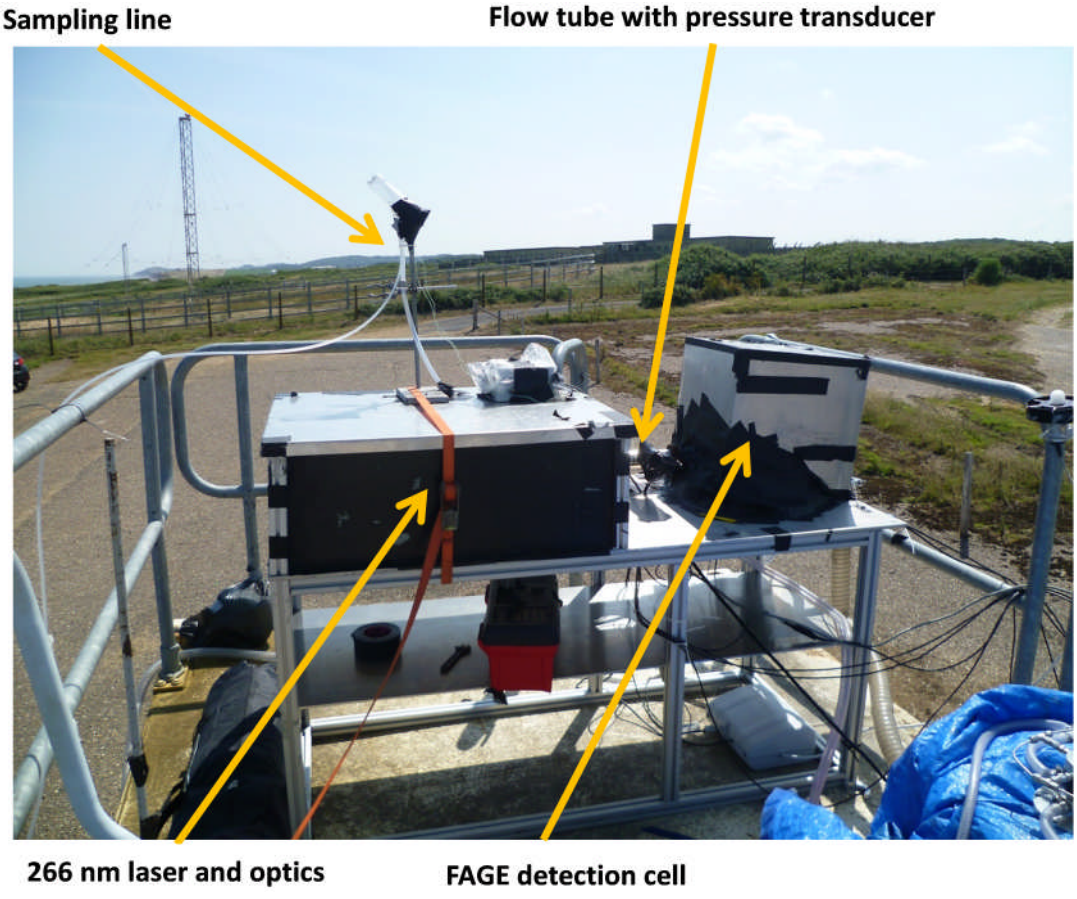

Figure 6.5: Photograph of the laser flash photolysis OH reactivity instrument whilst making measurements in ambient air during the ICOZA campaign at the Weybourne Atmospheric Observatory (WAO), key features are labelled.

Ambient levels of ozone (typically 30 – 50 ppb during the day) and water vapour (RH 38 – 98 %) were sufficiently large through the course of the campaign to achieve OH decays with good signal-to-noise during the set period when the FAGE apparatus recorded an online fluorescence signal which was typically 75s. It was not necessary to add additional ozone or water vapour to the OH reactivity instrument at any point during ICOZA. It was not necessary to correct the measurements to account for a difference in pressure between the flow tube of the instrument and ambient as was the case for the campaign in York (when the instrument was operated in configuration 1). This is because the use of a wider sampling line during ICOZA (when the instrument was operated in configuration 2) resulted in this pressure difference being negligible (<1 Torr).

OH reactivity was measured from 29/06/2015 to 22/07/2015 and all measurements made are displayed in Figure 6.6. Figure 6.6(a) shows the time series of OH reactivity plotted with error bars which represent the 1σ uncertainty (~±0.2 s^{-1} on average) determined through the uncertainties on the OH decay fits and the determination of $k'_{(zero)}$. The measurements are re-plotted in Figure 6.6(b) with the omission of error bars for clarity. Values ranged from 1.7 to 27.7 s^{-1} and the mean average k'_{OH} was 5.1 s^{-1} which is close to the 4.9 s^{-1} average OH reactivity reported by Lee et al. (2009) for the TORCH-2 campaign which took place at the WAO in May 2004. The plots were constructed using the mid-point of the period during which OH decay signals were summed (i.e. when the fluorescence signal was recorded by the FAGE instrument).

Higher OH reactivity was typically observed towards the start of the campaign on 01/07/2015 and 02/07/2015 which coincided with the heat wave. An event of particular importance occurred on 01/07/2015 where a rapid change in wind direction occurred which gave rise to a ~10 ˚C increase in temperature and not long after this OH reactivity was shown to increase. Following this the OH reactivity decreased on a longer time scale and this is described further in context of air mass origin according to back trajectories in Section 6.3.2.3. The OH reactivity data are examined for evidence of diurnal behaviour in Section 6.3.2.1, and correlations with other species / parameters measured are presented and discussed in Section 6.3.2.2.

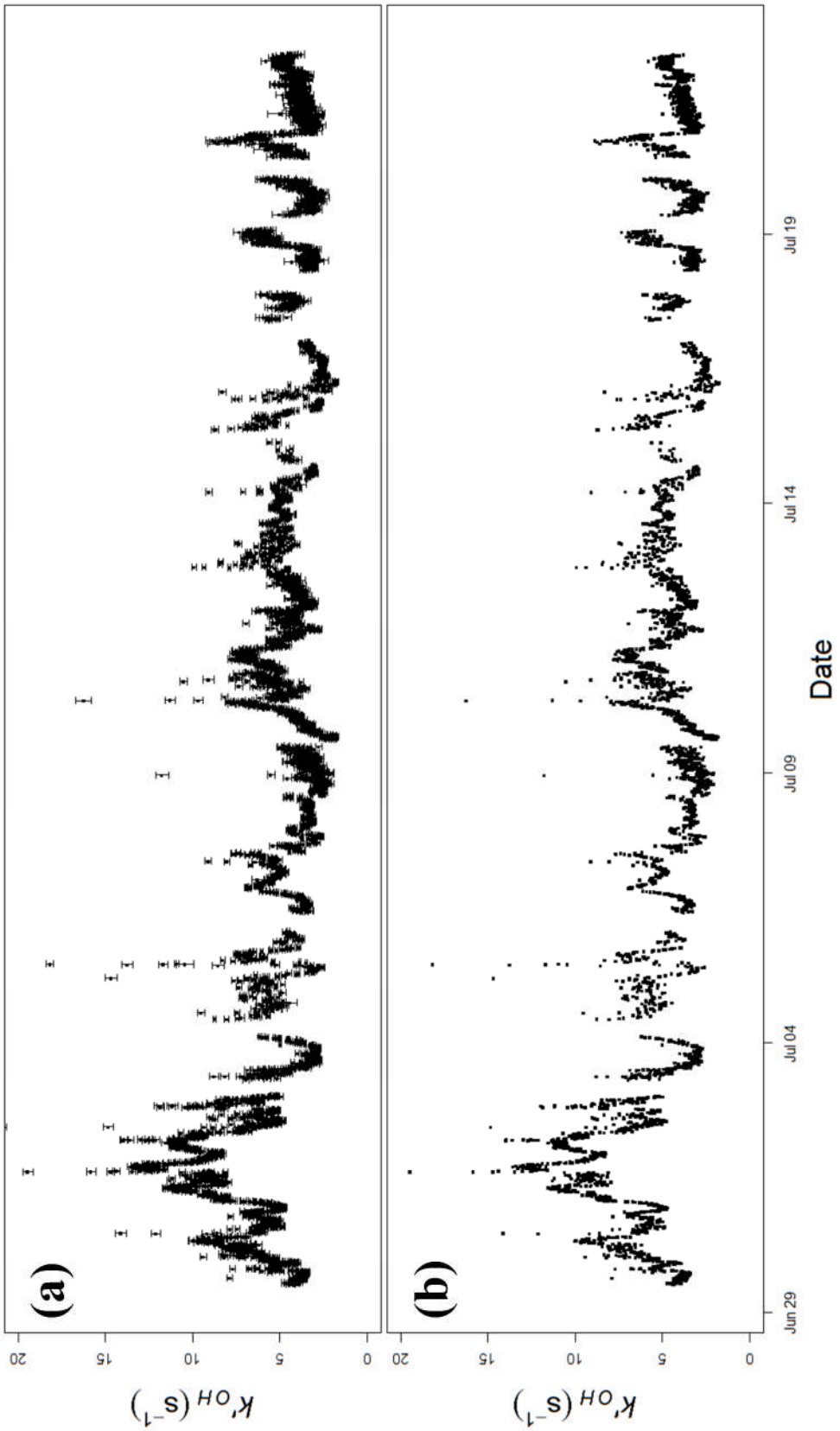

Figure 6.6: Time series of measured OH reactivity during the ICOZA campaign. (a) Data plotted with error bars representative of the 1σ uncertainty determined through combining the uncertainties of the decay fits and the determination of $k'_{OH(ZERO)}$. (b) Data plotted without error bars for clarity.

6.4.2 Interpretation of OH reactivity observations

6.4.2.1 Diurnal behaviour

It is often the case that where there are sources of OH reactive species that vary in a similar manner each day that a diurnal change in OH reactivity will be observed. Examples of this are morning rush hour peak at sites with strong anthropogenic influences such as that shown in Chapter 5 for the measurements made during the York 2014 'missing' OH reactivity campaign. Another example is measurements in forests such as those reported by Ren et al. (2006) from the PMTACS-NY Whiteface Mountain campaign where OH reactivity was typically higher during the day owing to the rate of biogenic VOC emission varying with the intensity of sunlight. To test whether there was any such source of OH reactive species acting on the air reaching the WAO during ICOZA, all OH reactivity measurements were averaged into 96 time bins with a mean value every 15 minutes using the timeAverage function of the openair package in R (Carslaw and Ropkins, 2012, Carslaw, 2015). These data are plotted in Figure 6.7.

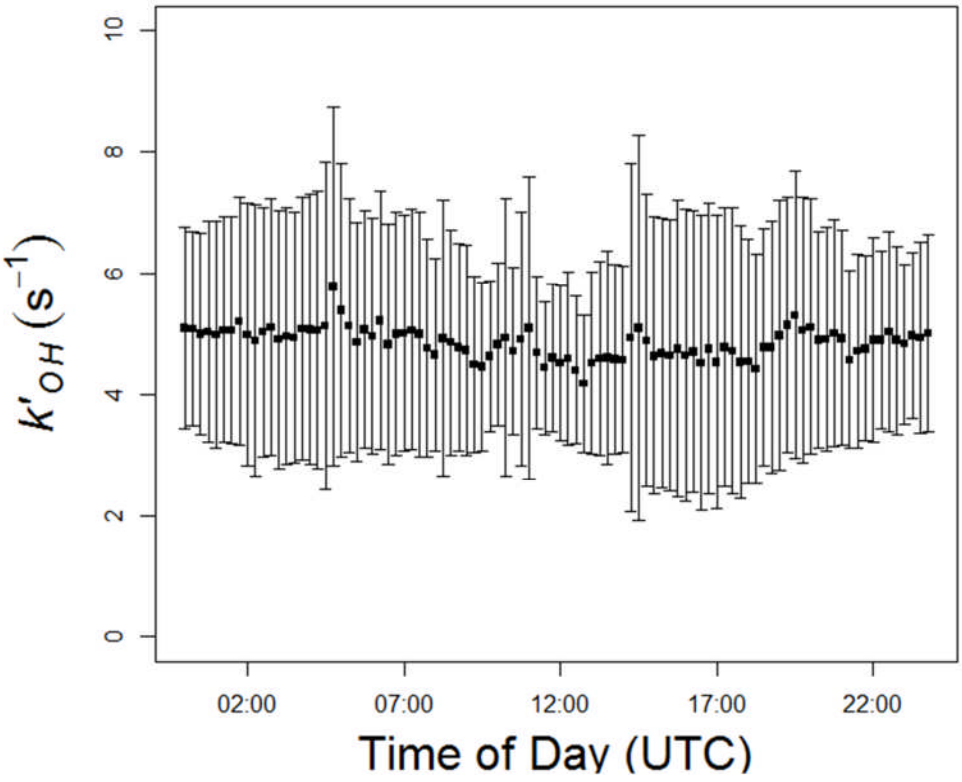

Figure 6.7: Diurnal profile of OH reactivity observed during the ICOZA campaign in 15 minute time bins. Error bars represent ± 1 σ standard deviation from the mean observation, and are a measure of the variability during a 15 minute time bin.

It can be seen that there is no clear structure in the points plotted indicating that there were no sources of OH reactive species that influenced the OH reactivity in a consistent manner daily. This was to be expected as the WAO campaign was chosen for the ICOZA campaign because it is subject to a wide variety of air masses; the lack of structure is likely a result of OH sinks from different sources reaching the site for varying periods of time each day. Previous measurements of OH reactivity at the WAO during the TORCH-2 campaign also showed no evidence of a diurnal trend. The absence of a diurnal trend in Figure 6.7 means it cannot be used to draw conclusions as to the 'average' behaviour of likely sources of OH reactive species (e.g. anthropogenic or biogenic VOCs). Correlations between OH reactivity and other species and parameters measured during ICOZA are presented and discussed in Section 6.3.2.2.

6.4.2.2 Correlations with other measurements

For the purpose of all analyses to examine the relationships between various species / parameters that were measured, all measurements were merged so that a common time base was shared. This was achieved using the timeAverage function of the openair package for R. Measurements of OH reactivity, individual OH sinks and meteorological parameters from the WAO tower were merged. Measurements recorded from 01/07/2015 13:00:00 – 25/07/2015 02:00:00 (UTC) were averaged into 15 minute bins. For the OH sinks measured using the GC-FID instrument, values were only recorded every ~90 minutes owing to the length of analysis time. Following the use of the timeAverage function on these data sets, gaps were filled by estimates obtained through linear interpolation between measurements.

The OH reactivity measured at the WAO during the TORCH-2 campaign was found to include a significant portion resulting from the presence of NO_x; NO and NO_2 contributed 0.087 s^{-1} and 0.722 s^{-1}, respectively, on average for the campaign (Lee et al., 2009). Correlations for measured OH reactivity with measured NO and NO_2 during ICOZA are presented in Figure 6.8.

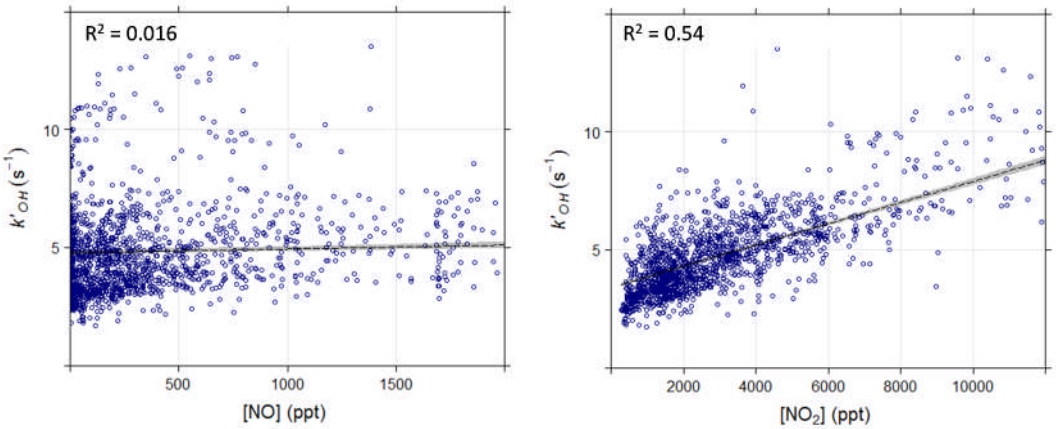

Figure 6.8: Plots of OH reactivity against both [NO] and [NO_2]. Data shown are 15 minute binned mean averages from measurements taken between 01/07/2015 13:00:00 – 25/07/2015 02:00:00 (UTC) during the ICOZA campaign. The shaded areas represent the 95% confidence intervals from the linear fits (least squares). NO and NO_2 data were supplied by Dr. James Lee, University of York.

There was no correlation between OH reactivity and NO during ICOZA indicating that NO was a minor contributor to the OH sink. The correlation with NO_2 is much stronger (R^2 = 0.54 compared with 0.016) and this indicates that NO_2 played a more dominant role in driving changes in OH reactivity that were observed, as was the case during TORCH-2. The strong correlation with NO_2 indicates that air masses containing pollution of anthropogenic origin were transported to the site as NO_2 is a secondary pollutant formed from the photo-oxidative processing of VOCs in the presence of NO (Wayne, 2000).

Also during TORCH-2 strong contributions to OH reactivity from alkenes and also OVOCs were reported, the campaign averages 0.262 s^{-1} and 0.563 s^{-1}. Correlations are shown in Figure 6.9 for measured OH reactivity with measured ethene (as an example alkene) and also the summed concentrations of measured MVK and MACR (as example OVOCs).

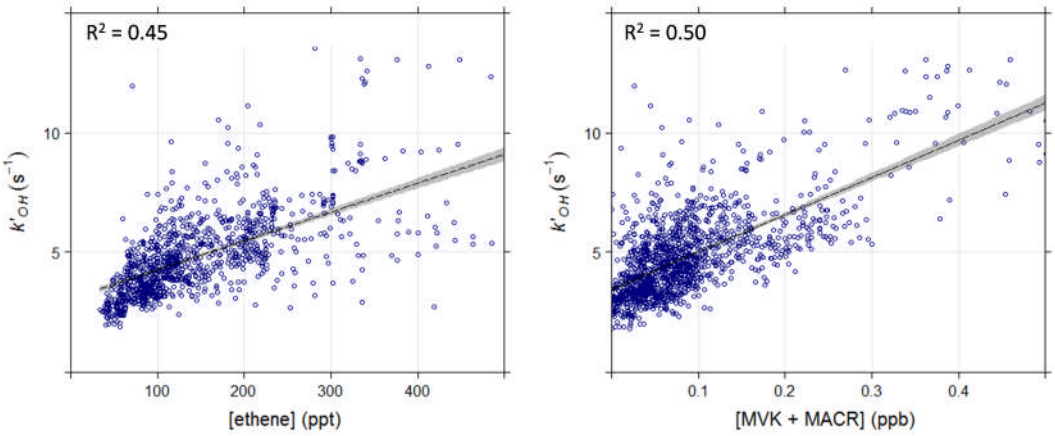

Figure 6.9: Plots of OH reactivity against both [ethene] and [MVK + MACR]. Data shown are 15 minute binned mean averages from measurements taken between 01/07/2015 13:00:00 – 25/07/2015 02:00:00 (UTC) during the ICOZA campaign. The shaded areas represent the 95% confidence intervals from the linear fits (least squares). VOC measurements provided by Dr. Grant Forster and Dr. David Oram, Unversity of East Anglia.

The plots show that there was strong correlation between OH reactivity and ethene and MVK + MACR (Methyl vinyl ketone and Methacrolein) (R^2 0.45 and 0.50, respectively). The correlation between OH reactivity and ethene supports the hypothesis that polluted air masses transported to the WAO were sampled during ICOZA. Ethene is known to be emitted from a variety of anthropogenic sources, such as biomass burning and fuel combustion; and natural sources such as outgassing from plants. However, plants are estimated to only contribute a small amount of total emissions (Aikin et al., 1982). The strength of the correlation between OH reactivity and MVK + MACR indicates that there was some influence from biogenic emissions at the site. Both are known photo-oxidation products of isoprene which is the dominant biogenic VOC emitted into the atmosphere (Zhao et al., 2004, Stone et al., 2011). Given the correlation of OH reactivity shown with MVK + MACR it should follow that there was some correlation between OH reactivity and isoprene, and also temperature; plots demonstrating these relationships are shown in Figure 6.10.

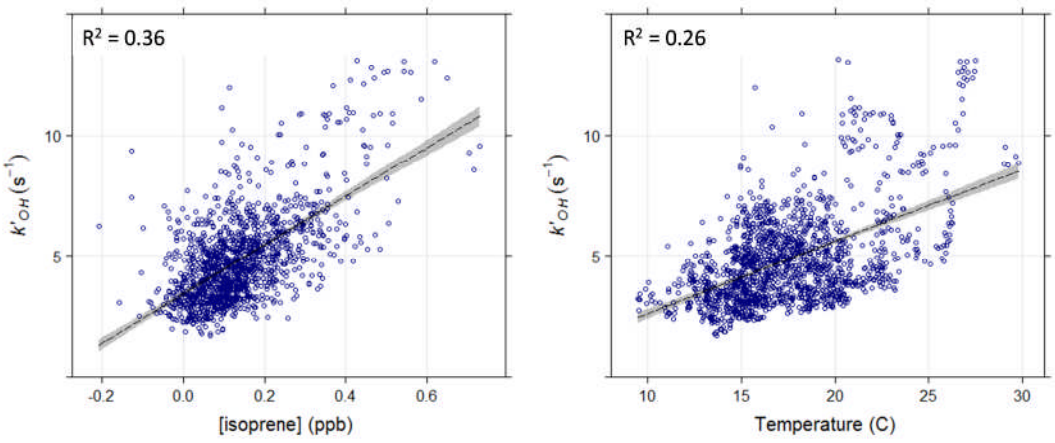

Figure 6.10: Plots of OH reactivity against both temperature in degrees C and [isoprene]. Data shown are 15 minute binned mean averages from measurements taken between 01/07/2015 13:00:00 – 25/07/2015 02:00:00 (UTC) during the ICOZA campaign. The shaded areas represent the 95% confidence intervals from the linear fits (least squares).

It is shown that there are moderate correlations between OH reactivity and both isoprene and temperature (R^2 = 0.36 and 0.26, respectively). The correlation with isoprene provides confirmation that biogenic emissions played some role in driving changes seen in OH reactivity during ICOZA. Biogenic emissions such as isoprene are known to increase with temperature (Di Carlo et al., 2004, Hansen et al., 2014). It is likely the correlation observed here is partly due to increased biogenic emissions. A full analysis of the potential drivers of changes in OH reactivity is given in the remaining subsections of Section 6.3.2.

6.4.2.3 Relationship with wind direction and air mass origin

To gain further insight into the sources of the varying levels measured of OH reactivity during ICOZA, the relationship with wind direction was examined and the percentileRose function of the openair R package was used for this. The 15 minute OH reactivity measurements, and wind directions measured at the top of the WAO tower in the merged data set described in Section 6.3.2.2 were used. A wind rose is shown in Figure 6.11(b) summarises the relationship between OH reactivity and wind direction during ICOZA.

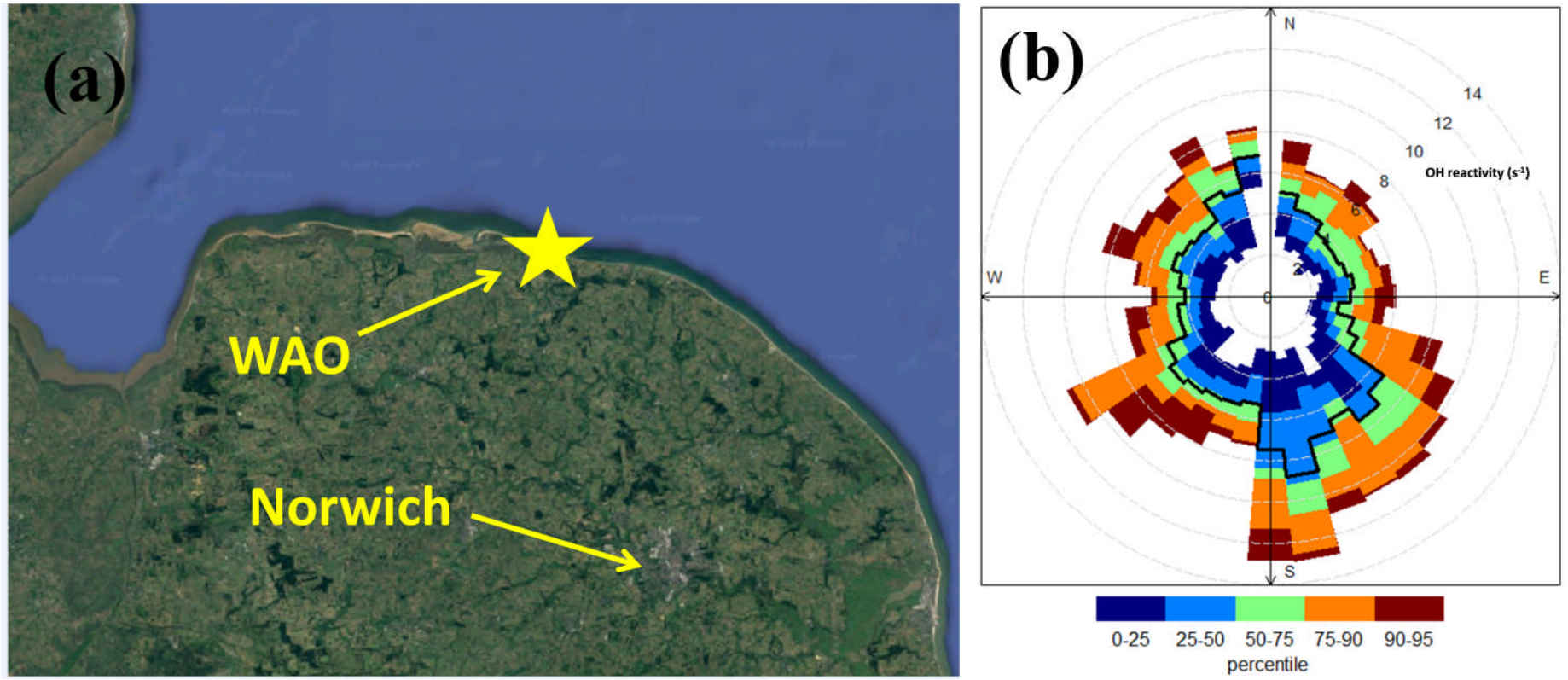

Figure 6.11: (a) Map to show the locational relationship between the Weybourne Atmospheric Observatory (WAO) and the city of Norwich. (b) Wind rose to demonstrate the dependence of measured OH reactivity on wind direction during the ICOZA campaign. The black line represents the mean observed value for a given wind sector. Coloured areas represent the percentile levels for a given wind sector.

During ICOZA the OH reactivity varied with wind direction, the black line in Figure 6.11(a) represents the mean values for the different wind sectors and shows that measurements were typically higher on average (~6-9 s^{-1}) when winds were southerly to south easterly. This is unsurprising considering that these winds blew from the land towards the sea and would have been expected to be more polluted and have a higher loading of OH sinks. A satellite image in Figure 6.11(b) illustrates the location of the city of Norwich relative to the WAO; Norwich is shown to be south-southeast of the WAO. It is concluded that the higher mean OH reactivity recorded when the wind was southerly to south easterly was likely a result of VOCs and other OH reactive pollutants transported from Norwich. Figure 5.11(b) also shows that on average for the campaign, the wind sectors with the lowest mean values were typically between easterly, northerly and westerly. This comes as no surprise considering that the air reaching the site in this case would be typically be less polluted as it is of marine origin.

Whilst Figure 6.11 shows evidence for a dependency of OH reactivity observations on wind direction, there are limitations to such an approach, as only speculative conclusions can be made as to the location of sink sources. To investigate the possible sources of sinks that contributed to OH reactivity during ICOZA, the measurements were examined in the context of their origin as determined through the calculation of the back trajectories of the ambient air that was sampled. The Hybrid Single Particle Lagrangian Integrated Trajectory Model (HYSPLIT) was used to calculate back trajectories using archived meteorological data provided by the National Oceanic and Atmospheric Administration (NOAA) for air reaching the WAO. The history of the air mass reaching the WAO was calculated for the previous four days at a starting height of 10 m every three hours for July 2015. It should be noted that whilst the back trajectories started at a height of 10 m, changes in altitude of the air during transport to the measurement site are not considered. Analyses which utilised back trajectories presented in this chapter should be considered as preliminary. Future work should include a detailed assessment of the impact variations in altitude could have on the results presented here.

Following the computation of back trajectories as described above, the openair trajPlot function was used to examine the relationship between various back trajectories, and the observed levels of OH reactivity. The results from such analysis

for 01/07/2014 and 02/07/2014 during the heat wave at the beginning of the campaign where high OH reactivity was recorded are summarised in Figure 6.12.

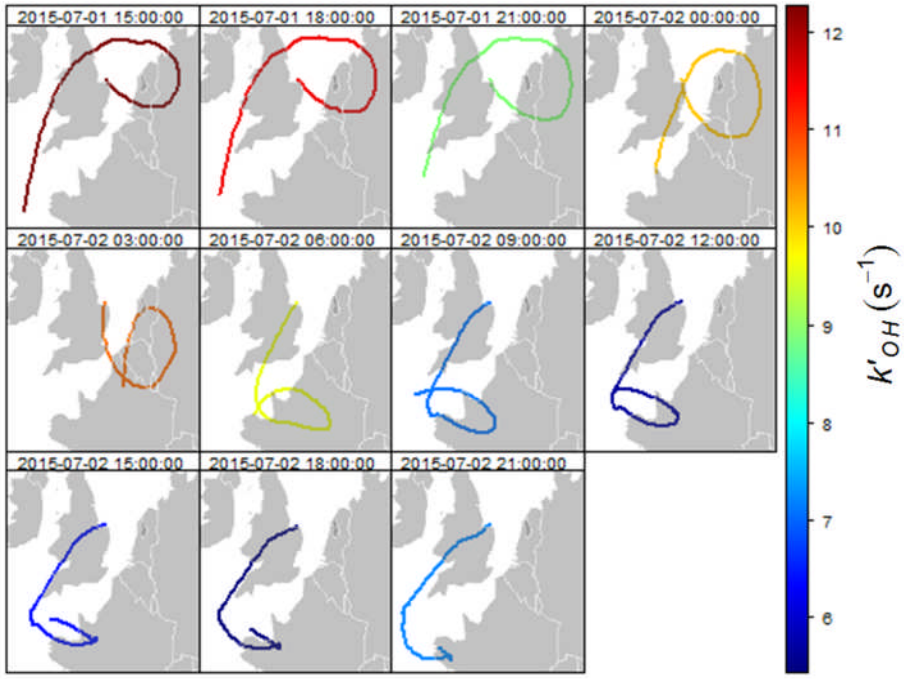

Figure 6.12: Four day back trajectories calculated using HYSPLIT (10 m starting height) for air reaching the WAO every three hours during ICOZA from 01/07/2015 13:00:00 to 02/07/2015 21:00:00. The colour of each back trajectory represents the mean OH reactivity for the hour.

From the afternoon to the end of 01/07/2015 the back trajectories show that the air mass had spent considerable time over the UK and continental Europe. During this time the three hour average OH reactivity measured ranged between ~10 – 12 s^{-1} which were the highest levels measured during the campaign. Following this in the early hours of 02/07/2015 the origin of the air mass transitioned so that the air reaching the WAO has spent less time passing over continental Europe. By the afternoon the back trajectories show that the air mass reaching the WAO had spent minimal time passing over continental Europe in the four days prior to arrival. Through the course of this change in air mass the measured OH reactivity is shown to drop to between 6 - 8 s^{-1}.

To broadly investigate the origin of the sinks that contributed to the OH reactivity measured at the site all of the back trajectories that were calculated for July 2014 were classified according to their profile using a cluster analysis, the openair trajCluster function was used for this to assign clusters based on the Euclidian

(straight line) distances between each pair of back trajectories. This analysis showed that the four day back trajectories for the air reaching the WAO during ICOZA fell into three distinct categories. These are defined as Local, Northerly and Westerly; they are summarised in Figure 6.13.

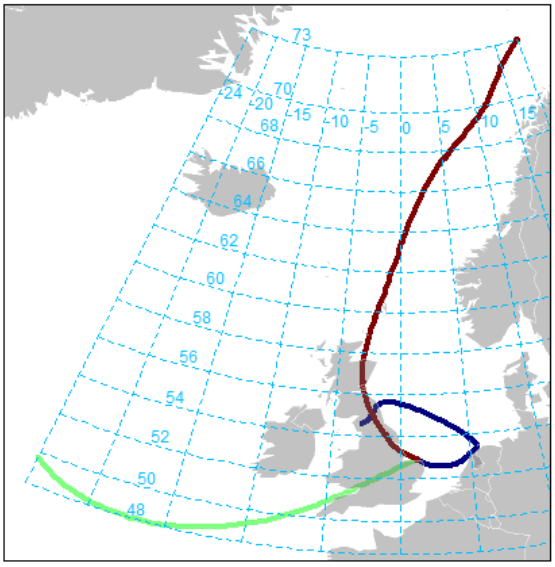

Figure 6.13: Clustered four day back trajectories determined using the openair trajCluster function to analyse back trajectories calculated every 3 three hours during ICOZA from 01/07/2015 13:00:00 – 25/07/2015 02:00:00 (UTC). The blue line represents the path of Local air, the red line represents the path of Northerly air and the green line represents the path of Westerly air.

The OH reactivity measurements were grouped according to the classification of air mass that was sampled. Figure 6.14 shows daily averages of OH reactivity, the heights of the bars are split according to the proportion of time each air mass type reached the site.

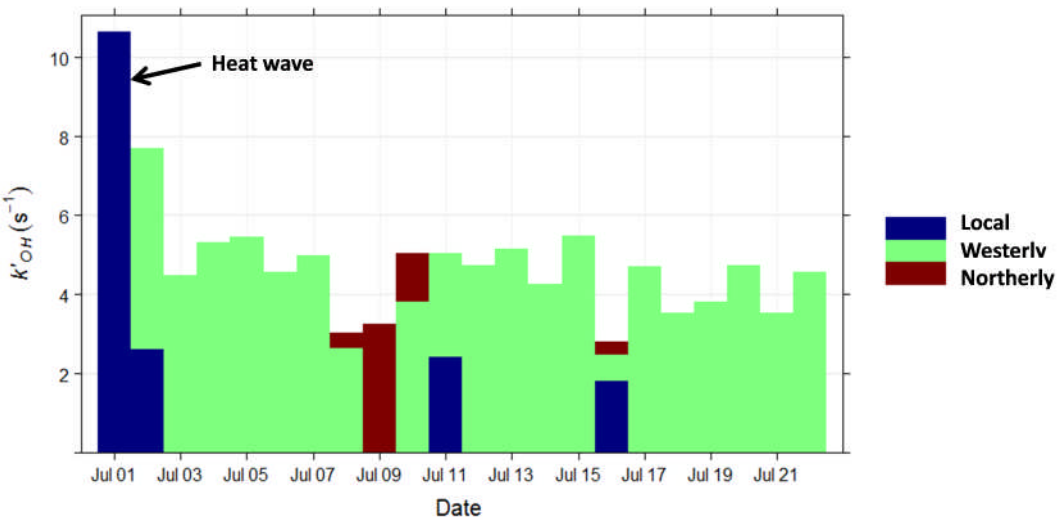

Figure 6.14: Bar chart to show the average daily OH reactivities recorded during ICOZA. Averages were calculated using data from 01/07/2015 13:00:00 – 25/07/2015 02:00:00 (UTC) and the height of each bar represents the portion of time that air of each classification reached the site. See Figure 5.14 for definition of air mass.

It is shown that for most of the campaign, air of Westerly origin was dominant, air masses of Local and Northerly origin reached the site less frequently. The highest average daily OH reactivity was recorded at the beginning of the campaign during the heat wave and further details regarding the variation in the origin of the air mass at this time are described above. The origin of the air mass transitioned from Local to Westerly. Following the heat wave Local air masses were only sampled twice again on 11/07/2016 and 16/07/2016. On these occasions the OH reactivity sampled did not reach the daily average levels that were recorded during the heatwave, it is likely that the high OH reactivity recorded during the heatwave included a greater contribution from products of VOC photo-oxidation, or temperature enhanced emissions. When the air reaching the WAO was of Northerly origin OH reactivity was typically lower and this is likely due to the predominantly oceanic and so less polluted nature of the back trajectory for this classification. Whilst the cluster analysis of the back trajectories can give indications as to the location of potential sink sources, it is not possible to draw conclusions on the specific locations of sources that contributed to OH reactivity as these could have been anywhere in the path of the back trajectory. To gain further insight into the specific locations of sink sources during ICOZA, the Concentration Weighted Trajectory (CWT) approach was utilised using the openair trajLevel function. Figure 6.15 shows the CWT mean

average levels of OH reactivity that contributed to the observations at the WAO during ICOZA.

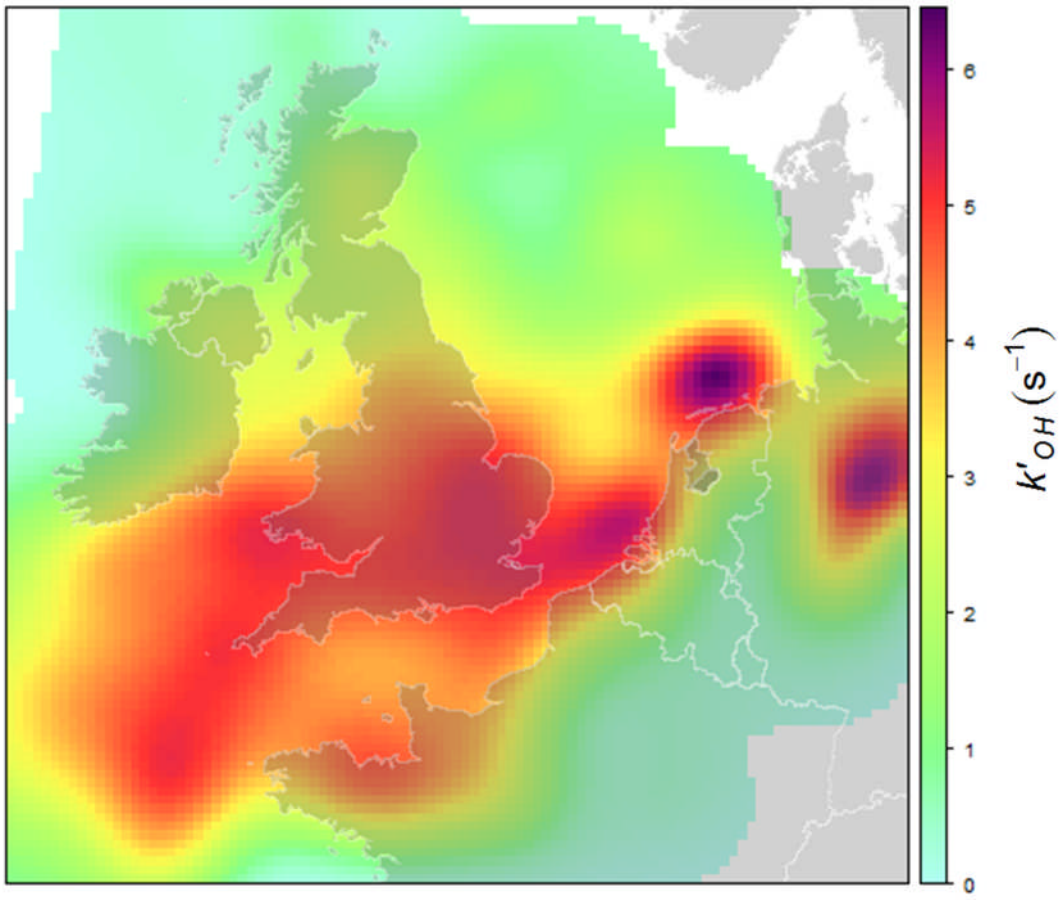

Figure 6.15: Concentration Weighted Trajectory (CWT) mean contribution to OH reactivity measured at the WAO during ICOZA. Values were determined based on 15 minute OH reactivity data and three hourly back trajectories during ICOZA from 01/07/2015 13:00:00 – 25/07/2015 02:00:00 (UTC).

The choropleth map represents the CWT mean contribution to the OH reactivity that was measured at the WAO during the whole of ICOZA. The areas which likely contributed the most to OH reactivity are darker whereas the lighter areas likely contributed less. It is shown that the biggest contributions to the measurements originated from the coastal area to the north of the Netherlands and also central Germany, and the coastal area near the Belgium-Netherlands boarder where the port of Rotterdam is situated. The contribution from the northern Netherlands coast is to be expected as there are high volumes of shipping in this area as there are a number of ports here and many vessels pass through these waters on their way to the German port of Hamburg. Also, the port of Rotterdam is the largest in Europe so it is so it is to be expected that shipping emissions originating from here contributed to

the measured OH reactivity when air was transported from here to the WAO. The high CWT mean contribution shown over central Germany lies over the city of Hanover which is home to many factories and other industrial developments which are all likely to emit pollutants that could have contributed to the OH reactivity measured. During the heat wave on 01/07/2015 the back trajectories passed over all three of the areas described above, as shown in Figure 6.12. It is possible that had there not been a heatwave at this time the CWT mean contributions for these areas would not have been as high as those shown in Figure 6.15 if a large portion of the reactivity measured at this time was accounted for by products of photo-oxidation. It can also be seen from Figure 6.15 that the CWT mean contribution was higher over England, Wales and surrounding waters than over Scotland and its surrounding waters. The results of the cluster analysis discussed above support this by showing that air originating from the North Sea, which may or may not have passed over Scotland, reached the WAO for only a small portion of ICOZA. Figure 6.14 showed that lowest daily average OH reactivities recorded were subject to air originating from the North Sea. In order to further understand the nature of the OH reactivity measured it was calculated using concentrations of co-measured sinks. Section 6.3.2.4 describes the method for this calculation and Section 6.3.2.5 compares and discussed the measured and calculated values.

6.4.2.4 Calculation of OH reactivity

The merged 15 minute data set described in Section 6.3.2.2 was used for the calculation of OH reactivity. Mixing ratios of OH sinks were converted to concentrations using the temperatures and pressures contained within the meteorological data. The resulting OH sink concentrations were used in conjunction with corresponding bimolecular rate coefficients for the reaction between each sink and OH as in E1.3 (reproduced below) to calculate a value of OH reactivity for each 15 minute bin. The sinks which were used to calculate OH reactivity for the ICOZA campaign are listed in Table 6.2.

$$k'_{OH(calc)} = \sum_{j} k^{j}_{OH+Aj} [A_j] \qquad \textbf{E1.3}$$

Sink	Class	$k_{sink + OH}$ (cm^3 $molecule^{-1}$ s^{-1})	Contribution to OH reactivity (s-1)	Instrument
O_3	O_3	7.3×10^{-14}	0.06	Thermo 49 Series
NO	NO	9.8×10^{-12}	0.11	Air Quality Design Inc. Chemiluminescence with LED NO_2 converter
NO_2	NO_2	9.9×10^{-12}	0.84	
CO	CO	2.3×10^{-13}	0.66	Ametek monitor
HONO	NO_z	6.0×10^{-12}	0.01	LOPAP
Methanol	Alcohol	9.0×10^{-13}	0.06	PTR-TOF-MS
Ethane	Alkane	2.4×10^{-13}	0.07	GC-FID
Propane		1.1×10^{-12}		GC-FID
Methylpropane		2.2×10^{-12}		GC-FID
Butane		2.4×10^{-12}		GC-FID
2-Methylbutane		3.7×10^{-12}		GC-FID
Pentane		4.0×10^{-12}		GC-FID
2-Methylpentane		5.3×10^{-12}		GC-FID
Hexane		5.5×10^{-12}		GC-FID
Acetylene	Alkene and	7.5×10^{-13}	0.12	GC-FID
Ethene	Alkyne	7.8×10^{-12}		GC-FID
Propene		2.8×10^{-11}		GC-FID
trans-But-2-ene		6.4×10^{-11}		GC-FID
But-1-ene		3.1×10^{-11}		GC-FID
cis-But-2-ene		5.6×10^{-11}		GC-FID
Benzene	Aromatic	1.2×10^{-12}	0.01	PTR-TOF-MS
Toluene		5.6×10^{-12}		PTR-TOF-MS
Formaldehyde	Carbonyl	8.5×10^{-12}	0.40	LIF
Acetaldehyde		1.5×10^{-11}		PTR-TOF-MS
Acetone		1.8×10^{-13}		PTR-TOF-MS
Methacrolein		2.9×10^{-11}		PTR-TOF-MS
Methyl vinyl ketone		2.0×10^{-11}		PTR-TOF-MS
Methyl ethyl ketone		1.1×10^{-12}		PTR-TOF-MS
1,3-Butadiene	Dialkene	6.7×10^{-11}	0.33	GC-FID
Isoprene		1.0×10^{-10}		PTR-TOF-MS
Acetonitrile	Unclassified	2.2×10^{-14}	0.05	PTR-TOF-MS
Dimethyl Sulfide		7.0×10^{-12}		PTR-TOF-MS
SO_2		8.9×10^{-13}		Thermo 43 Series

Table 6.2: OH sinks measured during the ICOZA campaign used in the calculation of OH reactivity. Species were assigned classes according to their functionality. Bimolecular rate coefficients for the reaction with OH at 298 K and 1 Atmosphere are shown however pressure and temperature dependencies were used in the calculation of OH reactivity. Campaign average contributions to OH reactivity are also shown for each sink classification in addition to details of the instrument used for the measurement of each species.

Each sink was assigned to a class according to its functionality, so that grouped contributions to calculated OH reactivity could be determined, these are also listed with their campaign average contributions. Details of the instrument used to measure each species are provided in addition to bimolecular rate coefficients for reaction with OH. The values shown are those calculated at a temperature of 298 K and pressure of 1 Atmosphere. For the calculation of OH reactivity, the values used were determined using the temperature and pressure dependencies in conjunction with measured temperatures and pressures by the WAO meteorological station. All expressions for rate coefficients were IUPAC recommended values taken from the Master Chemical Mechanism (MCM) v3.3 (Jenkin et al., 1997, Saunders et al., 2003), with the exception of acetonitrile which was taken from directly from IUPAC owing to it being absent from the MCM. The measured OH reactivity is presented in

Section 6.3.2.5 in addition to discussion of its relationship with the measured OH reactivity.

6.4.2.5 Measured and calculated OH reactivity

The method for the calculation of OH reactivity using data from co-measurements of OH sinks was described in Section 6.3.2.4. The resulting values are plotted in Figure 6.17 along with the measured values for comparison. The measured values are significantly higher than the calculated values for the majority of the campaign, implying the presence of 'missing' OH reactivity. The mean average measured OH reactivity was 4.8 s^{-1} and the mean average of the calculated values, determined where there was a corresponding measured value, was 2.7 s^{-1}. The 'missing' OH reactivity was 44 % on average for the campaign which is close to that determined by Lee et al. (2009) for TORCH-2 (40 %, when a similar suite of VOCs were measured at the WAO) when only measured species were used to calculate OH reactivity. The correlation between measured and calculated OH reactivity is presented in Figure 6.16. The majority of points typically occupy space around and just above the line representing 50% underestimation by the calculation of OH reactivity, which is not surprising considering that the 'missing' OH reactivity is 44 %. The linear least squares gradient is 0.56.

To gain further insight into factors which may have influenced the level of 'missing' OH reactivity, the agreements between the measured and calculated values for individual days are considered. The plots in Figure 6.18, Figure 6.19 and Figure 6.20 compare measured and calculated OH reactivity for each day. In each plot the measured OH reactivity is represented by the red line and the cumulative calculated OH reactivity is represented by the top of the stacked structures. Each coloured band represents a contribution to calculated OH reactivity from groups of measured OH sinks (summarised in Table 5.2) that were measured. The categories of OH sinks in order from the bottom of the stacked structures were: Dialkenes, Carbonyls, Alkenes and Alkynes, Alkanes, NO_2, NO and CO. To aid clarity, OH sink categories with an average contribution of less than 0.1 s^{-1} have been omitted unless they were found to contribute significantly (>0.5 s^{-1}) at any point. The daily comparisons show that there is significant variation in the discrepancy between the measured and calculated OH reactivity. The greatest differences (as high as ~70 %) are shown for 01/07/2015 and 02/07/2015 which coincided with elevated temperatures during the heatwave

when the air mass is known to have spent considerable time passing over continental Europe. The contribution to calculated OH reactivity from NO_2 on these days is also the highest for the campaign which indicates that the air sampled was most polluted at this time.

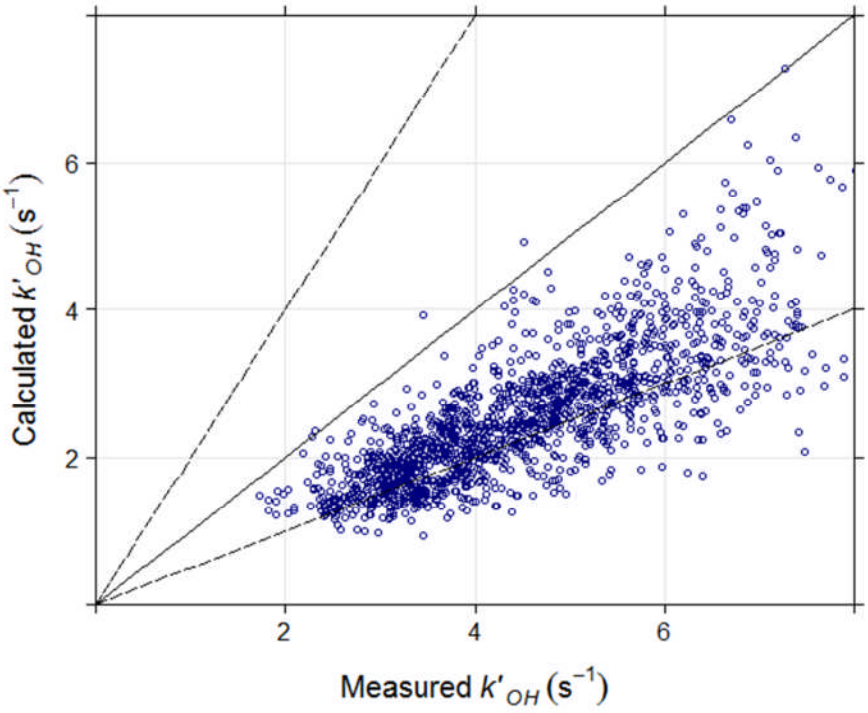

Figure 6.16: Correlation plot to show the relationship between calculated and measured OH reactivity during the ICOZA campaign. The solid line represents 1:1 agreement and the two dashed lines represent 50 % over or underestimation. Linear least squares gradient: 0.56, R^2: 0.57.

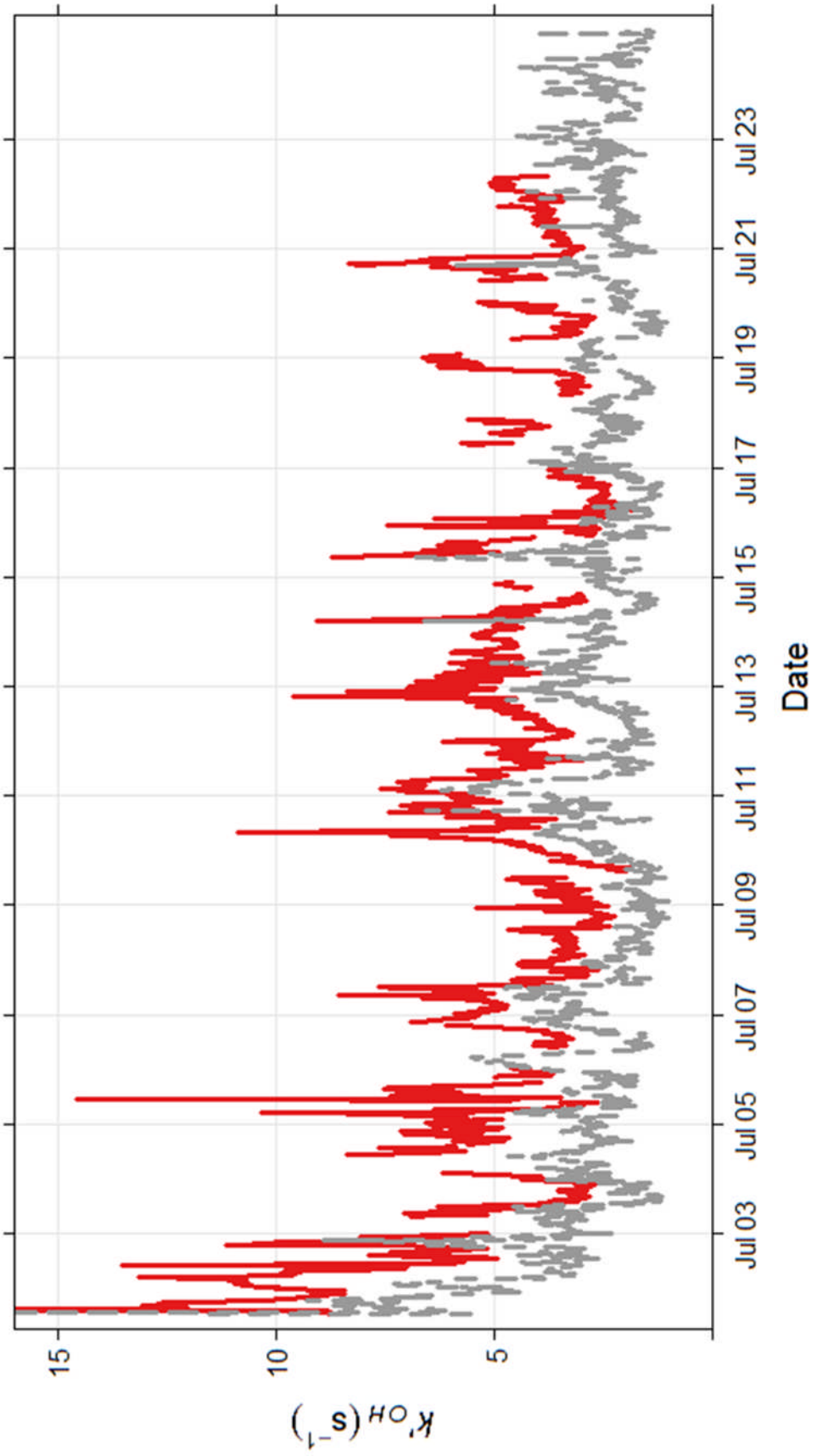

Figure 6.17: Measured OH reactivity (red line) and calculated OH reactivity (grey dashed line) for the ICOZA campaign. Data are plotted at 15 minute time intervals.

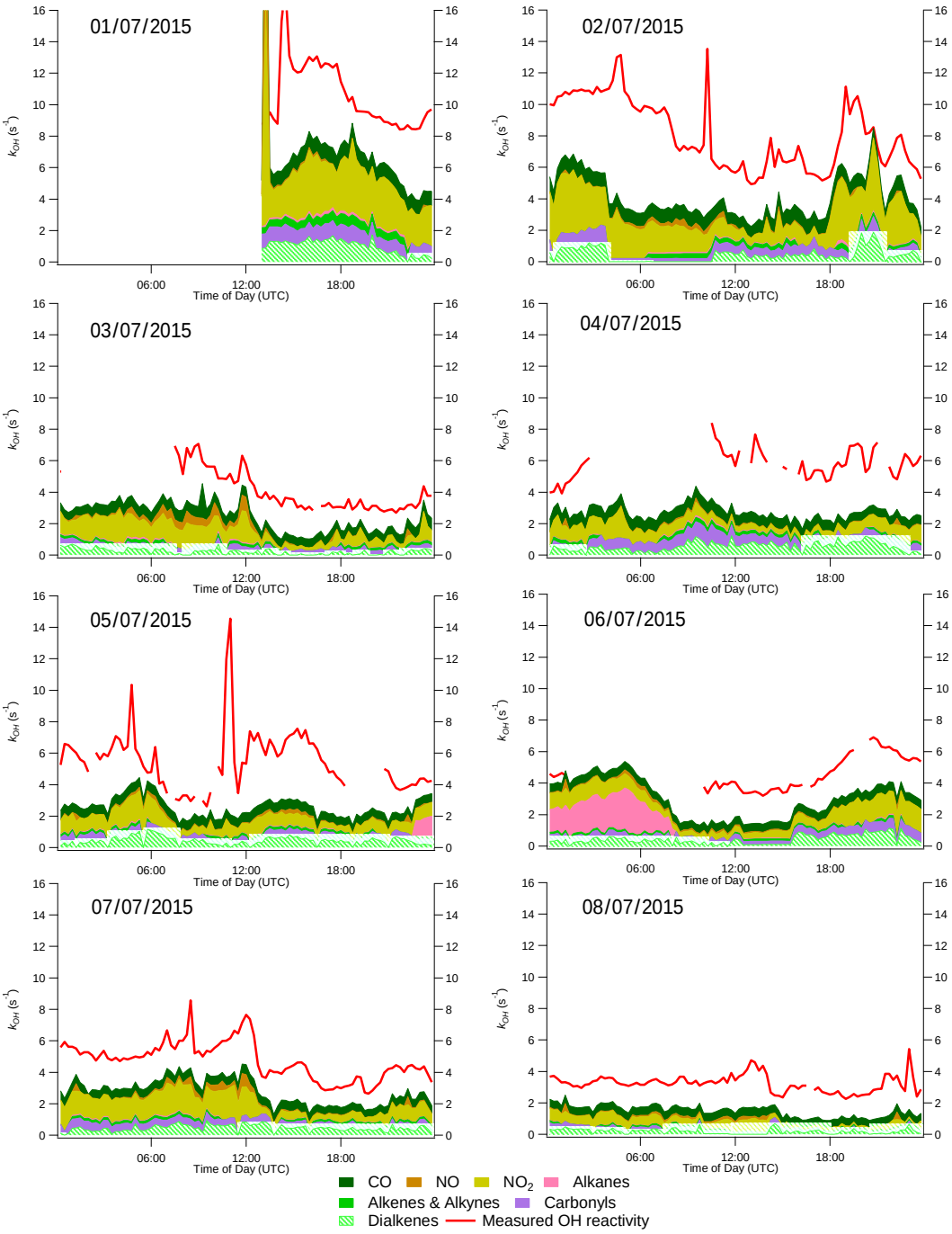

Figure 6.18: Daily comparisons (1st July – 8th July 2015) of measured total OH reactivity (red line) with cumulative calculated OH reactivity (stacked coloured structures) from the ICOZA campaign. Calculated contributions for each OH sink classification were determined using data for all species measured that are summarised in Table 6.2.

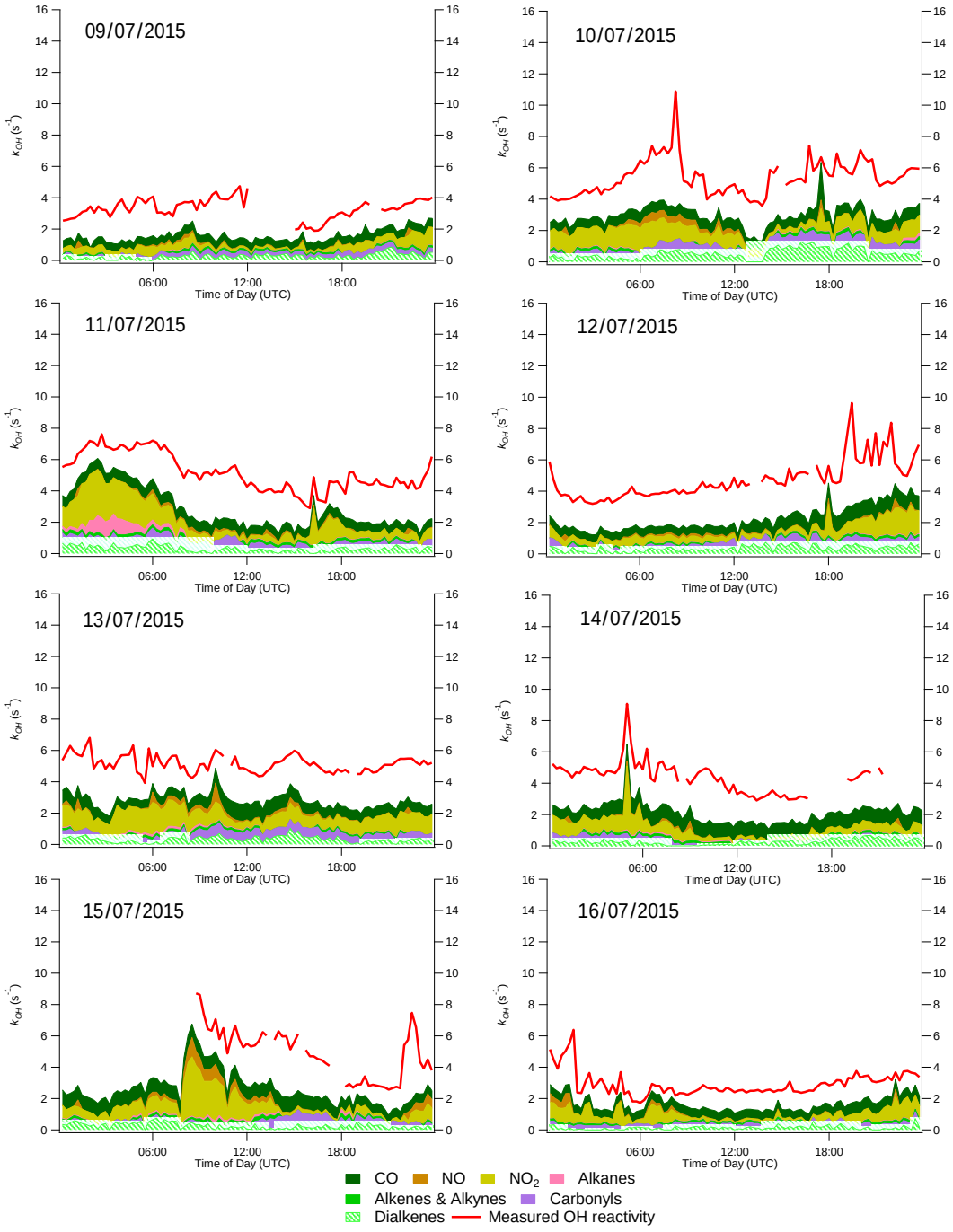

Figure 6.19: Daily comparisons (9th July – 16th July 2015) of measured total OH reactivity (red line) with cumulative calculated OH reactivity (stacked coloured structures) from the ICOZA campaign. Calculated contributions for each OH sink classification were determined using data for all species measured that are summarised in Table 6.2.

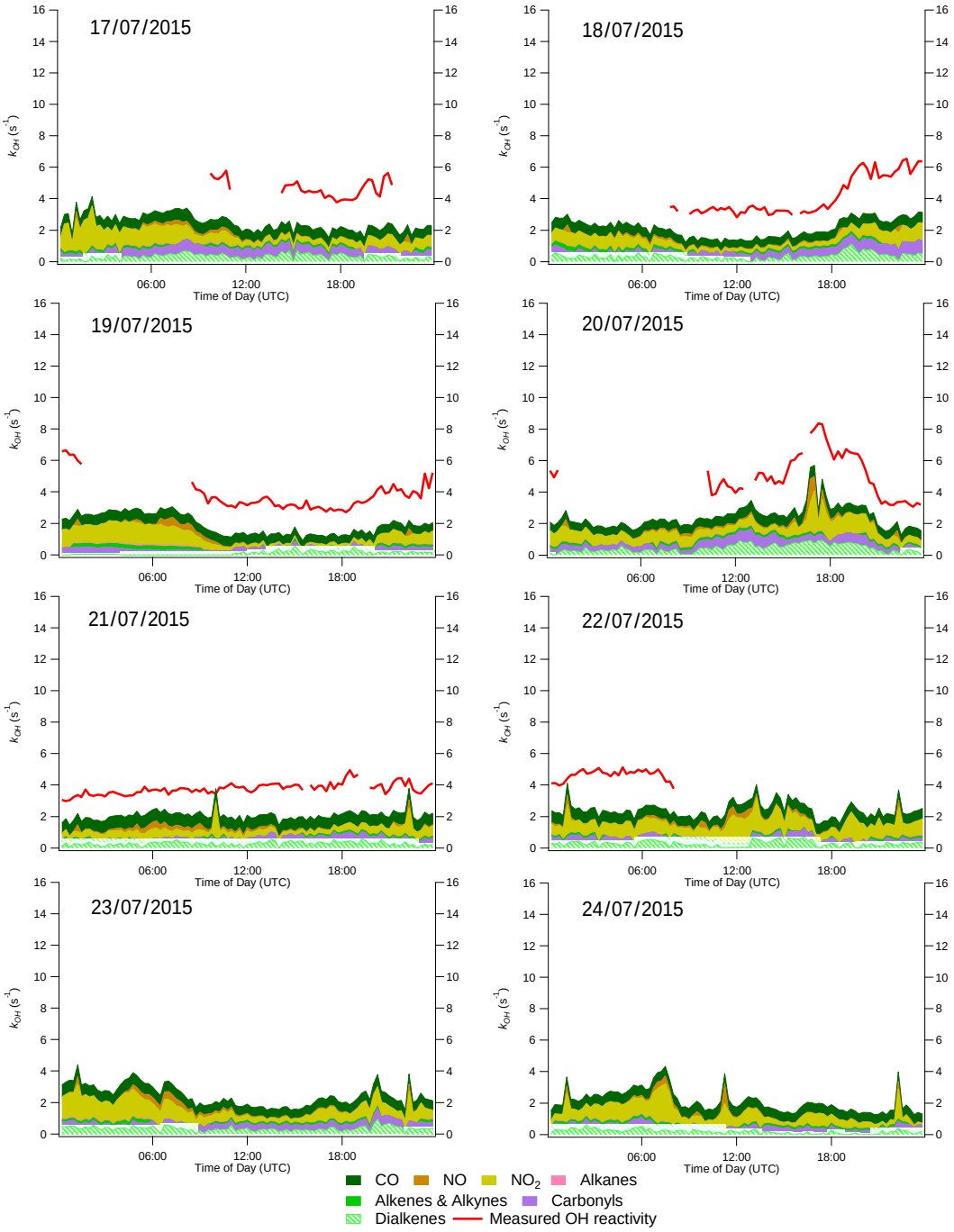

Figure 6.20: Daily comparisons (17th July – 24th July 2015) of measured total OH reactivity (red line) with cumulative calculated OH reactivity (stacked coloured structures) from the ICOZA campaign. Calculated contributions for each OH sink classification were determined using data for all species measured that are summarised in Table 6.2.

The plots for individual days demonstrate how the measured OH reactivity varies typically in the same way as the calculated values. However, there are periods of time where the profile of the measured values does not track that of the calculated. For example the spikes in measured OH reactivity just before 1200 on 02/07/2015 and 05/07/2015. It is likely that these are the result of a short lived elevated concentration of an OH sink that either was not measured, or was measured but rose and fell in concentration during the time where, for example, GC-FID measurements were linearly interpolated to achieve 15 minute time resolution.

The contribution from NO_2 to the calculated values is significantly more variable than those for other classifications of OH sink, and that changes in measured OH reactivity were almost always accompanied by a change in the calculated contribution from NO_2. This is expected considering the strength of the correlation with NO_2 presented in Section 6.3.2.2 and indicates that for the majority of ICOZA anthropogenic emissions drove the observed changes in OH reactivity.

Contributions from classes of OH sink other than NO_2 do not vary to the same extent on most days for which data are shown in Figure 6.18, Figure 6.19 and Figure 6.20. The class that showed the most variation after NO_2 is the dialkenes which includes contributions from isoprene and butadiene. These were shown to contribute the most to OH reactivity on 01/07/2015 and 02/07/2015 during and following the heat wave. This contribution from dialkenes at this time was almost exclusively driven by isoprene, which accounted for 91 % on 01/07/2015 and 99 % on 02/07/2015. This indicates that biogenic emissions, and their photo-oxidation products contributed to the OH reactivity measured during the heat wave as well as anthropogenic emissions.

On 01/07/2015 the daily average contribution from carbonyls to calculated OH reactivity (0.86 s^{-1}) was the highest recorded during the campaign. The largest contributor was acetaldehyde (50 %) followed by MVK + MACR (23 %) and formaldehyde (24 %). The largest atmospheric acetaldehyde source is thought to be the photochemical degradation of VOCs such as small alkanes and alkenes (Atkinson et al., 2006). The campaign average contribution from acetaldehyde to the carbonyl class was 31 % which is significantly lower than it was on 01/07/2015. This supports the hypothesis that a large portion of the OH reactivity during the heat wave could be attributed to increased photo-chemical processing of anthropogenic

VOCs, such as those from vehicles. Small alkanes and alkenes such as ethane, propane and propene are known to be directly emitted from combustion engines and these could have been processed more rapidly (Nakashima et al., 2012). Acetaldehyde is also known to be emitted from sea water as a result of photochemical degradation of dissolved organic matter, a source which has been postulated to be the second largest globally (Millet et al., 2010, Kieber et al., 1990). The campaign average contribution from MVK + MACR was 12 % which, similarly to acetaldehyde, is lower than it was on 01/07/2015. This observation further supports the hypothesis that biogenic emissions could have played a significant role in driving changes in OH reactivity during the start of campaign heat wave. It should be noted here that the contribution from formaldehyde to the carbonyl class is an estimate based on the average level measured from 08/07/2015 – 24/07/2015. This was necessary due to problems encountered with the HCHO LIF instrument at the beginning of the campaign. The contribution from HCHO here could have been far greater considering that the high temperatures that would have likely resulted in the most rapid photo-chemical processing of VOCs during the campaign.

As discussed above the discrepancy between the measured and calculated OH reactivity during ICOZA was greatest during the heatwave and a significant portion could be accounted for by a combination of anthropogenic and biogenic emissions, and their photo-oxidation products. Lee et al. (2009) reported that during the TORCH-2 campaign when a model was used to simulate the production of photo-oxidation products (which were not measured), the 'missing' reactivity was reduced from 40 % to 30 %. The use of a zero dimensional chemical box model to calculate the OH reactivity during ICOZA would also reduce the 'missing' OH reactivity. This should form the basis of future work on the study of OH reactivity during ICOZA.

Whalley et al. (2016) reported that a steady state concentration of RO_2 ($[RO_2]_{ss}$) can be calculated using E6.1, when it is assumed that the reaction between OH and NO to form HONO is a temporary radical sink, and that the reaction between OH and NO_2 is a permanent radical sink. It was also reported that the $[RO_2]_{ss}$ can be used to estimate the rate of ozone production ($P(O_3)$) from the reaction of RO_2 with NO (to form NO_2 which is subsequently photolysed leading to O_3 production) minus a correction to account for reaction of NO_2 with OH (which makes it unavailable for O_3 production), E6.2.

$$[RO_2]_{ss} = (k'_{OH} - (k_{OH+NO_2}[NO_2] + k_{OH+NO}[NO] + k_{OH+O_3}[O_3] + k_{OH+CO}[CO] + k_{OH+HCHO}[HCHO])[OH]) / (k_{RO_2+NO}[NO]) \quad \textbf{E6.1}$$

$$P(O_3) = k_{RO_2+NO}[RO_2]_{ss}[NO] - k_{OH+NO_2}[OH][NO_2] \quad \textbf{E6.2}$$

The average daytime (from 0600 – 2000 UTC) OH reactivity measured during ICOZA was 4.75 s^{-1}. This was used in conjunction with average daytime values of $[NO_2]$, [NO], $[O_3]$, [HCHO], and preliminary daytime average [OH] (5×10^6 molecule cm^{-3}) as in E6.1. $[RO_2]_{ss}$ was found to be equal to 4.3×10^8 molecule cm^{-3} for ICOZA, this corresponded to a daily average estimated $P(O_3)$ value of ~39 ppb d^{-1} as calculated using E6.2. In both calculations rate coefficients used were those shown in Table 6.2 with the exception of k_{RO_2+NO}that was assumed to be equal to $k_{C_2H_5OO+NO}$ at 298 K (2.6×10^{-12} cm^3 $molecule^{-1}$ s^{-1}, DeMore et al. (1997)). When the average daytime calculated OH reactivity is used in E6.1, in place of the measured OH reactivity, the value of $[RO_2]_{ss}$ determined is 2.0×10^8 molecule cm^{-3} (a 53 % reduction) and corresponds to a daily average estimated $P(O_3)$ value of ~12 ppb. This analysis means that ~27 ppb d^{-1} (~69 %) of the daily average O_3 production during ICOZA could have resulted from photo-oxidative processing of VOCs that were not measured (assuming that the missing OH reactivity was attributable to VOCs) and demonstrates the value of OH reactivity as a measurement. If the method reported by Ehlers et al. (2016) had been used to calculate O_3 production rates for ICOZA, using the calculated OH reactivity attributable to measured VOCs, and the calculated OH reactivity that is attributable to measured NO_2 with a computer model simulation, O_3 production would have been severely underestimated. Based on the assumption that 'missing' OH reactivity reported for ICOZA was exclusively due to unmeasured VOCs, the average daily production rate would be underestimated by ~69 %. However, it is likely that a significant portion of the discrepancy could be accounted for by unmeasured products of photo-oxidation. As mentioned above, future work should include a computer modelling study to assess the contribution from unmeasured photo-oxidation products, of measured VOCs, to the measured OH reactivity during ICOZA. The estimation of a third daily average O_3 production rate, using the OH reactivity predicted by the model, should be compared with the estimates above to further investigate sources of O_3. Further to this, the estimated production rates

should be compared with those directly measured by the POPR instrument (University of Birmingham).

6.5 Formaldehyde

6.5.1 Formaldehyde observations

The LIF instrument for the measurement of HCHO was deployed for the ICOZA campaign and was operated in configuration 3 as described in Section 2.3.6. The instrument was placed inside the WAO laboratory and measurements were made from a glass manifold which sampled ambient air from the top of the tower (described in Section 6.2). It was not possible to measure HCHO at the beginning of the campaign owing to problems encountered with communication between the instrument computer and the photon counting card, and also low laser power resulting from an electronic fault within the control unit of the fibre laser. Both of these problems were resolved by 08/07/2015 and measurements were made near continuously following this. The only unplanned gap in the data arose from a run down battery in the photodiode which meant it was not possible to normalise the LIF signal for laser power for some time on 14/07/2015 and 15/07/2015. The photograph in Figure 6 shows the instrument inside the WAO laboratory during the ICOZA campaign.

The levels of HCHO observed were found to vary significantly during the course of the ICOZA campaign; the observed levels were typically between 500 and 2000 ppt with a mean average of ~990 ppt. A complete time series for the ICOZA measurements is shown in Figure 6.21. The daily trend in HCHO levels was largely consistent through the campaign; increases were typically seen through the late morning and daytime hours and decreases were typically seen through the night time and early morning hours. The diurnal behaviour is discussed in detail in Section 6.4.2.1.

Figure 66.21: Photograph of the LIF HCHO instrument inside the WAO laboratory during the ICOZA campaign.

On the 08/07/2015 and 09/07/2015 HCHO was typically less than 1000 ppt before increasing on the 10/07/2015 where levels were typically higher than 1000 ppt and showed greater variation through the course of each day (~1000 ppt to ~ 2000 ppt). From the 21/07/2015 the measurements were typically lower until the end of the campaign. An exception to this is a period where large rapid excursions are shown during the early hours of the 25/07/2015 which coincided with a heavy thunderstorm. These data are plotted in Figure 6.22 to enable closer inspection.

During the storm the level of HCHO was shown to fluctuate by as much as ~1000 ppt on an order of minutes. The storm is known to have started at ~2200 on 24/07/2015 and ended at ~0600 on 25/07/2015. Figure 6.22 shows that HCHO levels behaved in a similar manner from ~0600 - ~1200 on 25/07/2015. The mean level of HCHO for ICOZA was ~985 ppt when the data from the storm were not considered. A more detailed discussion of the HCHO observed during and following the storm is given in Section 6.4.2.3.

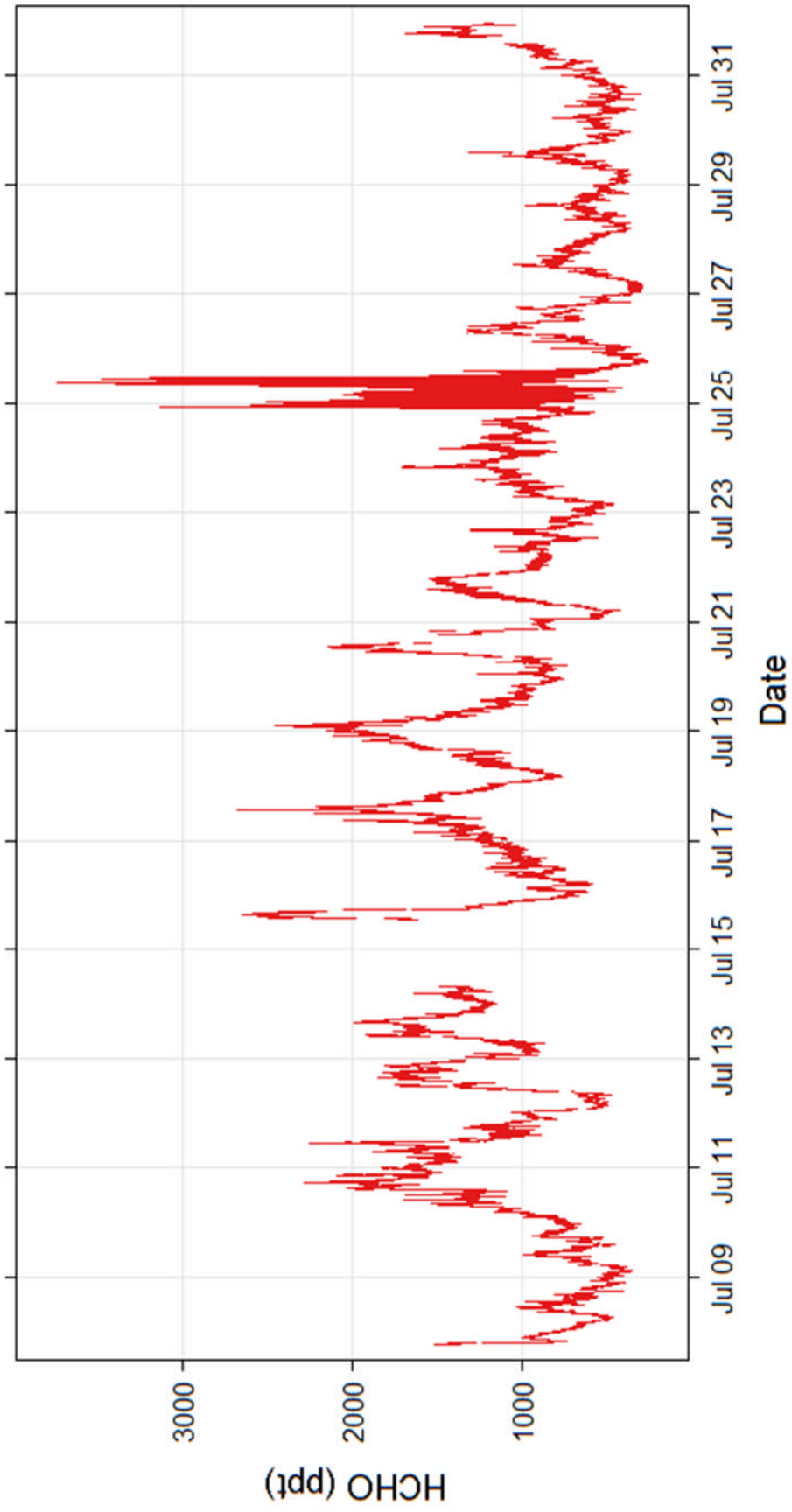

Figure 6.21: Time series of measured [HCHO] during the ICOZA campaign. Data are plotted with 1 minute time resultion. The unusual behaviour on July 25th coincided with a thunder storm at the site.

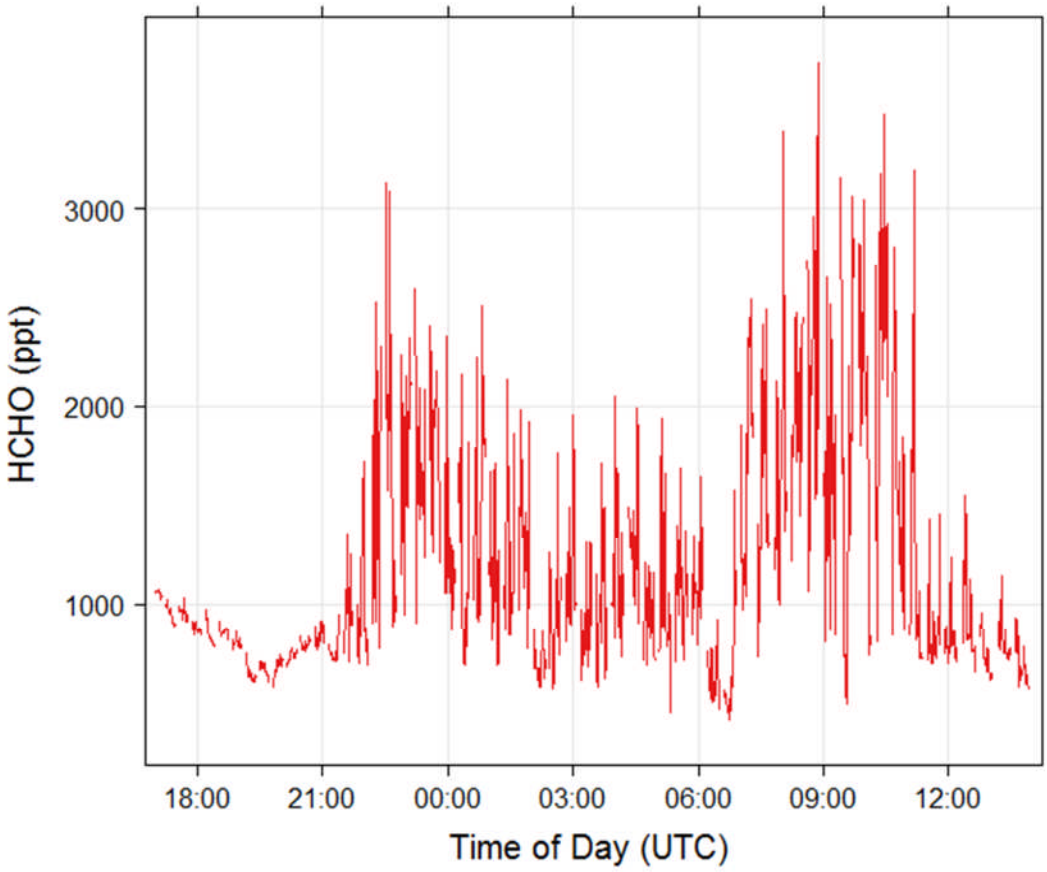

Figure 6.22: HCHO measurements plotted at 1 minute time intervals for 17:00:00 24/07/2015 – 14:00:00 25/07/2015 during the storm.

6.5.2 Interpretation of formaldehyde observations

6.5.2.1 Diurnal behaviour

The time series of HCHO measurements made during the ICOZA campaign presented in Section 6.4.1 showed that the daily trend was fairly similar on most days of the campaign where measurements were made. To enable a broad examination of the major drivers of the HCHO levels observed with respect to its chemistry, a diurnal profile was calculated for the 'average day'. Measurements were averaged into 96 time bins with a mean value every 15 minutes; Figure 6.23 shows the resulting diurnal profile.

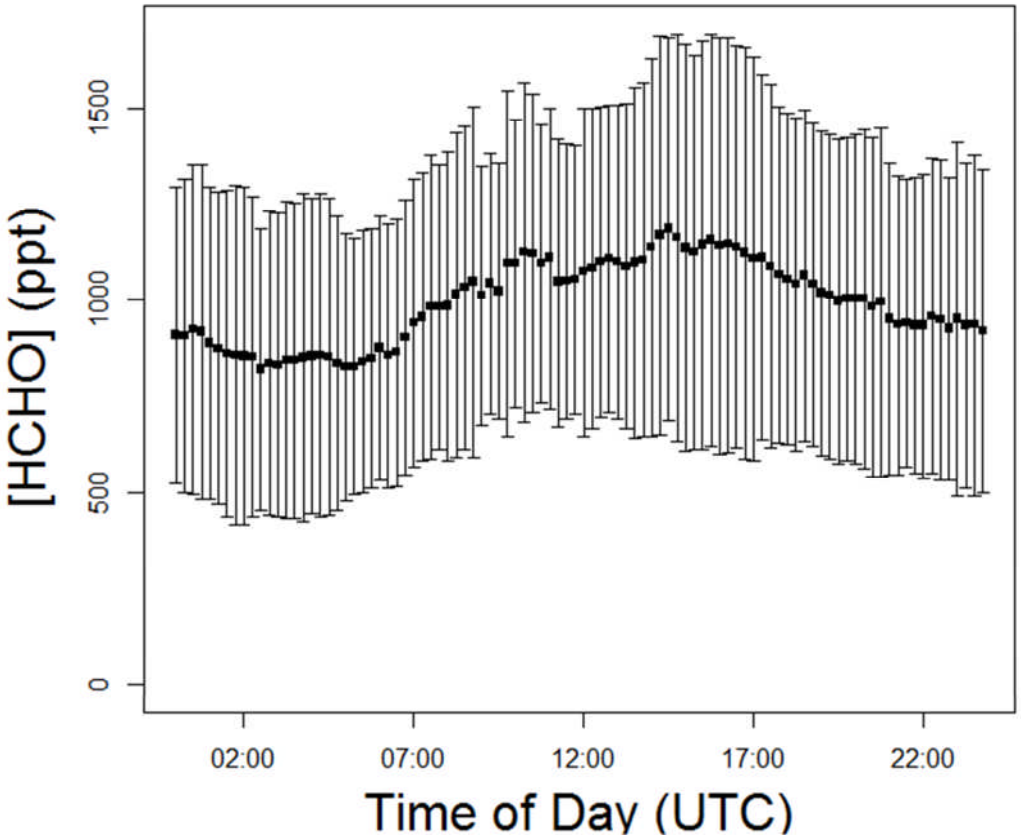

Figure 6.23: Diurnal profile of [HCHO] observed during the ICOZA campaign in 15 minute time bins. Error bars ± 1 σ standard deviation from the mean observation, and are a measure of the variability of HCHO levels during a 15 minute time bin.

Formaldehyde levels demonstrated clear diurnal behaviour during ICOZA and the profile is very typical of that for an environment where formaldehyde production is largely driven by photo-oxidation of VOCs. For example, the shape is very similar to that reported in the literature for clean marine environments. Ayers et al. (1997) reported a diurnal profile in 1993 measurements made in Cape Grim, Tasmania, and is consistent with there being net photochemical production during the daylight hours with more or less continuous loss to deposition which led to net loss in the night time hours. The level of HCHO is shown to increase from ~0600 and continue to rise until it plateaued towards a maximum at ~1600 when the sunlight driving the photochemical source would have been less intense. Following this a decrease is seen through the night until sunrise.

6.5.2.2 Correlations with other species measured

The relationship between the observed levels of HCHO and other species / parameters measured was examined to further investigate the nature of potential sources. The shape of the diurnal profile in Figure 6.26 indicates that the dominant source of HCHO during ICOZA was photochemical rather than direct emissions, e.g. those from engine combustion, industrial processes or the ocean. To assess the likelihood as to whether or not a such a direct emission source significantly impacted the HCHO measurements the relationship with NO_x was assessed. Correlation plots to demonstrate these relationships are shown in Figure 6.24.

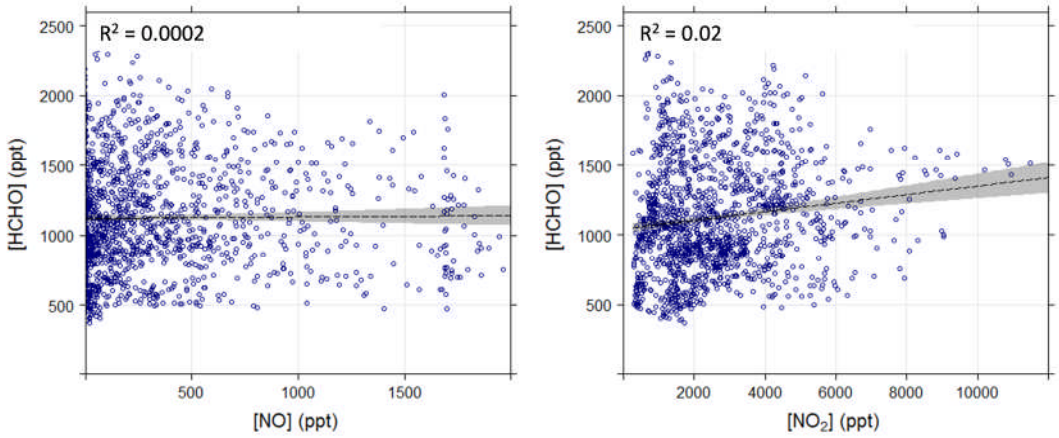

Figure 6.24: Plots of measured [HCHO] against both [NO] and [NO_2]. Data shown are 15 minute binned mean averages from measurements taken between 01/07/2015 13:00:00 – 25/07/2015 02:00:00 (UTC) during the ICOZA campaign. The shaded areas represent the 95% confidence intervals from the linear fits (least squares).[NO] and [NO_2] measurements were provided by Dr. James Lee, University of York.

Measured HCHO did not correlate with either NO or NO_2 during ICOZA, supporting the conclusion that the main source and driver of change in the HCHO observed was photochemical in origin. If a strong direct emission source impacted the measurements, some level of correlation would have been expected, as NO_x, similar to HCHO is a major by-product of fuel combustion and many industrial processes. To further investigate the photolytic HCHO source, the relationships with temperature and $J(O^1D)$ were examined. Correlation plots to demonstrate these relationships are shown in Figure 6.25.

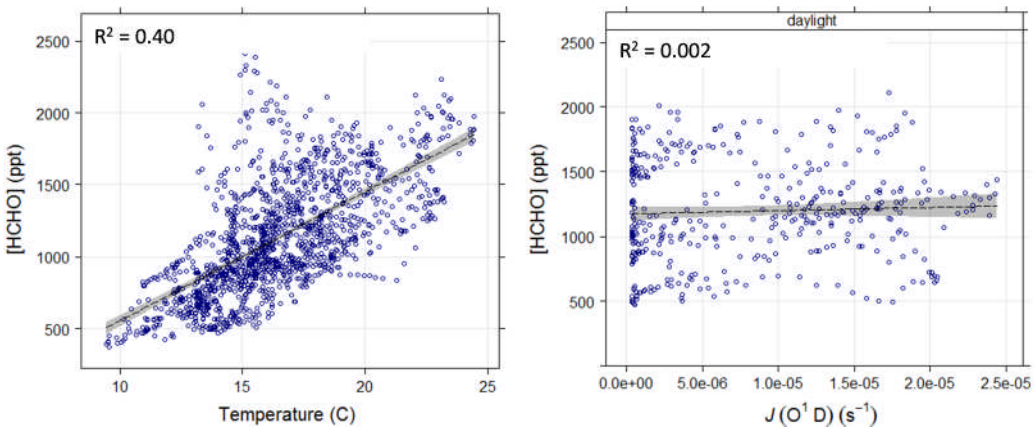

Figure 6.25: Plots of measured [HCHO] against both temperature and $J(O^1D)$. Data shown are 15 minute binned mean averages from measurements taken between 01/07/2015 13:00:00 – 25/07/2015 02:00:00 (UTC) during the ICOZA campaign. The shaded areas represent the 95% confidence intervals from the linear fits (least squares).

A clear correlation is shown between the level HCHO and the temperature of ambient air (R^2 = 0.40). This supports the conclusion that a large portion of the HCHO source during ICOZA was photochemical, as higher temperatures typically coincide with with more rapid photo-oxidation of VOCs. However, it is possible that to some extent that the correlation was influenced by direct biogenic emissions of HCHO as the comparison of OH reactivity and individually measured sinks (Section 6.3.2.2) showed evidence that there was some biogenic influence. It has been reported that direct HCHO emissions from plants have a positive temperature dependency (DiGangi et al., 2011). It is also shown that there was no correlation between the level of HCHO observed and the photolytic production rate of O^1D, $J(O^1D)$, which at first is surprising. However, it must be considered that the WAO is regularly subjected to air masses which are transported from considerable distances and that HCHO would be formed photochemically during this transport. HCHO typically has an atmospheric lifetime of a few hours (Jones et al., 2009) and so could be present in an air mass reaching the site having been produced a considerable distance away. If the air mass had been static during ICOZA, some level of correlation with $J(O^1D)$ would be expected. During the York 2014 'missing' OH reactivity campaign a reasonably strong correlation (R^2 = 0.32) was reported (Chapter 5). During this campaign wind speeds were much lower (0.35 m s^{-1} compared with 5.6 m s^{-1}) and so a greater portion of the photochemically produced

HCHO would have been formed locally through reactions involving locally produced O^1D.

Unfortunately, numerous instruments failed during the thunder storm between 24-25th July. Data that were available (NO_y, CO, metorological and PTR measured species) were used to investigate any possible relationship with HCHO. No correlations could be identified for this period. Although the temporal resolution is remarkable, it is not possible to draw conclusions here on potential sources of HCHO during the storm. A discussion of the possible cause of the HCHO during the storm is presented in Section 6.4.2.3 in the context of the origin of air mass as determined by the calculations of back trajectories.

6.5.2.3 Relationship with wind direction and air mass origin

During TORCH-2 HCHO was reported to be dependent on wind direction (Lee et al., 2009). It was found that HCHO was typically higher when the wind blew from the land than from the sea. When the wind was westerly to southerly to easterly the level of HCHO reported was ~750 – 1100 ppt. Whereas when the wind was westerly to northerly to easterly the levels were typically ~500 – 750 ppt. To investigate the relationship between HCHO and wind direction during ICOZA, the openair percentileRose function used. The 15 minute HCHO measurements, and the wind directions measured at the top of the WAO tower in the merged data set described in Section 6.3.2.2 were used. Figure 6.26 shows a wind rose for the HCHO measured during ICOZA and a map to show the location of the WAO. Data recorded during the storm were not included in this analysis.

It is shown that the highest (~1000 – 1500 ppt) mean HCHO was recorded when the wind was southerly to south westerly and similar to TORCH-2 the wind sector mean values were all greater than 500 ppt from westerly to southerly to easterly. The lowest mean values were observed for wind sectors from northerly to easterly which was also the case during TORCH-2. The dependence of HCHO levels on wind direction varies from that observed for OH reactivity where the highest mean values were shown to be for south easterly air, caused by higher values that were recorded during the heatwave at the beginning of the campaign. This is not reflected for HCHO in Figure 6.27 because measurements did not start until after the heatwave.

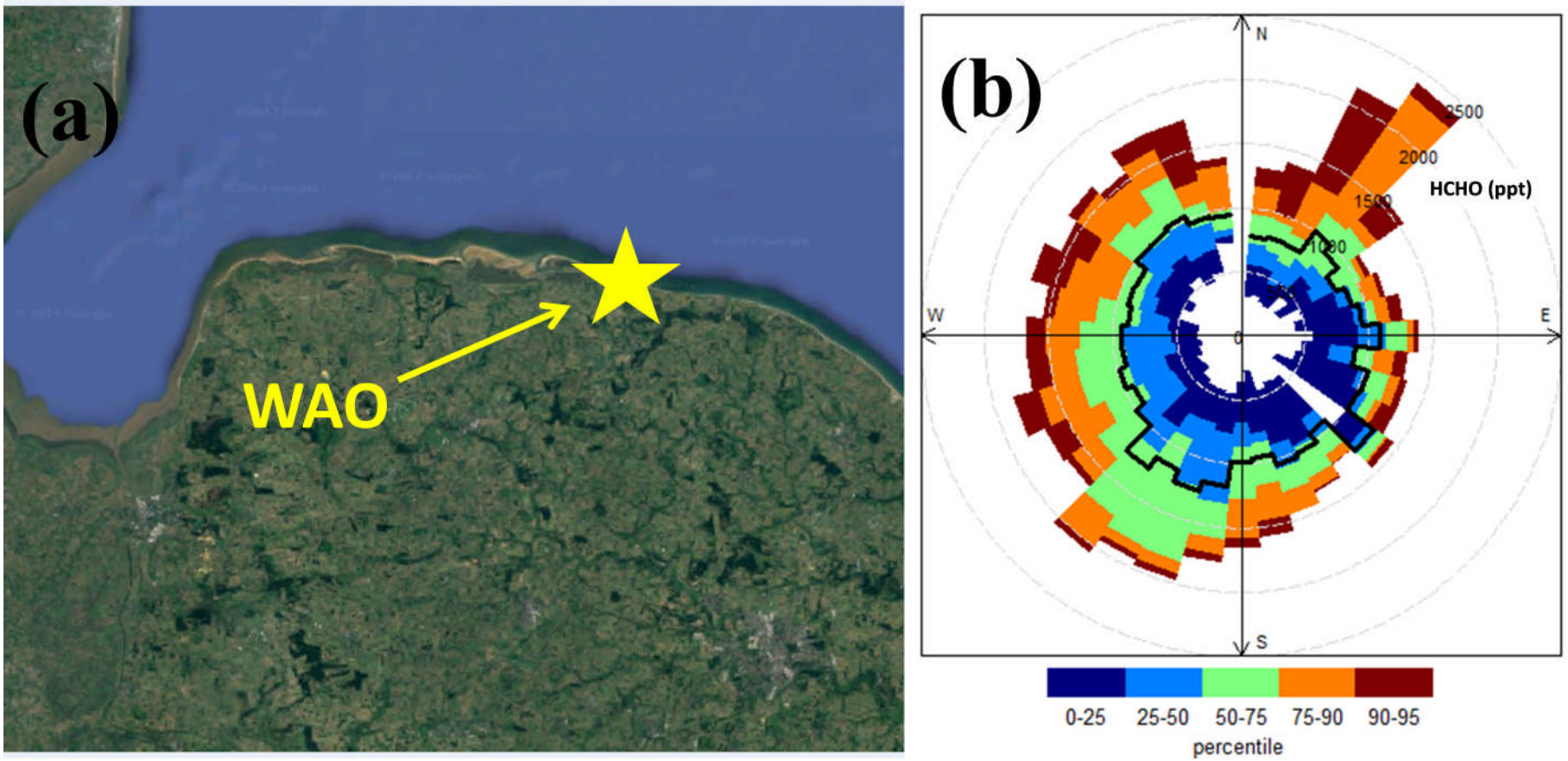

Figure 6.26: Wind rose to demonstrate the dependence of measured [HCHO] on wind direction during the ICOZA campaign. The black line represents the mean observed value for a given wind sector. Coloured areas represent the percentile levels for a given wind sector.

It was not possible to conduct a similar analysis as conducted for OH reactivity using back trajectories to identify possible source locations for HCHO for the whole of ICOZA. As stated above, the majority of the HCHO observed is thought to have been photo chemically produced and so would have been produced *in situ* during transport to the WAO. An exception to this was the 24-25/07/2015 storm which occurred during the night when there would have been no photochemical source. Figure 6 shows how the level of HCHO observed changed with the course of the back trajectory of the air reaching the WAO during the storm. The back trajectories were calculated as described in Section 6.3.2.3.

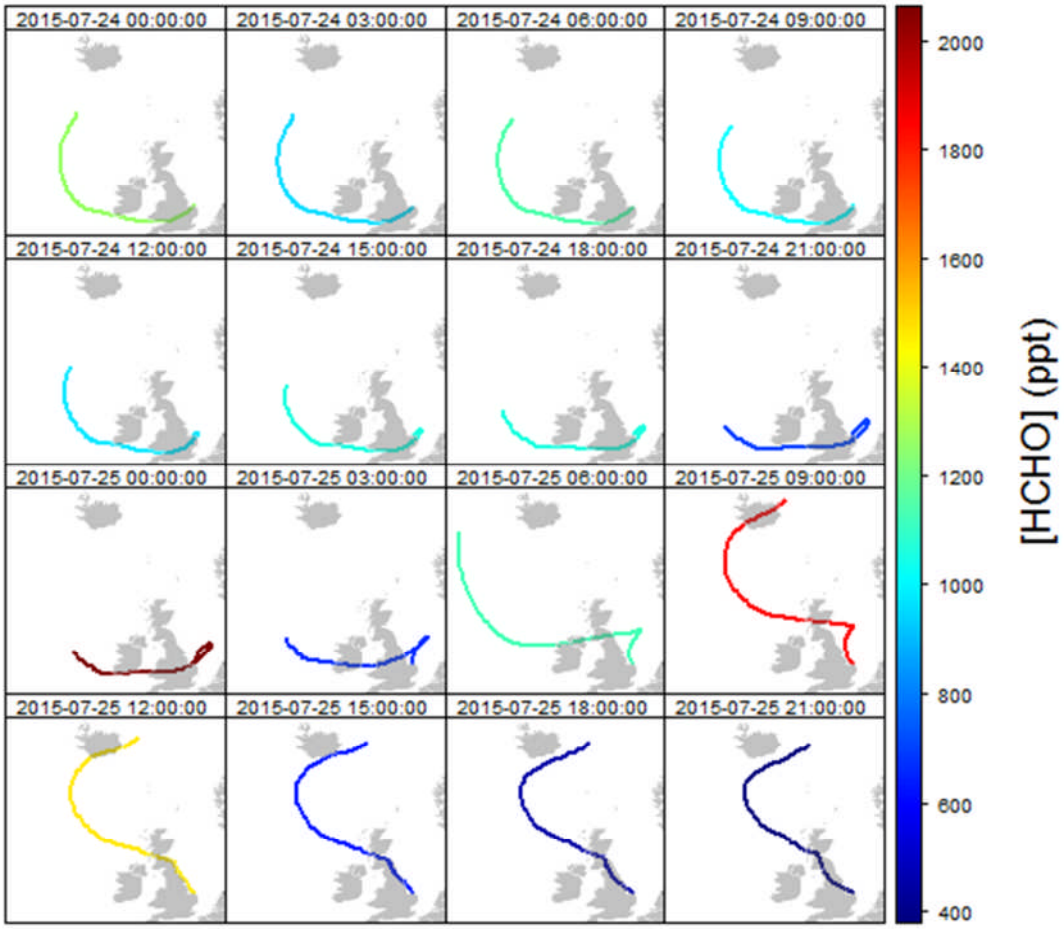

Figure 66.28: Four day back trajectories calculated using HYSPLIT (10 m starting height) for air reaching the WAO every three hours during ICOZA from 24/07/2015 00:00:00 to 25/07/2015 21:00:00 (UTC). The colour of each back trajectory represents the mean [HCHO] for the hour. Thundersorm onset was at ~2200 on 24/07/2015.

The back trajectories show a change in air mass simultaneous with the onset of the storm. Prior to the storm air of Atlantic origin was transported across southern England to the North Norfolk coast. As the storm began at ~2100 on 24/07/2015 the

back trajectories show that the air sampled had a brief excursion over the North Sea before returning to the coast where it was sampled at the WAO. It is not possible to draw any conclusions here as to the cause of the behaviour of HCHO during the night time storm. Following cessation of the storm at ~0600 on 25/07/2015 the back trajectories show that the path travelled changed so that it no longer passed over Southern England. It passed from the North Atlantic over Scotland into the North Sea before taking a sharp change in course to reach the WAO. At ~1200 on 25/07/2015 it is shown that the path travelled changed again so that transport into the North Sea did not occur and a more direct path was taken from the North Atlantic.

Figure 6.22 showed a pause in the rapid fluctuations of HCHO observed at ~0600 on 25/07/2015 when the storm ended. Following this the HCHO measurements started to behave in a similar manner to during the night-time storm until ~1200 when the profile of and level of HCHO returned to that typical for the rest of the campaign. On the morning of 25/07/2015 before ~1200 the waves in the North Sea near the WAO were the biggest observed and the water was visibly the most turbulent during the whole of the ICOZA campaign, the sunlight was also intense at this time. It is possible the HCHO fluctuations on the morning after the storm were due to a combination of the rougher sea and increased irradiation as the sun rose. Dissolved organic matter in sea water is known to make HCHO when irradiated with sunlight and more of this matter may have been available for photolytic degradation when the sea was more turbulent (Kieber et al., 1990).

It should be stressed that the possible reasons given for the unusual HCHO behaviour observed during the storm are not conclusive. To the knowledge of the author there are no other examples of such behaviour reported in the literature. Unfortunately due to the failure of other instruments during the storm only a limited analysis in the context of other observations could be conducted. It is suggested that laboratory experiments are conducted where sea water disturbed and irradiated with a lamp of similar spectral output to that of the sun whilst HCHO is measured in the headspace. This would allow the hypothesis that photodegradation of organic matter was a source of HCHO that contributed to unusual behaviour following the storm to be tested. Further to investigation of the cause of the unusual behaviour of HCHO observed during the thunder storm, it is suggested that a zero-dimensional chemical

box modelling study is conducted, using the MCM, to further investigate the HCHO budget during ICOZA.

6.6 Summary and conclusions

Measurements of OH reactivity and formaldehyde are presented from the ICOZA campaign which took place at the WAO on the North Norfolk Coast in July 2015. The campaign formed as a collaboration between researchers at the University of Leeds, University of Birmingham, University of York, University of East Anglia and University of Leicester.

OH reactivity was measured near continuously from 29/06/2015 to 22/07/2015 with few unplanned gaps in the data coverage. Measurements stopped on 22/07/2015 due to a problem encountered with the signal of the reference cell used to tune the wavelength of the 308 nm probe laser for the detection of OH. Formaldehyde was measured near continuously from 08/07/2015 – 31/07/2015. It was not possible to measure formaldehyde at the beginning of the campaign due to problems encountered with the computer used to control the LIF instrument and also a problem with low laser power from the fibre laser.

The mean OH reactivity measured was 5.1 s^{-1} and individual measurements were shown to vary between 1.7 and 27.7 s^{-1}. The mean was similar to that reported previously at the WAO during TORCH-2 (4.8 s^{-1}). Some of the highest measurements were made during a heatwave at the beginning of the campaign when the maximum temperature recorded was ~29 ˚C on 01/07/2015. At this time back trajectory analysis showed that the air in which OH reactivity was measured had spent a considerable amount of time being transported over both the UK and continental Europe in the four days prior to arrival at the WAO. A cluster analysis of the back trajectories concluded that the air masses sampled during ICOZA could be assigned one of three distinct classifications. These were Atlantic, North Sea and Local European. Atlantic air masses, where the air had passed over Southern England, were found to dominate the majority of the campaign. Back trajectories were used to calculate CWT mean OH reactivities to investigate the locations of potential sources of OH reactivity. It was shown that the greatest sources of OH sinks were likely to be along the coast of the Netherlands, and central Germany. OH reactivity was calculated using the concentrations of co-measured identifiable OH sinks for 01/07/2015 – 22/07/2015. The average calculated OH reactivity for this

period was 2.7 s^{-1}, the 'missing' OH reactivity was 44 % which was comparable to that reported for TORCH-2 where 40 % was reported to be 'missing'. It was concluded that changes in the OH reactivity measured were largely driven by NO_x emissions and that the missing OH reactivity was likely due to a combination of primary and secondary unmeasured anthropogenic and biogenic VOCs. The measured OH reactivity and that calculated using concentrations of OH sinks, were each used to estimate a daily average production rate of O_3 through calculation of a steady state concentration of RO_2. When the measured OH reactivity was used, this was estimated at ~39 ppb d^{-1}, whereas when the calculated OH reactivity was used it was estimated at ~12 ppb d^{-1} (69 % lower). It is not known at present what portion of this difference could be reconciled by taking into account products of photo oxidation in the prediction of OH reactivity, using a computer model. It is suggested that further work relating to the OH reactivity measurements includes a modelling study to assess the magnitude of the contribution from products of the photo oxidation of measured species that may have contributed to OH reactivity. Following this the daily average O_3 production rate should be estimated using the model predicted OH reactivity to assess what portion of the 69 % discrepancy is accounted for by model generated intermediates. The estimated ozone production rates should also be compared with direct measurements made using the University of Birmingham POPR instrument.

The mean level of formaldehyde observed during ICOZA was ~990 ppt and was found to vary by ~1000 – 2000 ppt through the course of each day. Clear diurnal behaviour was observed and was consistent with what has been previously reported in the literature, for an environment where the dominant source of formaldehyde is the photochemical processing of VOCs. The dependence of measured formaldehyde levels on wind direction was roughly in line with what was reported at the WAO during TORCH-2. An interesting observation of formaldehyde during ICOZA was that which occurred during, and after a storm on 24-25/07/2015 where the concentration was seen to rapidly (on an order of minutes) fluctuate by up to ~1000 ppt. No correlation between formaldehyde and any other measurement could be found for this time period and many instruments failed during the storm. It was concluded that a possible source of some of the formaldehyde following the storm could have been due an increased flux from the sea. Formaldehyde formed from photo degradation of dissolved organic matter could have been a greater source at

this time due to the high swell of the sea. It is suggested that future work to further rationalise these observations takes the form of a laboratory experiment to try and simulate these conditions in a controlled setting whilst formaldehyde is measured.

6.7 References

AIKIN, A. C., HERMAN, J. R., MAIER, E. J. & MCQUILLAN, C. J. 1982. Atmospheric chemistry of ethane and ethylene. *Journal of Geophysical Research: Oceans,* 87**,** 3105-3118.

ATKINSON, R., BAULCH, D. L., COX, R. A., CROWLEY, J. N., HAMPSON, R. F., HYNES, R. G., JENKIN, M. E., ROSSI, M. J., TROE, J. & SUBCOMMITTEE, I. 2006. Evaluated kinetic and photochemical data for atmospheric chemistry: Volume II – gas phase reactions of organic species. *Atmos. Chem. Phys.,* 6**,** 3625-4055.

AYERS, G. P., GILLETT, R. W., GRANEK, H., DE SERVES, C. & COX, R. A. 1997. Formaldehyde production in clean marine air. *Geophysical Research Letters,* 24**,** 401-404.

BANNAN, T. J., BOOTH, A. M., BACAK, A., MULLER, J. B. A., LEATHER, K. E., LE BRETON, M., JONES, B., YOUNG, D., COE, H., ALLAN, J., VISSER, S., SLOWIK, J. G., FURGER, M., PRÉVÔT, A. S. H., LEE, J., DUNMORE, R. E., HOPKINS, J. R., HAMILTON, J. F., LEWIS, A. C., WHALLEY, L. K., SHARP, T., STONE, D., HEARD, D. E., FLEMING, Z. L., LEIGH, R., SHALLCROSS, D. E. & PERCIVAL, C. J. 2015. The first UK measurements of nitryl chloride using a chemical ionization mass spectrometer in central London in the summer of 2012, and an investigation of the role of Cl atom oxidation. *Journal of Geophysical Research: Atmospheres,* 120**,** 5638-5657.

BOHN, B., KRAUS, A., MÜLLER, M. & HOFZUMAHAUS, A. 2004. Measurement of atmospheric O3 → O(1D) photolysis frequencies using filterradiometry. *Journal of Geophysical Research: Atmospheres,* 109**,** D10S90.

CARSLAW, D. C. 2015. *The openair manual - open-source tools for analysing air pollution data. Manual for version 1.1-4,* King's College London.

CARSLAW, D. C. & ROPKINS, K. 2012. openair - an R package for air quality data analysis. *Environmental Modelling and Software,* 27-28**,** 52-61.

CAZORLA, M. & BRUNE, W. H. 2010. Measurement of Ozone Production Sensor. *Atmos. Meas. Tech.,* 3**,** 545-555.

DEMORE, W. B., SANDER, S. P., GOLDEN, D. M., HAMPSON, R. F., KURYLO, M. J., HOWARD, C. J., RAVISHANKARA, A. R., KOLB, C. E. & MOLINA, M. J. 1997. Chemical kinetics and photochemical data for use in stratospheric modeling. *JPL Publication,* 4.

DI CARLO, P., BRUNE, W. H., MARTINEZ, M., HARDER, H., LESHER, R., REN, X., THORNBERRY, T., CARROLL, M. A., YOUNG, V., SHEPSON, P. B., RIEMER, D., APEL, E. & CAMPBELL, C. 2004. Missing OH Reactivity in a Forest: Evidence for Unknown Reactive Biogenic VOCs. *Science,* 304**,** 722-725.

DIGANGI, J. P., BOYLE, E. S., KARL, T., HARLEY, P., TURNIPSEED, A., KIM, S., CANTRELL, C., MAUDLIN III, R. L., ZHENG, W., FLOCKE, F., HALL, S. R., ULLMANN, K., NAKASHIMA, Y., PAUL, J. B., WOLFE, G. M., DESAI, A. R., KAJII, Y., GUENTHER, A. & KEUTSCH, F. N. 2011. First direct measurements of formaldehyde flux via eddy covariance: implications for missing in-canopy formaldehyde sources. *Atmos. Chem. Phys.,* 11**,** 10565-10578.

EHLERS, C., KLEMP, D., ROHRER, F., MIHELCIC, D., WEGENER, R., KIENDLER-SCHARR, A. & WAHNER, A. 2016. Twenty years of ambient observations of nitrogen oxides and specified hydrocarbons in air masses dominated by traffic emissions in Germany. *Faraday Discussions,* 189**,** 407-437.

HANSEN, R. F., GRIFFITH, S. M., DUSANTER, S., RICKLY, P. S., STEVENS, P. S., BERTMAN, S. B., CARROLL, M. A., ERICKSON, M. H., FLYNN, J. H., GROSSBERG, N., JOBSON, B. T., LEFER, B. L. & WALLACE, H. W. 2014. Measurements of total hydroxyl radical reactivity during CABINEX 2009 – Part 1: field measurements. *Atmos. Chem. Phys.,* 14**,** 2923-2937.

HEARD, D. E., READ, K. A., METHVEN, J., AL-HAIDER, S., BLOSS, W. J., JOHNSON, G. P., PILLING, M. J., SEAKINS, P. W., SMITH, S. C., SOMMARIVA, R., STANTON, J. C., STILL, T. J., INGHAM, T., BROOKS, B., DE LEEUW, G., JACKSON, A. V., MCQUAID, J. B., MORGAN, R., SMITH, M. H., CARPENTER, L. J., CARSLAW, N., HAMILTON, J., HOPKINS, J. R., LEE, J. D., LEWIS, A. C., PURVIS, R. M., WEVILL, D. J., BROUGH, N., GREEN, T., MILLS, G., PENKETT, S. A., PLANE, J. M. C., SAIZ-LOPEZ, A., WORTON, D., MONKS, P. S., FLEMING, Z., RICKARD, A. R., ALFARRA, M. R., ALLAN, J. D., BOWER, K., COE, H., CUBISON, M., FLYNN, M., MCFIGGANS, G., GALLAGHER, M., NORTON, E. G., O'DOWD, C. D., SHILLITO, J., TOPPING, D., VAUGHAN, G., WILLIAMS, P., BITTER, M., BALL, S. M., JONES, R. L., POVEY, I. M., O'DOHERTY, S., SIMMONDS, P. G., ALLEN, A., KINNERSLEY, R. P., BEDDOWS, D. C. S., DALL'OSTO, M., HARRISON, R. M., DONOVAN, R. J., HEAL, M. R., JENNINGS, S. G., NOONE, C. & SPAIN, G. 2006. The North Atlantic Marine Boundary Layer Experiment(NAMBLEX). Overview of the campaign held at Mace Head, Ireland, in summer 2002. *Atmos. Chem. Phys.,* 6**,** 2241-2272.

HELAND, J., KLEFFMANN, J., KURTENBACH, R. & WIESEN, P. 2001. A New Instrument To Measure Gaseous Nitrous Acid (HONO) in the Atmosphere. *Environmental Science & Technology,* 35**,** 3207-3212.

HOFZUMAHAUS, A. 2006. Measurement of Photolysis Frequencies in the Atmosphere. *In:* HEARD, D. (ed.) *Analytical Techniques for Atmospheric Measurement.* Blackwell Publishing Ltd.

JENKIN, M. E., SAUNDERS, S. M. & PILLING, M. J. 1997. The tropospheric degradation of volatile organic compounds: a protocol for mechanism development. *Atmospheric Environment,* 31**,** 81-104.

JONES, N. B., RIEDEL, K., ALLAN, W., WOOD, S., PALMER, P. I., CHANCE, K. & NOTHOLT, J. 2009. Long-term tropospheric formaldehyde

concentrations deduced from ground-based fourier transform solar infrared measurements. *Atmos. Chem. Phys.,* 9**,** 7131-7142.

KIEBER, R. J., ZHOU, X. & MOPPER, K. 1990. Formation of carbonyl compounds from UV-induced photodegradation of humic substances in natural waters: Fate of riverine carbon in the sea. *Limnology and Oceanography,* 35**,** 1503-1515.

KRUPA, S. V., NOSAL, M. & LEGGE, A. H. 1998. A numerical analysis of the combined open-top chamber data from the USA and Europe on ambient ozone and negative crop responses. *Environmental Pollution,* 101**,** 157-160.

LANGRIDGE, J. M., BALL, S. M. & JONES, R. L. 2006. A compact broadband cavity enhanced absorption spectrometer for detection of atmospheric NO(2) using light emitting diodes. *Analyst,* 131**,** 916-22.

LEE, J. D., YOUNG, J. C., READ, K. A., HAMILTON, J. F., HOPKINS, J. R., LEWIS, A. C., BANDY, B. J., DAVEY, J., EDWARDS, P., INGHAM, T., SELF, D. E., SMITH, S. C., PILLING, M. J. & HEARD, D. E. 2009. Measurement and calculation of OH reactivity at a United Kingdom coastal site. *Journal of atmospheric chemistry,* 64**,** 53-76.

MILLET, D. B., GUENTHER, A., SIEGEL, D. A., NELSON, N. B., SINGH, H. B., DE GOUW, J. A., WARNEKE, C., WILLIAMS, J., EERDEKENS, G., SINHA, V., KARL, T., FLOCKE, F., APEL, E., RIEMER, D. D., PALMER, P. I. & BARKLEY, M. 2010. Global atmospheric budget of acetaldehyde: 3-D model analysis and constraints from in-situ and satellite observations. *Atmos. Chem. Phys.,* 10**,** 3405-3425.

MURPHY, J. G., ORAM, D. E. & REEVES, C. E. 2010. Measurements of volatile organic compounds over West Africa. *Atmos. Chem. Phys.,* 10**,** 5281-5294.

NAKASHIMA, Y., TSURUMARU, H., IMAMURA, T., BEJAN, I., WENGER, J. C. & KAJII, Y. 2012. Total OH reactivity measurements in laboratory studies of the photooxidation of isoprene. *Atmospheric Environment,* 62**,** 243-247.

PENKETT, S. A., PLANE, J. M. C., COMES, F. J., CLEMITSHAW, K. C. & COE, H. 1999. The Weybourne Atmospheric Observatory. *Journal of Atmospheric Chemistry,* 33**,** 107-110.

REN, X., BRUNE, W. H., OLIGER, A., METCALF, A. R., SIMPAS, J. B., SHIRLEY, T., SCHWAB, J. J., BAI, C., ROYCHOWDHURY, U., LI, Y., CAI, C., DEMERJIAN, K. L., HE, Y., ZHOU, X., GAO, H. & HOU, J. 2006. OH, HO2, and OH reactivity during the PMTACS-NY Whiteface Mountain 2002 campaign: Observations and model comparison. *J. Geophys. Res,* 111**,** D10S03.

ROBBINS, R. C., BORG, K. M. & ROBINSON, E. 1968. Carbon Monoxide in the Atmosphere. *Journal of the Air Pollution Control Association,* 18**,** 106-110.

SAUNDERS, S. M., JENKIN, M. E., DERWENT, R. G. & PILLING, M. J. 2003. Protocol for the development of the Master Chemical Mechanism, MCM v3 (Part A): tropospheric degradation of non-aromatic volatile organic compounds. *Atmospheric Chemistry and Physics,* 3**,** 161-180.

STONE, D., EVANS, M. J., EDWARDS, P. M., COMMANE, R., INGHAM, T., RICKARD, A. R., BROOKES, D. M., HOPKINS, J., LEIGH, R. J., LEWIS,

A. C., MONKS, P. S., ORAM, D., REEVES, C. E., STEWART, D. & HEARD, D. E. 2011. Isoprene oxidation mechanisms: measurements and modelling of OH and HO₂ over a South-East Asian tropical rainforest during the OP3 field campaign. *Atmos. Chem. Phys.,* 11**,** 6749-6771.

STONE, D., WHALLEY, L. K., INGHAM, T., EDWARDS, P. M., CRYER, D. R., BRUMBY, C. A., SEAKINS, P. W. & HEARD, D. E. 2016. Measurement of OH reactivity by laser flash photolysis coupled with laser-induced fluorescence spectroscopy. *Atmos. Meas. Tech.,* 9**,** 2827-2844.

WAYNE, R. P. 2000. *Chemistry of Atmospheres*, New York, Oxford University Press.

WEINHEIMER, A. J. 2006. Chemical Methods: Chemiluminescence, Chemical Amplification, Electrochemistry, and Derivitization. *In:* HEARD, D. (ed.) *Analytical Techniques for Atmospheric Measurement.* Blackwell Publishing Ltd.

WHALLEY, L. K., BLITZ, M. A., DESSERVETTAZ, M., SEAKINS, P. W. & HEARD, D. E. 2013. Reporting the sensitivity of laser-induced fluorescence instruments used for HO2 detection to an interference from RO2 radicals and introducing a novel approach that enables HO2 and certain RO2 types to be selectively measured. *Atmos. Meas. Tech.,* 6**,** 3425-3440.

WHALLEY, L. K., STONE, D., BANDY, B., DUNMORE, R., HAMILTON, J. F., HOPKINS, J., LEE, J. D., LEWIS, A. C. & HEARD, D. E. 2016. Atmospheric OH reactivity in central London: observations, model predictions and estimates of in situ ozone production. *Atmos. Chem. Phys.,* 16**,** 2109-2122.

WORLD HEALTH ORGANISATION, W. 2005. Air Quality Guidelines Global Update 2005.

ZHAO, J., ZHANG, R., FORTNER, E. C. & NORTH, S. W. 2004. Quantification of Hydroxycarbonyls from OH−Isoprene Reactions. *Journal of the American Chemical Society,* 126**,** 2686-2687.

Chapter 7 - Summary and future work

7.1 Summary

In Chapter 1 of this thesis the importance of measuring OH reactivity and HCHO in the atmosphere is highlighted. Measurement techniques available for the measurement of each of these parameters are summarised in addition to a discussion of field observations that have been reported in the literature. In Chapter 2 details are provided of the two instruments used to make measurements of OH reactivity and HCHO for this thesis. The operating principles are described in addition to details regarding the key components and methods for data acquisition utilised by each instrument.

In Chapter 3 of this thesis an intercomparison is described for OH reactivity instrumentation that took part at the SAPHIR chamber at Jülich Forschungszentrum, Germany in late autumn 2015. Measurements of OH reactivity made using the Leeds LFP-LIF instrument are compared with anonymised measurements made using eight other instruments. Results were shown for three experiments out of a total of ten that took place during the intercomparison. In these three experiments the measurements made using the Leeds instrument agreed well with calculated values and measurements made using other LIF type instruments. However, in some cases the Leeds measurements showed a slight positive bias probably caused due to contaminants in the Leeds sampling line, or in the system that was used to supply O_3 to the instrument flow tube during some experiments. A full analysis of the data reported from all participating instruments of the intercomparison study, in addition to discussion of the agreement of data will be form the basis of a future publication.

In Chapter 4 the laboratory characterisation is described for an OH flow reactor which was successfully coupled with a GC-TOF-MS system at the University of York to form a new instrument for the identification of ‘missing’ OH reactivity. Some preliminary observations in ambient air made using this instrument are

presented from the York 2014 'missing' OH reactivity campaign which took place at an urban background site.

Measurements of OH reactivity and HCHO from the York 2014 'missing' OH reactivity campaign are presented in Chapter 5. The mean OH reactivity was ~6.3 s^{-1} and measurements ranged from 2.8 – 17.4 s^{-1}. Diurnal behaviour in OH reactivity showed evidence that the site was influenced by morning 'rush hour' vehicular emissions. A diurnal morning peak was observed at ~8 s^{-1}. OH reactivity was calculated using measured concentrations of a very detailed suite of OH sinks, for example several classes of VOCs. The campaign average 'missing' OH reactivity was ~27 % when the measurements were compared with predictions made with a calculation that used measured concentrations of identifiable OH sinks. It was concluded that the cause of 'missing' OH reactivity was likely a combination of unidentified primary VOCs and products of VOC photo-oxidation that were not measured. Data collected using the new instrument described in Chapter 4 have the potential to chemically identify some of the species that contributed to the 'missing' OH reactivity. The York 2014 'missing' OH reactivity campaign was the first field deployment of the HCHO LIF instrument (described in Chapter 2). The average level of HCHO observed was ~1.3 ppb and measurements were typically in the range 0.5 – 2.0 ppb. The measurements demonstrated the value of using the LIF technique for the measurement of HCHO with high time resolution (1 sercond) as rapid HCHO fluctuations (on the order of a few seconds) were observed that would likely be missed if another technique with lower time resolution was used. Some evidence of a diurnal profile was observed for HCHO in York that indicated the biggest source of HCHO was photo-chemical, a steady rise was observed through the daytime hours. However, it was only possible to examine data for daytime HCHO as the instrument was switched off overnight throughout the campaign.

Further field measurements of OH reactivity and HCHO are presented in Chapter 6 from the WAO situated on the North Norfolk Coast during the ICOZA campaign. OH reactivity was calculated using the concentrations of measured OH sinks and compared with the observations. The mean OH reactivity was ~5.1 s^{-1} and measurements ranged from 1.7 – 27.7 s^{-1}. The average 'missing' OH reactivity was ~44 % which is comparable with what has been determined previously at the same site. The biggest discrepancies (as high as ~70 %) were observed during a heat wave (29 ˚C maximum temperature) indicating a greater contribution from products of

VOC photo-oxidation. The measured and calculated OH reactivity were used to estimate a daily average O_3 production rates of ~39 ppb d^{-1} and ~12 ppb d^{-1}, respectively. The ~69 % difference between these values demonstrates the value of measuring OH reactivity when studying *in situ* O_3 production. This observation demonstrates that production rates could be substantially underestimated if the suite of VOCs measured is not representative of the composition of the air mass. The average level of HCHO observed was ~1.0 ppb and measurements were typically in the range 0.5 – 2.0 ppb. Strong diurnal behaviour of HCHO was observed at Weybourne that was consistent with what has been reported in the literature for similar environments where the dominant source is photo-chemical. An interesting feature of the HCHO measurements was the behaviour that was observed during a heavy thunderstorm at the end of the campaign. Sharp fluctuations (~1 ppb) were observed on the order of minutes. However, it was not possible to fully investigate the cause of this in the context of other species and parameters measured due to the failure of most other instrumentation during the storm.

7.2 Future work

A summary of the research, key results and conclusions that are presented in this thesis is given in the previous section. The purpose of this final section is to suggest what should be considered for future work with regard to continuation of the research presented here.

The work from the OH reactivity intercomparison at the SAPHIR chamber, discussed in Chapter 3 is currently in preparation for publication. The proposed publication will present results from each experiment that was conducted, and will also include a detailed discussion of the agreement of data that were recorded by all participating instrumentation. Much of the analysis of data required for completion of this publication is still in progress and as such it is not possible to provide detailed suggestions for future work here.

Chapter 4 details the design, development and characterisation of an OH flow reactor as part of a new instrumentation for the identification of 'missing' OH reactivity through the analysis of ambient air. Preliminary results are presented from the York 2014 'missing' OH reactivity campaign (described in Chapter 5). However, these are only for a small period of the measurement campaign (~2 days out of ~1 month). Future work relating to Chapter 4 should include a complete analysis of all

of the data that were acquired by the new instrument in York. All identifiable species in the air that was sampled by the system should be quantified where the sample had, and had not been exposed to OH in the flow reactor. These data should then be used to re-quantify as accurately as possible, the relationship between the change in instrument response for OH reactive species identified, and the bimolecular rate coefficients for their reaction with OH. Further to this, the chemical identity of species that were not immediately identifiable, should be investigated through thorough analysis of the large library of mass spectral data that was acquired. Any such species should then be accounted for in the prediction of OH reactiivity (as in Chapter 5), through calculation and model simulation, to assess their significance as an OH sink. The new instrument discussed here has shown potential as a valuable tool for investigating the source of 'missing' OH reactivity. Future deployment of this instrument should be considered to environments with atmospheres for which significant 'missing' OH reactivity has been reported, such as a forest. However, before this can happen the system should be re-engineered as a portable field instrument. The measurements made in York were only logistically possible because the instrument was housed within a well equipped laboratory in a space much larger than what is typically available in the field.

In Chapter 6 measurements of OH reactivity and HCHO are presented from the ICOZA campaign in Weybourne. OH reactivity was measured and predicted through calculation using the concentrations of co-measured identifiable sinks. Products of VOC photo-oxidation have not yet been considered in the prediction of OH reactivity for ICOZA. Future work should include a computer modelling study using the MCM to simulate OH reactivity for ICOZA, so that the contribution to OH reactivity from products of photo-oxidation of the measured primary sinks can be assessed, the missing OH reactivity should also be re-quantified. Further to this, daily ozone production rates should be re-calculated, using the steady state approximation for RO2, to estimate the portion of daily ozone production in Weybourne that was attributable to the processing of OH sinks not accounted for in the model simulation. This calculation, and those presented in Chapter 6 should be repeated using a revised average daytime OH concentration as at the time of writing only a preliinary value was available. Future work relating to HCHO for ICOZA should include a computer modelling study using the MCM where levels are simulated and compared with the measurements. Unfortunately, due to technical

challeges with many instruments during the thunderstorm at end of ICOZA, it was not possible to fully investigate the cause of rapid flutuations in HCHO that were observed. In future the hypothesis that that the HCHO source was oceanic should be tested through laboratory experiments where the headspace of some seawater, under various simulated atmospheric conditions, is sampled by the HCHO LIF instrument. Numerous analyses are presented in Chapter 6 which utilise back trajectories that were calculated using the HYSPLIT model, whilst the starting height for the back trajectories calculated was set at 10 m, these analyses do not take into account variations in the altitude of air during transport to the site. Future work should include a detailed assessment of the variation in altitude through the course of each back trajectory calculated to determine the relevance of the preliminary conclusions relating to the origin of species contributing to OH reactivity during ICOZA.